ELECSHIP *98* PROCEEDINGS

International Conference
on
Electric Ship

1 September, 1998

Istanbul, TURKEY

Sponsored by: ⊚

US Office of Naval Research (Europe)

Organised by: ◐

Middle East Technical University

Editors: **Prof.Dr. H. Bülent Ertan**
Prof.Dr. Yıldırım Üçtuğ
Electrical and Electronics Engineering Department
Middle East Technical University
06531 Ankara, Turkey

REPORT DOCUMENTATION PAGE

Form Approved OMB No. 0704-0188

1. AGENCY USE ONLY (Leave blank)	2. REPORT DATE	3. REPORT TYPE AND DATES COVERED
		Final Report

4. TITLE AND SUBTITLE
Elecship 98 Proceedings. International Conference on Electric Ship. 1 September, 1998. Istanbul, Turkey.

5. FUNDING NUMBERS
N00014-98-1-1056

6. AUTHOR(S)
Multiple

7. PERFORMING ORGANIZATION NAME(S) AND ADDRESS(ES)

Middle East Technical University
Department of Electrical and Electronics Engineering
06531 Ankara Turkey

8. PERFORMING ORGANIZATION REPORT NUMBER

ISBN 975-429-129-2

9. SPONSORING/MONITORING AGENCY NAME(S) AND ADDRESS(ES)

Office of Naval Research
European Office
PSC 802, Box 39
FPO AE 09499-0039

10. SPONSORING/MONITORING AGENCY REPORT NUMBER

11. SUPPLEMENTARY NOTES
In conjunction with International Conference on Electrical Machines (ICEM'98).

This work relates to Department of the Navy Grant N00014-98-1-1056 issued by the Office of Naval Research International Field Office. The United States has a royalty free license throughout the world in all copyrightable material contained herein.
Best available copy.

12a. DISTRIBUTION/AVAILABILITY STATEMENT

Approved for Public Release; Distribution Unlimited.
Government Purpose Rights License. All other rights reserved by the copyright holders.

12b. DISTRIBUTION CODE
A

12. ABSTRACT (Maximum 200 words)

The conference papers were presented in five sessions which focused on: Country programs for all electric warships; miscellaneous topics, ship power systems; propulstion, and converters.

13. SUBJECT TERMS
Ship propulsion

15. NUMBER OF PAGES

16. PRICE CODE

17. SECURITY CLASSIFICATION OF REPORT	18. SECURITY CLASSIFICATION OF THIS PAGE	19. SECURITY CLASSIFICATION OF ABSTRACT	20. LIMITATION OF ABSTRACT
UNCLASSIFIED	UNCLASSIFIED	UNCLASSIFIED	UL

NSN 7540-01-280-5500

Standard Form 298 (Rev. 2-89)
Prescribed by ANSI Std. 239-18
298-102

ELECSHIP'*98* ORGANISING COMMITTEE

Chairman:

Dr. Peter MAJUMDAR, US Office of Naval Research (Europe)

Co-Chairman:

Prof. Dr. H. Bülent ERTAN, Middle East Technical University

Members:

Rear Admiral Savas ONUR, Turkish Navy

Prof. Dr. Bahri ERCAN, Hacettepe University

Prof. Dr. M. Yıldırım ÜÇTUĞ, Middle East Technical University

PROGRAMME TIMETABLE

TUESDAY, 1 SEPTEMBER 1998

09:00 - 09:15	FORMAL OPENING - Address of Welcome
09:15 - 09:30	KEYNOTE SPEECH RADM P.G. Gaffney, II, US Navy
09:30 - 10:15	INVITED PAPER Mr. Terry Ericsen, USA
10:15 - 10:45 COFFEE BREAK	
10:45 - 11:30	SESSION CP: COUNTRY PROGRAMS
11:30 - 12:15	SESSION MI: MISCELLANEOUS TOPICS
12:15 - 13:30 LUNCH	
13:30 - 15:00	SESSION SP: SHIP POWER SYSTEM
15:00 - 15:30 COFFEE BREAK	
15:30 - 16:30	SESSION PR: PROPULSION
16:30 - 17:00 COFFEE BREAK	
17:00 - 18:30	SESSION CO: CONVERTERS
18:45 - 20:00 COCKTAIL	

TABLE OF CONTENTS

OPENING SESSION

Tuesday, September 1   09:00 - 10:15

Chair: Prof.Dr. H.B. ERTAN

Keynote Speech
RADM P.G. Gaffney, II, USA

Invited Paper
Mr. T. Ericsen, USA

SESSION CP: COUNTRY PROGRAMS

Tuesday, September 1   10:45 - 11:30

Chair: Prof. W.F. WELDON

SESSION MI: MISCELLANEOUS TOPICS

Tuesday, September 1   11:30 - 12:15

Chair: Prof. W.F. WELDON

SESSION PS: SHIP POWER SYSTEM

Tuesday, September 1   13:30 - 15:00

Chair: Dr. I. LINGVAY

SESSION PR: PROPULSION

Tuesday, September 1   15:30 - 16:30

Chair: Dr. G. TINA

SESSION CO: CONVERTERS

Tuesday, September 1   17:00 - 18:30

Chair: Prof.Dr. L. RODRIGUES

iv

The All Electric Warship: An Overview of the U.S. Navy's Integrated Power System Development Programme

LCDR Timothy McCoy, US Navy
Naval Sea Systems Command
2531 Jefferson Davis Hwy.
Arlington, VA 22242 USA

Dr. Makhlouf Benatmane
Cegelec Projects, Ltd.
Boughton Road
Rugby, England CV21 1BU

Abstract

The advent of fast, high voltage, high power semiconductor switching devices is revolutionising the commercial marine industry. The "power station" concept, wherein all ship's loads (including propulsion) are powered from a common set of generators has become prevalent in many commercial marine and industrial markets including cruise ships, ferries and shuttle tankers. This is primarily because modern power electronics has made propulsion systems utilising variable speed AC motor drives in the multi-megawatt power range cost competitive with traditional segregated mechanical drive plants.

For the military ship, there are additional advantages in addition to the ownership cost improvements of electric propulsion. These include increased survivability and reliability, reduced maintenance and manning requirements and arrangement flexibility. However, the requirements of the military ship are more demanding than the commercial ship. The military ship demands higher power density components, imposes more stringent signature requirements and subjects components to a harsher environment, including weapons effects such as underwater shock.

To meet these military requirements, the U.S. Navy has embarked on a development programme that builds on the experience in the commercial marine market and adapts that technology to the military combatant ship application. This development is embodied in the U.S. Navy's Integrated Power System (IPS) programme. Presently, the IPS programme is well into its Full Scale Advanced Development (FSAD) phase where prototype hardware is being constructed for land based proof of concept testing. This paper outlines the IPS architecture, the development programme to date, future plans and technologies presently being used or considered for future insertion.

1.0 IPS architecture

IPS starts with the commercial marine "power station" architecture shown in Figure (1). However, the IPS architecture differs from commercial practice in several areas. First, a modular approach is taken to the design, in an effort to reduce the recurring engineering effort presently needed for the introduction of each new ship class. This modular approach will also facilitate future hardware upgrades within each module, as today's electronics will become obsolete long before the end of a ships useful life, typically 30-50 years for military ships.
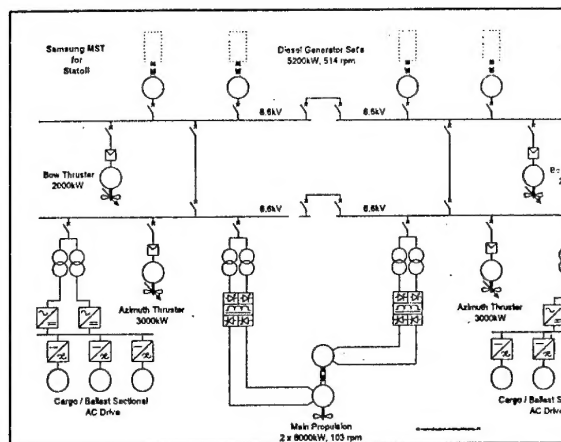
Figure 1: Power Station Architecture

To meet the military survivability and reliability requirements, the ship's service distribution system uses a zonal architecture and distributes power as high voltage DC. Regulated solid state power converters separate each zone and provide inversion to AC where necessary. See Figure (2).

1.1 DC Zonal DC Distribution

DC Distribution simultaneously accomplishes two goals for the military ship. First, it de-couples the loosely regulated propulsion bus with its high harmonic content from sensitive combat systems loads that require clean, continuos power. Second, DC distribution provides what has become known as "zonal fight through." Zonal fight through is defined as the ability of the ship's power system to sustain damage without any electrical disruption outside of the damaged zone.

A battle damage event will cause multiple electrical faults of various impedances. With conventional AC

distribution systems, protected by electromechanical circuit breakers, voltage sag from low impedance faults and high frequency disturbances from arcing faults are transmitted throughout the electrical system during the 0.1 – 0.3 seconds required for the circuit breakers to clear the faults. These electrical disturbances will cause sensitive electronics (computers and other combat system components) to trip offline or reset themselves. The ultimate result is a loss of mission capability until the computers can be restarted (which may take upwards of 1 hour).
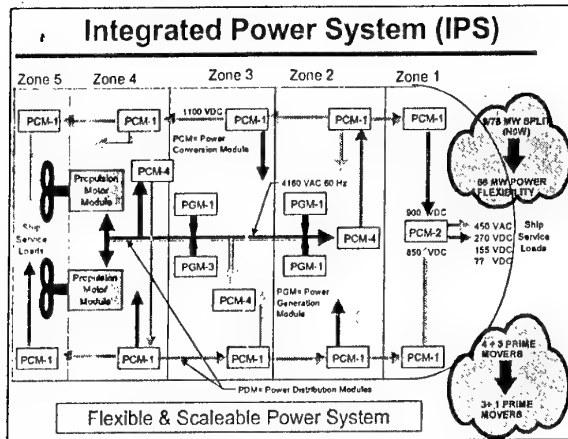
Figure 2: IPS Architecture

The DC-zonal distribution system that has been incorporated into the IPS architecture avoids this problem. Each zone is electrically isolated from all other zones by solid state power conversion equipment (indicated as PCM-1 in Figure 2). A fault within the zone will cause the PCM-1 to shut down, effectively isolating that fault. A fault on the longitudinal bus will cause the PCM-4 feeding that bus to shut down. The ship's control system then determines the fault location, reconfigures the affected bus and re-energises the un-faulted portion of the bus via the PCM-4. All vital loads, such as combat systems equipment, are provided power from both busses. Auctioneering diodes within the PCM-2 inverter modules allow the input to be switched from one bus to the other without any disruption to its output being passed on to the sensitive user load.

An added benefit of distributing DC power is the ability to tailor custom power interfaces for combat systems equipment. There is a steady trend toward more use of DC power within user equipment [1]. To date, these equipments have accepted 60 or 400 Hz AC input power because that was the only power available. With DC distribution, the output of the PCM-2 module shown in Figure 2 can be readily changed to any DC voltage the user equipment needs. This will allow the combat systems developer to eliminate most of his input power

supply. This custom power interface also eliminates the need for large input filters, presently required to meet power quality and EMI requirements. However, the component developers must match impedances to ensure stability of the DC system.

1.2 Generation and Propulsion

The Generation portion of the power system utilises commercially based 60 Hz equipment. Protection on the high voltage bus is via standard electromechanical switchgear. Presently, this is considered to be the lowest cost alternative to providing this function to the all-electric warship. Non-standard high frequency generators (~240 Hz) have been proposed by some researchers. However, as there is no commercial market for such unique equipment, development and production costs make such an approach unaffordable in light of today's declining military budgets.

In the propulsion area, commercial motors and drives are adequate for some military vessels, such as amphibious and auxiliary ships. However, the surface combatant has higher power and more stringent signature requirements. This forces deviations from strictly commercial. The IPS programme has attempted to develop a prototype drive that meets the military requirements while still being commercially based [2].

1.3 System Control

The modular nature of the IPS system extends to system control as well. Presently there are three levels of control: system, zonal and local. System and zonal control software resides on the ship's computing and network infrastructure. Consequently, there are no fast control loops within either of these control tasks. Any fast control loop is pushed down into the local controllers that reside within each hardware module. This philosophy ensures that the power system does not tax the performance of the ship's infrastructure.

System control consists of power source management (generators), load shedding and fault recovery. Zonal control simply manages the number of online sources (PCM-2s) to optimise the power system's efficiency. The module local controllers perform all fault detection, equipment protection and high-speed regulation functions.

Additional functions, such as equipment health monitoring, embedded training, software redundancy, utilisation of secondary information sources are planned. However, these features are not built into the present control software.

2

2.0 Programme Status

The IPS programme has completed extensive computer modelling, ship fit studies and life cycle cost studies. These various studies predict the technologies being tested in the FSAD portion of the programme are technically feasible and will meet U.S. Navy ship requirements in a cost-effective manner.

Presently, the IPS programme is beginning the test portion of its Full Scale Advanced Development phase. The FSAD system represents a partial ship-set of prototype equipment that is sufficient to prove the IPS architecture concepts. A full ship-set of equipment depends on the actual ship type [3]. The equipment will be tested ashore at the Land Based Engineering Site (LBES) in Philadelphia, PA, USA.
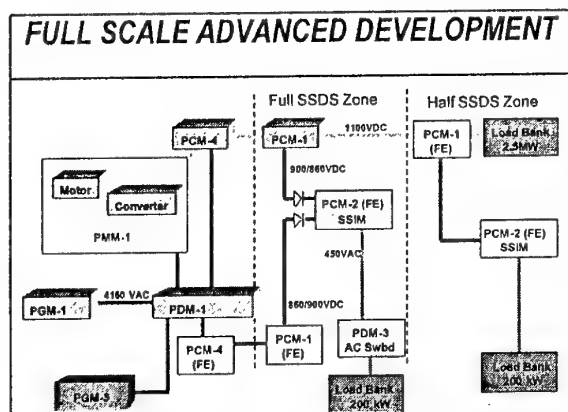
Figure 3: FSAD One-Line Diagram

Figure (3) shows a one-line diagram of the FSAD system. There is one 21MW commercially derived gas turbine generator module, one existing 3MW gas turbine generator, one propulsion motor and drive and 1.5 zones of ship service distribution equipment. In addition, there are various load banks, a waterbrake to load the propulsion motor and a computer network to host the control software.

The prototype propulsion motor module is based on a 15-phase PWM induction motor drive. At 19 MW, this drive is pushing PWM technology to a significantly higher power level than previously attained. The 21 MW generator module utilises an existing General Electric LM-2500 engine with commercially derived generator and module controller that have been procured for this programme. This equipment is described further in [2]. The 3MW generator module is an existing 450 V unit that is connected to the propulsion bus via a 450/4160V transformer.

The ship service system consists of two PCM-4 transformer/rectifiers, three PCM-1 DC/DC converters, two PCM-2 inverters and two 450 VAC switchgear. The FSAD PCM-1 includes two soft-switching Auxiliary Resonant Commutating Pole (ARCP) topology DC/DC converters. Similarly, the PCM-2 modules are ARCP design. Test results demonstrate the very clean (<3% total harmonic distortion) waveform produced from this design. The FSAD PCM-4 module is a 24-pulse transformer rectifier that uses an innovative series parallel input transformer to eliminate the need for inter-phase reactors.

Figure (4) depicts the land-based engineering site in Philadelphia, PA where testing will continue through early 1999.

3.0 Future Developments

The IPS programme aims to make any future ship that may benefit an IPS ship. Toward that end, the programme office is supporting various ship acquisition offices by providing engineering design and cost information allowing the designers of those ships to incorporate the advantages of IPS into their designs. Because of the novel acquisition strategy for the Navy's DD-21 destroyer, the IPS programme office is working closely with industry to ensure their designers become familiar with these novel concepts.

One of the key tenets of the IPS programme is the open system approach to interfaces. Specifying interfaces via commercial and industry standards allows multiple vendors to produce modules that will work together, even when utilising different technologies within those modules. This approach allows for simplified upgrades because the entire system does not have to be re-designed simply to replace ageing electronics within a module.

Table I briefly lists some of the open interfaces within the IPS architecture. Note that the DC interfaces within the ship service distribution system are not yet covered by industry standards. This is a relatively new area and the IPS programme office is working with various organisations to develop appropriate standards.

Interface	Applicable Standards
4160 VAC bus	IEEE 45
450 VAC bus	Mil-Std-1399
Communications	Ethernet / IEEE 802.3
1100 VDC	N/A
900/860 VDC	N/A
270 VDC	ISO/TC 20/SC 1

Table I: IPS Interface Standards
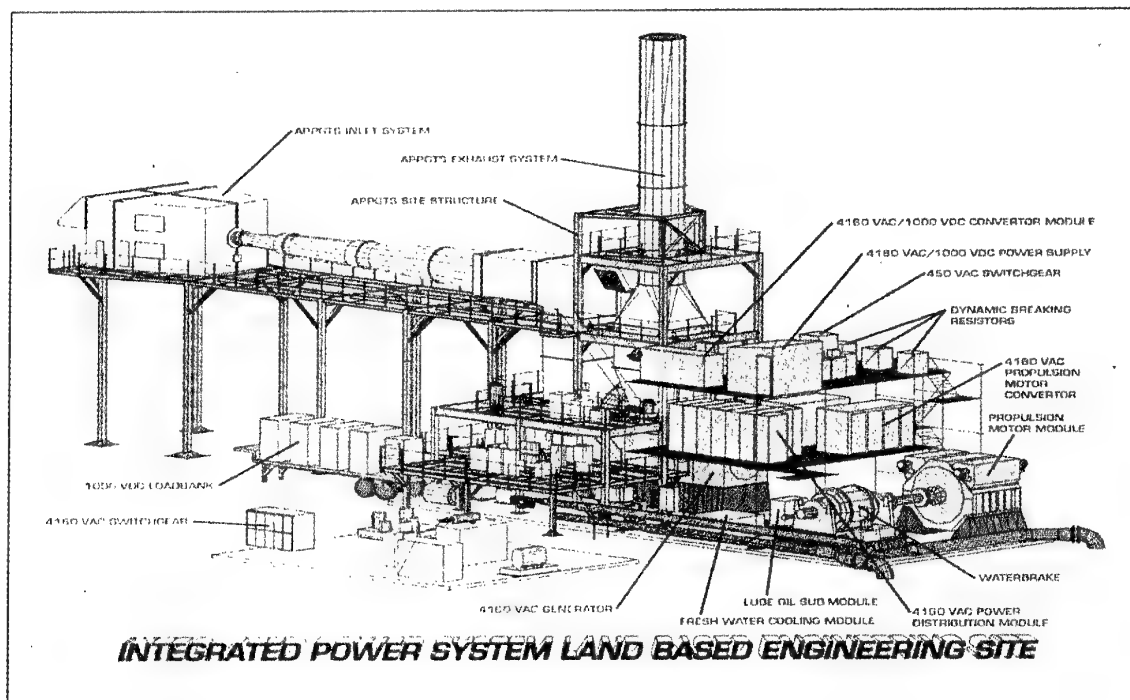
Figure 4: Land-based Engineering Site

There are significant technology advances in the offing that are could improve cost or performance of an Integrated Power System. Some examples are higher rated and faster power devices, large permanent magnet motors, PWM rectifiers, active filters and solid state circuit breakers, just to name a few. The open systems approach will allow these to be incorporated whenever they mature to the appropriate level.

4.0 Conclusions

The U.S. Navy's Integrated Power System programme is demonstrating that modern integrated electric propulsion can be adapted to meet the requirements of military ships in a cost-effective manner. The FSAD portion of the programme is proving the concept, as adapted for US Navy surface ship requirements. However, the technologies presented in this paper are in all likelihood not what will end up on the U.S. Navy's next ship design. Technology advances will surely render the power electronics obsolete as a minimum. One might then doubt the usefulness of the FSAD demonstration. On the contrary, the open systems approach eases the process of technology insertion and allows adaptation of the basic concept to other specific implementations.

5.0 References

[1]   Amy, J., Clayton, D., Kotacka, R., "Shipboard Electric Power Distribution: AC Versus DC Is Not the Issue, Rather, How Much of Each Is the Issue," All Electric Ship '98, London, U.K., September 1998.
[2]   Benatmane, M., McCoy, T., Dalton, T., Cooper, T., "Electric Power Generation and Propulsion Motor Development for U.S. Navy Surface Ships," All Electric Ship '98, London, U.K., September 1998.
[3]   Doerry, N., et. al., "Powering the Future with the Integrated Power System," Naval Engineers Journal, May 1996.
[4]   Benatmane, M., McCoy, T., "Development of a 19 MW PWM Converter for U.S. Navy Surface Ships," International Conference on Electric Machines, Istanbul, Turkey, September 1998.

THE UK ELECTRIC SHIP PROGRAMME

Cdr D.J. Mattick BSc, CEng, FIMarE, MIEE, MINucE, Royal Navy
Mr A.T. Luckett BSc, AMIEE, UK Ministry of Defence

Abstract

The United Kingdom Ministry of Defence (MOD) anticipates adopting Integrated Full Electric Propulsion (IFEP) for future classes of surface warships including the Future Escort (FE), primarily to minimise the total cost of ownership. This paper identifies various issues relevant to small warships that need to be resolved before IFEP can be fully realised. It then broadly outlines the current state of the MOD programme and the key technical achievements to date.

1 Introduction

Significant developments in warship marine propulsion have been characterised by infrequent step changes in technology followed by long periods of evolution and improvement. In the case of surface warships the last such change from steam to gas turbine propulsion was some 30 years ago. Gas turbines will continue to be at the heart of surface ship prime movers, but it is now clear that IFEP with the aid of advanced cycle gas turbines, permanent magnet motors and compact power electronics heralds the prospect of another step change with significant benefits.

The commercial marine sector has found that electric propulsion achieves significant through life cost savings by reducing the running costs, however the propulsion plant initial cost, volume and weight all typically increase. MOD studies have found that by adopting novel technologies and Electric Ship architectures these can all be minimised to enable this technology to be pulled through into naval use.

2 Cost

The Electric Ship concept was developed from IFEP to lower the Unit Purchase Cost (UPC) but still retain IFEP's Running Cost (RC) savings. Merchant Navy applications of IFEP have the advantage of space, thus they can easily accommodate commercially available equipment. A much more important advantage was also noted: the willingness of the Merchant Navy operator to accept increased UPC in order to gain reduced Through Life Cost (TLC).

$$TLC = UPC + RC \ (1)$$

For the Royal Navy, UPC must be minimised together with TLC and in order to achieve this the Naval Electric Ship has two main features in addition to those usually found in a traditional IFEP vessel:

- **Minimum Generator Operation**: The UPC and space constraints require fewer more highly rated prime movers than would be found in a merchant IFEP vessel. In order to restore the fuel savings conceded by fitting fewer prime movers the ES runs under a regime of minimum generator operation, often with only one prime mover operational. This brings improvements in fuel consumption but more significantly in maintenance costs due to the minimised engine running hours.

- **Electrification of Auxiliaries**: Additional maintenance and manpower reductions can also be achieved by using electric auxiliaries wherever possible. Whilst these are also expected to bring significant cost savings these are proving difficult to quantify at this stage. When coupled with the centralised energy storage and high reliability ship wide electric power systems this policy will allow the overall weight of equipment fitted to be reduced.

3 Volume & Weight

Clearly volume and weight are important criteria for any warship in order to maximise its weapon payload. However, for 30 knot escort vessels at some 4,500 tonnes displacement it is not just desirable, but essential that the size and weight of commercial IFEP systems are driven down in order to meet the tight constraints imposed by these relatively small hull forms.

Whilst it is possible to achieve IFEP using a geared synchronous motor, it is not desirable to do so for signature reasons. This decided the UK MOD to fund development of a novel Permanent Magnet Propulsion Motor (PMPM) which current predictions indicate will be approximately a quarter of the volume and mass of a corresponding conventional machine.

Similarly, MOD is also required to invest in the development of the next generation of advanced cycle gas turbines to provide power dense prime movers with near diesel fuel efficiencies.

However, one of the main areas where industry is forging ahead without any significant government funding is in the field of power electronics, where the ongoing power electronics revolution is continuing to drive down the cost, size and weight of devices.

4 The electric ship programme

First and most importantly UK MOD Electric Ship Programme continues in existence. Although as might be expected funding difficulties are occupying much of the available manpower, the Programme remains viable and the possibility of Electric Warships forming the core of the Royal Navy in the next Century is still probable. Industry and Foreign Governments continue to support the Programme with secondees into the MOD led team.

Studies are currently underway to establish the precise configuration of the IFEP power system, but for the meantime the configuration shown in Figure 1 below represents the baseline power system architecture for a 30 knot monohull of some 4,500 tonnes displacement.
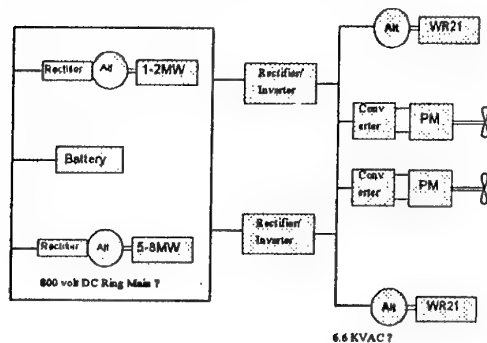
Figure 1 - Electric Ship Frigate Power System

An important feature of the design is that of single generator operation, which is made possible by the incorporation of an energy storage device, depicted as a battery.

The battery backed DC ring main provides electrical power for conversion locally to any particular supply required by a consumer. It is interconnected to a medium voltage AC propulsion busbar by reversible inverter rectifiers which allows any one of the four prime movers to supply both propulsion and ship service loads.

The medium voltage AC bus bar is supplied by two advanced cycle gas turbines, the WR21s, and this engine is currently undergoing development testing at DERA Pyestock. A single 5-8MW Cruise engine supplies the DC ring main along with a single small 1-2MW engine capable of efficiently supporting the harbour load.

The key developments within this power system are the advanced cycle gas turbines, the widespread use of power electronics and most importantly the development of an efficient and power dense permanent magnet propulsion motor.

Advanced Cycle Gas Turbines

The programme envisages the use of a family of three advanced cycle gas turbine alternators:

- 25MW GTA - development of the WR21 gas turbine is well underway in collaboration with the USA and France.

- 5-8MW GTA - Initial studies have shown this engine to be currently unaffordable and development has therefore been postponed pending other nations and sectors of industry expressing their interest in a collaborative development.

- 1-2MW GTA - The UK have recently completed joint feasibility studies with The Netherlands and a collaborative development is currently being considered involving France, The Netherlands and the UK.

The Intercooled and Recuperated (ICR) WR21 is designed to achieve 30% propulsion fuel savings across a typical surface warship operating profile when compared to the current USN engine. These fuel savings are achieved by adding hardware to a simple cycle engine. Hardware additions inside the enclosure, when compared to an existing engine include the on-engine intercooler system, Variable Area Nozzle (VAN), and recuperator system (see Figure 2 below).
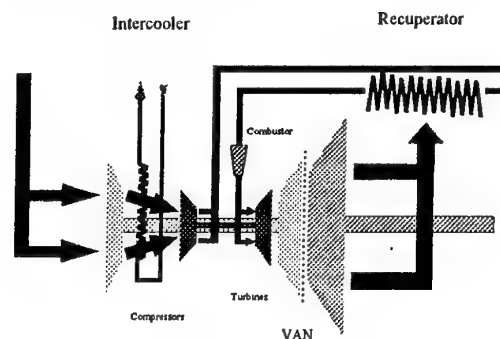
Figure 2 - ICR Gas Turbine Schematic

It is a common perception that adding hardware decreases accessibility, increases maintenance and support costs, and generally makes maintenance more difficult. This can be true if the hardware is added independently without a stringent design process in place to ensure that maintainability requirements receive the attention they require. This served to define some of the WR21 design challenges.

The WR21 design team has met these challenges by selecting mature, modular components with high reliability, designing an accessible enclosure, and by diligently following a development plan that pays special attention to maintainability and accessibility throughout the design and test phases of the program. A major success of the design effort has been the achievement of a maintainable and flexible system while incorporating the fuel savings and hardware into the existing footprint.

6

The compression process is split approximately 30:70 between the low and the high pressure compressors with intercooling in between. Air leaving the low pressure stage is cooled by rejecting heat, via an on-engine heat exchanger, into a closed freshwater/glycol intermediate loop which itself is cooled in a freshwater/seawater heat exchanger .

Air leaving the high pressure compressor is preheated in an exhaust heat recuperator prior to combustion, thereby reducing the amount of fuel required to reach the desired turbine inlet temperature. After passing through the gas generator turbines, which drive the compressors, gas enters the free power turbine via a first stage VAN.

The recuperator, intercooler and VAN are the three key features providing the improvements to the specific fuel consumption (SFC) that the WR21 offers when compared with an equivalent simple cycle gas turbine. The recuperator uses exhaust gas energy to increase the combustion inlet temperature, thereby reducing the fuel needed to achieve the required cycle temperatures. This provides a basic improvement in SFC and achieves a fuel efficiency close to that of a diesel engine (see Figure 3 below).
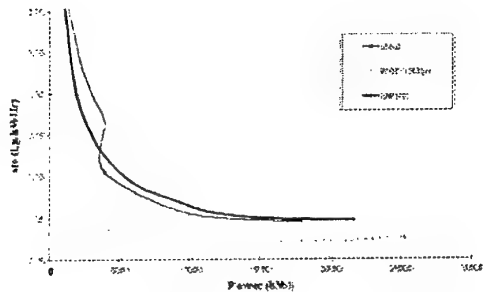
Figure 3 - Gas Turbine Specific Fuel Consumption

Intake air, after compression in the low pressure compressor , is cooled through an on-engine intercooler which reduces the work required to further compress the air and thus improves the high pressure compressor spool efficiency and raises the net output power. Another advantage is that intercooling reduces the compressor discharge temperature thereby increasing the effectiveness of the recuperator because of an increased air to gas temperature differential.

The VAN closes progressively with diminishing power to reduce the power turbine mass flow rate. Thus at part-load high cycle temperatures are maintained. This increases the recuperator air to gas temperature differential and the associated recuperator heat transfer which results in an improved part load SFC.

Maintenance evaluations at the test site are a significant part of the test program and every in-place maintenance procedure intended to be accomplished inside of the enclosure at DERA Pyestock has been demonstrated.

Other significant maintenance improvements are planned for future applications and users. The WR21 maintenance program will continue to evolve and when production begins a flexible and fuel efficient system will be delivered to a variety of users.

However, it is in the area of emissions where the gas turbines excel when compared to a diesel engine. The emission profile depicted by Figure 4 below, compares the performance of a gas turbine with a typical suite of medium speed diesels. It can clearly be seen from this graph that gas turbines outperform diesel counterparts and are capable of meeting emerging MARPOL emissions legislation. Furthermore, with additional design enhancements it is possible to significantly improve upon this profile by modification of the burners if necessary to meet more stringent legislation in the future.
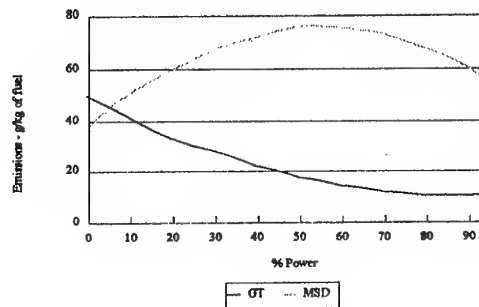
Figure 4 - Comparison of NOx Emissions

It is interesting to note that Royal Caribbean cruise liners have recently selected a hybrid gas turbine prime mover fit for their Millennium and Voyager Class cruise liners, citing an 80% reduction in NOx and a 90% reduction in SOx emissions as one of the reasons.

Power Electronics

MOD is investing very little in this area at present due to the overwhelming power electronics revolution that is sweeping through the industry, both at a device and at a converter level.

On the device level our baseline assumption is that Electric Ship installations can utilise Insulated Gate Bipolar Transistors (IGBT's) as they are readily available at the power ratings required. However, the technology is moving so fast it is likely that alternative devices will become available by the time that production contracts are placed. MOD is therefore maintaining a watching brief on the following device developments:

- MOSFET Controlled Thyristor (MCT)
- Fast Turn Off Device (FTO)
- Integrated Gate Commutating Thyristor (IGCT)
- MOS Turn Off Thyristor (MTO)
- Emitter Turn Off Thyristor (ETO)

7

Similarly, the baseline assumption for the converter topology is that a Pulse Width Modulated (PWM) converter will be used, but it is not inconceivable that one of the following topologies will come to the fore:

- Resonant Converters
- Matrix Converters
- Sequential Capacitive Discharge Converters

What is perhaps more important at this stage is the development of a strategy for the systematic and efficient use of power electronics within the power system architecture.

Permanent Magnet Propulsion Motor (PMPM)

The MOD has chosen Transverse Flux as the topology to be used for further development in the technology demonstration programme for its PMPM. The work will result in a representative machine and converter being constructed, and is being led by Rolls Royce Marine Power with the Machine being constructed by Peebles in Edinburgh, and with converter development under sub-contract to CEGELEC Projects Ltd who also have responsibility for system integration.

A key feature of the motor and converter is the separation of the windings and inverter power circuits for each phase. Consequently, the converter comprises eight single-phase fully-controlled inverter bridges. This greatly improves the fault tolerance and possibilities for reversionary modes. The preferred converter type for this application is a Pulse Width Modulated (PWM) voltage source inverter. The high fundamental frequency (195 'HZ at full speed) together with a need for close control of the current waveform and a compact overall arrangement mean that the preferred semi-conductor power devices are IGBT's. The DC link voltage and peak phase current suggests that there is a need for devices in series and parallel. As designed, the converter is directly water-cooled, with the power devices for each phase mounted onto a common water-cooled aluminium heat sink using appropriate insulating wafers. The need for Electro-Magnetic Compatibility and to minimise earth leakage currents is achieved principally by earthing the semi-conductor heat sinks at the mid-point of the DC link and ensuring that the devices are arranged for optimum dv/dt cancellation. The effective rating for each single phase bridge is given by the product of DC link voltage and peak phase current.

The full-scale PMPM, to be rated for 20MW at 180RPM, is expected to comprise of four discs each with four rims (see Figure 5 below). The predicted efficiency of the motor at full load is comfortably in excess of 98% and detailed calculations have shown that it remains close to 98% at least down to 30% speed.
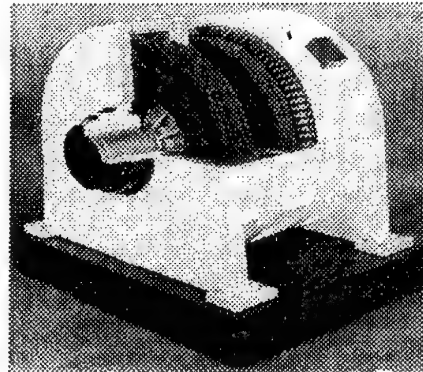
Figure 5 - PMPM Scale Model

Each pair of rotor rims forms just one phase of the TFM; this does not in itself produce a smooth continuous torque. A steady torque output requires at least two phases, with the phases appropriately displaced to minimise torque ripple. In the absence of saturation and with the motor fed from a sinusoidal supply, the torque produced by each phase closely approaches a sine-squared function; hence two phases separated by 90° electrical are sufficient to produce a smooth torque. In reality, the presence of saturation and the likelihood of non-sinusoidal excitation means that a higher phase number is desirable. The shaft torque is the resultant of all the phases acting together and is relatively free of ripple; however within the motor, the phases are separated so each of the rotor rims experiences 100% torque ripple. This has important implications for the design:

- Firstly the magnets and pole pieces have to be designed to withstand the cyclic stresses so produced.
- Secondly, the entire rotor and stator system has to be designed with recognition of the torsional dynamics of the system.

Clearly the larger diameter outer rims are able to produce higher torque than the inner rims. At low power the torque ripple is cancelled entirely within each disc by driving the inner phases harder than the outer ones. Applying this technique throughout the power range of the machine would reduce its overall potential since the outer phase would have to be driven at below its maximum capacity in order to balance the lower inner phase torque. In order to maximise the power of the machine the residual torque variation at high power (resulting from the inability of the inner phase to fully match the outer) will be balanced across discs, this in turn imposes additional design constraints on the machine. Figures 6 & 7 show the PMPM Construction and Phase Geometry respectively.

8
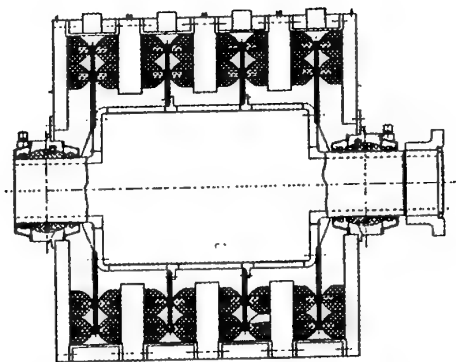
Figure 6 - PMPM Transverse Flux Topology
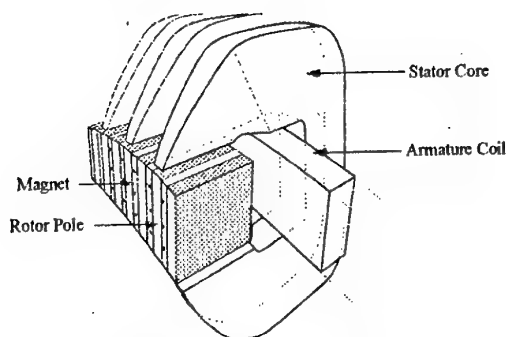
Figure 7 - PMPM Magnetic Circuit

Podded and Contra-rotating Propulsors

One of the major changes in marine electric propulsion systems over recent years has been the introduction of azimuthing podded propulsors. MOD UK studies to date have identified that up to 15% fuel savings can be achieved by a tractor pod (due to the improved hydrodynamic flow around the propeller) and that manoeuvrability is much improved. Whilst no development is included in the UK Electric Ship Programme such evident cost savings are not being ignored and study work is ongoing. There are a number of issues unique to warships to be investigated. For example:

- does the thrust transfer path significantly affect the design and construction of a small warship?

- can the cantilevered pod survive military underwater shock environments?

- does placing the motor outside the hull cause any signature problems?

- can the lateral forces caused by high speed turns be supported?

- do the availability, reliability and maintainability parameters being achieved by commercial installations meet military requirements?

A further 10% to 15% fuel savings are predicted for contra-rotating propeller installations. Despite the bearing and seal arrangements on the propeller shafts (which have traditionally proven difficult to engineer, install and maintain) there are a limited number of commercial ships with contra-rotating propulsion systems at significant powers. Whilst UK MOD continues to monitor these commercial installations, there is no plan to undertake any development at this time.

Programme Overview

The above developments are drawn together, along with many others not described in this paper, into a comprehensive programme that culminates in generic shore and sea demonstration in order to inform the future vessel equipment selection milestones. The Programme overview at Figure 8 shows development of pre-production units and the subsequent integration of some developments into a shore demonstrator prior to the Future Escort equipment selection milestone and also early enough to influence the Future Carrier (CV(F)). The assumption is that sea demonstration will be required (subject to review at various programme points) and that the UK Trimaran Demonstrator is likely to be the only available platform for this purpose, using phase two trials jointly with other nations.
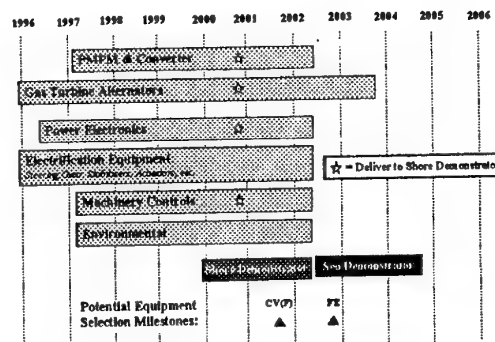
Figure 8 - Electric Ship Programme Overview

Demonstration is required in order to confirm that the newly developed equipment can be integrated together; that automated Damage Control facilities are satisfactory; that a control system can manage the installation and thus enable very low manning; that the system can accommodate power surges and motions in a seaway; and that equipment availability, reliability and maintainability targets are achieved in a marine environment. Of these, a sea demonstrator is currently considered essential only for the latter three.

Whilst it is expected that CV(F) will be the first platform to adopt the Electric Ship architectures described above, the hull form is large enough to accommodate a commercial electric propulsion fit as a fallback. However, this commercial option is not suitable for the much smaller FE, and it is therefore essential that developments are available by their respective equipment selection dates.

Whilst sea trial results will not be available until later than this, it is expected that the shore demonstrator will have proven the major design principles, and concurrent engineering will make it possible to accommodate modifications that may result from sea trials.

All these developments do not come cheaply and the UK programme has been costed at £150M, of which there is currently a significant funding shortfall. However, the savings associated with adopting IFEP and the corresponding electrification of auxiliaries is estimated to be in the region of £1.8 billion! It is therefore not surprising that the MOD is fully committed to identifying alternative ways of funding this shortfall, including development of partnership and collaborative opportunities wherever feasible.

5 Conclusion

The UK MOD Electric Ship Programme continues and the key development of the PMPM is now in hand as are the initial studies necessary to define the IFEP architecture more fully. Once again advances in both power electronic device and converter design offers much greater efficiency than hitherto believed possible. The application of IGBT PWM converters to the ES concept is now a practically proven option. However, the use of alternative rapidly developing power electronic devices must not be discounted, nor should the possibility of employing resonant soft switching in the converter itself.

The Electric Ship Concept has continued to show significant potential advantages for future warships, both in total cost of ownership and in system flexibility and operational capability. The Electric Ship Programme is now at a critical stage where decisions to be taken in the near future will have great significance for the Royal Navy's future operational capability. The engineering challenges are undoubtedly real and significant, but none are without evident methods of resolution; the opportunity to take advantage of all the benefits that technology offers remains within the Royal Navy's grasp, but only just.

The authors remain absolutely convinced that the Electric Ship is the self-evident choice for future warship design, they look forward with enthusiasm to the next years which promises much in engineering development challenge. They firmly believe that the original vision of the Electric Warship [1, 2, 3] now has substance in engineering fact.

References

[1] Cdr C.G. Hodge RN and Cdr D.J. Mattick RN, "The Electric Warship" IMarE Evening Paper, Tuesday 19 December 1995, IMarE Transactions Volume 108, 1996, Part 2.

[2] Cdr C.G. Hodge RN and Cdr D.J. Mattick RN, "The Electric Warship II" IMarE Evening Paper, Tuesday 10 December 1996, IMarE Transactions Volume 109, 1997, Part 2.

[3] Cdr C.G. Hodge RN and Cdr D.J. Mattick RN, "The Electric Warship III" IMarE Evening Paper, Tuesday 16 December 1997, IMarE Transactions Volume 110, 1997, Part 2.

STUDY AND RESEARCH OF ELECTROMAGNETIC SHIP PROPULSION IN ROMANIA

Ph.D. Nicolae. Badea   Ph.D. Dumitru. Calueanu   Ph.D.Razvan. Magureanu
Faculty of Naval and Electrical Engineering of the "Lower Danube" University of Galati
Domneasca Street No 47 Phone/Fax:+ 4036.460182

Abstract

The paper deals which the interaction between the electromagnetic and hydrodynamic field in the electromagnetic propeller of a ship. The set of equations associated with the dimensionless MHD field of anelectric type is solved by applying the finite element method on the dimensionless propeller channel The mathematical models of the interaction define the constant ruler of MHD interaction and their influence about energetically characteristics. The essential objectives of this paper are as follows:

1-the present method determination of flow and electric field distribution in the presence of intense magnetic fields;

2-the present experimental and theoretical aspects in electromagnetic ship propulsion by correlation length propeller with length interaction; ($\rho\, v_o /\sigma B^2$.)

1.Introduction

The idea of using electromagnetic ship propulsion for propelling seawater vehicles is not brand new idea. It has been examined in the past by investigators (Phillips 1962, Doragh 1963, Way 1968, Saji 1978, Hummert 1979, Swallow 1991, Doss 1993). All of these studies lead to one conclusion, that is, that a superconducting magnet with a high magnetic field must be used if one expects to achieve practical electromagnetic propulsion efficiency. In this time the Ship and Ocean Foundation in Japan launched a research and development program to develop techniques for electromagnetic ship propulsion, and to construct on experimental ship to demonstrate this concept with all the necessary machinery and equipment on board. The ship "YAMATO I" was completed in 1991 and is ready in sea trials during 1992. The model Yamato has a displacement of 185 tons; designs speed 8 knots and are propelled by two thrusters with cryogenic magnets of 4 Tesla. Because of the low magnetic field and small size of the thrusters, the predicted propulsion efficiency is very small (3%). The research domain of ship electromagnetic propulsion has proved to be of interest for researchers in Romania. Experimental achievements after the 1990 in electromagnetic propulsion have caused an increased interest in other countries as well, such as Yugoslavia, Romania etc. As for our countries by the contract the Ministry of Research and Technology finances this type of fundamental research within the Faculty of Naval and Electrical Engineering of the "Lower Danube" University of Galati. The present staff has come up with a systematic theory of the electromagnetic field-hydrodynamic field interaction in the propelling channel, starting from the deviation of the load carriers in an electromagnetic field and from generalizing the results of research published in articles of the magazines specializing in this type of propulsion.

On the basis of this theory the energy balance equations that have been obtained evince the possibility of getting superior efficiency by correlating the geometric dimensions of the propellers to the applied field input .

2. The mathematical model of MHD field in ship propulsion

Ship electromagnetic propulsion consists of the interaction between a magnetic field generated on shipboard and an injection (half-induced) electrical current in the sea water, as a result of this interaction the ship is moving The paper advances the vector field approach to the MHD field in an electromagnetically driven ship. The MHD interaction equations exposed locally for an infinitesimal sea water element are obtained from a combination of the electromagnetic and hydrodynamic field equations. The MHD field equations system is much simplified by neglecting the terms that do not play a significant role in the two-field interaction. Thus, the set of equations associated MHD ship is show in figure 1
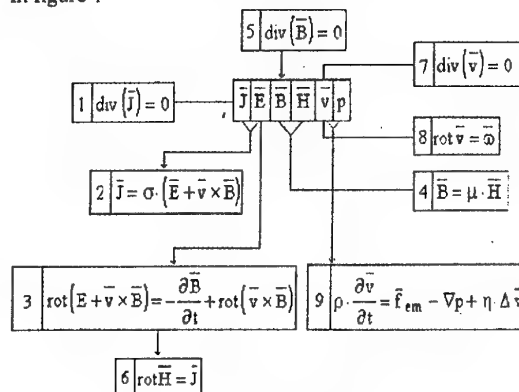
Figure 1 MHD equations

The complex phenomena that take place inside the propellers channel require to include some mechanical parameters($\rho\ V$)and electromagnetic parameters($\mu\sigma$) the condition in which said phenomena take place call for such parameters as water velocity , applied induction the channel size .For this reason the mhd field equations have been dimensionless Under the adimensional approach , the propeller channel dimensions are considered with respect to the characteristic distance -d- which is the channel outlet along the axis of the magnetic field applied. $r^* = r\,/\,d, \nabla^* = d\cdot\nabla, B^* = B\,/\,B_o$ The

sea water motion inside the channel induced on electrical field and assumption v_o speed of the enter zone channel . the speed dimensionless in the channel is $v_o^* = v / v_o$ and dimensionless electric field $E^* = E / v_o B$ where E -applied electrical field . With these assumptions the dimensionless governing equations are(for conduction propeller):
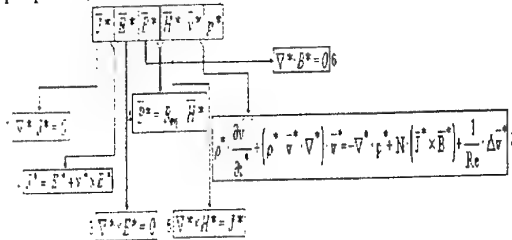
Figure 2 Adimensional MHD equations

where:

$$J = J / \sigma v_o \cdot B_o = E + v \times B, \nabla \times B = \Re_m \cdot J, f = J \times B$$

$N = d / \lambda$ -interaction   parameter

$\lambda = \rho \cdot v_o / \sigma \cdot B^2$ -length characteristic of interaction

2.1 The numerical simulation of the MHD system equations

The mathematical model of MHD ship propulsion was applied to a propeller channel placed under the hull. The duct of MHD propeller has a pair of electrically insulating walls which are perpendicular to the transverse magnetic field and a pair of highly conducting walls which are parallel to the field, as sketched in figure 3

Insulating Top
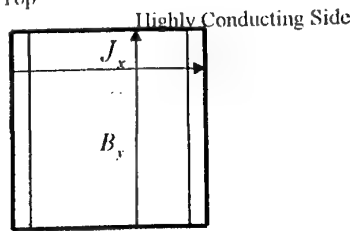
Fig.3 Cross section of duct

We assume: $V(0,0, v_z(x,y))$

$$J(J_x, J_y, 0),$$

$$\frac{\partial \cdot p}{\partial \cdot z} = J_x \times B_y \text{ in center cross}$$

- -steady state flow

The differential equations of the adimensional MHD field an finite element approximated is solved by the weighted residue methods. Galerkin procedure using software PDEase In essence the method of weighted residuals suppose are given a differential operator L and a function f(x) on a region duct satisfying L(f(x))=0. Then   for   "any"   function W(x). $\int_{Duct} W(x) \cdot L(f(x))dx = 0$ If we are given any

function g(x), then $\int W(x) \cdot L(g(x))dx = R$, is a measure of the residual error involved if g(x) is used as on approximate solution of L(f(x))=0 .Note that the shape of the weight function determines the weighting of the error at each point x in the region duct A special case of the method of weighted residuals is to use the same function as basis function and weigh function {W(x)=N- where N is interpolation function of finite element model). This case is called the Galerkin method. Finite element modeling has been the preferred method for converting the spatial components of complex sets of continuous partial differential equations (with well defined boundary values) to a set of discrete nodal equations for numerical solving. In this method the spatial area of duct is gridded into small patches called finite elements over which the variables are represented by simple polynomials. The second order adimensional equations are obtained from a combination a first order equations and result

$$\frac{\partial^2 v_z^*}{\partial \cdot x^{*2}} + \frac{\partial^2 \cdot v_z^*}{\partial \cdot y^{*2}} + H_a^2 (J_x^* B_y^*) = -p^*$$

(1)

$$\frac{\partial^2 \cdot \varphi^*}{\partial \cdot x^{*2}} + \frac{\partial^2 \cdot \varphi^*}{\partial \cdot y^{*2}} + B_y^* \frac{\partial \cdot v_z}{\partial \cdot y^*} = 0$$

with   boundary   condition

$$y^* = \pm 1 \cdot v_z^* = 0, \frac{\partial \cdot \varphi^*}{\partial \cdot x^*} = 0, x^* = \pm n, v_z^* = 0, \varphi^* = \pm m \cdot n$$

where: $H_a = B \cdot d \cdot \frac{\sqrt{\sigma}}{\sqrt{\eta}}$ Hartmann number ;

$$p^* = \frac{d^2}{\eta \cdot v_o}\left(\frac{\partial \cdot p}{\partial \cdot z}\right) \text{ pressure parameter}$$

$$\varphi^* = \frac{\varphi}{B \cdot v_o \cdot d} = \frac{\varphi / l}{B \cdot v_o \cdot d} \frac{l}{} = m \cdot n \quad \text{electric}$$

potential applied

In conclusion the MHD field distribution in ship propulsion can be determinate resolving the adimensional MHD equation at the adimensional channel. The solution of the two-dimensional MHD problem is obtained by PDEase software. The solution is obtained on a grid in the (x, y) coordinate space (fig. 4) for m=4, n =2 .The flow   profile   for   propeller   duct   is

a Stage=1 Grid#5 Nodes=664 Cells=303 PDE Err=0.0108 Mem=510k

Vol=-1.853057
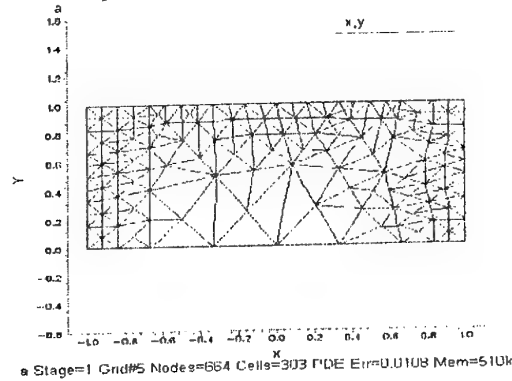
a Stage=1 Grid#5 Nodes=664 Cells=303 PDE Err=0.0108 Mem=510k
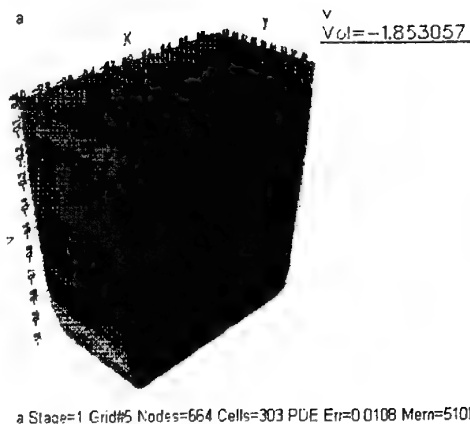
Fig. 4 Surface flow for $H_a = 26$

show in figure 4 for the Hartmann. In the core flow region .velocity is uniform but in vicinity walls decrease. The limit layer thickness at the conducting(fig.5) and insulating(fig.6) walls isn't identical Thus solving for two Hartmann number the limit layer thickness at the conducting walls is $\dfrac{\delta_{i1}}{\delta_{i2}} = \dfrac{\sqrt{H_{a2}}}{\sqrt{H_{a1}}}$, and the insulating walls is

$$\frac{\delta_{i1}}{\delta_{i2}} = \frac{H_{a2}}{H_{a1}}$$

a Stage=1 Grid#5 Nodes=664 Cells=303 PDE Err=0.0100 Mem=510k
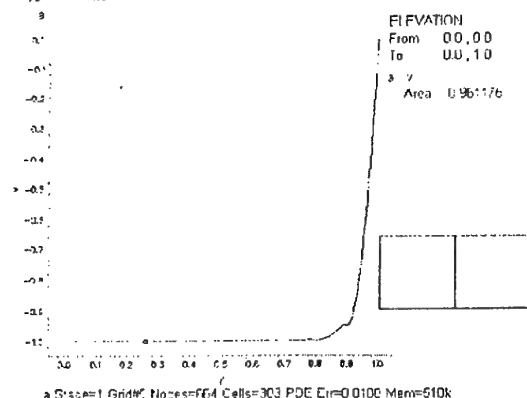
Fig.5 Elevation velocity at the insulating walls

a Stage=1 Grid#5 Nodes=664 Cells=303 PDE Err=0.0118 Mem=510k
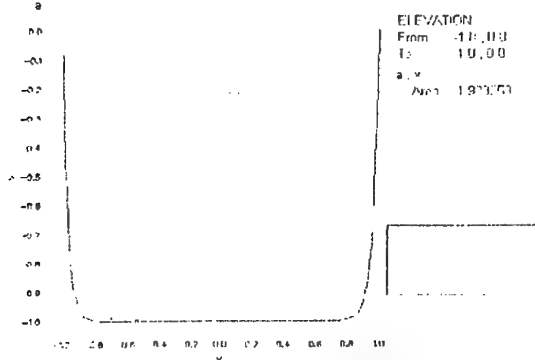
Fig.6 Elevation velocity at the conducting walls

3. The mathematical model of the MHD interaction and the energetic changes inside the propeller

The starting point of a MHD analysis is the particle deviation with in an electromagnetic field. As is well known, the sea water under the action of the electromagnetic field, dissociates into positive and negative ions of concentration n_+ and n_-.

The mathematical model of the MHD interaction assume:
- the sea water inside the MHD propulsion can be regarded as the results of two superimposed ion fluids:
- number of particles from each fluid per volume unit to keep concord to the following:

$$\frac{\partial n}{\partial t} + \nabla(n \cdot \bar{v}) = 0 \quad (2)$$

Decomposing the fluid velocities $\bar{V}_\perp$ and $\bar{V}_\parallel$ concord to two direction shown in fig.1, where v_D is perpendicular to the electric and magnetic field and $\bar{V}_\parallel$ is parallel to the electric field, we obtain by multiplying equation (2) by charges q_+ and q_- respectively and making to sum, the electric charge conservation low:

$$\frac{\partial \rho^*}{\partial t} + \nabla(\bar{J} + \rho^* \cdot \bar{v}_D) = 0 \quad (3)$$

where: $\bar{J} = n_+ q_+ \bar{V}_{H+} + n_- q_- \bar{V}_{H-}$ (4) stands for the current density associated which the motion to the electric field direction; $\rho^* = n_+ q_+ + n_- q_-$ (5) charge density.

In this case the volume electromagnetic force is:

$$\bar{f} = \bar{f}_i + \bar{f}_- = \rho^* \cdot \bar{E} + \rho^* \cdot \bar{v}_D \times \bar{B} + \bar{J} \times \bar{B} \quad (6)$$

where: $\rho^* \cdot \bar{E}$ - volume electric force due to the electric field applied; $\rho^* \cdot \bar{v}_D \times \bar{B}$ - force due to the reaction field; $\bar{J} \times \bar{B}$ - Lorentz force.

Decomposing ideal fluid motion equation assuming that the single infinitesimal sea water element with in propeller:

$$\rho \cdot \frac{d\bar{v}_{II}}{dt} = \rho^* \cdot (\bar{E} + \bar{v}_D \times \bar{B}) \quad (7) \text{ at } \bar{E} - \text{axis}$$

$$\rho \cdot \frac{d\bar{v}_D}{dt} = \bar{J} \times \bar{B} \quad (8) \text{ at flow axis}$$

Integrating the flow equation which $v_D = v_0 + v$:

$$\int_0^v \frac{dv}{u_0 - v_0 - v} = \int_0^x \frac{\sigma \cdot B^2 \, dx}{\rho \cdot v_0} \quad (9)$$

the solution is: $v = (u_0 - v_0) \cdot (1 - e^{x/\lambda})$ (10)

where. V_0 - velocity in the enter propeller; v - increase velocity in the channel which v_0. Assuming that the infinitesimal sea water element $d\Omega$ penetrate in the propeller zone with v_0 velocity as a result

dissociates the center velocities positive and negative ions at the x distance should be (fig.7)

Fig.7 Infinitesimal sea water element

Decomposing velocity center: $\overline{V}_+ = \overline{u}_0 + \overline{u}_+$

respectively $\overline{V}_- = \overline{u}_0 + \overline{u}_-$

(where: $\overline{u}_0 = \dfrac{\overline{E} \times \overline{B}}{B^2}$ seeming speed) in the enter

propeller zone $\overline{V}_+ = \overline{V}_- = \overline{u}_0$.

Covering x distance under electromagnetic field action, the electromagnetic force density what action ions is revolved angular $\beta = 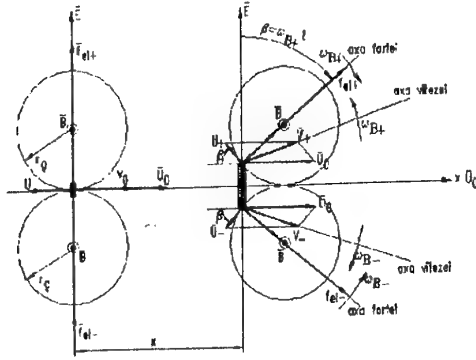\omega \cdot t$ and velocities which minus β. Associating electrical current density $\overline{J}_u = \sigma \cdot (\overline{u} \times \overline{B})$ at the direction resultant electrical field, covering x distance then electrical current density associated which the motion to the electric field applied is reduced:

$$J = \sigma \cdot (E - v_D \cdot B) = \sigma \cdot B \cdot (u_0 - v_0) \cdot e^{-x/\lambda} \quad (11)$$

and electromagnetic pressure:

$$p_{em} = \int_0^x J \cdot B \, dx = \rho \cdot v_0 \cdot (u_0 - v_0) \cdot (1 - e^{-x/\lambda}) \quad (12)$$

From short propeller channel $e^{-x/\lambda} \cong 1 - (x/\lambda)$ and the electric current density[4] and electromagnetic pressure[5] $: J = \sigma \cdot B \cdot (u_0 - v_0)$ (13) and

$$p_{em} = J \cdot B \cdot x \quad (14)$$

Because the electromagnetic propulsion is carried out in an orthogonal electric and magnetic field the difference of pressure at the ends of the propeller must be done by the electromagnetic pressure as a result of the magnetic field - electric current interaction throughout the length of the propeller channel. The electromagnetic power necessary to the propulsion of a fluid of $d\Omega$ can be determined by the relation [1]:

$$W_E = \int_{\mathscr{D}} \overline{E} \cdot \overline{J} \, d\Omega = \int_{\mathscr{D}} \left(\overline{J} \times \overline{B} \right) \cdot \overline{u}_0 \, d\Omega \quad (15)$$

The electromagnetic power necessary to the propulsion can determined by the relation [2]

$$\overline{f}_m \cdot \overline{u}_0 - p_j - p_\Delta = p_{mec} \quad (16) \text{ where}$$

$$J = \sigma \cdot (E - v_D \cdot B) = \sigma \cdot B \cdot (u_0 - v_0) \cdot e^{-x/\lambda} (17)$$

The integration of the specific power equation on the propeller channel volume leads to the following power distribution.
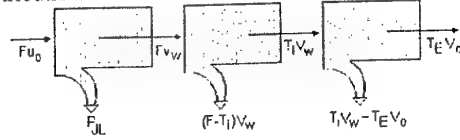
Fig.8 Power distribution

In the power distribution, from above, it was use the "s" sliding, defined between the electromagnetic field seeming speed and the water average speed from the propeller channel:

$$s = \frac{\overline{u}_0 - \overline{v}_W}{\overline{u}_0} \quad (18)$$

Under the action of the electromagnetic field the sea water from the channel leaves like a jet. Electromagnetic propeller efficiency represents the ratio between the propeller power and the input power

$$\eta_n = \frac{T_E \cdot v_0}{F \cdot u_0} = \frac{T'_E \cdot v_0}{T_i \cdot v_w} \cdot \frac{T_i \cdot v_w}{F \cdot v_w} \cdot \frac{F \cdot v_w}{F \cdot u_0} \quad (19)$$

$$= \eta_j \cdot \eta_p = \eta_j \cdot \eta_C \cdot \eta_E$$

3.1 The numerical simulation and the experimental determination of the energy transformations

The mathematical energy transformation model was applied to a propeller channel placed under the hull. The channel is characterized by the geometric dimensions L_C length, Δr radial opening and $\pi/6$ angular opening for one channel [2].

As in the energetic transformations there also intervene geometrical dimensions of the propeller (through the interaction volume) they where adimensioned like this[5]:
- the propeller length trough the ship length;
- the picking-up and spout area through the propeller channel area;
- the radial opening through the ray of the ship.

The studied variable was the dependence of the magnetic induction efficiency applied to the values given for other dimensions (v_0, A_C, L_C, Δr). In the numerical simulation for simplicity, assume that the overall drag on the vehicle is given by[4] :

$$\text{drag} = 1/2 C_D A_s \rho \cdot v_0^2, \quad (20)$$

where C_D is some effective coefficient of drag , A_s is some effective wetted surface area ,and v_0 is the velocity of the ship .For such a simple drag model the equality of

thrust versus drag defines a relation between the inlet and exit areas of the thruster. This can be seen from

$$\rho \cdot A_o v_o^2 \left(\frac{A_o}{A_j} - 1 \right) = 1/2 C_D A_s \rho \cdot v_o^2 \qquad (21)$$

Thus .for different A_j values corresponding A_o values can be determined so that the thrust is generated for any vehicle velocity. As a specific case[5] , assume the vehicle to be a generic attack -class submarine which is 110 m long ,12 m in diameter, 15 m/s speed(30 knots). A parametric study for magnetic field(fig.9)
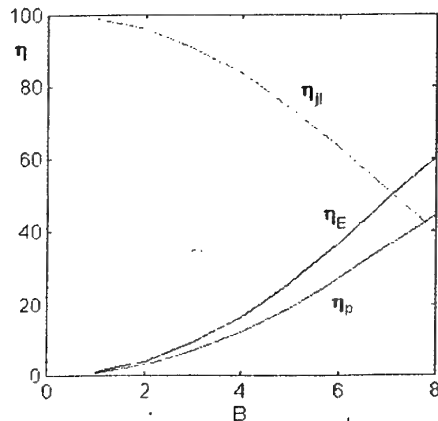
Fig .9 . Efficiency function induction

As a result the power level necessary to the propulsion is reduced while their distribution is to be found in figure 10
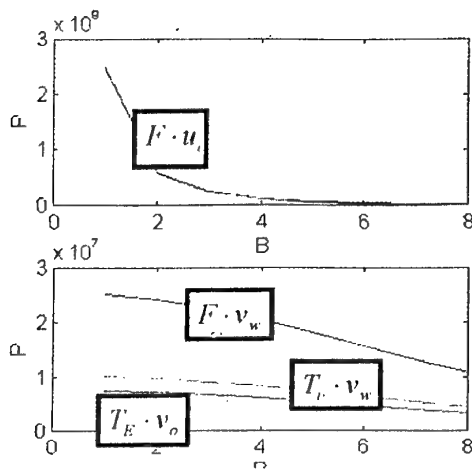
Fig. 10. Simulation power distribution

A parametric study has been perform over length thrut variable for B=6 Tesla , v_0=15 m/s , length ship 110m

and efficiency is show in
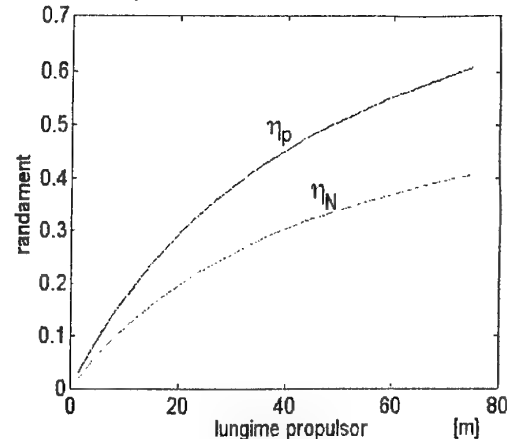
Figure 11 . Efficiency function length

Two electromagnetic driven ship models have been designed to check the principle of the electromagnetic ship propulsion and the energy transformations.
The experimental ship models corresponding to these two types of propulsion have been tested in the trial tank.(Ls=0.55m Lc=(25%)Ls. From the experimental results the energy transformations (12) have been determined.
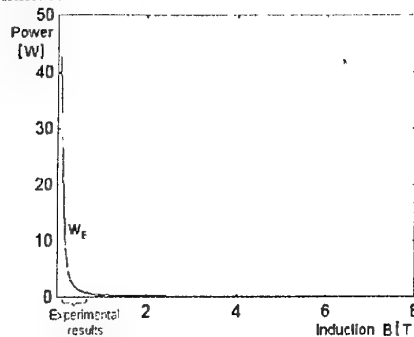
Fig. 12 . Experimental power

and efficiency propulsion(fig13):
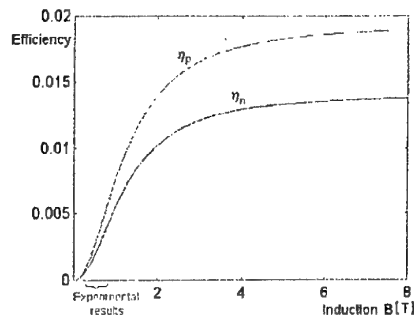
Fig .1 3 Experimental efficiency propulsion

15
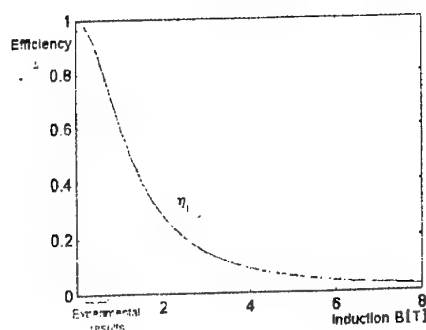
Fig. 13 b . Experimental efficiency Joule

These have subsequently been compared with those provided by the numerical simulations performed the mathematical model approached.

5.Conclusions

In conclusion, we can say that MHD field determination is possible find MHD systems equation in ship propulsion that can be determinate resolving the adimensional MHD equation at the adimensional channel. The mathematical model of the MHD interaction go to generalization of current density relation (11) and also pressure relation (12) for any propeller channel. On the basis of this theory the energy balance equations that have been obtained evince the possibility of getting superior efficiency by correlating the geometric dimensions of the propellers to the applied field inputted.

References

[1]   Badea,   N.   Aspecte   ale   interactiunii campelectromagnetic-apa de mare. **International Conference SIELMEC'97.** Chisinau. Moldova octomber 1997 p.270-274

[2]   Badea,   N..   Contributii   privind   propulsia electromagnetica a navelor.**Tesis of PhD,** iulie 1997 Galati. Romania

[3] Badea, N. The predetermination of the energetically and   geometrical   characteristics   of   an electromagnetic propeller. In: **The annals of "Dunarea de Jos"**, Galati.Romania 1994 p10-14.

[4] Doss, E. MHD Sea-water Propulsion. In: **Journal of Ship Research.**march 1993

[5] Swallow, D.. MHD Submarine Propulsion Systems. In

Naval Engineers Journal. ,may 1991,p.141

[6]-***-PDEase-software-Macsyma-USA-1994

THE COMPUTATION OF THE ELECTRIC FIELD STRENGTH OF A SEAGOING SHIP

T. Susanu**, I. Lingvay*, E. Petac**, F. Stoian*, C. Lingvay*

* Research Institute for Electrical Engineering - ICPE S.A.
Splaiul Unirii 313, Bucharest, Romania

** Naval Academy "Mircea cel Batran"
8700, Fulgerului 1, Constanta, Romania

Abstract. The paper presents an algorithm for the computation of the electric field around a seagoing ship.

1. GENERAL ASPECTS

It is well-known that the study of the electric field is performed taking into account some state variables. They can be scalar, vectorial etc. and they locally describe the state of the considered field.

Therefore, in order to establish the nature, the spatial distribution and the variation in time of such a field, one has to define:

- the flux of the state vector field and the flux density;
- the circulation of the state vector field;
- the spatial variations of some state scalars (for the case of scalar fields);
- the variation in time of the non-steady fields (locally described by the substantial derivates);
- the discontinuity of some fields.

For all these cases, the mathematic models are based on equations with partial derivates of various type, most of these equations being of second order. In order to determine the strength of an electric field on three spatial directions, we first introduce a mathematical model and then, an algorithm is developed.

2. THEORETICAL BACKROUND

The intensity of the electric field in a point can be computed by means of the gradient of the electric potential function on that point. This assume that by measurements and computation, the electric potential values are known on all the points concerned. What we do not know is the potential variation law.

To find the potential law, we consider a rectangular section of area $S = a \times b$, uniformly loaded with electric charge, and surface density ρ_S. (fig. 1)
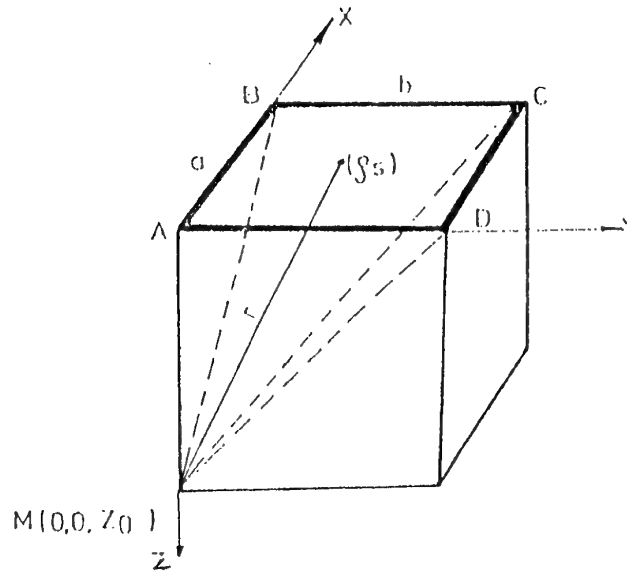
Fig.1 The rectangular section uniformly loaded with electric charge

The potential in point M $(0,0, z_0)$ is:

$$V_M = \rho_S / 4 \pi \varepsilon \int_S dS / r = \rho_S / 4 \pi \varepsilon \int d y \int d x / (x^2 + y^2 + z_0^2)^{1/2} \qquad (1)$$

By solving (1), with respect to x, one has:

$$V_M = \rho_S / 4 \pi \varepsilon \int \{\ln [a + (a^2 + y^2 + z_0^2)^{1/2}] - \ln (y^2 + z_0^2)^{1/2}\} d y \qquad (2)$$

By integration with respect to y [7], the arcsin is expressed in function of arctg and a constant is added, namely arctg (z_0 / a). Thus:

$$I_1 = \int \ln [a + (a^2 + y^2 + z_0^2)^{1/2}] d y = y \ln [a + (a^2 + y^2 + z_0^2)^{1/2}] + a \ln [\ln [y + (a^2 + y^2 + z_0^2)^{1/2}] - y + z_0 \arctg y / z_0 + z_0 \arctg a z_0 / [y_2 + z_0^2 + y (a^2 + y^2 + z_0^2)^{1/2}] \qquad (3)$$

Then:

$$V_M = \rho_S / 4 \pi \varepsilon [a \ln (b + \overline{MC}) / \overline{MB} + b \ln (a + \overline{MC}) / \overline{MD} - z_0 \arctg a \cdot b / z_0 \cdot \overline{MC}] \qquad (4)$$

From (4), if V_M is known, ρ_S can be determined and then, from (1) it follows:

$$\dot{\rho}_S = 4 \pi \varepsilon V_M / [a \ln (b + \overline{MC}) / \overline{MB} + b \ln (a + \overline{MC}) / \overline{MD} - z_0 \cdot \arctg a \cdot b / z_0 \cdot \overline{MC}] \qquad (5)$$

18

The electric field vector in M is given by:

$$E_M = - \text{grad } V_M = i \cdot E_x + j \cdot E_y + k \cdot E_z \qquad (6)$$

The strength of the electric field in M is:

$$E_M = \sqrt{E_x{}^2 + E_y{}^2 + E_z{}^2} \qquad (7)$$

3. THE ALGORITHM

The discrete grid we use for the computation of the electric field is shown in fig.2 (a part of the immersed bull of the ship).
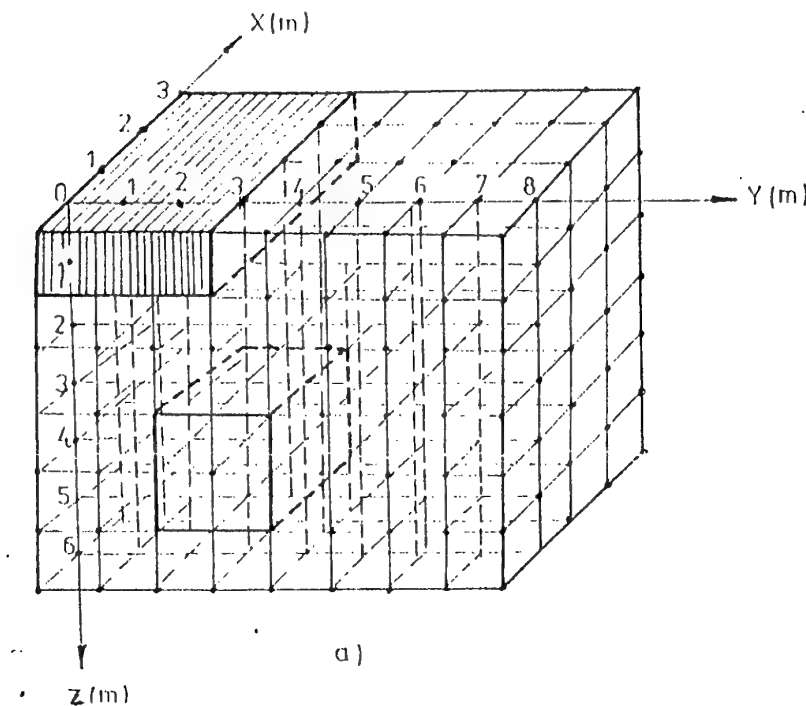
Fig.2 The cubic network for the computation of the electric field

The resolution of the grid on ox, oy and oz directions is of 1 meter. The domain to be considered in the sequel (for $x = -1 \div 3$ and $y = 3 \div 8$ - the area $(xoy)_{z=0}$, $x = -1 \div 3$ and $y = 0 \div 3$ - area $(xoy)_{z=1}$ respectively) is thus divided in squares ($h = 1$ m). Each square has virtually a uniform charge distribution which can be determined with (5) for $a = b = h$. The electric field strength can be computed on oz direction for each square (fig.1), at k h distance, for $k = (1 ...6)$ m. Thus:

$$z = k \cdot h, \quad k = 1...6 \qquad (8)$$

19

Since direct computation is tedious, we simplify it as follows: taking into account that the potential gradient in a point is determined by the difference of the potentials of two points in its neighbourhood ($M(x, y, z)$ and $M(x + \Delta x, y, z)$; $M(x, y, z)$ and $M(x, y + \Delta y, z)$ or $M(x, y, z)$ and $M(x, y, z + \Delta z)$), with $\Delta x = \Delta y = \Delta z = h = 1$ m - fig.3).
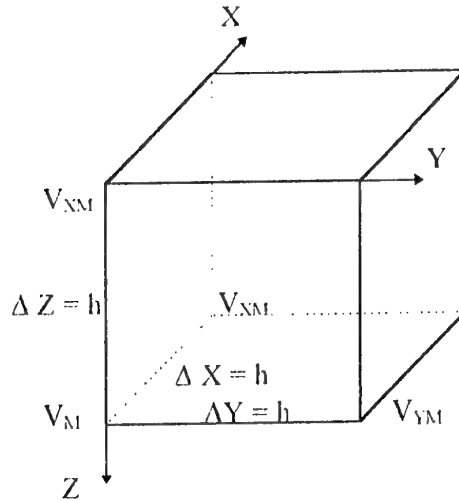
Fig.3 The potentials distribution on the three axis nearby $M(V_M)$

$$\Delta V(x) = V_M - V_{xM} \tag{9a}$$
$$\Delta V(y) = V_M - V_{yM} \tag{9b}$$
$$\Delta V(z) = V_M - V_{zM} \tag{9c}$$

which can be approximated by:

$$\Delta V(x) = (\partial V / \partial x) \Delta x = E_{xM} \cdot \Delta x \tag{10a}$$
$$\Delta V(y) = (\partial V / \partial y) \Delta y = E_{yM} \cdot \Delta y \tag{10b}$$
$$\Delta V(z) = (\partial V / \partial z) \Delta z = E_{zM} \cdot \Delta z \tag{10c}$$

The components on point M of the electric field on the three directions are:

$$E_{xM} = \Delta V(x) / \Delta x = (V_M - V_{xM}) / \Delta x = (V_M - V_{xM}) / h \tag{11a}$$
$$E_{yM} = \Delta V(y) / \Delta y = (V_M - V_{yM}) / \Delta y = (V_M - V_{yM}) / h \tag{11b}$$
$$E_{zM} = \Delta V(z) / \Delta z = (V_M - V_{zM}) / \Delta z = (V_M - V_{zM}) / h \tag{11c}$$

From 11 (a, b, c) it appears that the three components of the electric field on point M depend only of the potential difference in M and the points at $h = 1$ m in its neighbourhood, on the three directions.
The electric field strength on M is:

$$E_M = \sqrt{E_{xM}{}^2 + E_{yM}{}^2 + E_{zM}{}^2} \tag{12}$$

As above, the electric field strength on all the points of the cubic network can be determined.

4. CONCLUSIONS

The strength of the electric field generated by a ship (trade or naval) at a certain depth or a certain distance from the ship, is of considerable importance (e.g. for active anticorrosive protection of the ship).

The strength of the electric field is of great importance in the case of a military conflict; if the marine unconnecting mines'explosion are known, the appropriate measures in order to minimise the electric field of the ship can be taken

A model for the computation of the electric field has been presented. The derived algorithm is simply enough to be implemented on an IBM PC computer.

REFERENCES

[1] Dumitrescu I. - " Simularea cimpurilor potentiale", Romanian Academy Edition, Bucharest 1983

[2] Landau L.D. - "Teoria cimpurilor", Technical Edition, Bucharest 1963

[3] Nicolau E. - "Cimpuri si unde electromagnetice", Romanian Academy Edition, Bucharest 1983

[4] Radulet R. - "Bazele teoretice ale electrotehnicii", Bucharest 1955

[5] Durand E. , "Electrostatique", Tome I - "Les distributions", Masson et C - ie, Editeurs, · Paris 1966, pp 245

[6] Susanu T. , Calueanu D. , Lingvay I. , Alexa M. - "Potential measurements on the hull of a seagoing ship. Methods and results." - The International Conference "Optim 91", "Transilvania" University, Brasov , Oct. 10 - 13, 1991

[7] Susanu T. , Lingvay I. , Stoian F. , Petac. E - "The finite Differences Method to Determine the Potential Function Values in the Three - Dimensional Space Around a Seagoins Ship"

THE FINITE DIFFERENCES METHOD TO DETERMINE THE POTENTIAL FUNCTION VALUES IN THE THREE-DIMENSIONAL SPACE AROUND A SEAGOING SHIP (FINDI)

T. Susanu**, I. Lingvay*, F. Stoian*, E. Petac**

* Research Institute for Electrical Engineering - ICPE S.A.
Splaiul Unirii 313, Bucharest, Romania

** Naval Academy "Mircea cel Batran"
8700, Fulgerului 1, Constanta, Romania

Abstract. The purpose of the paper is to present an algorithm, based on the Finite Differences Method (FINDI), for the computation of the electric potential on the three spatial directions around a seagoing ship.

1. INTRODUCTION

The electric field of a sea-going ship assumes a slow rate variation in time, if energy conversions are negligible. The equations with partial derivates which describe the main magnitudes are of elliptical type. Thus, the study of the field phenomena is processed in the framework of the scalar potential theory.

A potential field having the divergence of the state vector equally zero in all the points P, in a domain Ω, namely:

$$(\text{div } E)_P = 0, \ \forall \ P \in \Omega \tag{1}$$

is called a "Laplace" field in the domain Ω.

The potential function V (defined by E= - gradV) verifies in Ω the equation:

$$\Delta V = 0, \text{ called Laplace equation.} \tag{2}$$

In order to solve equation (2), the boundary conditions of the problem have to be find. There are many methods specialised to solve this kind of problems. For its simplicity and efficiency, "The Finite Differences Method" suits very well to such a problem. Besides, there is available a huge amount of computer code to solve it.

The "Finite Differences Method" replaces the equations with partial derivates (describing a problems with boundary conditions) by equations with finite differences. The result of this method consists of a series of digital data, representing the potential values in the nodes of a network (applied to a chosen domain). These digital data are obtained by solving a linear

algebraic system, the discrete counterpart of the equations with partial derivates in the nodes of the network.

The accuracy of the method depends of:
- the discrete network;
- the type of discretization for the equations with partial derivates;
- the precision of approximation for the boundary conditions;
- the computation techniques (methods and equipment).

In order to approximate a Laplace equation by the "Finite Differences Method" we choose a discrete model in a three-orthogonal Cartesian coordinates system formed by cubic network.

2. THE ELECTRIC POTENTIAL FOR BOUNDARY CONDITIONS OF FIRST TYPE (DIRICHLET)

The physical measurements were picked-up on a seagoing ship of small dimensions, having the immersed bull with the configuration shown in fig.1. The potential measurements, on the boundary and inside the chosen domain, were performed offshore of the Black Sea, in the region of Mangalia city. These determinations were necessary in order to get the potential values and to use them as boundary conditions in a Dirichlet problem.

It can be notice that the studied domain stretches between the frames C39 and C47, having the dimensions from fig.1. The cross plane of the ship, determined by the plane yoz and the hull is approximated by a rectangle 3 x 1 m.
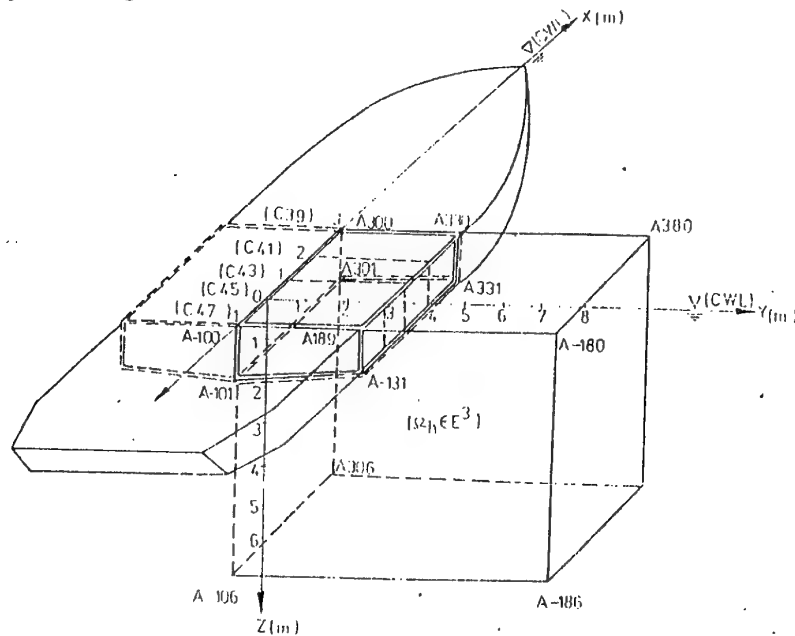
Fig. 1 The immersed bull of the ship and the measure domain Ω_h

The index of any point A in fig.1 indicates the coordinates of A in the 3D space. The values of the potential V(x,y,z), inside the chosen domain, was determined by solving the differential equation (2). For this, we have used an approximation with seven inner nodes in the 3D space.

These nodes are distributed as shown in fig.2, i.e., a discrete cubic network with a characteristic structure R7.

In fig.2b it can be seen that the node A_0 (x,y,z) is surrounded by the nodes $A_1 \ldots A_6$. The same notation is preserved for any inner node.
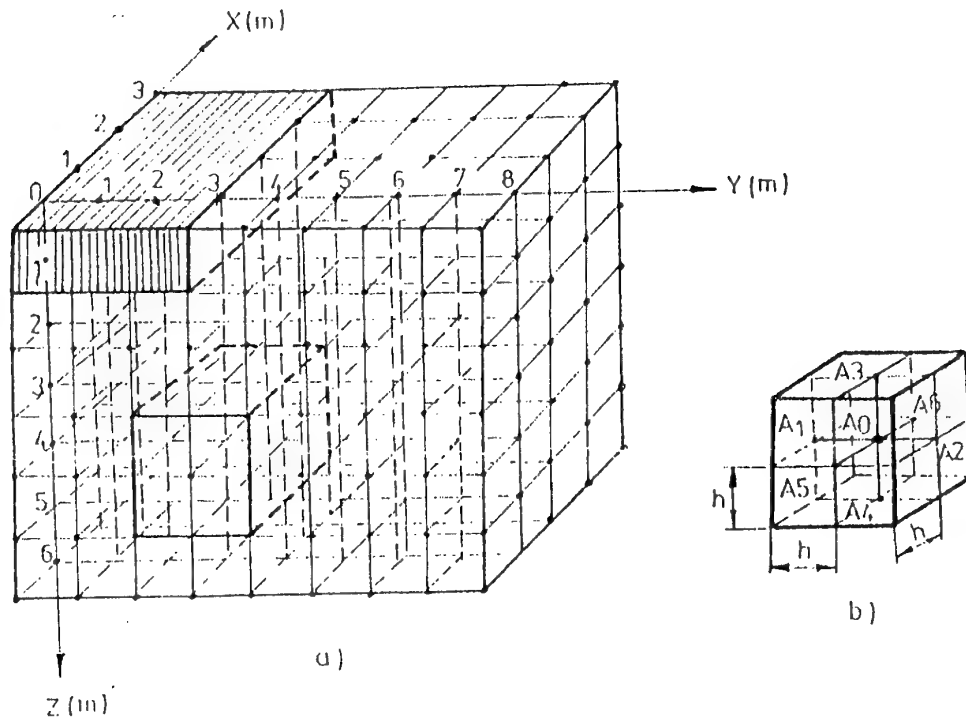
Fig. 2 The discrete cubic network :
   a) the discretization of the chosen domain
   b) the characteristic structure R7

In the case of first type boundary conditions the nodes A_0 will be located only inside the chosen domain. If we develop the potential V (x,y,z) after Taylor formula, around A_0 (x,y,z), the result is:

$$V(x_0+h,\ y_0+h,\ z_0+h) = V(x_0,\ y_0,\ z_0) + \Sigma\ 1/m! \cdot [(\partial V/\partial x)_{A_0}h+(\partial V/\partial y)_{A_0}h+(\partial V/\partial x)_{A_0} \cdot h +$$

$$+ (\partial V/\partial x)_{A_0}h]^m = V_0 + (\partial V/\partial x+\partial V/\partial y+\partial V/\partial z)_{A_0} \cdot h + 1/2!(\partial^2 V/\partial x^2+\partial^2 V/\partial y^2+\partial^2 V/\partial z^2)_{A_0} \cdot h^2 +$$

$$+\ 2/2! \cdot (\partial^2 V/\partial x\partial y+\partial^2 V/\partial x\partial z+\partial^2 V/\partial y\partial z)_{A_0} \cdot h^2 + 1/3!(\partial^3 V/\partial x^3+\partial^3 V/\partial y^3+\partial^3 V/\partial z^3)_{A_0} \cdot h^3 +$$

$$+ 3/3!(\partial^3 V/\partial x\partial y^2+\partial^3 V/\partial x\partial z^2+\partial^3 V/\partial x^2\partial y +\partial^3 V/\partial x^2\partial z+\partial^3 V/\partial z^2\partial y+\partial^3 V/\partial y^2\partial z)_{A_0} \cdot h^3 + \ldots \quad (3)$$

From a practical point of view, the accuracy of the computation is satisfactory, even without taking into account the terms of above second degree. In particular, the following equations with partial derivates are successively obtained:

- for the node A_1 (x_0, y_0 - h, z_0):

$$V_1 = V_0 - (\partial V/\partial y)_{A_0} \cdot h + 1/2! \cdot (\partial^2 V/\partial y^2)_{A_0} \cdot h^2 - \ldots \quad (4)$$

- for the node A_2 (x_0, y_0+h, z_0):

$$V_2 = V_0 + (\partial V/\partial y)_{A_0} \cdot h + 1/2! \cdot (\partial^2 V/\partial y^2)_{A_0} \cdot h^2 + \ldots \qquad (5)$$

- for the node A_3 $(x_0, y_0, z_0 - h)$:

$$V = V_0 - (\partial V/\partial z)_{A_0} \cdot h + 1/2! \cdot (\partial^2 V/\partial z^2)_{A_0} \cdot h^2 - \ldots \qquad (6)$$

- for the node A_4 $(x_0, y_0, z_0 + h)$:

$$V_4 = V_0 + (\partial V/\partial z)_{A_0} \cdot h + 1/2! \cdot (\partial^2 V/\partial z^2)_{A_0} \cdot h^2 + \ldots \qquad (7)$$

- for the node A_5 $(x_0 - h, y_0, z_0)$:

$$V_5 = V_0 - (\partial V/\partial x)_{A_0} \cdot h + 1/2! \cdot (\partial^2 V/\partial x^2)_{A_0} \cdot h^2 - \ldots \qquad (8)$$

- for the node A_1 $(x_0 + h, y_0, z_0)$:

$$V_6 = V_0 + (\partial V/\partial x)_{A_0} \cdot h + 1/2! \cdot (\partial^2 V/\partial x^2)_{A_0} \cdot h^2 + \ldots \qquad (9)$$

From relations $5 \div 10$ we have:

$$V_1 + V_2 + V_3 + V_4 + V_5 + V_6 = 6 V_0 + (\partial^2 V/\partial x^2 + \partial^2 V/\partial y^2 + \partial^2 V/\partial z^2)_{A_0} \cdot h^2 = 6 V_0 + \Delta V \cdot h^2 \quad (11)$$

Taking into account equation (2) for a Laplace field, we have:

$$V_1 + V_2 + V_3 + V_4 + V_5 + V_6 - 6 V_0 = 0 \qquad (12)$$

Similarly (for any point of the network) the following relation holds:

$$V_{x_0, y_0 - 1, z_0} + V_{x_0, y_0, z_0 - 1} + V_{x_0, y_0, z_0} + V_{x_0, y_0, z_0 + 1} + V_{x_0 - 1, y_0, z_0} + V_{x_0 + 1, y_0, z_0} - 6 V_{x_0, y_0, z_0} = 0 \quad (13)$$

These two expressions (12 & 13) are an approximation with finite differences of the Laplace's equation ($\Delta V = 0$), in seven nodes of the 3D space; the order of the error magnitude is of zero. Equation (13) is further iterated for each inner node of the chosen domain. In particular, for the domain shown in fig.2 a system of 96 linear algebraic equations with 96 unknown variables was found out. By solving the system the digital approximation of the electric potential function $V(x, y, z)$, $x, y, z \in \Omega_h$ is obtained.

3. CONCLUSIONS

The computation of the potential values on the entire immersed hull of a sea-going ship or in a volume around it, is a problem of considerable concern (e.g. to obtain information about the electrochemical corrosion gradient).
The proposed method has two stages as following:

25

- an experimental stage - the measured of the potential values, which will form the boundary conditions of Dirichlet type problem for the following computation stage, and will validate the computation as well
- a computation stage - to determine the potential values inside the considered volume

REFERENCES

[1] Aubin J. P. - "Approximation of elliptic boundary value problems" - Wiley Interscience, New York 1972

[2] Ciarlet P.G. - "Numerical analysis of the finite element method for elliptic boundary value problems" - North-Holland, Amsterdam 1977

[3] Collatz L. - "The numerical treatment of differential equations", Springer - Verlag, Berlin, Heidelberg, New York, 1966

[4] Dumitrescu I. - " Simularea cimpurilor potentiale", Romanian Academy Edition, Bucharest 1983

[5] Greenspan D. - "Introductory numerical analysis of elliptic boundary value problems" Harper and Row, New York 1965

[6] Milne W.E. - "Numerical solution of differential equations", John Wiley and Sons, New York 1953

[7] Racoveanu N. , Dodescu Gh. , Mincu I. - "Metode numerice pentru ecuatii cu derivate partiale de tip hiperbolic" - Technical Edition, Bucharest 1976

[8] Smith G.D. - Numerical solution of partial derivate equations", Oxford University Press, London 1965

[9] Susanu T. , Calueanu D. , Lingvay I. , Alexa M. - "Potential measurements on the hull of a seagoing ship. Methods and results." - The International Conference "Optim 91", "Transilvania" University, Brasov , Oct. 10 - 13, 1991

[10] x x x "Numerical solution of partial differential equations", New York, Academic Press, 1967

THE VIRTUAL TEST BED:
AN ENVIRONMENT FOR VIRTUAL PROTOTYPING

Charles W. Brice, Levent U. Gökdere, Roger A. Dougal
Department of Electrical & Computer Engineering
University of South Carolina
Columbia, SC 29208
USA
brice@engr.sc.edu

Abstract

The Virtual Test Bed (VTB) is a software environment that supports design, analysis, and virtual prototyping of electric power systems, with an emphasis on naval applications. This paper describes the status of development of the VTB and its use in the multi-technical field of ship power systems.

1 Introduction

The Virtual Test Bed (VTB) is a software environment that supports design, analysis, and virtual prototyping of electric systems. The VTB is being developed as a part of the Power Electronic Building Block (PEBB) program to support both that program and the more general task of integrating power electronics into the more electric ships of the 21st century Navy.

This paper describes the VTB Program, its value to multidisciplinary engineering systems, how an engineer would use it, and concludes with an example application.

2 The VTB Program

The VTB development team initially adopted four overarching principles to rule development of this software. First, the VTB should recognize and preserve the value and utility of the abundance of existing ship system models and the skills of those who created those models. Second, the VTB should support both top-down and bottom-up engineering methodologies. Third, the VTB should make extensive use of visualization to increase the value of the software, both in terms of ease of use and in efficiency of conveying to the user an intuitive understanding of computed results. Finally, the VTB should be useable by all of those who need to use it. Hence it should be platform independent and should exploit distributed and network-oriented computing to allow virtually unlimited power and widespread access.

The VTB development team encompasses six universities. The team is lead by a group at the University of South Carolina, and supported by efforts at Georgia Institute of Technology, Purdue University, Pennsylvania State University, University of Missouri/Rolla, and Taganrog State University of Radio Engineering (Taganrog, Russia).

The fundamental value of the VTB can be attributed to its capability for integrating into one simulation environment models that have been created in a variety of languages, each as appropriate to the particular component that it describes. This allows one to construct a comprehensive virtual prototype of the entire multi-technical world of the electric ship. Electronic components can be described by SPICE files (Simulation Program with Integrated Circuit Emphasis), dynamic systems by ACSL files (Advanced Continuous Simulation Language, MGA Software), power electronics by Saber© (Analogy, Inc.) files, and so on. Each component of the entire ship system can be described in the most appropriate language by an expert who understands that particular component and that particular language, then the multitude of components can be assembled into the greater ship system. These models are then brought into the VTB environment by the process of translation, as will be explained later. Figure 1 shows the basic structure of the VTB as it now exists.

A basic benefit of the multi-lingual approach is that a particular component of the electric system can be represented by a plethora of models, depending on the objective of the investigation. These models can be of various orders and can exist in many languages. High-level, reduced-order, models can be used when studying the basic performance of a large system, while detailed, high-order models can be used when studying the dynamics of a microcosm of the system where more detail is necessary. This inherently
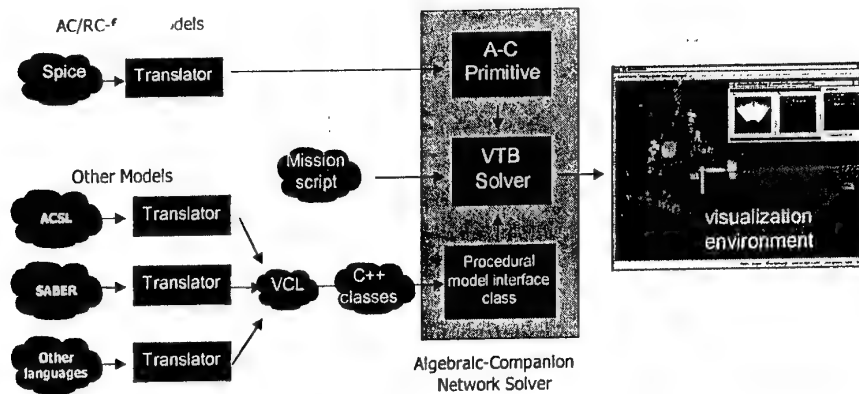
Figure 1. General architecture of the Virtual Test Bed (Version 2).

supports both top-down and bottom-up engineering approaches.

Visualization technologies are heavily employed to enhance the value of the Virtual Test Bed. Beyond the now-standard visual user interface, the VTB provides advanced displays of simulation results including full-motion animation of mechanical components, oscilloscope-like displays of waveform data, and imaginative mappings of computed results onto the system topology in ways that can increase user comprehension of system behavior and yield new insight into problems and problem resolutions.

The VTB provides two views of the virtual system. One is a physical view, which shows the physical structure including component placement within its environment (ship structure, etc.). The other is a schematic view that provides more rapid definition and assimilation of the connectivity of the system.

The VTB environment is distributable. In the present incarnation (Version 2), network simulations execute on a single processor, while visualizations can run concurrently on a separate system. Upcoming versions of the software will distribute the network simulation itself in several ways.

When models are submitted to the VTB library, they are translated to the VTB Common Language (VCL) and subsequently output as C++ classes. Model source code in one of the supported simulation languages is first scanned and parsed. Semantics (i.e., meaning) is added to yield the model
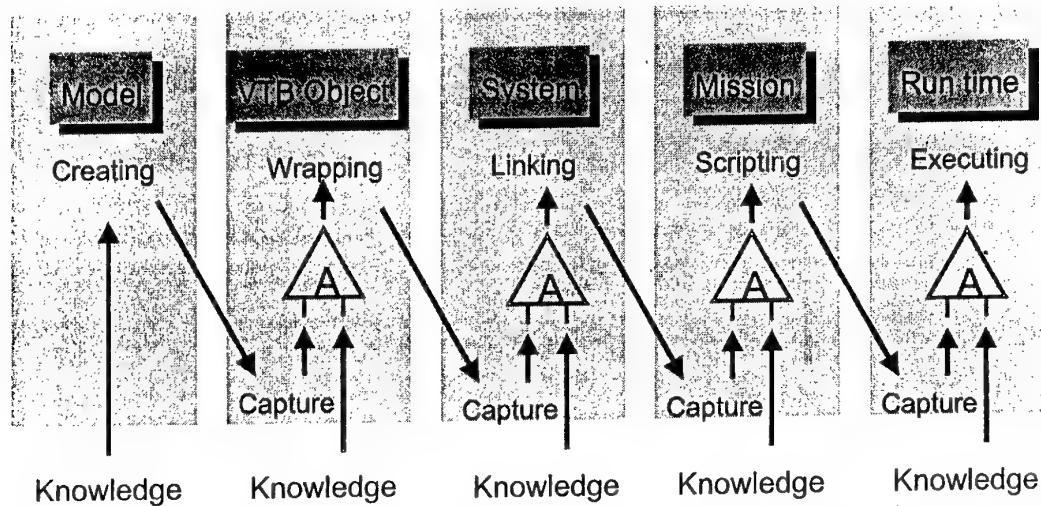
Figure 2. At each step in the modeling and simulation process, VTB captures and amplifies user knowledge.

28

description in the VTB Common Language (VCL), which is then converted to C++ classes to yield access to the highly optimized execution environment. Finally, a DLL (dynamically linked library) is created so that the model can be linked into the simulation at runtime. This obviates the need to recompile the simulation scenario each time that an object is changed.

The Solver uses an extension to the resistive companion form network solution method called the algebraic companion method [1]. Because of compatibilities between SPICE netlists and the algebraic companion method, the translation process is bypassed and instead algebraic companion primitives are directly formed for each SPICE primitive.

The VTB provides more than a flexible environment for simulating electric ship systems; it captures and amplifies the knowledge of the users at each step. Consider the process of using the VTB as a sequence of steps, as shown in Figure 2, starting with building a model of a component or process, and ending with running a system simulation. Each step may be done by a different member of a team or by team members working together but perhaps at different times and different locations. The VTB

supports this work environment by capturing as much knowledge as possible at each step. The computer is then used as a tool to amplify that knowledge.

3 Application to Ship Electric Systems

Electric systems of 21st century naval platforms will be more distributed, more intelligent, more fault-tolerant, and more multi-technical than existing systems. Furthermore, these new topologies for ship electric power distribution will have no historical precedents and so they must be more thoroughly tested than current systems. Power electronics and intelligent controls will increasingly allow more competent systems but with smaller safety margins. The small margins yield great benefit in terms of system size, cost, and flexibility, but can threaten system robustness. It is the purpose of the Virtual Test Bed to ensure that these systems will work when they are challenged.

Figure 3 shows a simplified view of an advanced electric-drive ship power system that uses a zonal power distribution architecture. The propulsion motors are fed from an AC system while most of the ship service power is distributed by a DC zonal system. PEBB's are used in various places to tie the
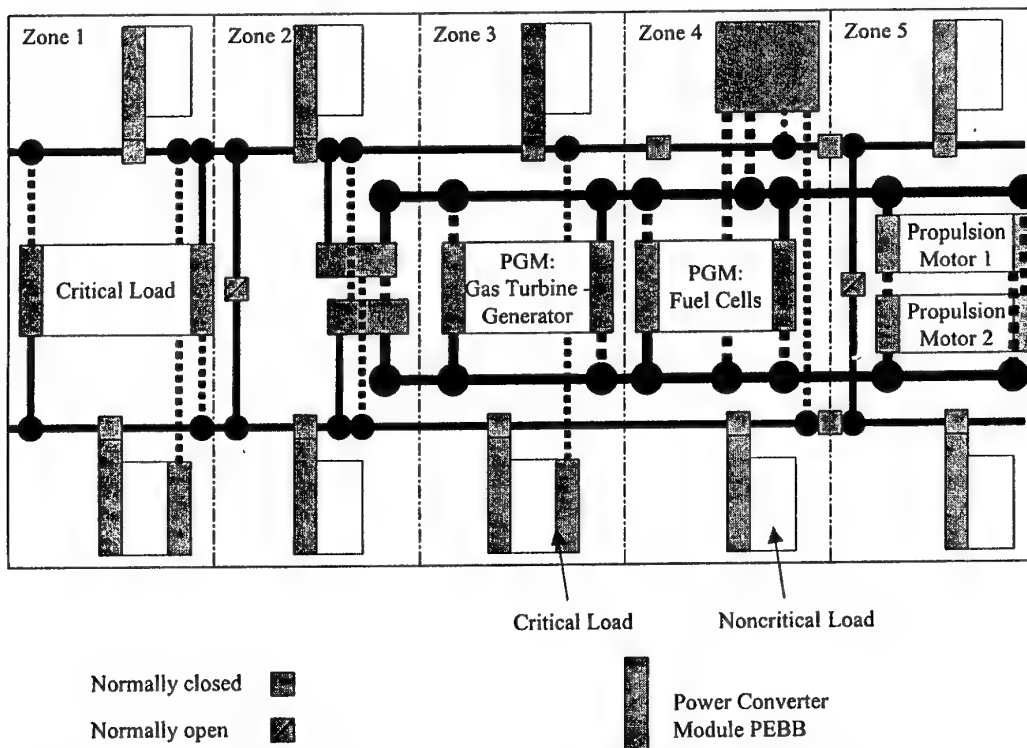
Figure 3. Advanced ship power system with electric-drive propulsion, fuel cell power generation modules for base load and gas-turbine-generators for peaking power.

system together, providing protection and control functions in addition to simple inversion from DC to AC. Base power is provided by fuel cells, while peaking power is provided by gas turbines. Although greatly simplified, something similar to this system could be used in the next generation of warships.

Figure 3 illustrates some, but not all, aspects of the next generation of ship power systems. In particular, we expect to see DC distribution and advanced motor controllers having high switching frequencies. Notwithstanding the use of DC power distribution, AC motors will likely be used for powering of most mechanical systems. These motors may be of an unconventional design, perhaps supplied at higher frequencies than commonly used today. In any case, it is important to accurately model the high-frequency response of power converters, motors and other devices in the system. It is also essential to include appropriate control system actions, and to

accurately represent the system itself. With that in mind, the VTB project includes development of high-frequency motor models [2], development of efficient models for motors and motor drives [3], innovative motion control concepts [4], development of tools for calculating parasitic effects [5], and development of models that account for thermal loading. Since many technical disciplines are involved, we describe the ship systems as multi-technical.

Imagine now that you wish to use the VTB to analyze the dynamic performance of a ship system similar to the one illustrated in Figure 3. First, define the system by selecting models from a model library. You can browse the library using a tool called the model librarian that has a familiar look and feel; it appears to be just like a web browser. You find a set of models of the fuel cell that you want to include, and the librarian aids you in finding the one with the level of detail that you want. Since this model has already
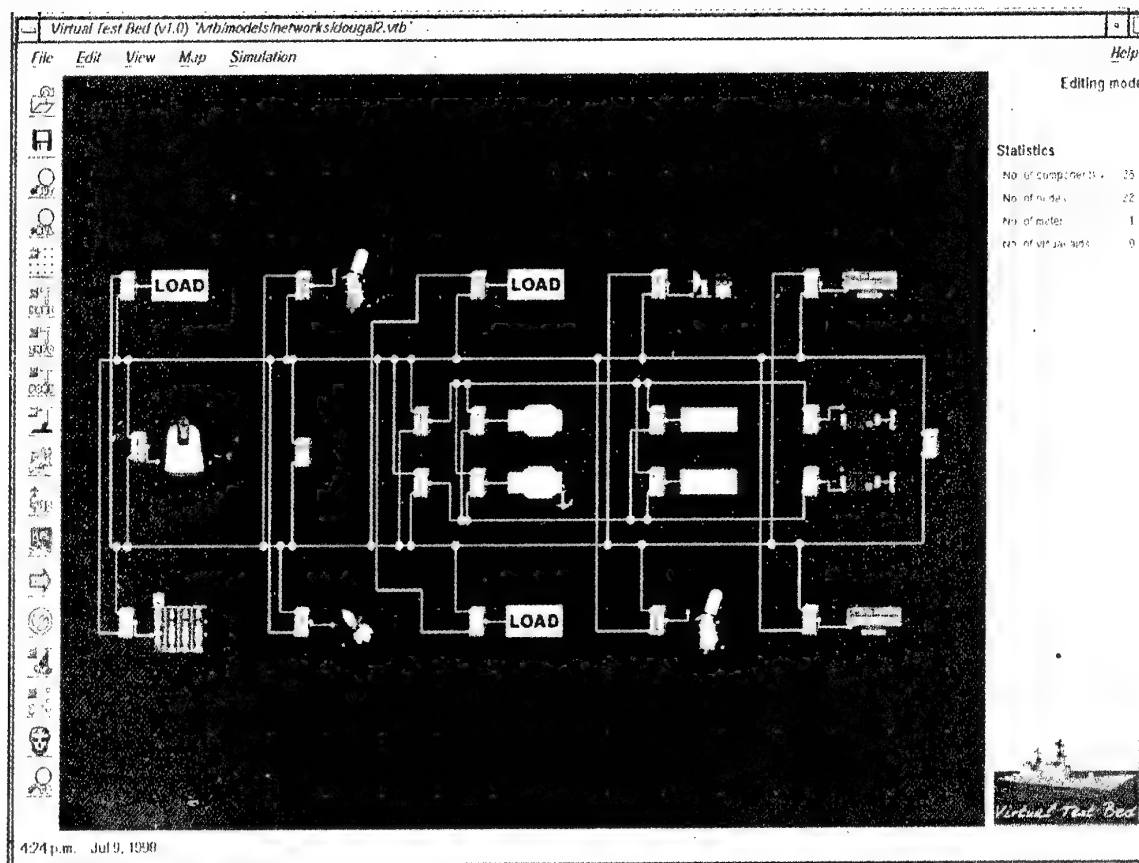
Figure 4. User screen of the VTB.

been translated from the simulation language that the model developer used to create it, and it has been wrapped to become a VTB object, you can simply click to insert it into the system. You then find other objects similarly. If you wish to define a new object, you can do that by using any of a variety of languages; you can write C++ code directly, you can create an ACSL *.csl file, or a Saber netlist. Or, if the new object is just a collection of simple circuit elements, perhaps a SPICE netlist would suffice. To import that new object into the VTB library, it is necessary to specify things such as the interface variables and any internal variables that you wish to interact with. The Librarian assists as you do this. Now wire the components together to define the network topology.

At this point a model of a power system exists, and system studies could be performed. Instead, your goal is run a whole series of simulation studies to check the performance of the power system under many different scenarios. The VTB supports this by providing a mission scripting facility that allows full real-time support, if needed.

As the simulation runs, or after it runs if you don't want to interact with it, you can view the data in a variety of ways. The VTB makes use of visualization plug-ins to customize the visual displays in meaningful ways. The most straightforward visual display may be a simple oscillographic view of waveform data. But displays can be much more complicated. In the most advanced forms, physical systems can be animated to show how they behave, or some parameter of the system can be mapped onto the system topology to yield a new way of looking at complex data sets.

At this point, the simulation can be highly interactive. A user can insert or delete system components on the fly and immediately see updated data. The simulation need not be compiled before it is run, thanks to the use of the dynamically linked libraries that define system components.

4 Conclusions

This paper described the Virtual Test Bed (VTB) and its application to multidisciplinary engineering systems such as naval ships.

The fundamental value of the VTB can be attributed to its capability for integrating into one simulation environment models that have been created in a variety of languages, each as appropriate to the particular component that it describes. This allows one to construct a comprehensive virtual prototype of the entire multi-technical world of the electric ship.

Acknowledgment

References

[1] A.P.S. Meliopoulos and G.J. Cokkinides, "A Time Domain Model for Flicker Analysis," **Proceedings of the IPST'97**, pp. 365-368, Seattle, WA, June 22-26, 1997.

[2] S.D. Sudhoff, J.L. Tichenor, J.L. Drewniak, "Wide-Bandwidth Multi-Resolutional Analysis of a Surface-Mounted PM Synchronous Machine," submitted to **IEEE Transactions on Energy Conversion.**

[3] S.D. Pekarek, O. Wasynczuk, H.J. Hegner, "An Efficient and Accurate Model for the Simulation and Analysis of Synchronous Machine/Converter Systems," **IEEE Transactions on Energy Conversion**, Vol. 13, No. 1, pp. 42-48, March 1998.

[4] L.U. Gökdere and C. W. Brice, "Energy Shaping and Input-Output Linearization Controllers for Induction Motors," **Proceedings of the 1997 IEEE Conference on Control Applications**, Hartford, CT, Oct. 1997.

[5] R.A. Lewis and J.L. Hudgins, "The Effects Due to Package Parasitics of a PEBB-1 Module in an ARCP Circuit," **Proceedings of the Power Electronics Specialist Conference**, May 1998.

Grounding Design Approach In The Integrated Power System For US Navy Surface Ships

Thomas C. Dalton
ICEM '98 Conference Office
Department of Electrical and Electronics Engineering
Middle East Technical University
Ankara, 06531 TURKEY

ABSTRACT

Grounding of power distribution systems at medium voltage levels for safety of personnel and protection of equipment is a fairly routine practice for shore based industrial and utility facilities. However, grounding quickly becomes more complex in a marine application because low voltage shipboard electric plants are ungrounded to maintain power availability to ship service loads. As the integrated shipboard electric plant power demand increases to support the ship propulsion loads in all electric concept, higher voltage systems are required. These two traditional design approaches of grounding power systems ashore for equipment protection and personnel safety and not grounding shipboard systems for enhanced system reliability conflict each other. Fortunately, high impedance grounding resolves this conflict by placating the requirements of both of these system applications. Unfortunately, some aspects of high impedance grounding aboard a merchant ship become more sensitive to implement in naval ship applications designed to emphasize survivability in battle and reliability with minimal maintenance.

Accordingly, this paper reviews the basic aspects of grounding[1,2] and shipboard grounding applications for merchant and naval ships. The unique impact associated with the newer solid state technology pulse width modulated (PWM) power converters being developed to control propulsion motors in future USN surface naval ships is also addressed. Thoughts on the challenge of implementing high impedance grounding in higher medium voltage systems for larger naval ships (such as aircraft carriers) are discussed, too. This paper concludes with suggested high impedance grounding design applications for generic surface naval ships, including aircraft carriers and propulsion systems incorporating PWM power converter technology.

PURPOSE OF GROUNDING

The first power distribution systems were ungrounded because the problems with ungrounded systems and benefits of grounded systems were not fully understood. This occurred because grounding equipment is an additional cost associated with a casualty event that could be tolerated in an ungrounded system. The unintentionally grounding of one phase simply does not necessarily cause the system to protectively shutdown (i.e., two phases must become grounded for a phase to phase fault to cause a protective device response).

The purpose of grounding is multifold. Its primary function is to protect personnel from shock hazard and equipment from insulation damage by preventing excessive ground fault overvoltages and limiting ground fault current. A secondary function of grounding is to identify when a ground fault condition exists. Most grounding is designed to respond to a grounding fault by removing the power source from the system to protect it and the faulted equipment from damage. Grounding schemes are not capable of determining the location of the ground fault or removing it from the system. This is the protective function of the differential phase relay in the switchboard circuit breakers. However, one grounding scheme (high resistance or impedance) is designed for continuous operation under a ground fault condition to prevent disruption of power to loads until such time as repairs can conveniently be made to remove the ground fault.

GROUNDING EFFECTS

Grounding an ungrounded higher voltage power distribution system provides protection against shock to personnel by creating a path of lower resistance to ground than a person. This intentional path to ground on a chassis or frame precludes the possibility of any significant voltage level occurring on any exposed metal components that personnel could readily contact.

Grounding an ungrounded power system also protects equipment from exposure to resonant effects resulting from ground fault restrikes building up the voltage to as much as ten to twenty times the nominal system voltage rating. This develops as a result of the characteristic zero crossings of the sinusoidal voltage waveform coupled to the inherent resonant effect of the capacitive and inductive nature of any power distribution system. A resulting voltage phenomena is created at each restrike cycle that tends to steadily charge the voltage in higher repetitive incremental steps as potentially large as the system voltage rating itself. Thus, most ungrounded systems must have an insulation system rated much higher than the nominal system voltage rating for grounded systems or additional insulation damage may occur anywhere within that system during a ground fault condition. This does not apply for low voltage systems because the insulation capability far exceeds the nominal
voltage rating.

The other protective features of grounding an ungrounded power system are the ability to identify a ground fault occurrence and limit ground fault current impact on system components by reducing its duration and magnitude. An intentional ground connection also provides a convenient place to monitor for any ground fault conditions occurring anywhere in the system. Once a ground condition is identified, the power sources can be removed from service to protect them, the associated system components and the equipment that is ground faulted from excessive ground fault current. Resistance is often added to a ground connection to limit the magnitude of a ground fault current. This prevents any potential damage during the response period required for protective devices to function. In addition, some grounding schemes operate continuously under ground fault conditions, like an ungrounded system, without the excessive associated ground fault overvoltage and current to maintain continuity of service.

GROUNDING SCHEMES

An ungrounded higher voltage power distribution system is actually indirectly grounded via its inherent system capacitances. This capacitive grounding effect is essentially simulated by high resistive grounding since a system with infinite resistance in effect becomes an ungrounded system. Solid and low resistive

grounding are other options that are essentially direct ground connections through no resistance or a rather minimal resistance, respectively. Reactance and resonance grounding use a reactor rather than a resistor to connect to ground. A resonance ground is just a tuned reactor that is designed to provide an equal compensating current to oppose the capacitive charging current of the system. Similarly, high impedance grounding is merely a high resistance grounding via a grounding transformer that naturally adds inductance into the circuit for an overall impedance effect.

An overview of the usage and features of these types of grounding schemes appear in Tables 1 and 2. Ungrounded systems provide enhanced reliability in terms of power availability. Solid grounding is primarily used to economically provide single phase power inherently available for lower voltage loads.

TABLE 1
GENERAL GROUNDING METHOD
APPLICATIONS[4]

GROUNDING METHODS	SYSTEM USAGE
Ungrounded	Low voltage (600 V) for shipboard ship service electric plants
Solid Ground	Low (600 V) to medium (12.5 KV) voltage for industrial plants
Reactance Ground	Medium (34.5 KV) to high (115 KV) voltage for utility power substation
Resonance Ground	Medium (34.5 KV) to high (115 KV) voltage for utility power transmission
Low Resistance Ground	Medium (15 KV to 34.5 KV) voltage for local utility distribution
High Resistance Ground	Medium (5 KV to 15 KV) voltage for industrial plants and shipboard power generation/ship propulsion

High resistance or impedance grounding is designed to sufficiently limit the ground fault current to sustain a continuous ground fault condition indefinitely without damaging the equipment suffering that ground fault, which

33

TABLE 2
FEATURES OF VARIOUS GROUNDING SCHEMES AVAIALBLE[4]

FEATURE	COMPARISON OF GROUNDING METHOD CHARACTERISTICS					
	UN	S	R	RES	LR	HR
Immediate isolation from the ground fault	X	X			X	
No tripping of feeder breakers on occurrence of first ground fault so service continuity maintained						X
Minimum shock hazard to personnel during ground fault		X				
Minimum flash hazard to personnel during ground fault						X
Minimum arcing fault damage to equipment during ground fault regardless of fault location						X
Provides for line-to-neutral single phase loads at a lower voltage without the use of a transformer		X				
Practical suppression of transient overvoltage due to arcing ground fault		X				
Practical reduction of equipment burndown due to high impedance fault·		X			X	X
Reduce voltage dip due to ground fault						X

S: Solid   LR: Low-resistance   RES: Resonance   UN: Ungrounded   HR: High-resistance   R: Reactance

permits continuity of power service until the ground fault can conveniently be cleared. Low resistance, reactance and resonant grounding also limit ground fault current, but are designed to immediately protect the power source by removing it off line.

The optimum approach for grounding a particular power system depends on the performance priorities set for that system. There are two basic limitations associated with grounding design for a system. First, continuous current levels beyond 10 A at a ground fault in a power distribution system are not allowed because it would propagate insulation damage. Secondly, to ensure discrimination between a ground fault current and the system capacitive charging current present in a system, the ground fault current must be allowed to achieve a level at or above the system capacitive charging current to prevent a false ground fault response.

As a result of the capacitance from equipment in the power system, continuous duty ground fault operation with high impedance grounding is often limited to the 5 KV class and below[3] as illustrated by Tables 3 and 4. Other grounding techniques that immediately implement a protective device response to remove the power source while limiting ground fault current must be used when the capacitive charging current and

the associated allowed ground fault current of the system exceeds 10 A. Note that grounding designs for continuous duty ground fault operation also require the grounding equipment to be sized for continuous versus momentary service, which increases the cost, weight and space of the grounding components.

GROUNDING OPTIONS

Besides the operating duration of a grounding design, the location, quantity and interconnectability of grounds are design options tailored to the power distribution system application at higher voltage levels. Since the power source is the most important and likely equipment to be damaged by a ground fault (other than the equipment having the ground fault itself), grounding is normally integral to each power source. This approach makes it convenient to implement the grounding for the power source within its terminal box and ensure grounding protection is always activated when the power source is on line. The early concept of locating grounding at loads has long been discontinued because the power source could be left ungrounded if the load was removed.

In particular, there are several options for grounding the power system. For instance, the

TABLE 3
TYPICAL CAPACITIVE CHARGING CURRENT OF EQUIPMENT AT VARIOUS VOLTAGE LEVELS[4]

EQUIPMENT	SYSTEM CAPACITIVE CHARGING CURRENT	
	5 KV	15 KV
Transformers	Negligible	
Cabling – (sample 350 MCM – 3 conductor)	.23 A (per 1000 FT)	.71 A
Generators - high speed	.02 A/MW	.06 A/MW
- low speed	.08 A/MW	.25 A/MW
Power Converters –		
- Cyclo type	.03 A/MW	.10 A/MW
- Pulse width modulated*	.09 A/MW	.26 A/MW
- Synchronous (LCI)		
- w/o by-pass capacitor	.47 A/MW	1.41 A/MW
- w/by-pass capacitor	.28 A/MW	.84 A/MW
AC motors (ind or sync)	.05 A/ KHP	.15 A/KHP

* includes by-pass capacitor

grounding location may be at either the switchboard or the power source. Another option to the system designer is whether or not to have one or several grounding points within a system. Typically, multiple point grounding occurs when several power sources are involved or a system is split into several sections. Since multiple grounding points usually create grounding current loops (particular for the third harmonic), high impedance grounding is used to restrict and dampen any resonant circulating grounding currents. Another method for eliminating ground loop circulating currents is to provide a common neutral, which is just a solid connection in-between all the desired grounding points to collect them into one singular ground point. A common neutral often becomes impractical because all the ground points have to be located in immediate proximity of each other (such as a power station) to preclude the

possibility of any equipment becoming ungrounded by disconnection of the neutral conductor from that equipment.

A concern for multiple point resistive or impedance grounding is its impact on protective device settings or the potential for independently switched grounds to be inadvertently deactivated. Therefore, if multiple point grounding is used, the grounding points are usually fixed relative to the equipment they

TABLE 4
TYPICAL SYSTEM CAPACITIVE CHARGING CURRENT AT VARIOUS VOLTAGE LEVELS FOR INDUSTRIAL APPLICATIONS[4]

SYSTEM VOLTAGES	SYSTEM CAPACITIVE CHARGING CURRENT
480 V	1 A to 5 A
2400 V to 4160 V	2 A to 7 A
13,800 V	10 A to 20 A

protect, except for disconnect links that are necessary to ensure the equipment remains isolated during maintenance if a ground fault occurs.

Protective settings of multiple point grounding are addressed in two ways. The preferred method is to size the resistance or impedance for the capacitive charging current of that equipment or system segment being protected. In this approach equipment or system segments can be added or removed with their respective grounding design without concern for the protective settings changing because the system inherently adjusts itself to the capacitive charging current of the new system configuration.

The other approach is to size each resistance or impedance for the entire system. When the entire system is interconnected, this approach requires the unnecessary grounding points to be removed or resetting the protective devices to a lower value corresponding to the additional ground fault paths available. If the same system was operated in a split mode, then the original settings of the protective devices will be acceptable, but they will permit a greater ground fault current related to the number of grounding paths available.

Grounding points are often easiest to obtain at the power source since transformers and generators generally offer a neutral grounding point that is readily available. A grounding transformer off a switchboard circuit breaker is required to develop a grounding point from a system, which adds cost, space and weight impacts.

The resistor for high resistance or impedance grounding of a generator is typically sized for momentary duty to fit within the limited space in the attached cable termination box. High resistance or impedance grounding at switchboards is more likely to be rated for continuous duty and the impedance could be sized for the entire power distribution system since there is already an obvious acceptance of the space, weight and cost impact. High impedance grounding may also have several independently switched resistors sized for the entire system to ensure at least one ground is always available.

When many generators with grounds appear likely in a power distribution system design, a better approach is to incorporate fewer grounding points at the major switchboards of the power system. Grounding at the switchboard versus the generators also makes more sense when the dominant capacitive charging currents are from the cabling or the loads in the system rather than the power sources (i.e., transformers used as power source or generator configuration has minimal impact on total system capacitance).

Another interesting aspect of grounding design is dependent on the capacitive charging current characteristic of power converters. Motor loads are often controlled via power controllers and when these power converters are directly connected into the system without transformer isolation, significantly more capacitive charging current may occur as indicated in Table 3. The commonly used synchronous or load commutated converter (LCI) derives a considerable amount of its capacitance at 60 HZ from the supply and machine bridges, motor itself and associated cabling. However, the DC link of a synchronous converter provides the major contribution of capacitance at a common mode frequency of 180 HZ. As Table 3 shows, a by-pass capacitor at the grounding equipment can lessen the effect of the DC link capacitance dramatically. Cycloconverters have substantially less capacitive charging current because there is no DC link in the cycloconverter. The newer PWM converter technology also has a DC link, but the

impact of the DC link is minimized from a by-pass capacitor as well. However, the primary purpose of this by-pass capacitor is to prevent the large stray PWM carrier frequency (2 KHZ and up) common mode current from severely overloading the grounding resistor.

Since power converters offer a current limiting capability, ground fault protection between the power converter and its motor is not necessary despite the length of cabling involved. However, if a PWM power converter is directly connected to a grounded power system (i.e., no transformer isolation from power sources) a ground fault will cause that converter to protectively shut itself down due the associated voltage shift impact on its stability. This peculiarity of the PWM power converter is a result of the converter being grounded at its neutral point in the DC link to accommodate the circulation of the carrier frequency common mode current.

MERCHANT SHIP GROUNDING APPLICATIONS

None of the US regulatory bodies require any specific type of grounding method for shipboard power distribution systems at medium voltage levels. In addition, no US regulatory bodies have any reliability requirements for continuous operation of the electric plant under ground fault conditions because adequate electric plant reliability is achieved from the minimum quantity of interconnectable generators and switchboards required. In fact, the US regulatory bodies actually require a ground fault to be removed once it is detected in a shipboard electric propulsion system. The US regulatory bodies further specify that ground fault currents can not exceed 20 A.

This requirement to remove the generators off line to protect them from a ground fault is unacceptable for an integrated shipboard electric plant that must continue to provide power for ship service loads.
Since high impedance grounding best simulates the superior reliability of ungrounded low voltage systems traditionally used aboard ships, this grounding approach is the only feasible solution for an integrated shipboard electric plant to support the all electric ship concept. Note that if PWM power converters are used without isolation transformers, a split shipboard electric plant or transformer isolation must be provided between the generators and the propulsion loads

to preclude loss of all propulsion upon a ground fault condition.

Given that high impedance grounding is not possible under continuous duty above 10 A of ground fault current and not recommended at ground fault current levels beyond 20 A on a momentary basis, high impedance grounding will be effective for most merchant ship applications. This is based on the shipboard power distribution system not being exceptionally large in size, having transformers to isolate major load capacitances (propulsion converters and associated motors in particular) and remaining at a relatively lower medium voltage level (15 KV and below). Table 5 illustrates this design sensitivity to the system capacitive charging current for basic merchant ship designs at the two medium voltage classes with and without transformer isolation for propulsion loads.

Accordingly, high impedance grounding becomes questionable for merchant ships with a larger power system at higher medium voltages or if no transformer isolation is provided for propulsion loads. If the shipboard power system for merchant ships develops excessive capacitive charging current, the electric plant will have to be segregated into reasonable system sections to accommodate the high impedance grounding fault current limitations. Hopefully, such subdivision of the shipboard electric plant would reduce the individual system capacitive charging current enough to preclude the use of low resistance grounding. Although it would not normally be necessary, a by-pass capacitor could be used to lower the system capacitive charging current if transformer isolation of propulsion loads was not reasonable.

Other high impedance grounding design aspects concerning the number and location of grounding points (all power sources or most switchboards) and resistor size (limiting current for an entire system or a specific equipment or system section) remain subject to the preference of the designer and tailoring to the shipboard application. Service vessels, utility ships, cargo ships and tankers that have very little ship service load with respect to the ship propulsion load usually ground at the generator. This occurs because of the fewer generators required to power the ship and the minimal capacitance from loads and associated cabling. Icebreakers (such as the USCG HEALY - WAGB 20) or other ships requiring greater reliability may elect to install grounding at several switchboards that are sized for the

entire system. This precludes the possibility of not having a full system ground available.

Generators tend to dominate the system capacitance for cruiseships since many of the major loads, except for a few large high voltage service motors, are isolated via transformers located near the main switchboards. As a result cruiseships often ground each generator individually. Grounding can also occur at shipboard switchboards whenever a better economy of fewer grounding points is desired due to the significant quantity of generators, including feedback ship service transformers, or the lack of system capacitance dominance by the generators.

GENERAL NAVAL SHIP GROUNDING APPLICATIONS

The design of power distribution systems at medium voltage levels for naval ships is very similar to that for merchant ships. Naval ships do, however, require a much greater power level for combat systems and larger propulsion loads. Survivability after battle damage and a higher a degree of reliability to address the minimal manning for maintenance on long term deployments is another key difference between naval and merchant ships. Thus most naval ship grounding designs will be similar to those for

TABLE 5
SYSTEM CAPACITIVE CHARGING CURRENT[+] FOR GENERIC MERCHANT SHIP APPLICATIONS[4]

SYSTEM VOLTAGE	SHIP TYPE & TOTAL POWER	CHARGING CURRENT
	(in MW)	PROPULSION CONFIGURATION XFMR DIRECT*
5,000 V	Service Vessel – 5	1.3 A 4.6 A
	Utility Ship – 10	2.7 A 7.4 A
	Tanker – 15	3.8 A 10.8 A
	Icebreaker** – 20	5.4 A 5.4 A
	Cruiseship – 30	7.2 A 21.2 A
15,000 V	Service vessel – 5	3.9 A 13.8 A
	Utility Ship – 10	8.1 A 22.2 A
	Tanker – 15	11.4 A 32.4 A
	Icebreaker** – 20	16.2 A 16.2 A
	Cruiseship – 30	21.6 A 63.1 A

* synchronous   ** cycloconverter
[+] no major HV service motor loads considered

merchant ships, but the design emphasis may change from economically obtaining an acceptable level of reliability that protects the system to maximizing reliability and survivability at greater power levels.

Certainly the possibility of loosing a ground or not having a ground available would be unacceptable for any naval ship. Most high impedance grounding approaches used for merchant ships preclude this possibility by providing multiple ground points at generators or switchboards. Some naval auxiliaries can use either of these grounding options for merchant ships. However, naval combatants must have a grounding design that maintains a maximum level of reliability, as some merchant ships do, to optimize survivability during battle. Any auxiliaries could also be designed this way if their service or payload warranted such optimization of the grounding design for greater survivability.

GROUNDING APPLICATIONS WITH USN NAVAL SHIPS

One of the latest research and development programs ongoing within the US Navy is an all electric ship concept called the Integrated Power System (IPS). IPS is a fully integrated power generation/distribution, ship propulsion and ship service electric plant design formulated for future USN surface ships (such as the DD21 or 21ST Century Combatant).

The prototype IPS propulsion configuration[5] is at 5 KV without transformer isolation of the propulsion loads to minimize space, weight and cost impacts. The capacitive charging current of these IPS propulsion loads will cause some difficulty in developing a continuous duty high impedance grounding design for most naval combatants (particularly amphibious ships and aircraft carriers as shown in Table 6). Further development of the prototype IPS configuration at a higher medium voltage levels will further exacerbate this aspect for any USN naval ship design and likely split the shipboard electric plant into several segments. Even at the 5 KV voltage level, this IPS configuration would require an aircraft carrier to split its shipboard electric plant into several segments, too. Although higher voltages are better suited to deliver the larger amount of power required for aircraft carriers, it is unlikely that this IPS configuration without isolation for propulsion loads could be applied to an aircraft carrier at higher medium voltages. However, the addition

of transformers to isolate these IPS propulsion loads would make a segmented shipboard electric plant possible for aircraft carriers at higher medium voltages. Similarly, this IPS configuration with isolation transformers would improve the prospect of providing a singular shipboard electric plant at lower medium voltages.

Another limitation with the prototype IPS propulsion configuration stems from the PWM power converter itself and the lack of transformer isolation for the propulsion loads. The penalty of using a PWM power converter is the required transformer isolation of the propulsion loads or split in the shipboard electric plant to prevent the entire loss of propulsion upon a ground fault condition. This means that an IPS design configuration consisting of an odd number of generators and an even quantity of propulsion motors (such as three generators and two motors as expected for a destroyer) cannot provide the full rated propulsion power available and yet prevent risking a complete loss of propulsion.

TABLE 6
SYSTEM CAPACITIVE CHARGING CURRENT[+]
FOR GENERIC
USN NAVAL SHIP APPLICATIONS

SYSTEM VOLTAGE	SHIP TYPE & TOTAL POWER	CHARGING CURRENT	
	(in MW)	PROPULSION CONFIGURATION	
		XFMR	DIRECT*
5,000 V	Destroyer – 60	3.8 A	9.2 A
	Auxiliary – 40	2.7 A	6.3 A
	Amphibious – 60	6.3 A	11.4 A
	Aircraft Carrier – 210	15.2 A	34.1 A
15,000 V	Destroyer – 60	11.4 A	27.6 A
	Auxiliary – 40	8.1 A	18.9 A
	Amphibious – 60	18.9 A	34.2 A
	Aircraft Carrier – 210	45.6 A	102 A

* PWM
[+] no major HV service motor loads considered

CONCLUSIONS

USN naval ships must use high impedance grounding in a manner similar to that employed on merchant ships. High impedance grounding for USN naval ships must be installed at and resistors sized for each generator or major switchboard to maintain acceptable simplistic grounding continuity and flexibility for all the shipboard electric plant configurations possible.

For IPS to be universally applicable to all USN naval ships, the issue of propulsion continuity must be addressed. Smaller USN

naval ships with a prototype IPS configuration (i.e., no transformer isolation for propulsion loads) must devise a coordinated control scheme that provides segregation of the shipboard electric plant before the PWM converter can protectively shutdown upon a ground fault condition. This permits operation of an IPS electric plant in its entirety whenever the system capacitive charging current is less than 10 A and diminishes the concern for odd numbers of generators powering even quantities of propulsion motors in a split plant mode.

Thus, most smaller USN naval ships with IPS as presently configured will be able to achieve full rated propulsion power as a singular electric plant without risking complete loss of propulsion. This would at least permit many other larger USN naval ships, except aircraft carriers, with IPS to retain sufficient propulsion reliability and provide cruise mode economy as a singular electric plant. Aircraft carriers with IPS must avoid this propulsion continuity issue via isolation transformers for the propulsion loads. This should not be too difficult since these ships as well as other large naval ships have the space to accommodate isolation transformers. Such a design configuration change to the prototype IPS has the added benefit of reducing the capacitive charging current. Accordingly, full rated propulsion power would be more achievable as a singular electric plant on most USN naval ships. However, the additional space and weight impact of these isolation transformers may be prohibitive for smaller USN naval ships.

REFERENCES

[1] IEEE STD-142-1991, "IEEE Recommended Practice for Grounding of Industrial and Commercial power Systems"

[2] Irwin Lazar, "Electrical Systems Analysis and Design for Industrial Plants", McGraw-Hill Book Company

[3] J.R. Dunki-Jacobs, "The Reality of High Resistance Grounding", 23RD Annual Petroleum and Chemical Industry Conference, 30-31 August 1976, Philadelphia, PA, USA

[4] Baldwin Bridger, JR. & Wallace E. DeHart, "High Resistance Grounding", IAS Annual Meeting,1977

[5] LCDR Timothy McCoy & Dr. Makhlouf Benatmane, "An Overview of the U.S. Navy's Integrated Power System Development Program", ICEM '98 Conference, 1 September 1998, Istanbul, Turkey

A Framework for Electric Survivability of Electric Shipboard Distribution Systems

D. Niebur, C. Nwankpa, R. Fischl, H. Kwatny

Center for Electric Power Engineering
Drexel University
Philadelphia, PA 19104

Abstract

This paper presents a framework for security and survivability evaluation of shipboard power systems. We further discuss some inherent similarities between terrestrial and shipboard power systems. Though these similarities exist it will pointed out that shipboard power systems are unique with its security and survivability evaluation differing substantially from the process accepted in their terrestrial counter parts.

1. Objectives

It is the objective of this paper to establish a framework for shipboard power system security and electric survivability assessment as part of a future autonomous shipboard management system.

Autonomous shipboard electric power system operation is one of the major goals of the Navy in order to ensure safe, reliable and economic system operation. We discuss our approach in the context of a novel architecture of shipboard electric distribution systems commonly referred to as the integrated power system (IPS). This architecture consists of generation and propulsion blocks, service distribution blocks and zonal distribution blocks, each of them comprising of individual power system components such as generators, machines, transformers and converters. These future shipboard systems are currently in the design phase and the dynamic behavior of the electric shipboard system and its implications on ship security, vulnerability and survivability are yet to be explored.

Because electrical modeling and simulation and experimental evaluation techniques are fairly well known for terrestrial power systems, it is reasonable to assume, that part of them can be used to model shipboard power distribution systems which thus become excellent candidates for shipboard automation. However, because DC systems represent only a very small part of terrestrial power systems, modeling of terrestrial power systems traditionally concentrates on AC (usually 60 Hz) modeling aspects. This is different for shipboard systems where the electric networks serves important DC loads in addition to an AC component operating at several frequency levels thus involving several time scales.

In this paper we look at terrestrial power system security models and discuss their range of validity for electric

shipboard system security and survivability. We further explore how to analyze areas where terrestrial system models are not valid. The ultimate goal of this approach is to define an electric security and survivability hierarchy which incorporate the complex nature of the multi-time scale environment of the shipboard electric distribution system.

2. Methodology

Terrestrial power systems have a long tradition of modeling and simulation. Models and software for state estimation, line overflow detection, outage and vulnerability prediction and dynamic system simulation are standard tools used by many electric utilities on a daily basis (see Balu et al., 1992 for an overview on the presented concepts). However, not all modeling assumptions in terrestrial power systems are valid for shipboard power systems. The following phenomena exist in both terrestrial and shipboard systems but their impact on the sensitivity, accuracy or complexity of the electric model system is different:

a) Low electric inertia.
b) Strong harmonic interaction.
c) Power quality.
d) System restoration.
e) Operational control of AC-DC coupling

For example operational control of the shipboard distribution AC and DC equipment may be comparatively simple, but the level of detail modeling needed is much higher than that done in terrestrial power system studies. Power quality issues may be of higher priority in shipboard power systems and requirements for system restoration may be in the order of 100 ms instead of times up to several hours for private customers in terrestrial distribution systems (see Butler et al, 98). On the other hand terrestrial power system restoration is a hard combinatorial problem because of the large number of possible configurations. Harmonic interaction in steady state are still of minor albeit increasing importance to terrestrial utilities and only recently some efforts were dedicated
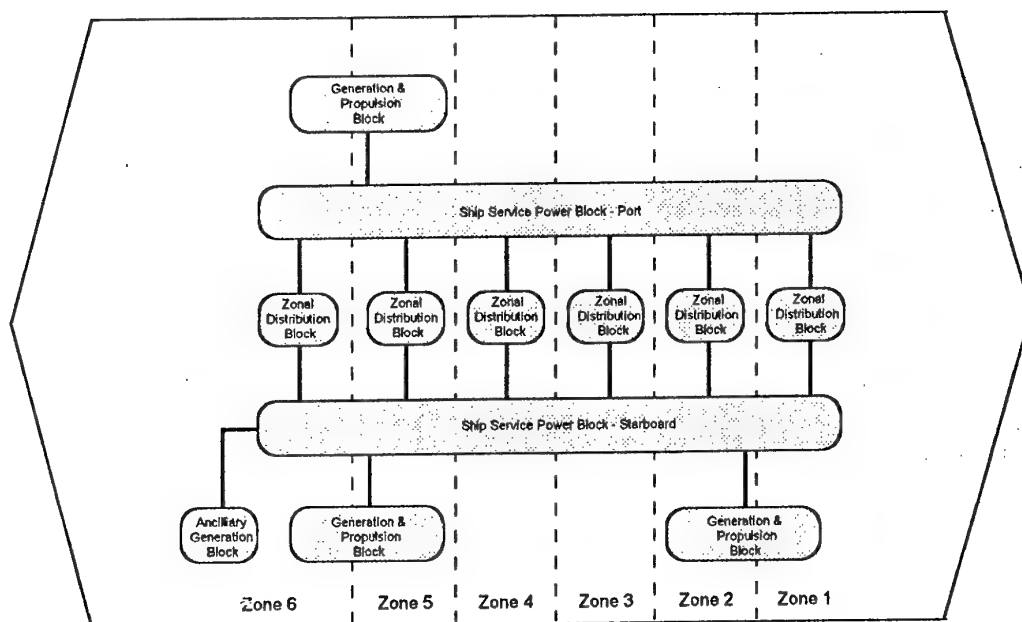
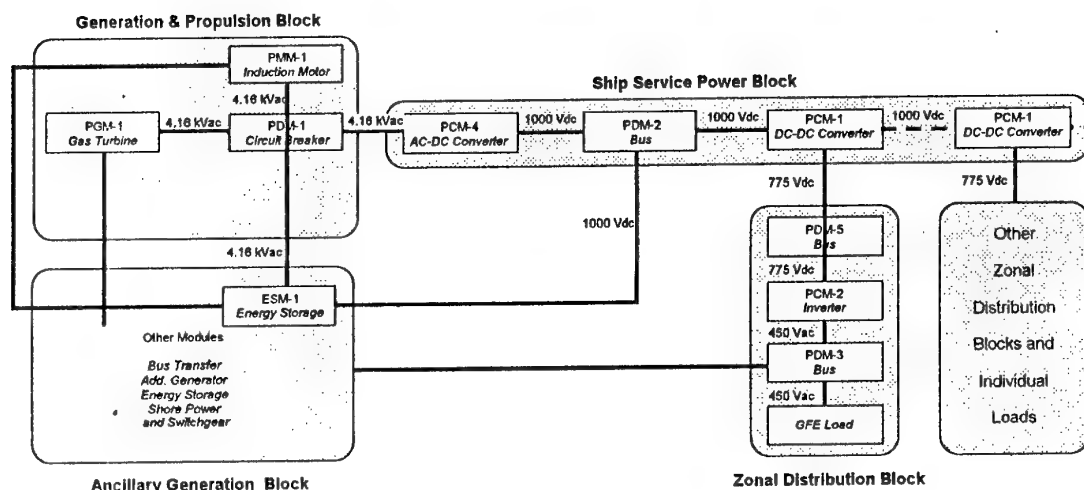*Figure 1:* Zonal Architecture of the Integrated Power System

Figure 2: Configuration of IPS blocks

to modeling of harmonics for dynamic stability (see Lefebvre et al., 95). For shipboard systems however, harmonic dynamics have a salient impact on the system performance because of the comparatively large number of power electronic equipment used for the AC-DC operation of the system.

The success of terrestrial *Energy Management Systems (EMS)* in maximizing the performance of *terrestrial electric power systems* in terms of reducing the number of power blackouts and brownouts and operating the system at minimum cost is well known. The main function of the EMS system is to improve the power

system's security at minimum cost, that is minimize the probability of losing load due to unexpected disturbances. This is achieved by a methodology called *security assessment (SA) and security enhancement (SE)*.

The key to SA and SE is the characterization of all the power system's operating points by a set of security levels (called *security states*) which are defined in terms of the type of operating limits that are either satisfied or violated under a set of contingencies, see Stott *et al.* 1987. For terrestrial power systems these security limits are traditionally discussed for the AC

41

system only although with the integration of FACTS devices the focus is shifting to the DC system as well as the AC/DC coupling. The security limits are given as thermal, voltage, frequency and stability limits. Note that system security is traditionally measured in terms of the number of contingencies it can withstand. This represents the system's electric robustness.

With respect to shipboard power systems it is necessary to state differences that exist between the terms security and survivability. Shipboard power system security can be looked upon as an analogy to its terrestrial counterpart. Survivability can be viewed as power system security with naval specific constraints, static and/or dynamic. For example, a given ship's power system may be considered secure in the traditional sense but non-survivable if its zones cannot operate in isolation of one another for a given period of time. The reverse may also hold true. We focus on the concept of electric security and survivability assessment from the shipboard system's perspective by discussing statically and dynamically secure and insecure states for the AC-DC system with respect to the different time scales of the electric system. We rely on the terrestrial power system model and techniques whenever this is appropriate, see Niebur and Fischl, 1997. This framework will be implemented through

- Definition of electric security and survivability limits for the static and dynamic AC and DC system.
- Determination of the possible power system security states and security levels.
- Assessment of the data pool necessary to be monitored in order to determine the security levels.
- Definition of the underlying electrical model in order to simulate and predict electric security and survivability states and levels.

To develop an EMS which is able to assess the electric security and survivability of the shipboard power system, one needs to develop simple accurate static and dynamic AC and DC models. This is a nontrivial task, since a study by [Belkhayat et al., 1995] has shown that depending on the system parameters, a dynamic model of a simple non-linear shipboard power system comprising of a single non-linear load may exhibit unstable behavior, bifurcation and limit cycles. These phenomena were also identified by us when performing analytical studies of the dynamics of a small terrestrial power system [Kwatny, Fischl and Nwankpa, 1995].

3. Integrated Power System Architecture

The Integrated Power System Architecture (IPS) consists of blocks and modules which provide electrical power for propulsion and ship service loads for a wide range of ships including submarines, surface combatants, aircraft carriers and others, [Doerry and Davis, 1994]. Figure 1 shows the schematic architecture of the IPS.

In this example, the ship is divided into 6 zones, which are supplied by 6 independent zonal electric distribution system blocks (ZDB). Two distribution circuits on the port and the starboard side connect these ZDBs which are supplied by 3 independent generation and propulsion blocks as well as an ancillary generation block, see Clayton, 1998. The modular approach improves reliability and survivability of the ship.

Figure 2 shows the configuration of the four (4) IPS Building blocks: Generation and Propulsion Block, the Ship Service Power Block, the Zonal Distribution block and the Ancillary Generation Block. Each IPS block further consists of up to 7 different generic modules: A power generation module (PGM), a power distribution module (PDM), a power conversion module (PCM), a power load module (PLM), a propulsion motor module (PMM), an energy storage module (ESM) and a system control module (SCM) (not shown), which consists of software packages.

4. Security Framework

In Figure 3 we show the AC system, DC system and their diverse coupling as they occur in Zone 2, 5 and 6 of the example. (The system and coupling aspects are simpler for the other zones.) Thus the security framework of the ship system will be discussed on the following hierarchy levels shown in Figure 4:

1. AC/DC coupling system
2. AC/AC coupling
3. AC system
4. DC/DC coupling
5. DC system

With respect to AC/DC Coupling Security the main problem is over-voltage or over-current security (depending on the converter type, Voltage Source Inverter (VSI) or Current Source Inverter (CSI) resp.)

It should be noted that the AC/DC Coupling Security is on a higher security level than the individual AC Security and DC Security. The reason for this is the main assumption that a power system is considered intact, when both AC and DC systems are electrically connected to each other. This implies the time-scales of these two systems must be of a shorter time frame then the coupling. In Clayton, 1998, the time-scale was specified to be in the order of milliseconds.

AC/AC and DC/DC Coupling involves similar problems as the AC/DC Coupling, i.e. over-voltage and over-current problems.
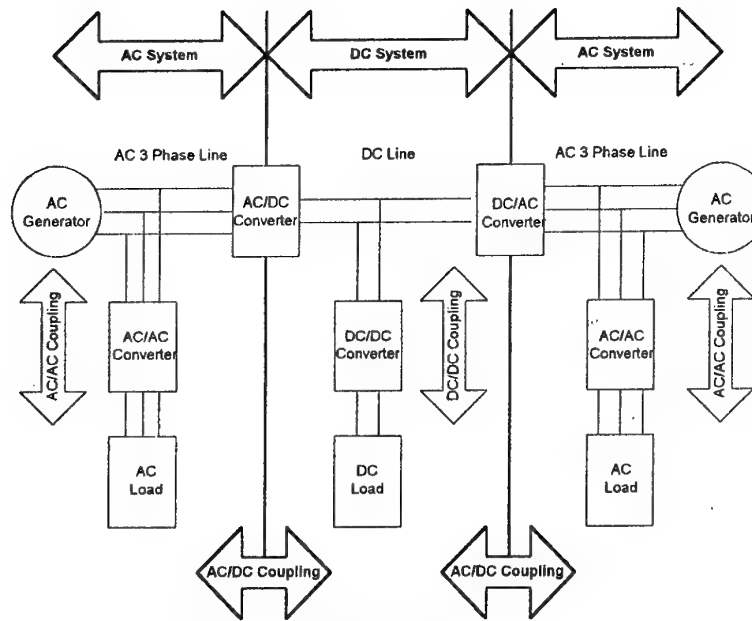
Figure 3: IPS Subsystems and Coupling

For all three coupling types we have to consider the switch characteristics which include dv/dt and di/dt limits.

In the context of system security and survivability, the level of importance of harmonic effects is lower than the afore-mentioned. Harmonic distortion falls into the class of system reliability. However on the component level, harmonics is a security problem.

With respect to the AC System, see Figure 4, security involves problems consisting of overloads, voltage, small signal and transient stability problems, etc. These security limits are extensively discussed in the terrestrial power system literature, see Balu *et al.*, 1992. In addition to the above security issues DC System security also involves current stability.

With respect to the AC Component Security evaluation one is referring to problems associated with loads: voltage drops, speed-up/speed-down, frequency problems, etc. The same holds true for DC Component security evaluation except for non-existence of frequency problems.

What has been mentioned and shown in Figure 4 is mainly a classification for shipboard security assessment. Whether control should be implemented in a hierarchical or distributed manner requires further system studies. With respect to the time-scale one would expect a distributed control system to be achievable in a quicker time-frame than hierarchical

control based on computational limitations as well as reliability considerations. In addition the Navy requires that their components be required to operate in isolation for short periods of time which again lends credit to distributed control.

6. Conclusion

In this paper we present a framework for shipboard system electric security and survivability. This framework is essential for shipboard system design, analysis, operation and control. Shipboard electric distribution analysis has traditionally focussed on component analysis. However with the growing complexity and interaction of shipboard AC and DC components, system security can not be directly extrapolated from component performance. With a well-established system security and survivability framework control actions and restorative actions allow state transitions from alert or emergency states to secure states. Benefits of this approach include reduced crew size, more safe, economical and reliable ship operation, energy efficiency, simulation models and tools for emergency prevention and management and ultimately either remote or autonomous ship control.
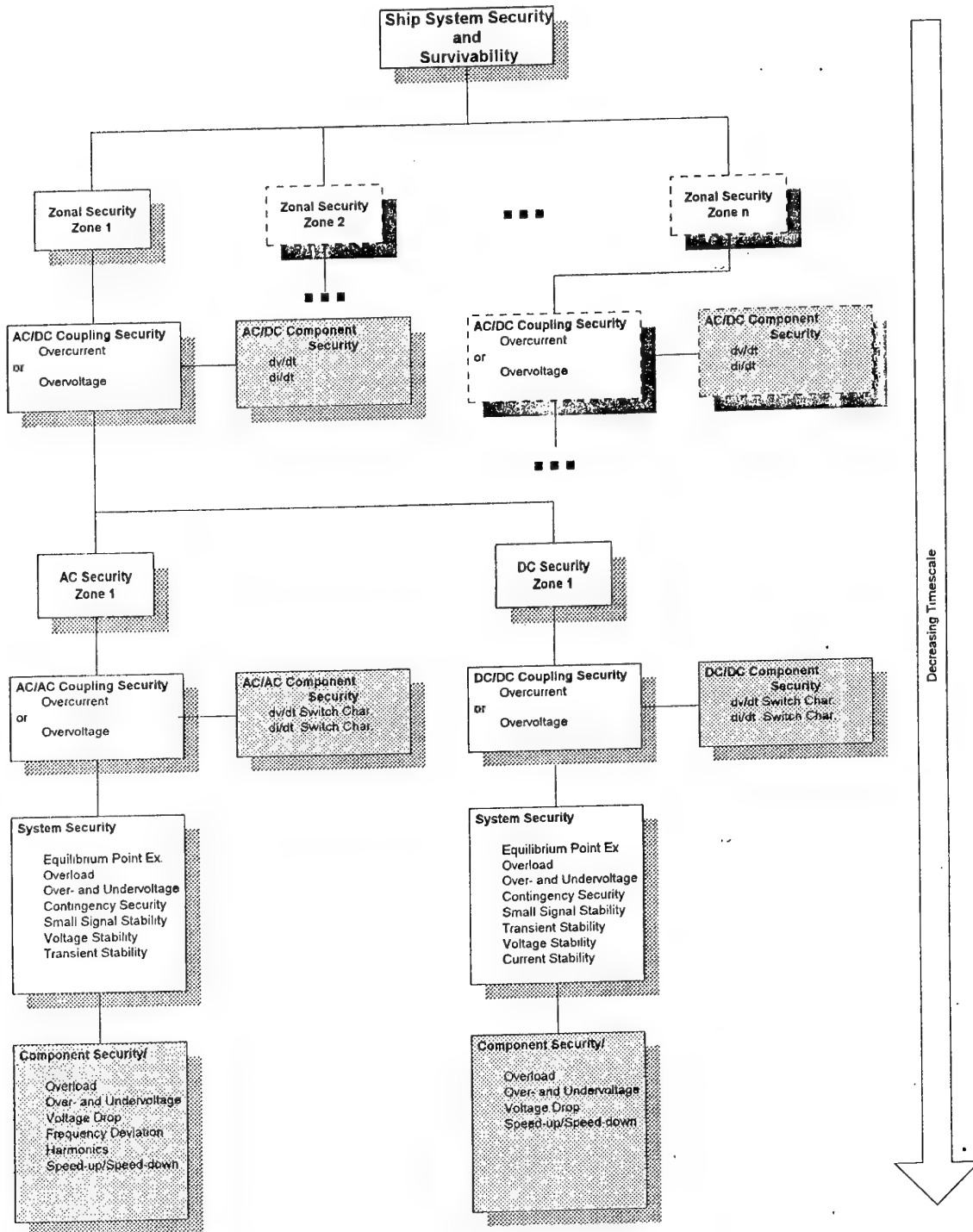
Figure 4: Security Hierarchy

References

1. Balu, N. et al., "On-line power system security analysis," Procs. of the IEEE, Vol. 80, No. 2, Feb. 1992, 262-280.

2. Butler, K., Sarma, N. D. R., Whitcomb, C., Do Carmo, H. and Zhang, H., "Shipboard systems deploy automated protection," IEEE Computer Applications in Power, April 1998, 31-36.

3. Belkhayat, M., Cooley, R. and Abed, E. H., "Stability and dynamics of power systems with regulated converters," *Proceedings of IEEE Int. Symposium on Circuits and Systems*, Seattle, May 1995.

4. Clayton, D., "Integrated Power System (IPS)- Next Generation Navy Power System Architecture" *Proc. of the 1998 ONR-Drexel-NSWC Workshop on Electric Shipboard System Modeling, Simulation and Control*, Drexel University, Philadelphia, PA, June 22-23,1998.

5. Doerry, N. H. and Davis, J. C., "Integrated Power System for Marine Applications," *Naval Engineers Journal*, May 94, 77-90.

6. Kwatny, H. G., Fischl R. F. and Nwankpa C. O. "Local bifurcation in power systems - Theory, computation and application," *Proceedings of the IEEE*, Vol. 83, No. 11, Nov. 1995, 1456-1483.

7. Lefebvre S., Gole A. M., Reeve, J., Pilotto, L., Martins, N. and Bhattacharya, S., "IEEE Working Group on Dynamic Performance: Modeling of DC systems and power electronics for transmission systems - Report on test systems for AC/DC interaction studies," *IEEE Transactions on Power Delivery*, Vol. 10, No. 4, Oct. 1995, 2027-2034.

8. Niebur, D. and Fischl, R., " Power system monitoring and control for naval shipboard distribution systems- phase I," *Report to Naval Surface Warfare Center*, Carderock Division, July 1997.

9. Stott, B., Alsac, O. and Monticelli, A. J., "Security Analysis and Optimization," *Proceedings of the IEEE*, Vol. 75, No. 12, December 1987, 1623-1643.

Performance Analysis of a Shaft Generator System
and Consideration of its Operation Limit

Shoji Nishikata, Yohei Koishikawa, Akihiro Odaka, and Teruo Kataoka

Department of Electrical Engineering, Tokyo Denki University

2-2 Kanda-Nishikicho, Chiyoda-ku, Tokyo, 101-8457 Japan

Abstract

Performance analysis of a main-engine-driven shaft generator system is presented. A set of system equations, by which THD of the output voltage, for example, can be estimated, is derived first, and the system performance including its operation limit is analyzed. It is shown that if reactance of AC reactor is small and the leading angle of commutation of the inverter is large, the operating range of the system is widened with an increase of the THD. A way of considering system losses is then introduced, and it is shown that the maximum output of the system is reduced by at most 20% when the losses are considered. The effects of the leading angle on the characteristics of the field current and the apparent capacity of synchronous condenser are also investigated. The validity of the theory introduced here is confirmed through the experimental investigations with a tested system.

1 Introduction

A shaft generator system is used in a ship to feed sufficient power to the electric apparatus by using a part of the power produced by the main engine [1]. This type of power generating system has been used since 60's mainly in large ships because it can reduce fuel and operating costs. Recently, a large shaft generator system has its capacity as much as some thousand kVA.

A typical shaft generator system is shown in figure 1. Since the speed of the main engine can vary over a wide range when the ship makes a voyage, the output voltage and frequency of the shaft generator driven by the main engine can also be changed. Hence, as in the figure AC power produced by the shaft generator is converted into DC power with the thyristor rectifier, and then the DC power is converted again into AC power with constant voltage and frequency with the externally commutated thyristor inverter. The synchronous condenser, which is connected in parallel with three phase load, is used to provide reactive power for loads and for commutation of inverter thyristors. In the system, an AC reactor to reduce the harmonic

SG : Shaft Generator, SC : Synchronous Condenser, DCL : DC reactor, ACL : AC reactor, REC : Thyristor rectifier, INV : Externally Commutated Thyristor Inverter
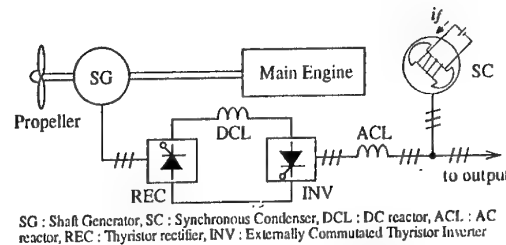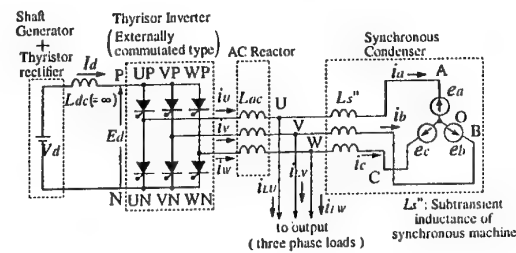
Fig. 1. Shaft generator system.

Fig. 2. Equivalent circuit.

components of the output voltage is also located in the output side of the thyristor inverter. The output voltage and frequency of the system are kept to be constant with controlling the field current and the speed, respectively, of the synchronous condenser. Also, the output voltage of the rectifier is regulated almost constant for a wide range of generator speed with the field current of the shaft generator and/or the firing angle of the thyristor rectifier.

The performance characteristics of the · shaft generator system have been discussed little, and in this paper a detailed analysis of the system considering losses is presented and the operation limit of the system is discussed.

2 System equations

Figure 2 shows the equivalent circuit of the shaft generator system given in figure 1, and this circuit is needed to discuss the steady-state performance of the system. As shown in the figure, the thyristor rectifier in figure 1 is represented as a DC voltage source. The equivalent circuit for synchronous condenser is

obtained by referring to [2]. The armature resistances of the condenser are neglected for the present, and in the event of discussing the system performance with taking the losses into account these resistances will be considered.

We assume here the output terminal phase voltages without jumping and sinking due to commutation of thyristors to be sinusoidal. The voltage equation for U-phase, for example, can be written:

$$e_U = \sqrt{2} V_p \sin\left(\theta - \gamma + \frac{\pi}{6}\right) \quad (1)$$

where, γ is leading angle of commutation, and the origin of θ is chosen to be the instant of the commutation from thyristor WP to UP.

The voltage equations for V-, and W-phases are of also sinusoidal with phase lags of $2\pi/3$, and $4\pi/3$, respectively, with respect to e_U.

U-phase output current i_{LU} can be assumed to be of sinusoidal because most loads are of inductive.

$$i_{LU} = \sqrt{2} I_L \sin\left(\theta - \gamma + \frac{\pi}{6} - \varphi\right) \quad (2)$$

where, φ is lagging angle determined by the load.

V-, and W-phase output currents are sinusoidal with phase lags of $2\pi/3$, and $4\pi/3$, respectively, with respect to i_{LU}.

When the inductance in DC link L_{dc} is very large, output current of the inverter can be regarded as constant in the conducting periods of inverter except for the commutation periods, and e_U can be expressed as

$$e_U = L_s'' \frac{di_a}{dt} + e_a = L_s'' \frac{d(i_U - i_{LU})}{dt} + e_a$$
$$= -L_s'' \frac{di_{LU}}{dt} + e_a \quad (3)$$

Here, e_a is a-phase armature induced voltage of the synchronous condenser and can be assumed to be sinusoidal provided that the condenser has damper windings [2].

Therefore, we have equation for e_a as follows:

$$e_a = e_U + L_s'' \frac{d i_{LU}}{d t}$$
$$= \sqrt{2} V_p \sin(\theta - \gamma + \pi/6)$$
$$+ \sqrt{2} I_L X_s'' \cos(\theta - \gamma + \pi/6 - \varphi)$$
$$\equiv \sqrt{2} V_i \sin(\theta - \gamma + \pi/6 + \varepsilon) \quad (4)$$
$$V_i = \sqrt{(V_p + I_L X_s'' \sin\varphi)^2 + (I_L X_s'' \cos\varphi)^2} \quad (5)$$
$$\varepsilon = \tan^{-1} \frac{I_L X_s'' \cos\varphi}{V_p + I_L X_s'' \sin\varphi} \quad (6)$$

where, $X_s'' = \omega \cdot L_s''$, ω is angular velocity for θ.

Similarly, equations for e_b and e_c are obtained.

From the foregoing equations, we have a phasor diagram of the system from which the relationships among the fundamental components of currents and the voltages in the three phase load, in the output-side of
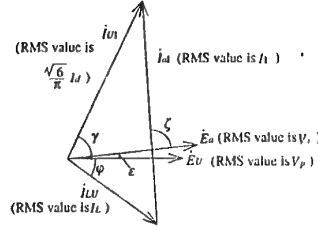

Fig. 3. Phasor diagram.

the inverter, and in the synchronous condenser can be clarified.

Figure 3 shows such a phasor diagram, in which '1' denotes fundamental component. It should be noted that I_{a1} leads $\dot{E}_a$ by $90°$ ($\zeta = 90°$) if losses are neglected. Also, RMS value of $(\sqrt{6}/\pi) \cdot I_d$ for I_{U1} is derived from the trapezoidal waveform of inverter output currents [2].

From figure 3, RMS value of the armature current of the synchronous condenser is

$$I_1 = \sqrt{\left(\frac{\sqrt{6}}{\pi} I_d\right)^2 + I_L^2 - 2\frac{\sqrt{6}}{\pi} I_d I_L \cos(\gamma + \varphi - u/2)} \quad (7)$$

where, u is angle of overlap of inverter output currents.

On the other hand, on referring to figure 2, voltage difference between P and O e_{PO} and current equations in the period of overlap at the commutation from WP to UP, for example, are

$$e_{PO} = L_{ac} \frac{di_U}{dt} + L_s'' \frac{di_a}{dt} + e_a \quad (8)$$
$$e_{PO} = L_{ac} \frac{di_W}{dt} + L_s'' \frac{di_c}{dt} + e_c \quad (9)$$
$$i_U = i_{LU} + i_a \quad (10)$$
$$i_W = i_{LW} + i_c \quad (11)$$
$$i_U + i_W = I_d = \text{constant.} \quad (12)$$

By subtracting (8) from (9), and using (10) - (12) and (4), we have

$$0 = L_{ac} \frac{d}{dt}(i_W - i_U) + L_s'' \frac{d}{dt}(i_c - i_a) + (e_c - e_a)$$
$$= -2(L_{ac} + L_s'') \frac{d}{dt} i_U + L_s'' \frac{d}{dt}(-i_{LW} + i_{LU}) + (e_c - e_a)$$
$$= -2(L_{ac} + L_s'') \frac{d}{dt} i_U + (e_W - e_U) \quad (13)$$

Based on this equation, the inverter current in incoming phase i_U can be obtained as follows:

$$i_U = \frac{1}{2(X_{ac} + X_s'')} \int_0^\theta \left(-\sqrt{6} V_p \sin(\theta - \gamma)\right) d\theta$$
$$= \frac{\sqrt{6} V_p}{2(X_{ac} + X_s'')} \left(\cos(\theta - \gamma) - \cos\gamma\right) \quad (14)$$

where, $X_{ac} = \omega \cdot L_{ac}$.

Since i_U becomes I_d when the commutation is completed at $\theta = u$, we have the relationship between I_d and u:

$$u = \gamma - \cos^{-1}\left(\frac{2(X_{ac} + X_s'') \cdot I_d}{\sqrt{6} V_p} + \cos\gamma\right) \quad (15)$$

On the other hand, by adding (8) and (9), and using (10) - (12) and (4), we get

47

$$e_{PO} = \frac{1}{2}(e_a + e_c) + \frac{1}{2}L_s'' \frac{d}{dt}(i_a + i_c)$$
$$= \frac{1}{2}(e_a + e_c) - \frac{1}{2}L_s'' \frac{d}{dt}(i_{LU} + i_{LW})$$
$$= \frac{1}{2}(e_U + e_W) \tag{16}$$

By using (10) - (12) and (4), phase voltages e_{UO} and e_{WO}, and line-to-line voltage e_{WU} are expressed as

$$e_{UO} = e_{PO} - X_{ac}\frac{d}{d\theta}i_U = \frac{e_U + e_W}{2} - \frac{X_{ac}}{2(X_{ac} + X_s'')}(e_W - e_U)$$

$$= e_U - \frac{X_s''}{(X_{ac} + X_s'')}\frac{\sqrt{6}V_p}{2}\sin(\theta - \gamma)$$

$$= e_U + X_s''\frac{di_U}{d\theta} \tag{17}$$

$$e_{WO} = e_{PO} - X_{ac}\frac{d}{d\theta}i_W = e_W + X_s''\frac{di_W}{d\theta} \tag{18}$$

$$e_{WU} = e_{WO} - e_{UO} = 2X_{ac}\frac{d}{d\theta}i_U$$

$$= -\frac{X_{ac}}{(X_{ac} + X_s'')}\sqrt{6}V_p\sin(\theta - \gamma)$$

$$= \frac{X_{ac}}{(X_{ac} + X_s'')}\cdot(e_W - e_U) \tag{19}$$

Similar manner is used to obtain the voltage equations for the other commutation periods.

In the meanwhile the average value of inverter dc side voltage E_d can be expressed by :

$$E_d = \frac{3\sqrt{6}}{\pi}V_p\frac{(\cos\overline{\gamma - u} + \cos\gamma)}{2} \tag{20}$$

Based on the equations derived above, we can discuss the steady-state performance of the system as well as the quality of the output terminal voltage.

3 THD of output voltage and operation limit

Figure 4 (a) shows an example of measured output voltage waveform of tested shaft generator system. In the tested system, the synchronous condenser is of salient-pole type with damper windings, and its ratings are : 2.77kVA, 200V, 50Hz, 4 poles ($X_s'' = 1.77\Omega$). In this case $X_{ac} = 1.32\Omega$, $V_d = 220$V, $I_d = 6.2$A, and $\gamma = 45°$. It is shown that there are voltage jumping and sinking caused by commutation of inverter thyristors. The calculated waveform for the measured waveform in figure 4 (a) is given in figure 4 (b). It can be seen that the calculated waveform coincides well with the measured one, supporting the validity of the theory introduced here.

The total harmonic distortion (THD) of the output voltage is given by the ratio of the distortion component in the output voltage V_h to the fundamental component V_1. Thus

$$THD = V_h/V_1 = \sqrt{V_0^2 - V_1^2} / V_1 \tag{21}$$

where, V_0 : RMS value of output terminal phase voltage.

From voltage equations derived in the foregoing section, we have the equation for V_0 :
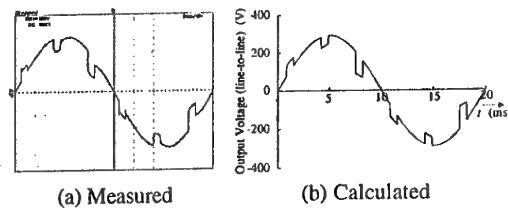
(100V/div, 2ms/div)

(a) Measured   (b) Calculated

Fig. 4. Output voltage waveforms (line-to-line)

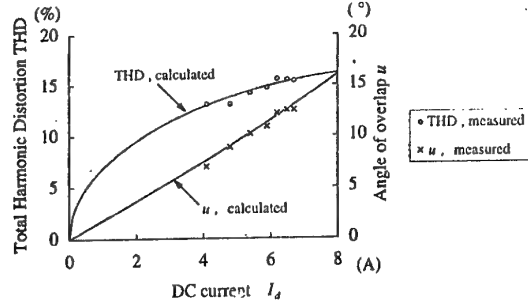$X_s'' = 1.77\Omega$, $X_{ac} = 1.32\Omega$, $\gamma = 45°$, $\sqrt{3}V_0 = 200$V, 50Hz

Fig. 5. THD and u vs. I_d.

$$V_0 = V_p\sqrt{1 + \frac{2}{\pi}(k^2 - \sqrt{3}k)(u - \sin u\cos\overline{2\gamma - u})} \tag{22}$$

where, $k = \frac{\sqrt{3}}{2}X_s'' / (X_{ac} + X_s'')$.

For the fundamental component of the output voltage V_1, we get

$$V_1 = \sqrt{a_1^2 + b_1^2} / \sqrt{2}$$

$$= V_p\sqrt{\left(1 + \frac{\sqrt{3}}{\pi}k(-u + \sin u\cos\overline{2\gamma - u})\right)^2}$$

$$\qquad + \frac{3}{\pi^2}k^2\sin^2 u\sin^2\overline{2\gamma - u} \tag{23}$$

where,

$$a_1 = \sqrt{2}V_p\left(-\sin\overline{\gamma - \frac{\pi}{6}} + \frac{\sqrt{3}k}{\pi}\cdot\left(\sin\overline{\gamma + \frac{\pi}{6} - u}\sin u + u\sin\overline{\gamma - \frac{\pi}{6}}\right)\right) \tag{24}$$

$$b_1 = \sqrt{2}V_p\left(\cos\overline{\gamma - \frac{\pi}{6}} + \frac{\sqrt{3}k}{\pi}\left(\cos\overline{\gamma + \frac{\pi}{6} - u}\sin u - u\cos\overline{\gamma - \frac{\pi}{6}}\right)\right) \tag{25}$$

Accordingly, THD can be expressed as :

$$THD = \sqrt{\frac{1 + \frac{2}{\pi}(k^2 - \sqrt{3}k)(u - \sin u\cos\overline{2\gamma - u})}{\left(1 + \frac{\sqrt{3}}{\pi}k(-u + \sin u\cos\overline{2\gamma - u})\right)^2 + \frac{3}{\pi^2}k^2\sin^2 u\sin^2\overline{2\gamma - u}} - 1} \tag{26}$$

It should be noted here that THD for line-to-line voltage is the same as (26).

In figure 5 the measured and calculated characteristics of THD of the output voltage and angle of overlap u are shown for various values of dc input current I_d. In this case, the condition except I_d was the same as in figure 4, and RMS value of output terminal line-to-line voltage was 200V (constant). A set of R-L load, in which its power factor was not always constant, was used in the system. It is shown that a good agreement between the measured and calculated results is obtained.
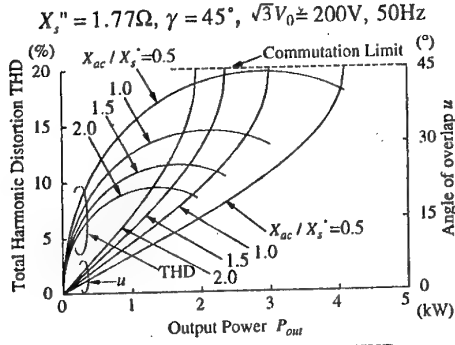
$X_s'' = 1.77\Omega$, $\gamma = 45°$, $\sqrt{3}V_0 \fallingdotseq 200V$, 50Hz

Fig. 6. Effects of X_{ac} on u and THD.

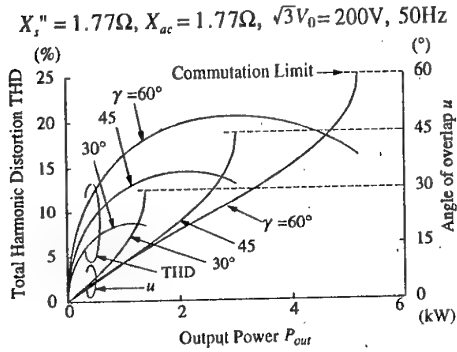$X_s'' = 1.77\Omega$, $X_{ac} = 1.77\Omega$, $\sqrt{3}V_0 = 200V$, 50Hz

Fig. 7. Effects of γ on u and THD.

Let us now explore the effects of the reactance of AC reactor X_{ac} and the leading angle γ on THD and u, and clarify the operation limit of the system.

In figure 6, the characteristics of THD and angle of overlap u versus output power of the system P_{out}, which is equal to the input power to the inverter if losses can be neglected, are shown for various values of X_{ac}. It can be seen from the figure that the smaller X_{ac} is, the wider the operating range becomes, whereas THD increases when X_{ac} is small. From (15) overlapping angle for a large value of X_{ac} becomes larger, resulting in reduction of maximum output as in the figure.

Figure 7 gives the characteristics of THD and u versus P_{out} for various values of leading angle of commutation γ. It is clarified that if γ is large, u becomes small because large commutation voltage is obtained for a large value of γ, and operating range of the system can be widened with an increase of THD.

4 Performance Analysis Considering Losses

Although the equations and calculated results mentioned above are useful in discussing the steady-state performance of the shaft generator system, system losses must be incorporated to the analysis when we desire to obtain more accurate results.

4.1 System Equations Considering Losses

The major loss in the shaft generator system is that of the synchronous condenser. (27) denotes an approximate equation for the synchronous condenser loss, which is composed of a fixed part independent of armature current of the synchronous condenser, and a part regarded as being proportional to the square of the armature current.

$$P_{loss} = P_m + 3 \times \left(I_a^2 \times r\right) \tag{27}$$

where, P_m : fixed loss (mechanical loss + no-load iron loss), I_a : RMS value of the armature current of synchronous condenser, r : equivalent armature resistance including the effects of damper loss and stray load loss (per phase).

Now, input power to the inverter P_{in} is given as

$$P_{in} = E_d \cdot I_d = \frac{3\sqrt{6}}{\pi} V_p \left(\frac{\cos \overline{\gamma - u} + \cos \gamma}{2}\right) \times I_d \tag{28}$$

On the other hand, the equation for the output power P_{out} drawn from the three-phase output terminals of the system is

$$P_{out} = 3V_p I_L \cos \varphi + 3V_p I_L \frac{k}{\pi}\left\{-u\sqrt{3}\cos \varphi \right.$$
$$\left. + \frac{\sqrt{3}}{2}\sin \overline{2u - 2\gamma - \varphi} + \frac{\sqrt{3}}{2}\sin \overline{2\gamma + \varphi}\right\} \tag{29}$$

It is noted that the voltage distortion due to commutation is considered in this equation.

Hence, if the losses in the AC reactor and the inverter are neglected, we have an equation for power balance as

$$P_{in} = P_{out} + P_{loss} \tag{30}$$

Since the inverter output current can be regarded as trapezoid, armature current I_a in (27) is expressed as

$$I_a = \sqrt{\frac{1}{\pi}\left\{\left(\frac{2\pi}{3} - \frac{u}{3}\right)I_d^2 + \pi I_L^2\right\}}{}^*$$
$${}^* \overline{+ \frac{1}{\pi}\left\{\frac{2\sqrt{6}}{u}I_d I_L\left(\sin \overline{\gamma + \varphi - u} - \sin \overline{\gamma + \varphi}\right)\right\}} \tag{31}$$

Also, by using (24) and (25), the relationship between the lagging angle φ in (2) and the power-factor angle of the load φ_L is given by

$$\varphi_L = \varphi + \tan^{-1}\left(a_1 / b_1\right) + \gamma - \pi / 6 \tag{32}$$

Next, let us derive the equations concerning the field current of the synchronous condenser. On referring to [2], RMS value of EMF induced in the armature winding of the condenser V_i is expressed through gap flux linkage Ψ_g :

$$V_i = \omega \Psi_g / \sqrt{2} = p\omega_m \Psi_g / \sqrt{2} \tag{33}$$

$$\Psi_g = \sqrt{\left(L_{af}i_f + k_d\Psi_{d0}\right)^2 + \left(-k_q\Psi_{q0}\right)^2} \tag{34}$$

where, p : number of pair of poles, ω_m : mechanical angular velocity, Ψ_{do}, Ψ_{qo} : flux linkages of d-, and q-axis damper windings, $k_d = L_{add}/L_{dd0}$, $k_q = L_{adq}/L_{dq0}$, L_{af}, L_{add}, L_{adq} : maximum value of mutual inductance

between armature winding (one phase) and field winding, d-axis damper winding and q-axis damper winding, respectively, i_f : field current.

Ψ_{d0} , Ψ_{q0} in (34) are determined by the fundamental component of the armature current in the condenser, and are expressed as

$$\Psi_{d0} = -\frac{3}{2}\sqrt{2}I_1 L_{add} \sin\left(-\alpha + \zeta\right) \qquad (35)$$

$$\Psi_{q0} = \frac{3}{2}\sqrt{2}I_1 L_{adq} \cos\left(-\alpha + \zeta\right) \qquad (36)$$

$$\tan\alpha = \frac{-k_q \Psi_{q0}}{L_{af}i_f + k_d \Psi_{d0}} \qquad (37)$$

As to ζ, we regard as $\zeta < 90°$ when the losses are considered, i. e.,

$$\zeta = \pi - \left(\varphi + \varepsilon\right) - \sin^{-1}\left\{\frac{\sqrt{6}I_d}{\pi I_1} \sin\left(\gamma + \varphi - \frac{u}{2}\right)\right\} \qquad (38)$$

Based on the equations derived above, we can now analyze the system performances when the losses are taken into account.

4.2 Effects of System Parameters on Operation Limit

Figure 8 shows the characteristics of output power and losses versus dc current I_d. In the figure, the measured values and calculated ones with and without considering losses are shown. It can be seen that the calculated values taking the losses into account are close to measured ones, supporting the validity of the theory.

Tables 1 and 2 give the effects of various system parameters on the maximum output power of the system for the cases with and without considering the losses. It should be noted that the maximum power is obtained when commutation failure in the inverter occurs (u becomes γ). In table 1 the effects of X_{ac} are shown, and it can be seen that a large maximum output is obtained for a small value of X_{ac} as expected from figure 6. Table 2 gives the effects of γ, and it is clarified that maximum output is increased when γ is large as seen in figure 7. From these tables the maximum output power is reduced when the losses are considered. Hence, we can say that the losses should be taken into account to obtain accurate results.

4.3 Consideration of Field Current of the Synchronous Condenser

The field current of the synchronous condenser i_f has an important role in controlling the output voltage of the system. Figure 9 shows i_f-I_d characteristics of the tested system for constant output voltage and frequency. It is clear that the calculated results agree well with experimental values, demonstrating the validity of the theory.

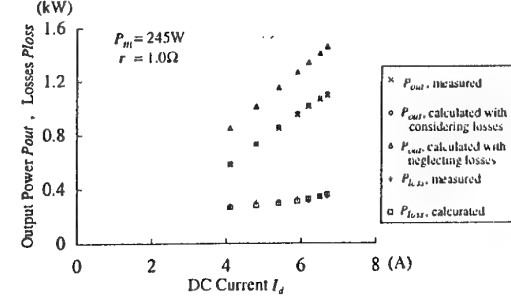$X_s" = 1.77\Omega$, $X_{ac} = 1.32\Omega$, $\gamma = 45°$, $\sqrt{3}V_0 = 200V$, 50Hz

Fig. 8. Output power P_{out} and loss P_{loss} vs. dc current I_d .

Table 1. Effects of X_{ac} on operation limit.
($\gamma = 45°$, $\cos\varphi_L = 0.8$, $\sqrt{3}V_0 = 200V$, 50Hz)

$X_{ac}/X_s"$ ($X_s" = 1.77\Omega$)	Maximum output (opration limit) P_{outmax}(kW)	
	Considering losses	Neglecting losses
0.5	3.50	4.09
1.0	2.55	3.00
1.5	1.98	2.36

Table 2. Effects of γ on operation limit.
($X_s" / X_{ac} = 1.0$, $\cos\varphi_L = 0.8$, $\sqrt{3}V_0 = 200V$, 50Hz)

γ (°)	Maximum output (opration limit) P_{outmax}(kW)	
	Considering losses	Neglecting losses
30	1.11	1.39
45	2.55	3.00
60	4.26	5.18

$X_s" = 1.77\Omega$, $X_{ac} = 1.32\Omega$, $\gamma = 45°$, $\sqrt{3}V_0 = 200V$, 50Hz

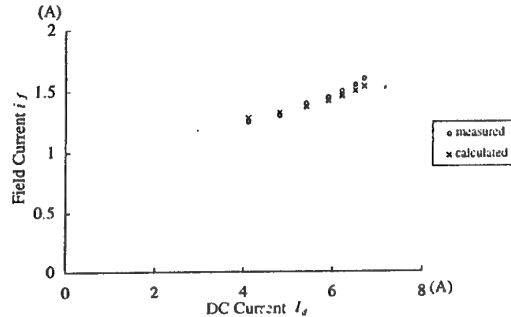
Fig. 9. Field current i_f vs. dc current I_d .

Figure 10 gives the characteristics of i_f versus output power P_{out} for various values of γ. It is shown that i_f should be increased to keep the output voltage and frequency constant when γ is large. This is because the armature current (i. e., armature reaction) of the synchronous condenser becomes large if γ is large, and consequently a large value of i_f is needed.
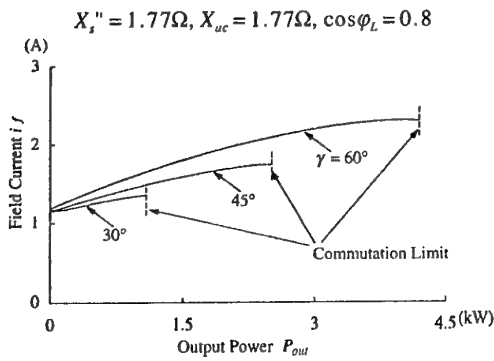
50

$X_s{''} = 1.77\Omega,\ X_{ac} = 1.77\Omega,\ \cos\varphi_L = 0.8$

Fig. 10. Effects of γ on i_f (Output voltage : 200V, 50Hz).

$X_s = 1.77\Omega, X_{ac} = 1.77\Omega,\ \cos\varphi_L = 0.8, \sqrt{3}V_0 = 200V,\ 50Hz$
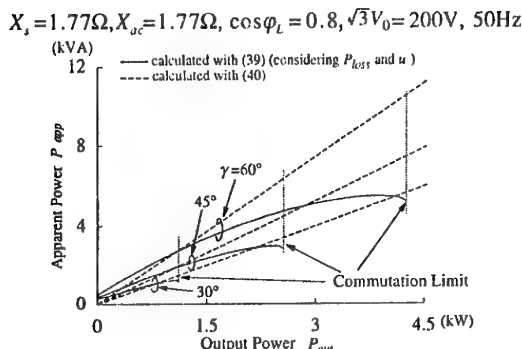

Fig. 11. Effects of γ on P_{app}.

4.4 Consideration of Apparent Capacity of the Synchronous Condenser

In this section, the characteristics of apparent capacity of the synchronous condenser are investigated. By using (22) and (31) the apparent power considering system losses P_{app} is expressed by

$$P_{app} = 3\,V_0 \cdot I_a \qquad (39)$$

On the other hand, for the case when the losses and overlapping phenomena in the inverter are neglected, we have the expression for P_{app} as

$$P_{app} = P_{out}\left(\tan\gamma + \tan\varphi_L\right) \qquad (40)$$

This equation is obtained on the basis of the fundamental component of armature current of the synchronous condenser [3].

Figure 11 shows the characteristics of P_{app} versus system output P_{out} for various values of γ. It can be seen from the figure that the apparent power is increased when γ is large since reactive power required in the inverter is increased for a large value of γ. Also, it is clarified that as P_{out} increases P_{app} calculated with (40) becomes larger than that with (39). This is based on the fact that angle of overlap increases as P_{out} increases, and the armature current considering the overlap becomes smaller when compared with the case of neglecting it.

5 Conclusion

A detailed performance analysis of a shaft generator system has been presented in this paper. A set of system equations, from which THD of output voltage as well as the operation limit of the system can be clarified, has first been derived. Based on the equations, the steady-state performance of the system is investigated. It has been shown that when the reactance of AC reactor is small and the leading angle of the inverter is large, the operating range of the system is widened with an increase of output voltage distortion. A way of taking the system losses into account is then introduced, and the effects of system parameters on the maximum output power have been clarified for the cases with and without considering the losses. It has been shown that the maximum output is reduced by about 14 - 20% when the losses are considered. Moreover, the performance of the field current of the synchronous condenser has been discussed. It has been revealed that the field current should be increased for the case of a large leading angle in order to keep the output voltage and frequency constant. Finally, the effects of the leading angle on the apparent power of the synchronous condenser have been calculated, and it has been clarified that the apparent power becomes large for a large value of leading angle, and that the losses must be considered to know accurate apparent capacity.

Although the equations and calculated results presented in this paper are useful in design and control of the shaft generator systems, such issues as reducing harmonics included in the output voltage without reduction of maximum output power are of importance. Moreover, dynamic performance of the system when loads are connected, for example, is also to be investigated. These are left for future study.

References

[1] J. Nishiyama, H. Kotera, T. Kishimoto, M. Yamaji, M. Tsuji : "Shaft driven AC generator for fixed pitch propeller," Journal of the M. S. J., 13, no. 6, pp.442-449, June 1978.

[2] T. Kataoka, and S. Nishikata, "Transient performance analysis of self-controlled synchronous motor," IEEE Trans. Industry Applications, IA-17, no. 2, pp.152-159, March/April 1981.

[3] I. Asada and S. Itano, "On the motoring mode operation of shaft generator systems," Trans. of Japan Society for Power Electronics, 17, pp.157-162, 1991.

POWER SUPPLY SYSTEM SAFETY FOR AN ELECTRIC SHIP

M. Dumitrescu, T. Munteanu, L. Dumitriu

"Dunarea de Jos" Galati University.
Electrical Engineering Department
Domneasca Street-111, Galati-6200, Romania
Fax 4.036.460182 E-mail: maridum @emae.ugal.ro

Abstract: Generalized stochastic Petri nets (GSPN) are the most commonly state-space model types used in dependability modeling. The great complexity of GSPN models, even for simple repairable systems, makes necessary a less complex model to be used. Combining the GSPN properties and high level Petri nets facilities, a structural simplified model Logical Explicit Stochastic Petri Nets (LESPN), having the same modeling power as GSPN, is built. Primitive architectural modules are used in repairable power systems dependability modeling (but not only). The paper presents a dependability comparative analysis, used in electric ship power plant safety study. Three Electrical Generators-Main Switchboard (EG-MS) coupling alternatives, for the electric ship power plant, are proposed and analyzed.

Keywords: generalized stochastic Petri nets, high level Petri nets, dependability, safety, electric ship power plant .

1. Introduction

Power systems safety study needs, in the designing phase, a set of different alternatives to be modeled. The proposed alternatives have to be fault-tolerant, all their vital elements need an important redundancy level. But the economics facilities play a major role in selecting the best alternative. The two aspects, adequacy and economics, can be consistently appraised by comparing the investment cost needed to achieve a certain level of adequacy, with adequacy worth. This type of economical purpose is a fundamental and important area of engineering applications.

To configure different design alternatives according to reliability criteria is the main problem, of power system safety study. To achieve this goal, a suitable model to configure all the design alternatives is necessary to be developed. Different kind of dependencies within subsystems can to be described by dependability model types. Dependability term means quality, correctness and continuity of service delivered by a system. Dependability encompasses measures as reliability, availability and safety.

Reliability uses several model types, such as reliability block diagrams, fault trees and Markov chains, have been used to evaluate various dependability metrics [4], [5]. These model types differ from one another, not only in the ease of use in a particular application, but in terms of modeling power. Modeling power of a model type is determined by the kinds of dependencies within subsystem to be modeled and the kind of dependability measures to be computed.

Scientific works as [4], [5] established a hierarchy, among the most commonly used types of dependability models, according to their modeling power. The Markov (state-space) model types (continuous-time Markov chains,

GSPN) are more powerful than combinatorial-model types, in that they can capture dependencies, such as a shared repair facility between system components. Markov models and are capable of handling phased missions, state dependent failure rates , common mode failures, physical interconnection dependencies, time dependent transitions, maintenance policies. But to describe the Markov chain (MC) for a complex system, became a very difficult task. In this case a stochastic Petri net (SPN) equivalent to MC, is usually used in modeling power system failure-repair behavior. The GSPN model is the most commonly used because it's ability to use in events modeling both kinds of transitions, timed and immediate transition.

This paper uses a power system dependability model based on GSPN model, but having a simplified structure. The model is used for a dependability comparative study of EG-MS coupling alternatives. A computerized tool, Stochastic Petri Nets Evaluation using Visual basic software, for 586 PC, predicting dependability metrics of complex repairable power system, was developed. Given input data in the form of Petri net structure, elements failure and repair rates and availability logical conditions, for candidate architectures during conceptual design of power system, the computation of the dependability metrics is straight forward .

Section 2 briefly introduces Generalized Stochastic, Logical Explicit Stochastic Petri Nets. Section 3 describes the LESPN simplified models for the EG-MS coupling alternatives. Section 4 gives the dependability metrics of the EG-MS coupling alternatives and makes the safety comparative study.

2. Petri nets in dependability modeling

The dynamic behavior of a system, according to Petri net theory, is determined by the movement of tokens based

on the firing of transition. A transition is enabled to fire if the number of tokens in each of its input places is at least equal to the multiplicity of the corresponding input arc from that place.

A marking of a Petri net is the distribution of the tokens in the set of places of Petri net. Each marking defines a state of the system. A marking is reachable from an original marking, if there is a sequence of transition firings starting from the original marking which results in that marking. The reachability graph (RG) of a Petri net is the set of all markings that are reachable from the initial marking. Most important firing times can be associated with transitions. When the distribution of firing times for all transitions is exponential, the net is a stochastic Petri net (SPN). Ajmone-Marsan [1] proposed in 1984 generalized stochastic Petri nets (GSPN) which allow transitions to have 0 firing time (immediate transitions) or exponentially distributed firing times (timed transitions). SPN and GSPN are equivalent to continuos time Markov chain (CTMC). There are two types of markings for a GSPN: vanishing (at least one immediate transition is enabled in that marking) and tangible (otherwise).

According to [5],GSPN dependability models consist of two subnets:the subnets modeling the stochastic failure-repair events (fig 1.a) and the logical subnets modeling AND or OR logical conditions of system performances (fig 1.b,c).

a

b

c
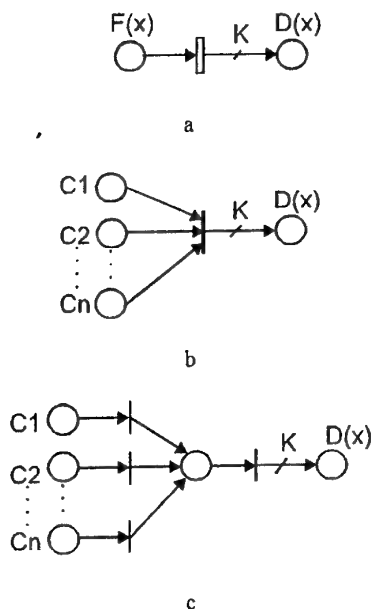
Fig 1. GSPN subnets modeling: a stochastic failure (repair) event (a), a AND logical condition (b), a OR logical condition (c),

This paper uses the new simplified LESPN model [2], extracting from inside GSPN model the logical subnets. The GSPN properties and the colorate Petri net facilities are combined, to create the set of primitive architectural modules. Primitive architectural modules are used to construct a modular architecture for this structural

simplified model, named logical explicit stochastic Petri nets (LESPN), because the logical conditions of system performance are explained outside the SPN model. Including predicate/ transitions nets facilities, a great structural simplification of the model is obtained. The arc label of the colorate Petri net dictates how many and which kinds of "colored" tokens will be removed from or added to the places.

3. Dependability models of EG-MS coupling alternatives

Naval power plant is an isolated system, usually having a single sectioned busbar system. The fault tolerant power system have automatically coupled Diesel generators to different busbar sections, improving the system availability. The Diesel generators are coupled to the MS, according to the three coupling alternatives presented in fig. 2.
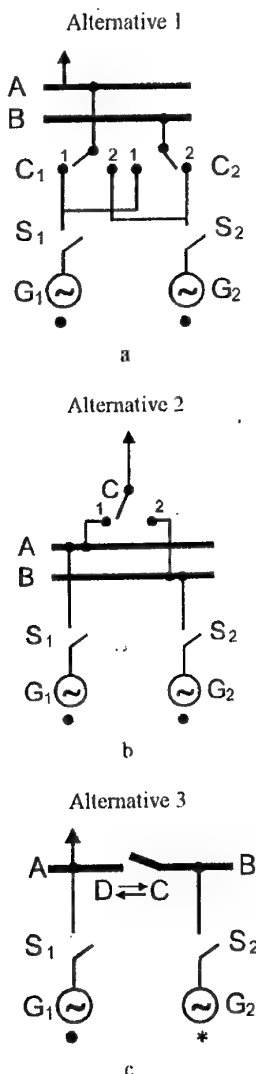
Alternative 1

a

Alternative 2

b

Alternative 3

c

Fig. 2. EG-MS coupling alternatives

53

The behavior, on reliability criteria, of each proposed alternatives 1, 2 and 3 is modeled, in the paper, using the LESPN model, as we can see in fig.3, fig.4, respectively fig.5. For all analyzed alternatives, the logical availability conditions are described in the "PERFORMANCE" table associated to the LESPN model.
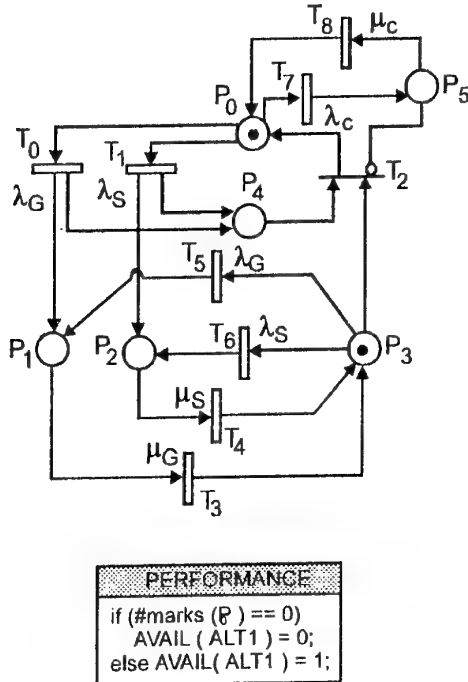
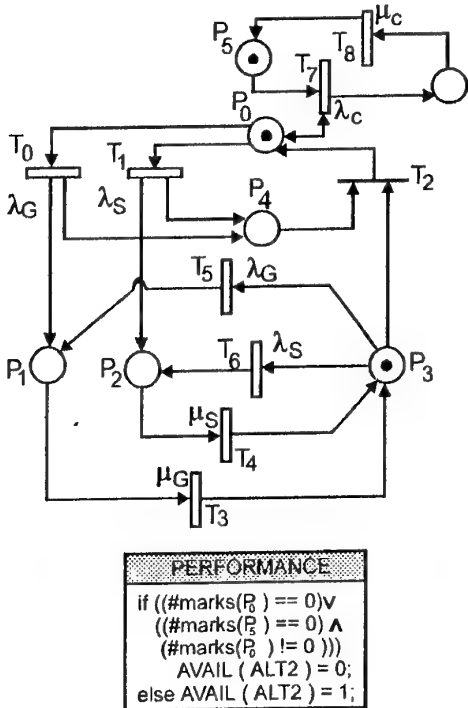The LESPN model for EG-MS alternative1 (fig.3) uses a set of locations modeling: $P_0/P_1/P_3$- the working /the failed/the stand-by generators number, P_4- the failed S switches number, P_5 the fail state of C separator, P_4 the stand-by generator command. The LESPN transitions have the following senses: $T_0, T_5/T_1, T_6/T_7$ -the generator/ S switch/ C separator failure event (conditioned by the good working of a generator), $T_3/T_4/T_8$ -the generator/ S switch/ C separator repair event, T_2 the stand-by generator coupling event (conditioned by the good working of the C separator).

The LESPN model for EG-MS alternative2 (fig.4) uses a set of locations modeling: $P_0/P_1/P_3$- the working /the failed/the stand-by generators number, P_4- the failed S switches number, P_5 the working state of C separator, P_6 the fail state of C separator, P_4 the stand-by generator command. The LESPN transitions have the following senses: $T_0, T_5/T_1, T_7$ -the generator/ S switch/ C separator failure event (conditioned by the good working of a generator), $T_3/T_4/T_8$ -the generator/ S switch/ C separator repair event, T_2 the stand-by generator coupling event (not conditioned by the good working of the C separator).

The LESPN model for EG-MS alternative3 (fig.5) uses a set of four colors (*,•,D,C), a set of predicates/ transition <x>, <y>, <z> and a set of locations modeling: $P_0/P_1/P_2$- the working G-S drives and the C separator state(C- connected, D- disconnected)/the failed generators number /the failed S switches number, P_3 the fail state of C separator. The LESPN transitions have the following senses: $T_0/T_2/T_6$ -the generator/ S switch/ C separator failure event (conditioned by the good working of a generator), $T_1/T_3/T_7$ -the generator/ S switch/ C separator repair event, T_4 the C separator connecting event (conditioned by the failure of a generator), T_5 the C separator disconnecting event (conditioned by the good working of both the generators).
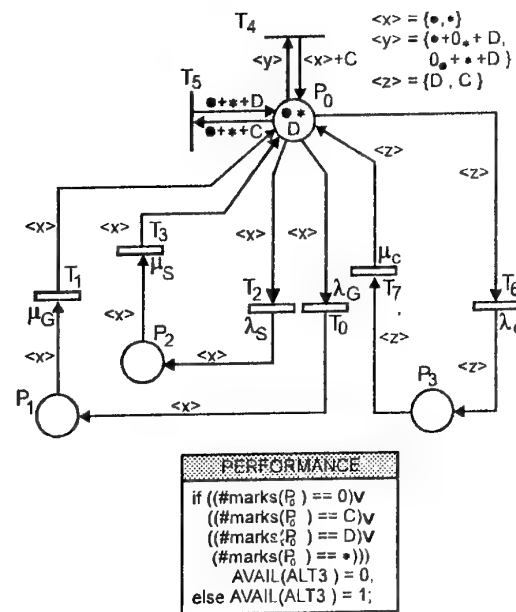

PERFORMANCE

```
if (#marks (P₅ ) == 0)
    AVAIL ( ALT1 ) = 0;
else AVAIL( ALT1 ) = 1;
```

Fig 3.The LESPN model for EG-MS, alternative 1.

PERFORMANCE

```
if ((#marks(P₀ ) == 0)v
    ((#marks(P₅ ) == 0) ∧
    (#marks(P₃ ) != 0 )))
        AVAIL ( ALT2 ) = 0;
else AVAIL ( ALT2 ) = 1;
```

Fig 4.The LESPN model for EG-MS, alternative 2.

PERFORMANCE

```
if ((#marks(P₀ ) == 0)v
    ((#marks(P₀ ) == C)v
    ((#marks(P₀ ) == D)v
    (#marks(P₀ ) == •)))
        AVAIL(ALT3 ) = 0;
else AVAIL(ALT3 ) = 1;
```

Fig 5.The LESPN model for EG-MS, alternative 3.

54

Table 1. Dependability metrics of EM-MS coupling alternatives

	NT/N	NS/NR	P_s	$M[\nu(T_P)]$	$M[\nu'(T_P)]$	$M[\alpha(T_P)]\times E+04$	$M[\beta(T_P)]$
Alternative 1	11/9	3/6	0.99814648	8.38414	53.1243	7.98517	148.2808
Alternative 2	16/12	3/9	0.99814644	8.38415	53.2193	7.98517	148.284
	3/3	1/2	0.99008135	16.7231	0	5.4312	255.37
Alternative 3	32/27	11/16	0.99984377	1.41449	216.072	7.99874	12.5377

4. Dependability comparative study

According to [2] dependability metrics for the EM-MS coupling alternatives, computed with the SPNE tool (considering a planned operational time T_p= 80000 h) are the following: general availability indices as system success probability P_s, system failure probability; and power system availability specific indices (PE 013/ 1994) as, the average of failure total time M [$\alpha(T_p)$], the average of success total time M [β (T_p)], the average of failure interruptions total number M [$\nu(T_p)$], the average of maneuver interruptions total number M [$\nu'(T_p)$] (table 1).

For the dependability metrics evaluation purpose, SPNE tool constructs the reachability graph (RG) of the bounded SPN, the reduced RG (obtained by reducing the vanishing markings), and the MC isomorphic to reduced RG, both modeling the failure-repair behavior of power system design alternative.The SPNE tool constructs the subset: success states, failure states.

Table 1 also shows the number of total / reduced states (NT/N), of success /failure states (NS/NR) associated to the EM-MS coupling alternatives.

For the EM-MS coupling alternative 2, two cases are studied: the complex case, with NR=16 states and N=12 states, considering the consumer availability (conditioned by the good working of the C separator) and the simple case of the MS availability, only. Obviously the complex case in EM-MS alternative2 must be compared with all the other alternatives, because the important task of the analyzed systems is the consumer power supply.

Comparative study results leads to the conclusion that the EM-MS elternative3 has the best availability indices. To achieve this goal a very large number of maneuvers, compared to the other alternatives, must be done. But an important increase of the electric ship power supply system safety is obtained.

5. Conclusions

The structural simplified model (LESPN), having the same modeling power as GSPN is more practical for engineering applications, more easy to understand and also very adequate in power system dependability modeling. Extracting the logical subnets from inside the GSPN model, the vanish markings and the immediate transitions associate to logical conditions does not appear in the reachability graph RG. Obviously the states number N, modeling the behavior of the analyzed system is very small, compared to GSPN model. This leads to a smaller computational effort and also to the possibility of increasing the complexity of the analyzed systems. Different dependability metrics may be evaluated using LESPN model and on this purpose a specialized software is created. In the designing phase this model and the associated tool can be easily used for dependability comparative study. The computed availability indices are used in techno-economical comparative study, for choosing the proper alternative system design. The comparative study may has two different stages: a simplified stage using simplified LESPN models for design alternatives and a complex stage using complex LESPN models for the vital areas power supply of the chosen system. The simplified stage purpose is to choose an adequate alternative and the complex stage purpose is to compare the dependability metrics for the system vital areas and to propose maintenance policies.

References

[1]   M. Ajmone-Marsan et. al. (1984)." A class of generalized stochastic Petri nets for the performance evaluation of multiprocessor systems", ACM Trans. Computer Systems, vol. 2, Apr. 1984, p 93-122.

[2]   M. Dumitrescu. "Contribution to the structure configuration and control of naval power system, on reliability criteria", Physics theses -Dunarea de Jos- University of Galati, 1997.

[3]   A. Johnson and M. Malek. "Survey of software tools for evaluating reliability, availability, and serviceability", ACM Computing Surveys, vol. 2, Apr. 1988, p 227-269.

[4]   M. Malhotra and K, S. Trivedi. "Power-Hierarchy for Dependability- Model Types". IEEE Trans. Reliability ,no 3, Sept.1994, p 34-42.

[5]   M. Malhotra and K, S. Trivedi. "Dependability modeling using Perti nets", IEEE Trans. Reliability, no 3, Sept. 1995, p 29-36.

Complex diagnostic system of ship electrical machines.

Y. Greivulis   A. Gasparian   A. Terebkov

Riga Tehnical University and Latvian Maritime Academy
Riga, Latvia

In Riga Technical University and Latvian Maritime Academy (Latvia) complex system of diagnostics of large ship electrical machines is developed. The given system is based on simultaneous registration both joint processing of a number of mechanical and electrical diagnostic parameters and allows to diagnose damages of a mechanical and electrical part of ship electrical machines and also to determine a residual resource. The described system of diagnostics is two-channel - contains the channel of registration both transformation of mechanical diagnostic parameters and channel of registration and processing of electrical diagnostic parameters. In each channel the primary processing of the diagnostic information is made by the microprocessor. Further the information is transferred for final processing to the personal computer. To one personal computer it is possible to connect 8... 16 diagnostic complete sets. Each complete set serves one electrical machine.

Mechanical diagnostic parameters are size vibroacceleration, measured two-plane - sensors directly in region both bearing units, angular speed, angular situation of rotor of a rather given point of zero situation, size and character of microdeformation of an external ring of the bearing. The signals from sensors act through convertor device on the microprocessor of the channel of processing of mechanical diagnostic parameters. In result of mathematical processing signals, proportional vibroacceleration, vibrospeed, vibrotransference for each plane each vibrosensor are allocated. Angular speed of a rotor and its angle of turn of a rather initial point of zero situation is determined also.

The channel of processing of electrical diagnostic parameters consists the microprocessor, convertor device and sensors of instantaneous magnitude three phase of currents and three phase of voltage. On instantaneous magnitude phase of currents and voltage instantaneous active and reactive power, harmonics structure of currents and voltage (control of amplitudes 3 ...7 harmonics), active resistance and temperature of a winding is de-termined and also appropriate working sizes [1].

The signals with both microprocessor channels act in the personal computer for final processing and accumulation in a database. The joint processing of electrical and mechanical diagnostic parameters allows to determine irregularity of angular speed and rotating moment for one revolution of a rotor. This irregularity can be caused as by defects of bearing units and irre-gularity

mechanisms. The analysis vibroinformation of bearing units allows to determine various defects - damage raseway of both rings and their skew, destruction of separator, deflection of the shaft At presence of the sensor of a moment on the shaft of the electrical machine is possible to supervise balance of mechanical and electrical power at all modes of operations of electrical machines - that allows to carry out complete diagnostics of the machine. If necessary increases of depth of diagnosing the driving unit can as be equipped by the appropriate sensors. Comparing at any moment and for any interval of time the balance of consumed electrical power and made mechanical, is possible to carry out diagnosing of given depth not only electrical machine, but also process equipment connected with it. For example, the large pump, except vibroacceleration sensors on bearings can have sensors of pressure and temperature on input and output branch pipes. Under the indications of these sensors it is possible to determine productivity and pressure of the pump and, hence, consumed power. For anchor- mooring arrangement installation of sensors of a tension of a cable and it length and etc. is necessary. An effective diameter of a drum, the weight of a cable determined automatically. In it case the microprocessor device makes as continuous comparison of electrical and mechanical power, account arrangement efficiency and etc. Comparing at any moment and for any interval of time the balance of consumed electrical power and made mechanical, is possible to carry out diagnosing of given depth not only electrical machine, but also process equipment connected with it. Any deviation of mechanical and electrical parameters from reference is an attribute of damage. The specified deviations with the help of a logic matrix of damage are analyzed in personal computer are compared with similar by data, stored in a database for certain period of time and in a final kind are given out to the operator.

The condition of the bearing can be described by functional dependence:

$$F = \{A (a, b, c) + B (d, e,) + C (g, h)\}, \qquad (1)$$

Where

A - current condition of an external ring of the bearing;

B - current condition of an internal ring of the bearing;

C - information on the previous condition of the bearing.

The account of parameter C requires presence of a database, which can be realized only with application of

The classical method of diagnostics bearing units is based on measurement and registration vibroacoustics signals and subsequent their mathematical processing (spectrum analysis, revealing of correlation dependences and other necessary parameters) [2]. At all advantages of this method it concerns to indirect methods of measurement. Direct metods of measurement of design parameters of bearing units are applied much less often. It is connected first of all to a complex design of the appropriate sensors and difficulty of their accommodation. In a certain measure these difficulties are solved in offered system (Fig.1).
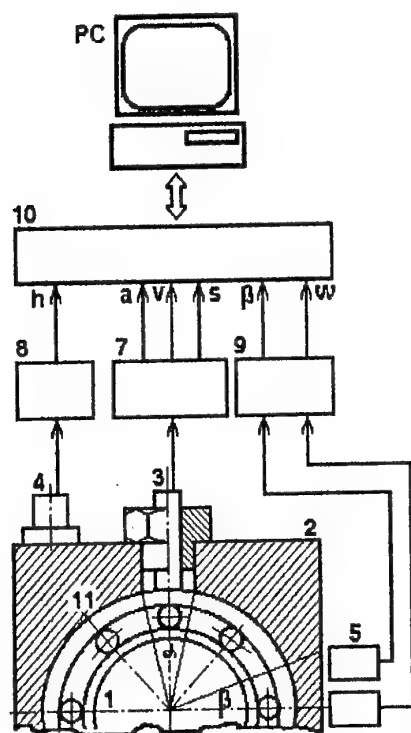
Fig.1. The scheme of system diagnostic with microdeformation sensor.

For increase of reliability and depth of diagnosing the offered system contains, except the sensor - piezoaccelaration 4, sensors of angular speed 6 and angle of turn 5, also sensor 3 microdeformations of an external ring 11 bearing 1. In the block 8 signals piezoaccelaration 4, proportional vibroaccelaration α, vibrospeed V, vibroway S will be transformed to the digital form and act in microprocesor - interface block 10. Through the converter 9 digital signals from sensors 5 and 6 angular speeds ω and angle of turn β act there. In the block 7 the information from the sensor of microdeformations 3 will be transformed. Measurement of character and size of microdeformations h (share and unit micron) external ring 11 of bearing allows directly to estimate a condition raceway both rings of the bearing and his balls. Microprocessor - interface block 10 contains 16 bits computer and 16 K bytes memory. For

further processing of the information under the given program the personal computer serves.

For very large and responsible electrical machines for increase of accuracy and the depth of diagnosing bearing units is possible to recommend modulation way of diagnostics. At direct measurement of low-frequency sites spectrum of noise of the bearing (share both unit Hz) and signals with small amplitude their registration is a difficult problem. For example, at registration with the help measuring magnet device at record such signals are modulated by high-frequency fluctuations from the special generator. In the given work a way of modulation of noise of the bearing high-frequency making of ultrasonic fluctuations directly in the bearing is offered by imposing them against each other and mutual displacement. High-frequency fluctuations pass through a zone of contact ball-ring-separator and mix up with noise of the bearing, generated in a zone of the specified contact. In result the high-frequency signal appear modulated on amplitude, phase and frequency by noise of the bearing. Sum signal consists harmonics with various parameters:

$$U = \sum_{k=1}^{N} \{a_k \cos(k\omega + \varphi) + b_k \sin(k\omega + \varphi)\} \quad (2)$$

At further detecting of a high-frequency signal the necessary information is allocated. The typical picture of spectral density of the specified signal is given on Fig. 2.
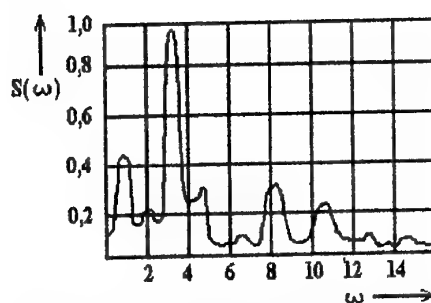

Fig. 2. The spectral density of ball track of the bearing - ring.

The specified way allows to register changes of diagnostic parameters there, where own generating ability of acoustic signals is small - for example, in slowly driving bearings.
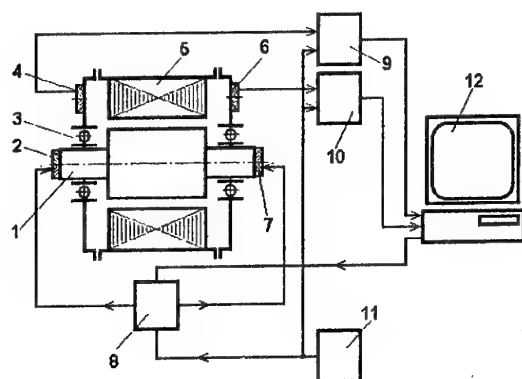
Principle of work explains Fig. 3.

Fig. 3.The scheme of modulating way of diagnostics bearing units.

1- shaft with a rotor of the electrical machine;
2, 7 - radiating high-frequency piezoelements;
3 - bearings;
4, 6 - piezoaccelerometers;
5 - stator;
8 - switchboard radiating high-frequency piezoelement;
9, 10 - synchronous detectors of amplitude, phase and frequency of modulated high frequency signals;
11 - high-frequency generator;
12 - personal computer.

The high-frequency ultrasonic signals from the generator 11 act on synchronous detectors 9 and 10 as basic and on the switchboard 8. The work of the switchboard 8 is operated by the personal computer 12. From an output of the switchboard 8 high-frequency signals alternately or according to the given program act on piezoceramic high-frequency radiators 2 and 7, placed in region internal rings of bearings 3. Further the high-frequency fluctuations through a zone of contacts an internal ring - ball - external ring act in bearing boards of the electrical machine, where are registered piezoacceleratometers 4 and 6. In a zone of contact ball - ring - ball the bearing generates own acoustic signals, which there modulate a high-frequency signal. In synchronous detectors 9 and 10 there is the processing high-frequency of a signal on allocation of changes of amplitude, frequency and phase of a modulating signal.From an output of synchronous detectors 9 and 10 transformation the received information for processing acts in the personal computer 12 for complete processing under the given program.

The given method allows to register diagnostic parameters in cases, when the own acoustic generation of bearings is small or is away at all - low rotation bearings or stopped mechanisms.

Economically expediently to apply complex system of diagnostics to electrical ship machines by capacity more than 50 kW.

[1] Y. Greivulis, A. Gasparian, A. Terebkov, Integrated parameters of quality of electrical energy and technical diagnostics of ship electrical machines. Energetics economy, electricity quality, electromagnetic compatibility on railway transport. · Russia, Moscow, MIIT, RAPS, 1997.
[2] R. Collacott, Mechanical fault diagnosis and condition monitoring, Chapman and Hall, London. 1977.

Evaluation about Reliability of Power Distribution Architecture in Electric Ship

G. Pessina *, M. Albenga **, P. Giraudi **
*Dipartimento di Ingegneria Elettrica Industriale - Politecnico di Torino
C.so Duca degli Abruzzi, 24 - 10129 Torino ITALY
** T.S. Industrial Support
Via Governolo, 24 - 10128 Torino ITALY

Abstract

Referring to naval appliances, this contribution deals with three catogories of loads: Interruptible Load, Uninterruptible Load and Absolutely Uninterruptible Load.

In order to get particular carachteristics in supplying load, nowaday system architectures are inspected. The study of these architectures reveals that the use of redundancies by themselves yields results which are not proportionate to the borne costs.

The results of this work lead to interesting conclusions: they show that a high level of reliability can be obtained from a careful design of the system architecture, rather than using redundancies.

Prearranging loads during project engirieering is the only way to obtain appreciable results.

Costs of reliability are considered in the last part of the contribution.

1. Introduction

This contribution examines the different kinds of architectures on which ships' electrical systems are based. Lowest-weight and smallest-dimensions architectures have been considered. These ones, with a very high degree of reliability, have been inspected considering degraded operations in the case of random faults.

From this point of view, nowaday carried out architectures of electrical equipments are shown.

The problem of redundancy is handled, as well. As we know, redundancies are necessary in order to increase the reliability and availability but their use must be attentively evaluated. In fact, an elaborate system is not always expected to lead to real advantage: it's not enough being redundant to increase the MTTF.

The contribution deals with three categories of loads: Interruptible Load, Uninterruptible Load and Absolutely Uninterruptible Load.

Even if the paper doesn't go into the matter of the importance we have to assign to the different kinds of load (it depends on the particular ship use), the three load features are described in detail.

The examined system architecture is shown in the following diagrams. As the systems we're dealing with consist of repairable functions, unrepairable functions and subsystems on the whole, evaluations about reliability are shown introducing the MTTF values and calculating the MTBF ones.

Results lead to interesting conclusions: they show that a high level of reliability can be obtained from a careful design of the system architecture, rather than using redundancies.

Reliability makes the system dearer: a modest increment can be very expensive.

As regards economic evaluations, costs of reliability are considered in the last part of the contribution.

The analysis of the costs which have to be borne is based on the authors' experience in project engineering (ripened in similar fields).

Essentially, the architecture of an electrical system of a ship consists of:

- an electric power generation system (usually a complicated one) supplying those loads which are essential to a complete management of the ship;
- loads having a different level of importance according to the intended purpose.

Loads may be devided in three different categories: normal loads, important loads, very important loads.

2. Load Features

2.1   First category: normal load (NL)

The definition of normal load can be given by dealing with a fault in the electric power generation side which causes the load to fail in performance. In this case, a load can be defined as a normal one when:

- the function which fails doesn't involve the failure of the basic requisites for the safety of the ship;
- its scanty way of working doesn't limit the complete operation of the ship (i.e.: it allows the ship to reach the destination or archieve the goal);
- MTTR is brief enough to allow the crew to restore the function before the development of the malfunction leads to overstep the limit which is represented by the complete operation of the ship.

As an example of normal load we can consider an air-conditioning unit used to control the temperature of a group of rooms.

2.2   Second category: important load (IL)

Also the definition of important load can be given by dealing with a fault in the electric power generation side which causes the load to fail in performance.

Owing to this event, a load can be regarded as an important one when:

- the function which fails doesn't involve the failure of the basic requisites for the safety of the ship;
- the malfunction causes a scanty way of working which makes the ship absolutely impossible to operate in a complete way; as long as the malfunction

persists the ship is not able to reach the destination or achieve the goal;

- MTTR is so long that the management of the navigation system can be seriously involved before they restore the initial performances of the function; thus, only a brief disconnection from the source of power is allowed.

Examples of important loads are compressors, electric motors (e.g.: motors used to circulate fluids), and, generally, those loads showing a time constant of the phenomenon longer than the time necessary to restore the electrical supply by an order of magnitude.

2.3 Third category: very important load (VIL)

As in the two foregoing definitions, the definition of very important load can be given by dealing with a fault in the electric power generation side which causes the load to fail in performance. On this assumption, a load can be defined as a very important load when:

- the function which fails does involve the failure of

the basic requisites for the safety of the ship at once, and risks the achievement of the goal;
- no circuit interruption is allowed.

Examples of very important loads are the process control systems. In this kind of systems, a microinterruption is enough to cause the suspension of the operation.

2.4 Times of disconnection from the source

It stands to reason that the source of electrical energy which supplies the three categories of loads is the weakest point of the chain of faults. From an electrical viewpoint, the three different kinds of loads can be defined in terms of the duration of the disconnection from the source of power; thus:

- normal load: no longer than an hour;
- important load: no longer than a minute;
- very important load: no interruption allowed.

On referring to the three categories of loads, the system architecture is developed in the schematic diagram shown in Fig. 1.
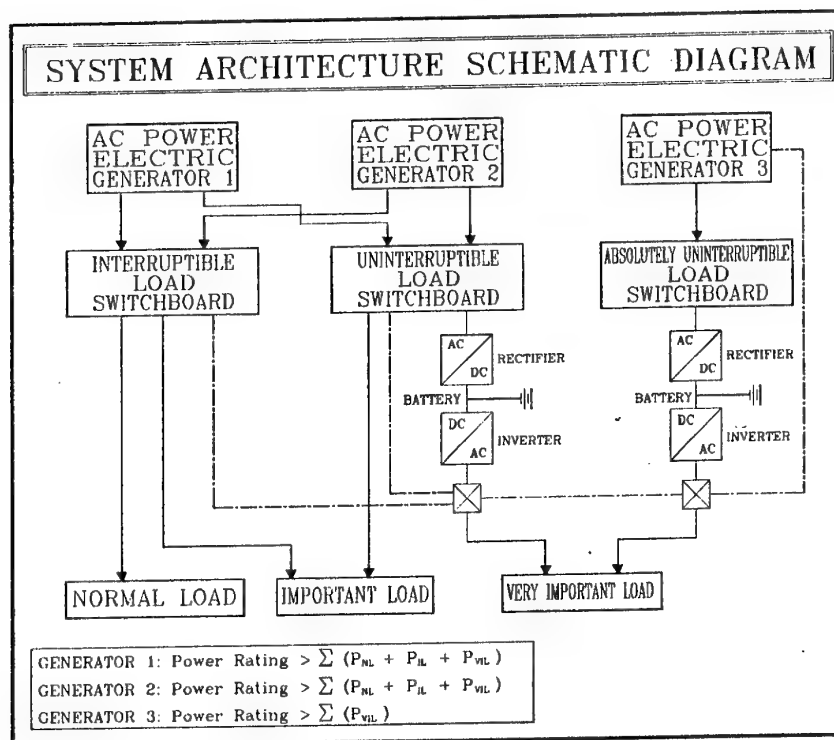
Fig. 1: System architecture

For those loads belonging to the first and second category, switching between supplies of electrical energy is allowed (in the case of electrical fault). On the contrary, for those loads belonging to the third category that operation is not allowed; in fact they are not in a position to endure any microinterruption.

In other words, power switching must take place with no disconnection from whichever source of electrical energy, in order to keep on supplying the very important loads in a continuous effective way.

3. Electrical power supplies for NL, IL, VIL

The schematic diagram of Fig. 1 shows an electrical system in which the three different categories of loads are supplied. Aboard a ship, of course, sources of electrical energy are self-governing generator sets. Fig. 1 shows three of these generators.

From the viewpoint of the electric power, generators 1 and 2 are the same; the two generator power outputs are:

$$P_{G1} = P_{G2} \geq P_{NL} + P_{IL} + P_{VIL} \qquad (1)$$

where:

- P_{G1}: power output of generator 1;
- P_{G2}: power output of generator 2;
- P_{NL}: summation of the normal load powers;
- P_{IL}: summation of the important load powers;
- P_{VIL}: summation of the very important load powers;

while the third generator power output is:

$$P_{G3} \geq P_{VIL} \qquad (2)$$

where:

- P_{G3}: power output of generator 3.

As shown in Fig. 1, each of two generators is able to supply all of the loads of the ship. This important function (supplying power to the loads) is duplicated to decrease the probability of failure. In fact, if one of the two generators is not able to supply power - owing to a fault or maintenance -, the second one will ensure supply to all of the loads.

Assume that the generators, under normal conditions, are:

- generator 1: operating;
- generator 2: stand-by not ready to operate;
- generator 3: operating.

Also assume that generators, electrical distribution systems and static switching systems are repairable systems.

As shown in the schematic diagram of Fig. 1, both generators 1 and 2 can be connected either to the switchboard pertinent to the normal loads or to the one pertinent to the important loads. It should be noted that the very important loads, however, can be supplied by all of the three generators and not only by generator 3.

As everybody knows what a UPS is, its functions won't be described. Notice that the time batteries can continue operating may be assumed at a value of:

$$T \geq 1,800 \text{ s} \qquad (3)$$

Usually this value is considered high enough to allow the generator set to start; it also includes possible failures in generator start-up.

4. Analysis of reliability parameters

From the reliability viewpoint, each UPS subsystem consists of a group of series connected elements, as shown in Fig. 2; each of them shows a certain failure rate λ and maintenance rate μ.
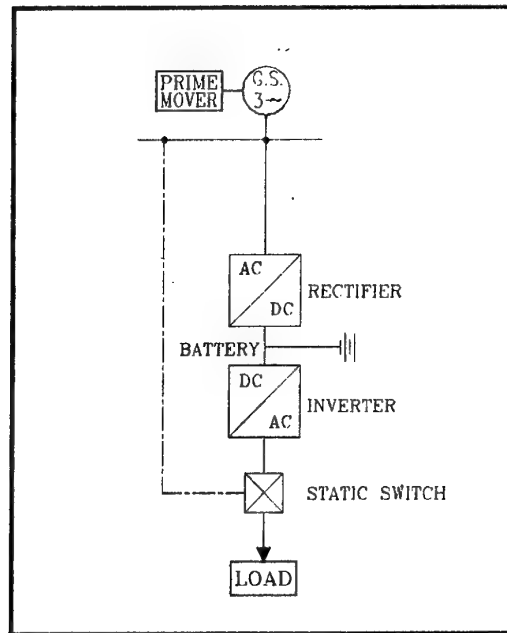
Fig. 2: UPS supplying load

Values of failure rate will be designated by the following subscripts:

- ac power supply system: λ_{NET};
- circuit-breaker on the supply side: λ_{MB};
- AC/DC converter: $\lambda_{AC/DC}$;
- DC/AC converter: λ_{INV};
- static switch: λ_{SSW};

whence:

$$\lambda_{UPS} = \lambda_{NET} + \lambda_{MB} + \lambda_{AC/DC} + \lambda_{INV} + \lambda_{SSW} \qquad (4)$$

As failure rates are constant in value, MTTF is:

$$MTTF_{UPS} = \lambda_{UPS}^{-1} \quad \text{[hours]} \qquad (5)$$

If redundancy is obtained by paralleling two subsystems which consist of the elements shown in Fig. 3, the Mean Time To Failure pertinent to the condition in which two UPS units are operating, is:

$$MTTF_{2UPS} = m_0 + 2 \lambda_{UPS} \cdot m_0 \cdot MTTF_{UPS} \qquad (6)$$

where:

$$m_0 = 1/(2 \lambda_{UPS} + \lambda_{NET} + \lambda_{SSW}) \qquad (7)$$

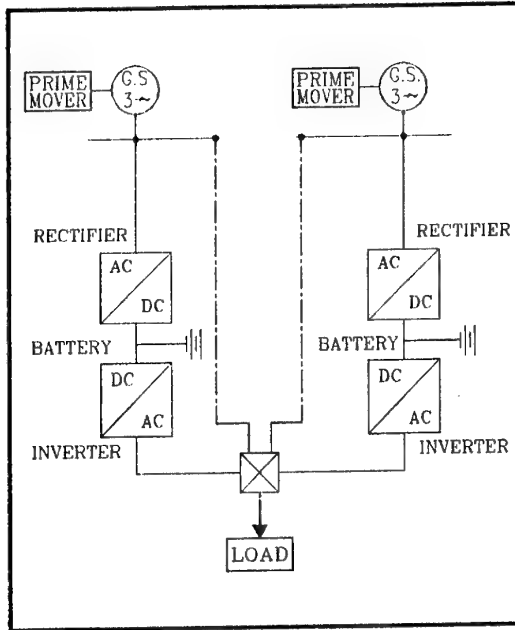- m_0: average time in the condition of correct operating.

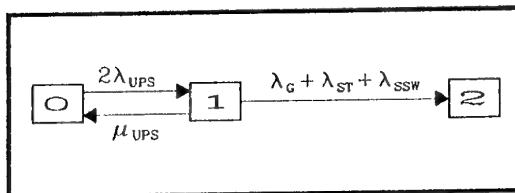Fig. 3: Paralleled subsystems

Further details may be found in Fig. 4.

Fig. 4: Events occuring in a system with two UPS.
Schematic block diagram

$MTTF_{2UPS}$ is the component of MTTF vector representing the average time between the failure of the system (e.g.: black-out) and the condition of correct operating throughout steps which show reduced performances in operating.

Referring to Fig. 3, the following failure rates are introduced

– supplying subsystem (generator): λ_G;
– start-up device of the generator: λ_{ST}.

As regards bypass, notice that the system of Fig. 3 is expected to be connected direct to the busbars of the generators through the static switch.

Bypass wire allows the system to remedy a UPS failure; in fact, bypass wire represents a second path through which generator supplies power to loads.

If a UPS unit is assumed to be in a stand-by condition not ready to operate, the way in which the electrical system evolves can be described as shown in Table 1. From developed computations [1; 2], with both of the UPS

units assumed to be operating the MTTR value increases very little, as shown in Table 2.

Table 1
Operation with one UPS unit. Failure rates and maintenance rates

Transition		Event causing the transition	λ; μ
From	To		
0	1	Generator fault	λ_G
1	0	Generator repair	μ_G
1	2	UPS fault	λ_{UPS}
2	1	UPS repair	μ_{UPS}
2	3	Static switch fault	λ_{SSW}
3	2	Static switch repair	μ_{SSW}
0	3	Static switch fault	λ_{SSW}
3	0	Static switch repair	μ_{SSW}

Table 2
Operation with both UPS units. Failure rates and maintenance rates

Transition		Event causing the transition	λ; μ
From	To		
0	1	UPS fault	λ_{UPS}
1	0	UPS repair	μ_{UPS}
1	2	Generator fault; start-up subsystem fault; static switch fault	λ_G + λ_{ST} + λ_{SSW}

From the supplying-system reliability viewpoint, the static switch can be regarded as a "neck of bottle"; it means that the static switch is a critical point in the architecture of the system. In fact, in the case of an electrical fault or damage of the static switch it will be possible to supply the very important loads by no means.

In order to solve this problem, assume that the generator subsystem is supplying the very important loads through electrically-separated paths, without the static switch which is shown in Fig. 3.

This solution is shown in Fig. 5.

The solution shown in Fig. 5 is a good one : In fact it shows a duplication of the supply circuitry.

5. Management of the system

It's clear that a system with the so-called very important loads can't be handled only by providing redundancies, that is duplicating crucial functions. In fact, the very "neck of bottle" is represented by the points of intersection of the system. To this regard, the duplication of the path through which electrical supply is ensured shows a good way of solving the problem; it does make redundancies indipendent.

Therefore, the management of the system has to involve:
A) two indipendent generators;
B) two UPS units (each of them with a bypass);

C) two indipendent generators supplying the so-called very important loads.

Only in this case, it's possible to provide preventive maintenance and rapid interventions intended to recondition the system without disconnecting loads.

By referring λ and μ to the values which can be inferred from MIL standards, technical literature and experience in this field, usually the magnitude of MTTF doesn't exceed 20,000 hours.

Fig. 5: System architecture leading to an increase of reliability

In accordance with the conditions shown in this paper, instead, when redundacies referred to the electric power generation side are really indipendent the MTTF is about 80,000 hours.

Once again we want to focus the attention on the following point: this result has been achieved by designing a system architecture directed to find out solutions which are pertinent to the power supply subsystem, rather than using too many redundancies.

6. Economic evaluations

From the foregoing, it's clear that the duplication of functions (redundancy) regarding the subsystem which supplies the very important loads involves high costs and doesn't lead to real advantages. The elimination of critical elements (neck of bottle) can't be obtained only by multiplying subsystems which are functionally the same.

The study of suitable system architectures, and conditions of management of the system itself is the best way of solving the problem in advance.

In this case, the presence of two generators (always available to ensure loads to be supplied), two paths

through which each generator is able to supply loads, and the independence of the electric power supply subsystems, yields a real advantage in terms of reliability without increasing costs.

The greatest care in providing preventive maintenance, and reducing the magnitude of MTTR is to be taken.

7. Conclusion

The evaluation of reliability parameters depends on the kind of fault occured in the electrical system.

Beyond personal intuitions supported by experience, computations show that the mere use of redundacies only increases costs without solving the problems. From the reliability viewpoint, real advantages can only be obtained by studying suitable architectures comprising independent supplies. These are the conditions we need to get a compromise between the costs which are to be borne and the high performances which are requested.

References

[1] G.Pessina, G.Vicario, C.Zimaglia, "Affidabilità di sistemi elettrici non riparabili: impostazione teorica e studio di configurazioni di base serie e parallelo", Automazione e Strumentazione, Febbraio 1985

[2] G.Pessina, G.Vicario, C.Zimaglia, "Valutazioni delle caratteristiche dell'affidabilità in configurazioni complesse di sistemi elettrici non riparabili", Automazione e Strumentazione, Aprile 1985

[3] E.R.Barlow, F.Proschan, "Mathematical theory of reliability", Wiley and Sons Inc.

[4] N.Feller, "An introduction to probability theory and its applications", Wiley and Sons Inc.

A FLEXIBLE NETWORK STRUCTURE FOR AN EFFICIENT ELECTRIC SHIP DISTRIBUTION SYSTEM

N. Messina, G. Spataro, G.M. Tina

Dipartimento Elettrico, Elettronico e Sistemistico
Engineering Faculty - University of Catania
Viale A. Doria, 6 - 95125 Catania (Italy)
Fax: +39 95 330793 - Email: gtina@dees.unict.it

Abstract

This paper proposes a change in shipboard electric power system: to modify the structure of its distribution network, leaving the traditional, essentially radial, scheme and using another more flexible one, which will be shown here, in order to get quickly the necessary network reconfigurations, according to the load changes, both in normal and failure situations. Then, as regards intelligent automatic management of this distribution system, a control algorithm logic is presented, which allows to determinate the various optimum configurations in simple way, without hard analytic tools. Moreover a particular application of the above mentioned ideas is shown, regarding the primary power network of a ferry ship. Finally some observations about the improvement of the system reliability by utilization of new circuit breakers based on solid state devices and of mineral isolation cables; then the conclusions about reached results and the possible future developments of the system proposed are drawn.

1.Introduction

A careful examination of the development of shipboard electric power networks puts in evidence, as regards devices and automation, that it is more and more useful to consider their problems like the industrial power plants ones. Really, today's naval power systems have some inherent characteristics that make them different from typical utility power system, so that typical power system models are not always appropriate for analysing shipboard dynamics, like, e.g., the war ships ones [1], [4]. However we think it is necessary and possible to improve the basis structure of shipboard electric plant: by introducing the new ideas regarding the industrial one, e.g. [2]. In fact a ship's electrical power system consists of some generators (both normal and emergency) connected to main switchboards usually in ring configuration; from which the various loads are fed, directly or by other distribution switchboards, in accordance with an essentially radial scheme, excepting a few particular loads (vital loads, frequency changers, etc.) for which two or more alternative sources of power are provided (fig. 1).

Then this kind of distribution network generally presents two weak points: almost singleness of primary power supply flows and few possibilities of reconfiguration (the latter is considered as new distribution of the loads supplies in relation to new feeders availability and particular functioning conditions of network), both in normal and fault condition, in the various operative phases

(sailing, working, loading, unloading, emergency, etc.) during the daily interval.

G=Generator   FC=Frequency Converter
c=commutator   MS=Main Switchboard
LCS=Load Center Switchboards
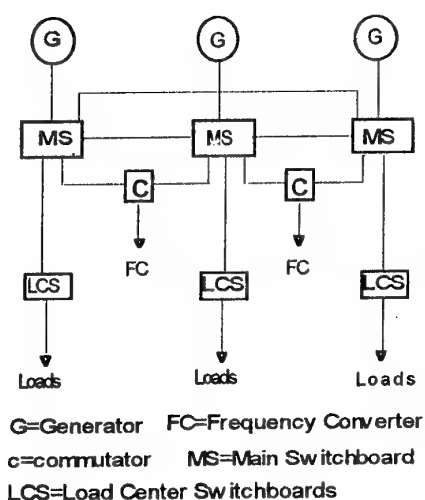
Figure 1: Typical ship's electric distribution system

So, these considerations and both technical and economic other ones, among which, overall, the great importance of power service quality, as regards continuity and reliability, in shipboard electric plant, make us imagine an innovative network structure, like the proposed one, which is flexible (it can be reconfigured in accordance with its maximum possible efficiency) and suitable for using intelligently the automation and control technologies that are available today.

2.Power network structure

An example of the above mentioned network structure is shown in figure 2.

It is a square type, supplied by main distribution switchboards, which are directly fed by generators (figure 3); its knots are distribution switchboards and have a double function: connecting each other's and supplying the loads (figure 4).

Every main switchboard feeder supplies a group of knots according to an essentially radial scheme, which is got by a suitable combination of the positions (on/off) of the relative knot switches.
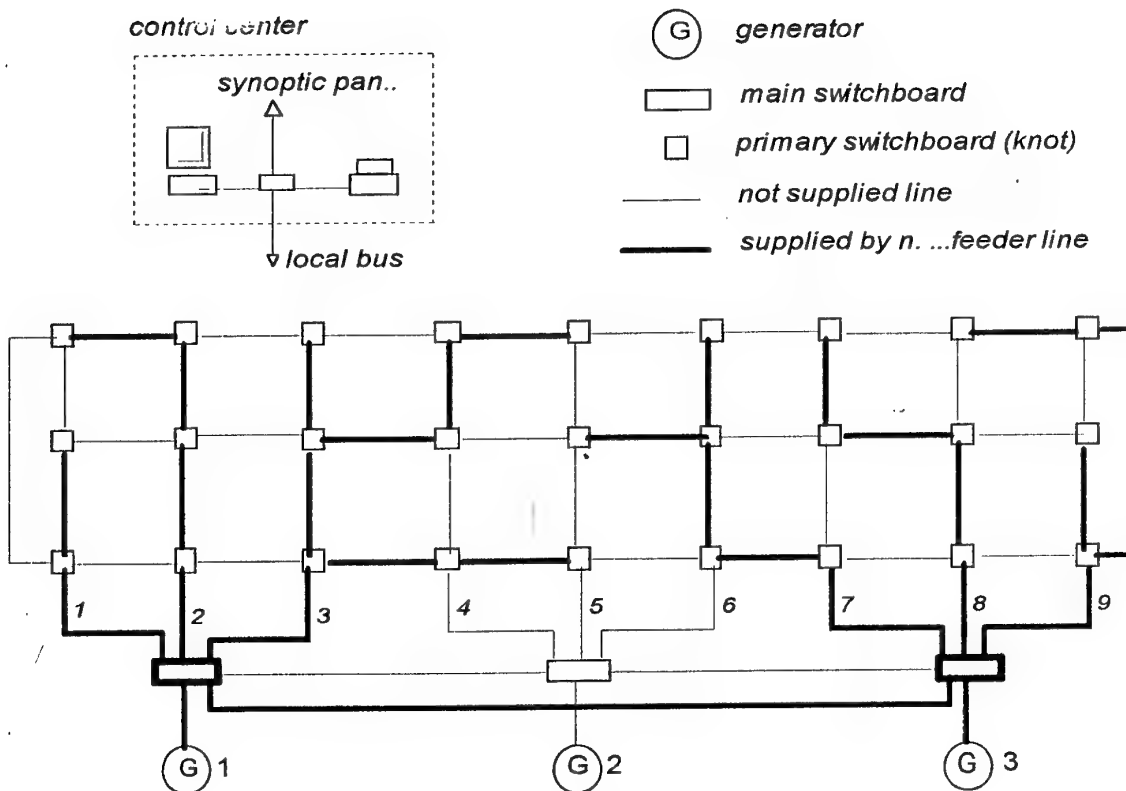
control center

synoptic pan..

↑

↓ **local bus**

Ⓖ **generator**

🔲 **main switchboard**

☐ **primary switchboard (knot)**

———— **not supplied line**

▬▬▬ **supplied by n. ...feeder line**

1 2 3 4 5 6 7 8 9

Ⓖ 1 Ⓖ 2 Ⓖ 3

Figure 2: Primary power network

Such a network is managed by an intelligent automation and control system, consisting of PLCs, which are installed in the distribution boards, and a PC station placed in the control center, all of them are connected by a local bus. This network structure has the following strong points:

- possibility of primary power supply flow change: every knot (distribution board) can be supplied by one of the various lines which are joined to it and the particular line can be supplied by one of the various feeders, so as to get the most suitable network configuration; then there is a double choice possibility: way and source, so that a great reliability and supply continuity are obtained;

- remarkable reduction of primary lines number: in the presented structure every feeder can supply more than one distribution board (primary load), whereas in the traditional one every feeder supplies just one primary load;

- uniformity of features of primary network components: it is better that the feeders are equal in order that is possible to exchange them in accordance with the various network reconfigurations, then there is a complete uniformity as regards switches, of the main board and knots, and primary connection lines. From it comes out that a remarkable reduction of electrical spare parts;

- possibility to modify the electric distribution system easily: every transformation is very simple, e.g., changing position of a board or installing a new one, and it is not necessary to modify the plant, as it is sufficient to connect it to the nearest knots, naturally, it is necessary to respect the network maximum load limits.

The following advantages arise from the above mentioned points:

- possibility of network on line automatic reconfiguration, according to the various operative phases, daily time intervals and situations of overload or fault event, getting the maximum advantage: thanks to the flexibility of the proposed structure and automation and control system it is possible, by the switching knots, to carry out network reconfiguration automatically on line, so that the various aims (uniform feeders loads, minimum losses, loads supply priority order, higher reliability), are obtained in the best way;

- possibility of boards supply by different ways;

- possibility of priority order change of loads power supply in any moment, just by intelligent automation and control system, without hardware modification;

- boards supply continuity also when some line is disconnected owing to maintenance, overload or fault event;

- simple and safe maintenance;

- easy management of the spare parts.

Further improvement of the flexibility of the studied network can be obtained by means different schemes of the switching knots. The simplest scheme shown in fig 4 can be adopted for supplying the node from one side, whereas more complex schemes can be used for supplying two lines from the other two sides independently. Of course a high level of complexity of the nodes improves the performance of the network in terms of flexibility and reconfigurability, which is a very important task when fault problems are concerned. On the other hand node complexity increases installation and management costs.
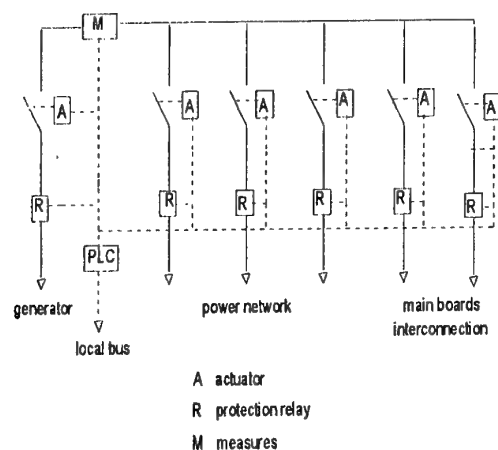
65

Figure 3: Main power distribution switchboard.

A actuator
R protection relay
M measures

3.Management and reconfiguration logic

The basis logic of control algorithm of the intelligent system aims to determinate and carry out -the best possible network configuration on line, in accordance with the particular situation of knots loads and generators power availability. Naturally, as such a configuration is the one which meets technical and economic requirements more (minimum losses, maximum reliability, priority order, maximum generators efficiency, etc.), the chief logic purpose is to get, as much as possible, uniformity of feeders total loads and, so, of generators output power too, when they are not interconnected. The logic procedure is the following one: the knots switches, after a first ideal condition in open position, are closed according to a prearranged succession: going from the knots directly connected to the main boards towards the most far ones; so that every knot connects the other nearest ones, in decreasing order of their load; moreover the knots are

jointed to the various feeders, always choosing, time by time, the feeder that is available and presents, at the moment, the littlest power output, on condition that the latter is less than the relative prefixed limit. If, once the first cycle of connections is completed, some knots are still disconnected, another one begins again, and so on till the whole network is completed or, anyway, the maximum feeders power out put is attained. Then, with the purpose to apply the above mentioned network structure and logic, some management criterions are here presented. In normal conditions network dynamics is observed according to the various ship's phases (sailing, working, loading, unloading, etc.) and daily time periods. So, first of all, is necessary to examine the load diagram of the network knots so as to determinate, for every operative phase, the various daily time periods in which it is possible to consider total loads knots practically stationary. For each one of such periods and relative distribution of loads knots, a particular network configuration, that we called basis configuration, is determinate, in accordance with the above examined logic. During the day, in normal conditions, the management intelligent system carries out these basis configurations; naturally it also takes into account the field data (measurements and alarms) and statistics load forecasts, so as to perform some little modification in the foreseen configuration, when it is necessary. In failure conditions, when a plant portion is disconnected by on field hardware protection devices, the intelligent system carries out an on line reconfiguration, still using the just described logic, and transforms the actual configuration in the nearest one. In this way the supply of not damaged parts, included by the above-mentioned portion, is restored, in advantage of the electric service continuity for the ship. Moreover a particular software is studied which is able to apply the above described reconfiguration logic. It essentially considers, like inputs, the load diagrams of the network knots and the maximum limit of feeders power supply. The outputs are the switchboards positions of the network knots, by which the reconfiguration is possible and other parameters concerning the feeders: power supply, identification of the relative fed knots and total line losses. .

network interconnections   local bus   loads

A   actuator   R   protection relay   M   measures
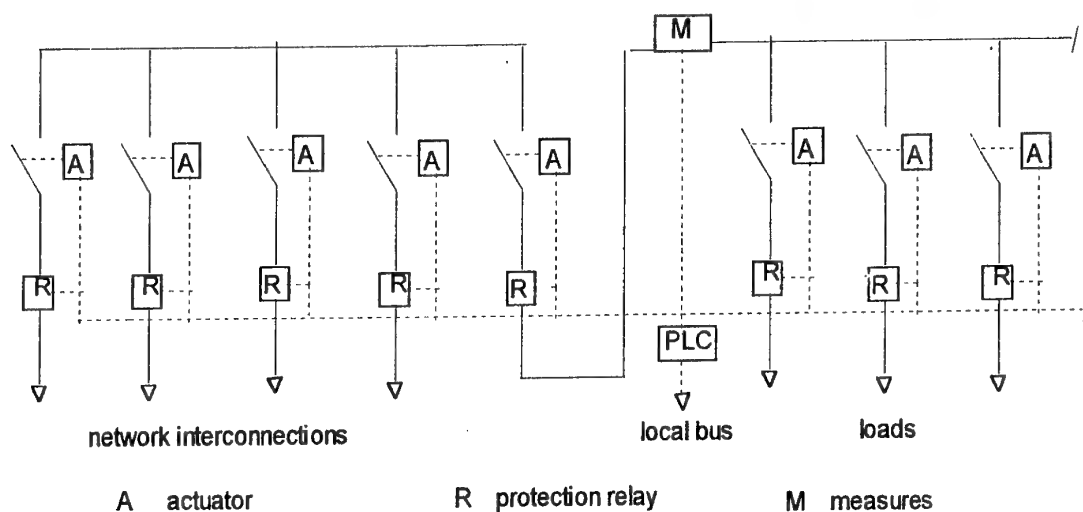
Figure 4: Knot of primary power distribution network.

4.A particular application

The suggested network structure and management logic are applied, in principle way, to the electric plant of a ferry ship, so as to study its primary power system according to the above mentioned ideas. In particular, such a network is normally supplied by two generators, which are cyclically and automatically chosen among three of them by the intelligent system; the fourth one is forecasted for the emergency situation. The generators are connected to relative main distribution switchboards (see fig.2), which are equipped with equal feeders and supply the various primary knots (see fig.3) of the distribution network.

The following simplifications and plan specifications are considered:

- all the lines of primary network are cables which have the same length and section;
- the load diagrams of the primary network knots are supposed of kind shown in figure 5;
- network total load: like table 1;
- total loads of network primary knots: like table 2 (for exposition simplicity just a few interesting data are indicated);
- nominal power of each normal feeder:100 kVA;
- nominal power of each emergency feeder: 80 kVA;
- normal generators power: n.3 x 315 kVA (2+1 cyclic reserve);
- emergency generator power: 250 kVA;
- generated and distributed power supply: ungrounded three phase system/440 V/60 Hz;
- primary network cable section: 3x120 mm2;
- phase resistance of each primary distribution line: 0,006 Ohm.
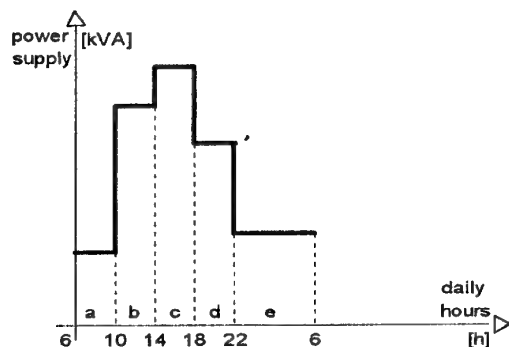
Figure 5: Load diagram of primary knot.

Table 1: Network total load in the various operative phases and daily intervals.

	NETWORK LOAD [kVA]				
OPERATIVE PHASE	06.00 10.00	10.00 14.00	14.00 18.00	18.00 22.00	22.00 06.00
SAILING	430	442	441	438	432
WORKING	425	435	440	430	420
LOADING/ UNLOADING	224	240·	245	224	210
EMERGENCY	172				

Table 2: Powers and priority order of knots.

	POWER SUPPLY [kVA]			
knot n.	RATED POWER	SAILING 14.00/18.00	EMERG -ENCY	SUPPLY PRIOR.
1	38	25.4	15.2	X
2	6	4.1		
3	41	27.7	16.5	X
4	38	25.4	15.2	X
5	23.1	15.4	9.2	X
6	3.4	2.2		
7	13	9.1		
8	9.4	6..3		
9	47	31.4		
10	41.4	27.7	16.5	X
11	50	33.5	20	X
12	93	62.7	37.4	X
13	27	18.4	11	X
14	4.4	2.9	1.7	X
15	20	13.7	8.2	X
16	14	9.7		
17	13	8.6		
18	15	10.1		
19	40	26.8		
20	28.7	19.2	11.4	X
21	38	25.4		
22	38	25.4		
23	13	8.7	5.2	X
24	10	6.7	4	x

By application of data and tools above described the network basis configurations in the considered phases and daily periods are determined; they are shown in figure 6, whereas the table 3 shows the values of the various feeders power supplies and the Joule losses of the distribution network in such configurations.

Table 3: Feeders' power supplies and power losses. of distribution network

PHASE/ INTERVAL	FEEDERS' POWERS [kVA]								
	1	2	3	4	5	6	7	8	9
POWER SUPPLY SAILING 14.00-18.00	65	70	60	82	81	83			
POWER LOSSES SAILING 14.00-18.00	2.8								
POWER SUPPLY EMERGENCY							68	64	40
POWER LOSSES EMERGENCY	1.4								
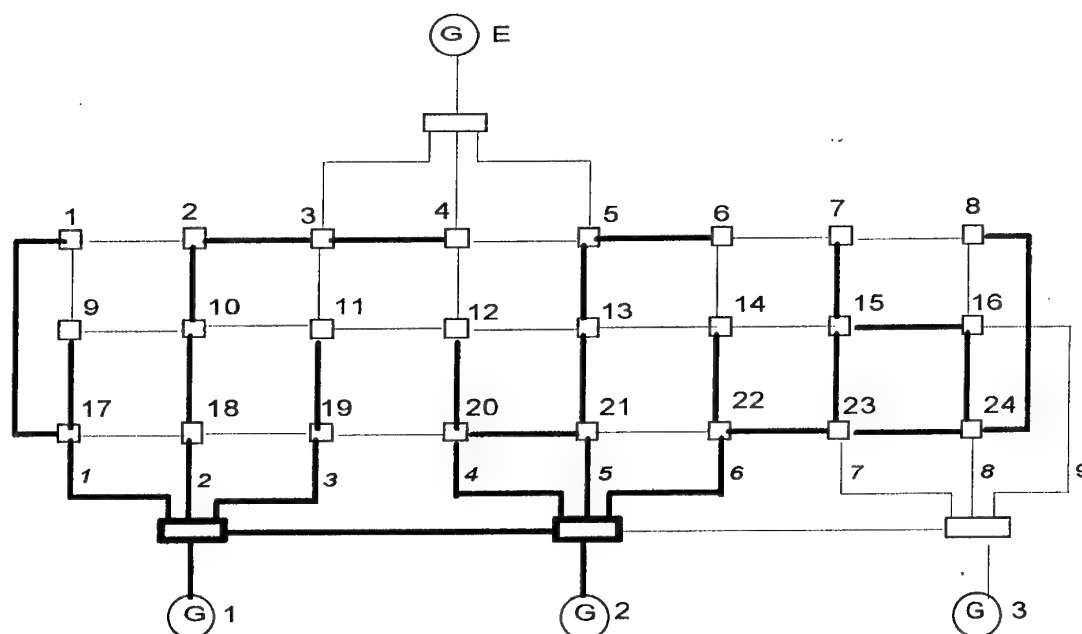
Figure 6: Network configuration in normal sailing phase, in daily interval 14.00/18.00.
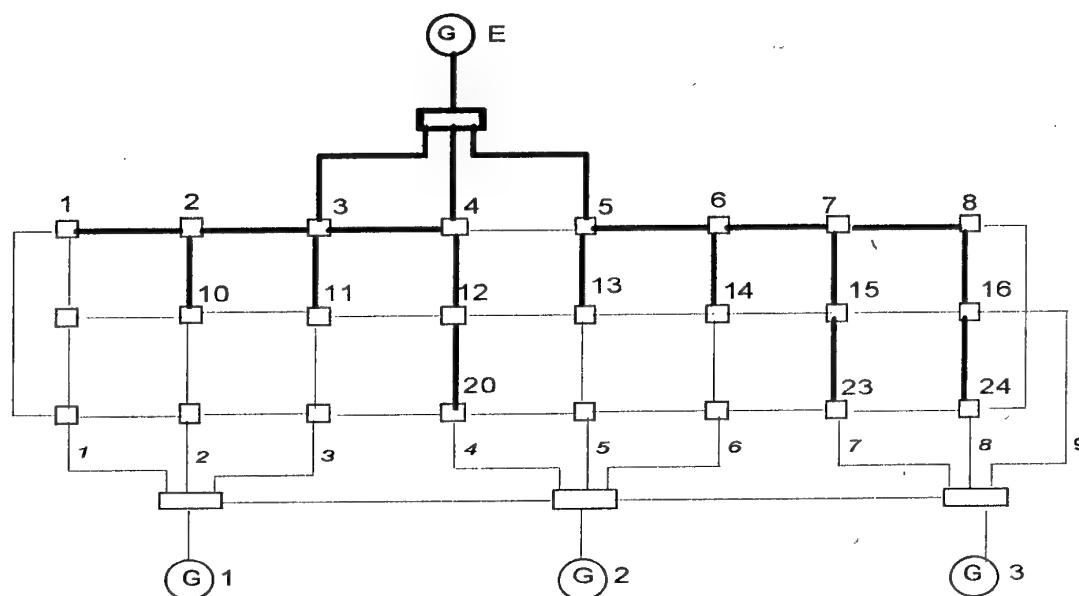
Figure 7: Network configuration in emergency phase.

5.Observations and conclusions

Surely it is possible to get further improvements of the suggested power distribution network, in terms of reliability and continuity of electric service. A first way is to use the new current limiting circuit breakers, based on solid states devices (a review is in [3]) and installing them in the main and knots switchboards (or, at least, in mains ones), to protect the primary lines. In fact this kind of breaker is very suitable in networks managed and automated by an intelligent system, as, thanks to its very short interruption time (not more than 1 ms) and its great ability for current limitation, very quick network reconfigurations can be got. This point of view is particularly important as regards, especially, the electronic loads, like control, communication or combat sensors, computers, converters, etc., as they are particularly sensitive to power interruptions and power quality. For

68

instance, interruptions of 70-100 ms can cause the entire combat system to shut down, with a long recovery time. Another idea to improve the primary shipboard electric network is to use cables with mineral isolation: the reduced number of lines which come out from the proposed main switchboards make us to thing of some utilization of these absolutely fire resistant cables, at least in certain particular ship's zones; overall it is to take into account they need just simple supports to be put in service and it is easier to look for the line failure when the latter occurs. Also in the case of MV networks the possibility of reducing the number of primary feeders and, in the same time, increasing their reliability, lets get optimum results. Really all these observations arise from a more general fact: the proposed structure simplifies the primary network, so that it allows, under the same its total expense, compared to the traditional one, to choose more reliable components, although they are certainly more expensive. In this direction we are developing our study regarding this proposed work: best application of the technologies that today are available for the network components.

Acknowledgement

References

[1] Karen L. Butler, N.D.R. Sarma, Cliff Whitcomb, Hider Do Carmo, Haibo Zhang: "Shipboard Systems Deploy Automated Protecion", IEEE Computer applications in power, april 1998.
[2] J.Hasegawa: "Flexible, Reliable and Intelligent Electric Energy Delivery System (FRIENDS)", Iasted Power '97, Plenary Talk, 1997.
[3] Charles W.Brice, Rouger A. Dougal, Jerry L.Hudgins: "Review of technologies for current-limiting low voltage circuit breakers", IEEE Transactions on industry applications, vol.32, no.5 Sept./Oct. 1996.
[4] G. Ercolini, R. Drago:" L'evoluzione dell'impianto elettrico delle Unità Navali della Marina Militare Italiana nel segno della sicurezza", Atti - Alimentazione di sicurezza e di riserva nei sistemi di sicurezza, Pisa, 1995.

Numerical Study Of a Double Star Synchronous Motor Drive For Electrical Propulsion

M.F. Benkhoris, F. Terrien and J.E. Boucher

'LARGE/GE 44',

Bd de l'Université, BP 406, 44602 Saint-Nazaire Cedex, FRANCE

1 Introduction

During the last years, an important achievement has been realised in the domaine of the variable speed A.C. drives. Among, the various solutions, the synchronous motor supplied by a current source inverter is widely used in the area of electrical propulsion [1][2]. The basic scheme is presend in figure 1. When supplied form conventional six-step current inverter, three phase synchronous machine exhibit a pulsating component of torque at six times the supply frequency. This causes excess mechanical vibration and poor system performance. By using two three phase current inverters to supply a machine with a double stator armature, the amplitude of the pulsating torque can be substantially reduced and the frequency of the pulsation torque shifted from six to tewelve times the supply frequency. To achieve this improved torque wavesphape, the two star armatures must be displaced by 30°. Two electrical structures are possible as shown in figure 2.

With the complexity of a such system under consideration and the level of electrical power used (some MW), the experimental study is very expansive. Then the numerical simulation becomes a powerful tool to predict the steady and transient state performances of the electric propulsion structure.

The physical system is composed of a power electronic converters which contain non-linear semi conductor components, taking either "on" or "off" state. State changes of these devices lead to topology change of the physical system. Thus the global system is represented by a "multiple model" depending on the supplied phases of the motor and the supply source, and the state of each converter. Hence, a specific methodology of modeling is required to describe the state of the power system.

The presented paper establishes an improved method for modeling and simulation of the electrical propulsion using a current source inverter.
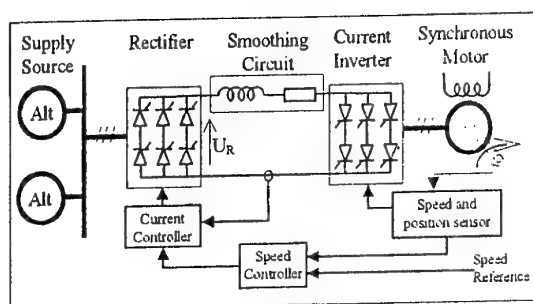
figure 1: basic scheme of the electrical propulsion
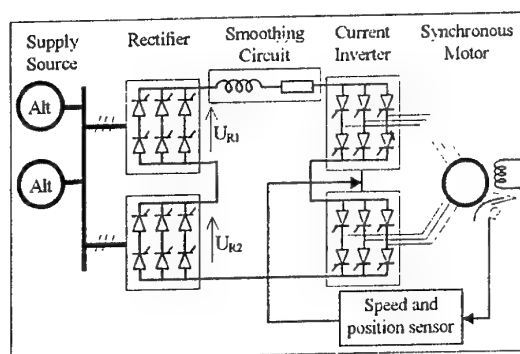
a) serie configuration
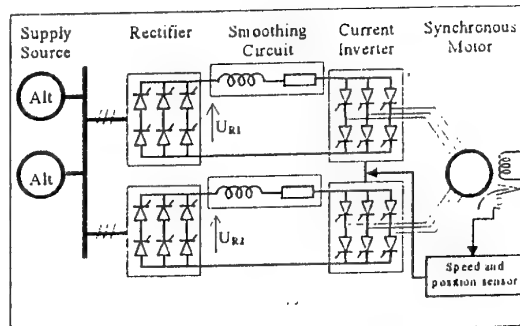
b) shunt configuration

figure 2: various used schemes

2 The methodology of the modeling: General electrical equation of the power system

For each studied structure, the power system is composed of the synchronous alternator, the smoothing circuit and the synchronous motor, which are connected together by the power electronic converters. The electrical equation of the power system can be deduced from the general electrical equation of the synchronous motor.

The double star synchronous motor under consideration is salient poles with field an unsymmetrical damper windings. The general electrical equation of the motor is given by:

$$[V] = \left[[R] + \omega.\frac{d[L]}{d\theta}\right][I] + [L]\frac{d[I]}{dt} \quad (1)$$

$[V]$ is the voltage vector, defined as:

$$[V] = \left[[V_{S_1}]^t [V_{S_2}]^t [V_R]^t\right]^t$$

where

$$[V_{S_i}] = [v_{a_i} \quad v_{b_i} \quad v_{c_i}]^t, \; i=1,2$$

$$[V_R] = [V_f \quad 0 \quad 0]^t$$

$[I]$ is the current vector, define as:

$$[I] = \left[[I_{S_1}]^t [I_{S_2}]^t [I_R]^t\right]^t$$

where

$$[I_{S_i}] = [i_{a_i} \quad i_{b_i} \quad i_{c_i}]^t, \; i=1,2$$

$$[I_R] = [I_f \quad I_D \quad I_Q]^t$$

$[R]$ is the resistance matrix:

$$[R] = \begin{bmatrix} [R_S] & [0] & [0] \\ [0] & [R_S] & [0] \\ [0] & [0] & [R_R] \end{bmatrix}$$

with:

$$[R_S] = r_s.\begin{bmatrix} 1 & 0 & 0 \\ 0 & 1 & 0 \\ 0 & 0 & 1 \end{bmatrix}, \; [R_R] = \begin{bmatrix} R_f & 0 & 0 \\ 0 & R_D & 0 \\ 0 & 0 & R_Q \end{bmatrix}$$

$[L]$ is the inductance matrix:

$$[L] = \begin{bmatrix} [L_{S_1}] & [L_{S_1 S_2}] & [L_{S_1 R}] \\ [L_{S_1 S_2}]^t & [L_{S_2}] & [L_{S_1 R}] \\ [L_{S_1 R}]^t & [L_{S_2 R}]^t & [L_R] \end{bmatrix}$$

where:

- $[L_x]$: is the matrix inductance of the x armature (x=S_1, S_2, R).

- $[L_{xy}]$: is the matrix mutuel inductance between the x and y armatures.

$$[L_{S_i}] = \begin{bmatrix} L_{S_i}(\theta) & M_{S_i}(\theta) & M_{S_i}(\theta) \\ M_{S_i}(\theta) & L_{S_i}(\theta) & M_{S_i}(\theta) \\ M_{S_i}(\theta) & M_{S_i}(\theta) & L_{S_i}(\theta) \end{bmatrix}, \; i=1,2$$

$$[L_{S_1 S_2}] = \begin{bmatrix} M_{a_1 a_2}(\theta) & M_{a_1 b_2}(\theta) & M_{a_1 c_2}(\theta) \\ M_{b_1 a_2}(\theta) & M_{b_1 b_2}(\theta) & M_{b_1 c_2}(\theta) \\ M_{c_1 a_2}(\theta) & M_{c_1 a_2}(\theta) & M_{c_1 c_2}(\theta) \end{bmatrix}$$

$$[L_{S_i R}] = \begin{bmatrix} M_{a_i F}(\theta) & M_{a_i D}(\theta) & M_{a_i Q}(\theta) \\ M_{b_i F}(\theta) & M_{b_i D}(\theta) & M_{b_i Q}(\theta) \\ M_{c_i F}(\theta) & M_{c_i D}(\theta) & M_{c_i Q}(\theta) \end{bmatrix}, \; i=1,2$$

$$[L_R] = \begin{bmatrix} L_F & M_{FD} & 0 \\ M_{FD} & L_D & 0 \\ 0 & 0 & L_Q \end{bmatrix}$$

with:
- L_x: the inductance of the x winding (x=S_1, S_2, F, D, Q).
- M_{xy}: the mutuel inductance between the x and y windings.
- $S1$: first star armature indix.
- $S2$: second star armature indix.
- F: the rotor winding.
- D: direct axis damper winding
- Q: quadrature axis damper winding

It is important to notice that inductance matrix $[L]$ depend on the angular position which varies with the time.

Using current source inverter structure, in normal conduction, only two phases of each star are supplied. The same phenomenon occures when a rectifier is supplied by a synchronous alternator. Hence a multiple model of the power system is required. Each possible configuration of power system is represented by a set of electrical equations which must be written in the state space form:

$$[\dot{X}] = [A][X] + [B][U]$$

71

The matrix $[A]$ and $[B]$ depend on the inverse of the matrix inductance. Which must be computed at each simulation step. An analytical method to inverse the matrix inductance is proposed.

For each operating mode the inductance matrix can be put in the following form:

$$[L_m] = \begin{bmatrix} [Am] & [Bm] \\ [Bm]^t & [Lr] \end{bmatrix}$$

The matrix inverse is:

$$[L_m]^{-1} = \begin{bmatrix} [X_1] & [X_2] \\ [X_3] & [X_4] \end{bmatrix}$$

where

$$[X_1] = \left[[Am] - [Bm][Lr]^{-1}[Bm]^t \right]^{-1}$$

$$[X_2] = \left[[Am] - [Bm][Lr]^{-1}[Bm]^t \right]^{-1} [Bm][Lr]^{-1}$$

$$[X_3] = -[Lr]^{-1}[Bm]^t \left[[Am] - [Bm][Lr]^{-1}[Bm]^t \right]^{-1}$$

$$[X_4] = [Lr]^{-1} + [Lr]^{-1}[Bm]^t \left[[Am] - [Bm][Lr]^{-1}[Bm]^t \right]^{-1} [Bm][Lr]^{-1}$$

2.1 Basic scheme of the electrical propulsion

The current source inverter-synchronous motor set (CSI-SM) can be have two operating modes. The first one corresponds to the normal conduction as shown in figure 3. The second one corresponds to the commutation mode as illustrated in figure 4. The same configuration can be possible in the synchronous alternator-rectifier (SA-RE). Hence four operating modes are possible for the global power system (table 1).

The principle of the modeling consists:
- to plot the corresponding electrical scheme for the operating mode under consideration
- to etablish the electrical equation based on the general electrical equation and the electrical circuit Kirchoff's law.
- to deduce the motor phase currents from the current in the smoothing circuit and the commutation current after solving the electrical equation [5].

CSI-SM	SA-RE	Power system
Normal conduction	Normal conduction	Mode 1
Normal conduction	Commutation	Mode 2
Commutation	Normal conduction	Mode 3
Commutation	Commutation	Mode 4

Table 1: operating mode of the basic scheme
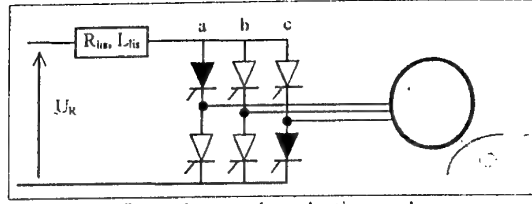
figure 4: normal conduction mode
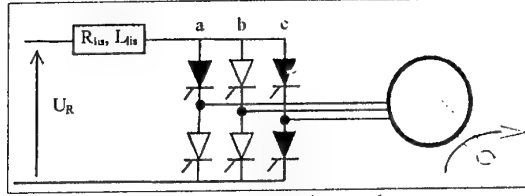
figur 5: commutation mode

2.2 Double star synchronous motor

As mentionned previously, in the case of a double star synchronous motor two configurations are possible. The table 2 summarises the operating modes of the current source inverter double star synchronous motor set (DSSM-CSI) corresponding to the shunt configuration (figure 2.b).

Star 1	Star 2	DSSM-CSI
Normal conduction	Normal conduction	Mode 1
Normal conduction	Commutation	Mode 2
Commutation	Normal conduction	Mode 3
Commutation	Commutation	Mode 4

Table 2: operating modes of DSSM-CSI (shunt configuration)

As an example we give the principle to etablish the electrical equation corresponding to the mode 1 of the DSSM-CSI power system. The studied configuration corresponds to figure 5. The a and b phases of the first star armature and the c and b phases of the second star armature are supplied. Hence the stator windings linked are by next equations:

$$U_{R_1} = R_{lis}.I_{R_1} + L_{lis}.\frac{dI_{R_1}}{dt} + v_{a_1} - v_{b_1} \qquad (2)$$

$$U_{R_2} = R_{lis}.I_{R_2} + L_{lis}.\frac{dI_{R_2}}{dt} + v_{c_2} - v_{b_2} \qquad (3)$$

$$i_{a_1} = +I_{R_1} \ , \ i_{b_1} = -I_{R_1} \ , \ i_{c_1} = 0 \qquad (4)$$

$$i_{a_2} = 0 \ , \ i_{b_2} = -I_{R_2} \ , \ i_{c_2} = +I_{R_2} \qquad (5)$$

The motor equations are deduced from the general equation of the double star synchronous motor.

According to the equation (1), (2), (3), (4) and (5) the electrical equation of the configuration presented in figure 5 can be written as follow:

$$[U_i] = [R_i][I_i] + [L_i]\frac{d[I_i]}{dt}$$

where

$$[U_i] = \begin{bmatrix} U_{R_1} & U_{R_2} & V_f & 0 \end{bmatrix}^t$$

$$[I_i] = \begin{bmatrix} I_{R_1} & I_{R_2} & I_f & I_D & I_Q \end{bmatrix}$$

$$[R_i] = \begin{bmatrix} [R_{S_i}] & [R_{SR_i}] \\ [R_{SR_i}]^t & [R_R] \end{bmatrix}$$

$$[L_i] = \begin{bmatrix} [L_{S_i}] & [L_{SR_i}] \\ [L_{SR_i}]^t & [L_R] \end{bmatrix}$$

$$[R_{S_i}] = \begin{bmatrix} R_{lis} + 2R_s + 2\omega(L_d - L_q).\sin(2\theta - \frac{2\pi}{3}) & 2\omega.(L_d - L_q).\sin(2\theta - \frac{\pi}{2}) \\ 2\omega.(L_d - L_q)\sin(2\theta - \frac{\pi}{2}) & R_i i_s + 2R_s + 2\omega.(L_d - L_q)\sin(2\theta - \frac{\pi}{3}) \end{bmatrix}$$

$$[R_{SR_i}]^t = \begin{bmatrix} -\sqrt{2}M_{fd}.\omega.\cos\left(\theta - \frac{\pi}{3}\right) & -\sqrt{2}M_{fd}.\omega.\cos\left(\theta - \frac{\pi}{6}\right) \\ -\sqrt{2}M_{dD}.\omega.\cos\left(\theta - \frac{\pi}{3}\right) & -\sqrt{2}M_{dD}.\omega.\cos\left(\theta - \frac{\pi}{6}\right) \\ \sqrt{2}M_{qQ}.\omega.\sin\left(\theta - \frac{\pi}{3}\right) & \sqrt{2}M_{qQ}.\omega.\sin\left(\theta - \frac{\pi}{6}\right) \end{bmatrix}$$

$$[L_{S_i}] = \begin{bmatrix} L_{lis} + L_d + L_q + (L_d - L_q).\cos(2\theta + \frac{\pi}{3}) & \frac{\sqrt{3}}{2}(L_{dm} + L_{qm}) + (L_d - L_q)\cos(2\theta - \frac{\pi}{2}) \\ \frac{\sqrt{3}}{2}(L_{dm} + L_{qm}) + (L_d - L_q)\cos(2\theta - \frac{\pi}{2}) & L_i i_s + L_d + L_q + (L_d - L_q).\cos(2\theta + \frac{2\pi}{3}) \end{bmatrix}$$

$$[L_{SR_i}]^t = \begin{bmatrix} -\sqrt{2}M_{fd}.\sin\left(\theta - \frac{\pi}{3}\right) & -\sqrt{2}M_{fd}.\sin\left(\theta - \frac{\pi}{6}\right) \\ -\sqrt{2}M_{dD}.\sin\left(\theta - \frac{\pi}{3}\right) & -\sqrt{2}M_{dD}.\sin\left(\theta - \frac{\pi}{6}\right) \\ -\sqrt{2}M_{qQ}.\cos\left(\theta - \frac{\pi}{3}\right) & -\sqrt{2}M_{qQ}.\cos\left(\theta - \frac{\pi}{6}\right) \end{bmatrix}$$

The same methodology principle can be applied to serie the configuration of the electrical propulsion. As the same D.C. current supply the two star armatures, the state space equation order is reduced. Hence the stator equation is deduced from equation (1) according to the next relation:

$$U_R = R_{lis}I_R + L_{lis}.\frac{dI_R}{dt} + v_{a_1} - v_{b_1} + v_{c_2} - v_{b_2}$$

$$i_a = i_{c_2} = I_R$$

$$i_{b_1} = i_{b_2} = -I_R$$

$$i_{c_1} = i_{a_2} = 0$$
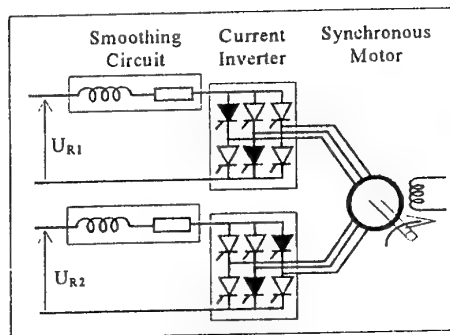
figure 5: electrical equivalent scheme of mode 1 (shunt configuartion)

3 Simulation of the electrical propulsion

The litterature of the last two decades is rich in number of simulation programs dealing with power electronic systems [3][4]. Hence several methods are developped.

As mentioned in the above paragraph, power electronic systems contain non-linear switching elements taking either "on" or "off" state. State changes of these devices lead to configuration changes of the system equations Each system configuration corresponds to a particular operation model. The global physical system is thus represented by a multiple model system.

At any time, the simulation program has to choose the appropriate model for the following computation step. This is a rather difficult task because the model changing, causes by the occurence of an event; are mainly unforeseeable, they are closely linked to the interaction of the "power system" (mains-converter-machine) and the control unit. Moreover, they are not synchronized with the step-by-step computation [4].

An event simulation methodology using Matlab-Simulink package software is applied to simulate the all structure of the electrical propulsion.

Figure 6 represents the simulation results corresponding to the basic scheme of the electrical propulsion. The supply source frequency is 60Hz and the inverter frequency is 50Hz.
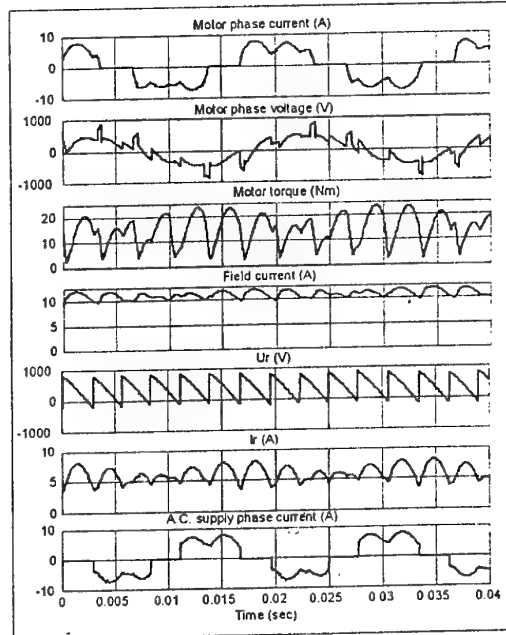
figure 6: simulation results of the basic scheme of the electrical propulsion

Figures 7 and 8 gives a phase motor current and the torque of the double star synchronous motor drive both for the serie and shunt configuration. The rectifier is modeled by a D.C. controlable voltage.
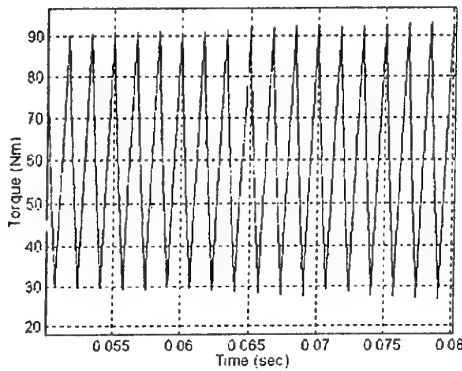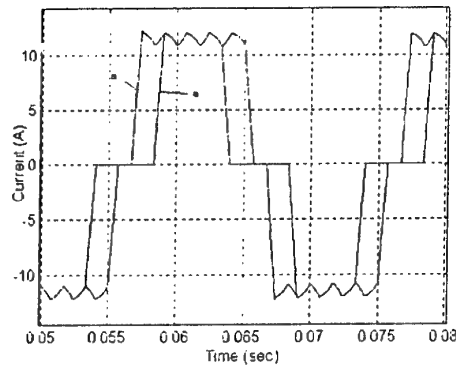
figure 7: simulation result - serie configuration
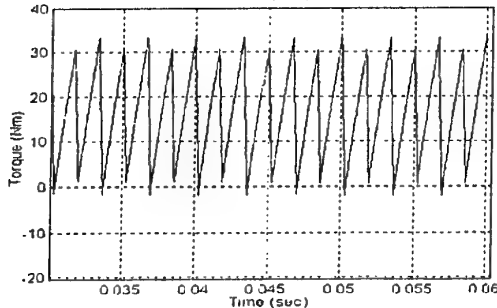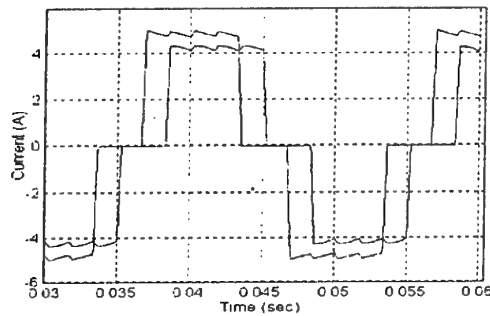

figure 8: simulation result - shunt configuration

4 Harmonic Analysis

The motor and the supply source harmonic current produce a motor torque ripple and network perturbation. The simulation program developped previously can be used to estimate the harmonic currents, the ripple, etc..

In order to estimate the motor harmonic currents, two approaches can be considered.

In the first approach, the rectifier and it's control unit are substituted by a constant gain. Hence the voltage at the output of the D.C. current controller represents the mean value of the voltage at the output of the rectifier. The inverter is controlled at 60Hz frequency.

In this case, the motor current presented in figure 9.a, is composed by a fundamental compoment and odd harmonics which are not a multiple of three (figure 10.a).

The second approach consists to take into account the rectifier. The frequency of the supply source is kept constant at 60Hz. The simulation is done respectively with two current inverter frequencies 50Hz (figure 9.b) and 60Hz (figure 9.c). The instantaneous current for the both cases is more different for the current obtained in the first approach. The harmonic analysis (figure 10) show that currents harmonics are odd multiple (non multiple of three) if the A.C. supply source and the inverter have the same frequency. Nevertheless harmonic amplitudes are differents from these obtained in the first approach (figure 10.b).

When the A.C. supply source and the inverter have not the same frequency the motor phase current presents some interharmonics (non characteristic harmonic due to intermodulation effect) (figure 10.c).

The same phenomenon is shown in the A.C. supply current. Generally harmonics and interharmonics frequencies can be calculated as follow:

$$f_v = \left[(P_1 . m) \pm 1\right] f_S \pm \left[P_2 . n\right] f_I$$

where:

P_1: rectifier phase number

P_2: inverter phase number

m,n: integer number

f_S: A.C. supply source frequency

f_I: current inverter frequency

74
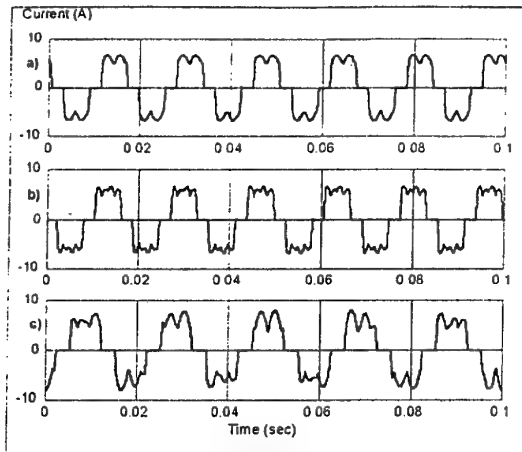
figure 9: motor phase current for different inverter frequency
a) first approach ($f_I = 60$Hz)
b) second approach ($f_S = 60$Hz, $f_I = 60$Hz)
c) second approach ($f_S = 60$Hz, $f_I = 50$Hz)
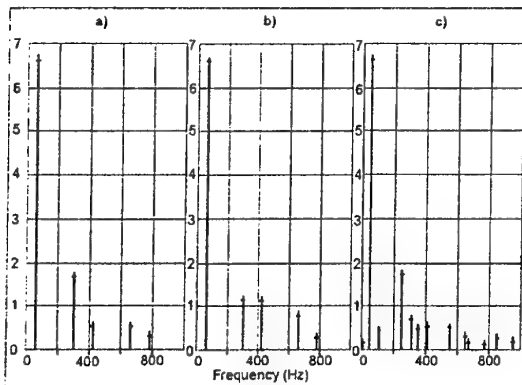
figure 10: harmonic analysis of the motor phase current for different inverter frequency
a) first approach ($f_I = 60$Hz)
b) second approach ($f_S = 60$Hz, $f_I = 60$Hz)
c) second approach ($f_S = 60$Hz, $f_I = 50$Hz)

5 Conclusion

In this paper we present a modeling and simulation methodology of electrical propulsion using current source inverter for both three phase and double star synchronous machine.

The developped model will enable us to investigate the behaviour and performance of this drive.

The network effect can be seen when the rectifier is taken into account, especially when the A.C. supply source and the inverter frequencies are differents. Then the motor current non characteristic harmonics due to the intermodulation effect produces a torque ripple.

References

[1] E. Moustafa, M. Poloujadoff, "Experimental determination of machine characteristics for a double star armature synchronous machine", **Electric Machines and Power Systems**, 8:103-112.

[2] L. Werren, "Synchronous machine with 2 three-phase windings, spatially displaced by 30° el. Commutation reactance and model for converter-performance simulation", **ICEM 84**, 2:781-794, sept. 1984, Lausanne, Switzerland.

[3] J.G. Kassakian, "Simulating power electronic systems. A new approch", **Proc. IEEE** 67, 1979

[4] R. Le Doeuff, M.F. Benkhoris, "General principles and new trends in the simulation of static converters and drives", **Mathematics and computers in simulation Elsevier Science** B.V. 38, 1995, p. 263-270.

[5] M.F. Benkhoris, S. Lasquellec, M. Féliachi, R. Le Doeuff, "Saturation effect on the simulation of the synchronous machine-power electronic converter set", **ICEM 98**, 2-4 sept. 1998, Istanbul, Turkey.

List of symbols

ω: electrical pulsation
L_d: inductance of the direct axis stator winding
L_q: inductance of the quadrature axis stator winding
L_D: inductance of the direct axis damper winding
L_Q: inductance of the quadrature axis damper winding
L_f: inductance of the field winding
M_{fd}: mutuel inductance between the field and the d axis stator windings
M_{FD}: mutuel inductance between the field and the d axis damper windings
M_{dD}: mutuel inductance between the d axis stator windings and the damper windings
M_{qQ}: mutuel inductance between the q axis stator windings and the damper windings
r_s: resistance of the stator phase winding
R_f: resistance of the field winding
R_D: resistance of the D axis damper winding
R_Q: resistance of the Q axis damper winding
R_{lis}: resistance of the smoothing circuit
L_{lis}: inductance of the smoothing circuit
v_{ai}, v_{bi}, v_{ci}: stator phase voltages of the star armature i
i_{ai}, i_{bi}, i_{ci}: stator phase current of the star armature i
I_f: field current
I_D: D damper winding current
I_Q: Q damper winding current
V_f: field voltage

75

Experiences of Azipod® propulsion systems onboard merchant vessels

R. Pakaste, K. Laukia, M. Wilhelmson, J. Kuuskoski
(ABB Azipod Oy)
Laivanrakentajantie 2
00980 Helsinki, FINLAND

Abstract

The Azipod (Azimuthing Electric Propulsion Drive) propulsion system has been developed jointly by ABB and Kvaerner Masa-Yards. The Azipod concept is a main propulsion system based on the ac-ac electric propulsion concept. Development work and references of ABB Azipod Oy are described. Also vessels ordered with the Azipod propulsion system are described.

As an example of the concept the propulsion machinery of the earlier *Fantasy-class* vessels and the seventh vessel of the series, the *M/S Elation*, are compared. Practical experience of the system is presented in a description of the sea trial experiences.

1 Introduction

This paper describes the history of the Azipod concept and in more detail the design of the Azipod propulsion system installed on the *M/S Elation* owned by Carnival Cruise Lines. The impact of the installation on the successful Fantasy-class cruise ship series is also described.

The results described in this paper can be achieved by installing the Azipod propulsion system on any newbuilding ship. When the vessel is designed from the beginning with the Azipod concept even further improvement in results can be expected.

In the marine field it takes several years before a new innovation is accepted to enter into the market. This means that systematic work and feed-back is needed before the product can be installed to a commercial vessel where its main task is to be profitable to its owner. When the Azipod concept was studied for the first time some seven years ago for a cruise liner, it was clear that certain steps were needed. In each step certain design aspects have been studied and realized in practice.

1. The Azipod unit installation on the waterway service vessel Seili proved the idea itself. An Azipod system can be built and installed, it is strong enough and fulfills all the basic requirements set for ship main propulsion.

2. The first high propulsion power installation for a commercial vessel, the 11.4 MW arctic tanker *Uikku*, proved the concept's superior capabilities in maneuvering and efficiency and have given valuable experience of high power applications.

3. The first pulling Azipod units were installed onboard the icebreaker Röthelstein in 1995. The comparison to pushing types was made and some very useful conclusions were drawn.

These vessels rapidly increased cumulative operating hours, thus giving valuable information and feed-back for the future designs.

The combination of these "full-scale applications" and a very extensive R&D program gave the basis for the Azipod cruise liner concept which was finally realized at the end of 1995.

2 History of the Azipod propulsion concept

The original idea for the Azipod system was developed when the Finnish Maritime Administration began to seek better solutions for the operation of icebreakers in ice channels. An important feature of an icebreaker is that it must be able to break out of an existing ice channel. This is important when the merchant ships that are being assisted, are using the ice channel and the icebreaker has to move around the operational area. To overcome this problem, the idea of a propulsion motor that could direct the thrust to any direction was created. The idea was presented to ABB and the concept of Azipod was drafted and patented.

Kvaerner Masa-Yards and ABB made an agreement in 1992 to develop and market the unit jointly. In 1993 the name Azipod was registered. After the order of the conversion of the *M/T Lunni* in 1994, the Kvaerner Masa-Azipod unit was founded.

Finally, on October 1, 1997 ABB, Fincantieri and Kvaerner Masa-Yards founded ABB Azipod Oy to market, design and produce Azipod propulsion systems.

YEAR	R&D STEPS	TARGET
1990	1,5 MW Azipod unit "SEILI"	Basic design wo
1993	11,4 MW Arctic tanker "Uikku"	Step in azimuth thruster's power Full scale hydrodynamic design check
1994	2x0,56 MW River icebreaker "Röthelstein"	Pulling propellers New ship concept (double acting)
1995	"SEILI" Azipod complete overhaul	Feed back after five years' operation
1997	2x14 MW Cruise liner M/S "Elation" sea trial	High power pulling Azipod units in operation
1998	"Uikku" Azipod complete overhaul	Feed back after four years' operation

Table 1. Azipod concept R&D steps in full scale.

3 Experiences onboard merchant vessels and references

M/S Seili
The first joint R&D project was the conversion of *Seili*, a waterway service vessel owned by the Finnish Maritime Administration, into the first Azipod ship in the world. This took place in 1991. The *Seili* continues to operate today, and its 1.5 MW unit has operated faultlessly since the conversion.

M/T Uikku and M/T Lunni
The next ship to be equipped with Azipod was a 16 000 DWT product tanker, the M/T Uikku, built in 1978 in Germany. The conversion work of Uikku was done in 1993. The power of Uikku's Azipod unit is 11,4 MW. The ship was built to ice class 1A Super and the Azipod to DnV ice 10 class. In 1995, Uikku's sister ship the M/T Lunni was similarly converted. Both ships have been in heavy commercial use since conversion. Their combined operating hours total well over 30,000. Of these, about 10,000 hours were on ice-infested waters. In 1997 Uikku became the first western cargo ship to navigate through the North-East Sea route. Uikku started its journey in Murmansk in western Russia in the beginning of September. Twelve days later Uikku arrived in Providenya, located in eastern Siberia south of the Bering Strait. The Uikku and The Lunni demonstrate the soundness of the basic design and construction chosen for the Azipod.

I/B Röthelstein
When the *M/T Lunni* was built, a small Austrian icebreaker, the *I/B Röthelstein*, was completed.

The power of each of the two Azipod units is 560 kW. The Röthelstein is a small river icebreaker that introduced new ice breaking technology, attacking the ice with pulling propellers. The icebreaker is driven stern first with the Azipod units pulling the vessel.

The icebreaking concept of going astern with pulling Azipod units demonstrates an icebreaking capability that surpasses all other technologies. It has also been tested with the *Lunni*. The tests showed that although the *Lunni* was not designed to operate stern first in heavy ice, it was able to operate in the toughest conditions found in Finnish waters without icebreaker assistance. Model and full scale test confirm that only 60% of the power needed when attacking the ice bow first is needed for this mode of icebreaking.

M/S Elation and *Paradise*
The good results and reliable operation of the Uikku and the Lunni enabled CCL (Carnival Cruise Lines) to choose Azipod for the *Elation* and the *Paradise* in the autumn of 1995. The power of each of the two units is 14 MW. The Azipod system of these vessels will be described in detail in chapter 4.

M/S Eagle I and *Eagle II*
The next Azipod system order came over a year later. It was placed for RCI (Royal Caribbean International). The biggest cruise ships ever ordered will be equipped with two 14 MW Azipod units and one 14 MW Fixipod, a non-rotating Azipod unit. The first ship will sail in the autumn of 2000. It is also one of the first cruise ships equipped with a DP-system. With the Azipod propulsion system and 3 x 4 MW bow thrusters, this system will be so powerful that the giant ship

will be able to stay on its designated place in winds, from any direction, of up to 18 m/second.

The MSV Botnica

In February 1997 Finnyards Oy ordered two 5 MW Azipod units for the multipurpose icebreaker *Botnica* it had on order for The Finnish Maritime Administration. The ship will operate in the Gulf of Finland in winter and in the North Sea oil fields for the rest of the year. To accomplish its offshore duties, the ship is equipped with a DnV Autro dp-class. The ship entered service at the North Sea in the summer of 1998. Excellent sea-trial experiences proved the system to make the ship very well suitable for the offshore work.

The *Botnica* is the first ship equipped with Azipod units and used in the offshore market and will provide a good reference for future applications.

Supply Ships for the Caspian Sea

In November 1997 Kvaerner Masa-Yards received an order for two small icebreaking supply ships the *Arcticaborg* and the *Antarcticaborg* powered by two 1620kW Azipod units. The ship's operation pattern in the Caspian Sea is made possible by the use of Azipod propulsion units. The ice conditions in the northern Caspian Sea are very severe, so the Azipod units will operate as ice lathes.

4 From Fantasy to Elation

The first ships in the Carnival Cruise Line's Fantasy-series were ordered in 1986 from the Kvaerner Masa-Yards shipyard in Helsinki (former Wärtsilä Marine). Over the years the Fantasy-series has grown to be the biggest series of purpose-built cruise ships ever constructed. A total of eight ships of the same design will be built. This design has proven to be very successful: both the builder and the owner have been satisfied with the ships.

For the two most recent units in the series, the *Elation* and the *Paradise*, CCL decided to adapt the Azipod propulsion concept already proven in service vessels and product tankers.

The Original Propulsion Machinery

In the original version the propulsion machinery consists of a diesel-electrical power plant connected to one busbar. Power is directed to the controllable pitch propellers with two 14 MW cycloconverter controlled propeller motors. The drive system provides smooth torque and speed control over the entire speed range.

To ensure maneuverability, the ships are equipped with three 1.5 MW tunnel thrusters in the bow and in the stern. Two rudders are also mounted in the stern

At that time the *Fantasy* represented the state of the art in propulsion and control technology. Today most new cruise vessels are equipped with electric propulsion.

In the Autumn of 1995, CCL and Kvaerner Masa-Yards determined to remain front-runners in applying new technology. CCL chose to use Azipod propulsion in their ships instead of the original propulsion described above. Electrical changes were minor: instead of running cables to the propeller motors, the cables were routed to the Azipod units and cabling work could be reduced since much of the equipment on the previous vessels were not installed.

Changes in the steel construction were avoided. For example, shaft tunnels inside the ship were turned into fresh water tanks. The main changes made included new construction for Azipod unit wells, head boxes, to allow the Azipod units to rotate 360° and cover plates for the three stern thrusters that had been eliminated.

All equipment and castings related to the shaft lines were removed. The steering gear hydraulic system was replaced by the Azipod hydraulic system. The cooling water system for the propulsion motors was extended to the Azipod room.

A summary of the changes in propulsion and maneuverability of the Elation compared with earlier ships in the Fantasy series is given in Table 2.

Item	Fantasy	Power	Elation	Power
Propulsion	2x14 MW	28 MW	2x14 MW	28 MW
Bow Thrusters	3x1.5 MW	4.5 MW	3x1.5MW	4.5 MW
Stern Thrusters	3x1.5 MW	4.5 MW	none	
Rudders	2 pcs		none	
		37 MW		32.5 MW

Table 2.

Design Aspects of the Azipod Propulsion System

Several aspects have to be taken into consideration when applying the Azipod concept: hull form, Azipod location, motor design parameters, propeller design and strength, hydrodynamic details, structural strength, vibration design and tuning, steering logic and operation modes, ship characteristics like course stability and heeling, behaviour in black-out situation and redundancy.

The Azipod turning shaft is located in the place of the old rudder vertical shaft. This allows full azimuthing angles and enough clearance to the baseline as well as sideways. The Azipod attachment to the ship hull is carefully designed according to the model scale tests and full scale experience. The synchronous electric propulsion motor design values, power and torque curves were kept identical to the sister vessels although savings in propulsion efficiency were expected.

Propellers

The fixed-pitch propeller diameter is 5,2 meters, as on the sister vessels. These propellers are the most powerful pulling propellers ever built. New operation modes created new challenges for the design. The task was successfully performed by making detailed hydrodynamic and FEM-calculations and by model scale tests.

The hydrodynamic optimization procedure resulted in inward rotating propellers. The Azipod was slightly inclined (six degrees) downwards in order to give a good inflow for the propeller. The results based on model scale tests estimated a several percentage improvement in propulsion efficiency.

Steel structure

The structural dimensioning was based on two basic load conditions: max. continuous loading in normal service and extreme loading (abnormal operation, e.g. if the control of the Azipod fails). The key design point was to adjust the dynamic behaviour. The excitation forces and moments were known from earlier projects. Excitation level is low due to the good wake field. The steel structure of the Azipod and ship hull was dimensioned so that the resonances were avoided in critical areas and in full powers. A special emphasis was placed on the Azipod attachment to the hull.

Steering system

The steering of the Azipod units is done by an electro-hydraulic steering system. A total of four hydraulic motors give the pod sufficient turning speed and redundancy. Steering logic had to be rethought e.g. the stability of the Azipod units, steering angles versus ship speed, power limitations and crash stop characteristics. Ship behaviour calculations during extreme maneuvering were done. The black-out situation was analyzed: Azipod system behaviour, dimensioning of the emergency network and starting sequence of the steering motors.

Also the redundancy was studied in order to prevent any failure in one pod to stop the other.

The Azipod units are mechanically, electrically and hydraulically independent.

Layout Modifications Onboard the Elation

Changes in the layout were kept to a minimum, except for the Azipod itself. The propeller motor room, no longer needed, actually offers new design possibilities because it makes available an additional 1200 m² of space. This space is as wide as the ship (32 m), 20 m in length, and two decks high, the height of the propeller motors. In the case of the Elation, the room was excellent for additional waste handling equipment:

An incinerator and a gray water treatment plant were installed in the propeller motor rooms of the original design and the old shaft tunnels were converted into fresh water tanks. Changes in the lay-out of the machinery spaces were minimal compared to the sister vessels. This was an advantage to the shipyard and the owner.

M/S *Elation* Sea-Trial Results

Efficiency

The following results were recorded during the sea trial in December 1997 in the Gulf of Finland. The increase in propulsion efficiency compared with the existing *Fantasy* class ships was 8%. The hull lines are the same on the Elation as on the previous ships in the Fantasy-series. The only changes were the local modification around the Azipod units and the closing of the stern holes for the thrusters.

Maneuverability

The maneuverability of a ship is best demonstrated by its full speed turning circle. The diameter of the turning circle of the *Elation* was about 30% smaller compared with the previous Fantasy-class vessels. The ability to turn the ship fast gives the master a better margin for maneuvering in tight situations and increases the safety of the ship.

The other important feature in a ship is its crash stop performance. The test was performed by reversing the propellers. An additional safety feature of a ship with Azipod units during a crash stop, is that the ship can be steered towards the desired stopping point.

Passenger comfort - vibrations

Reduction in noise and vibrations were also observed during the sea trials. This is mainly due to the very good wake field of the pulling propeller and resulting reduction in pressure pulses from the propeller to the hull. The passenger will observe the biggest difference in
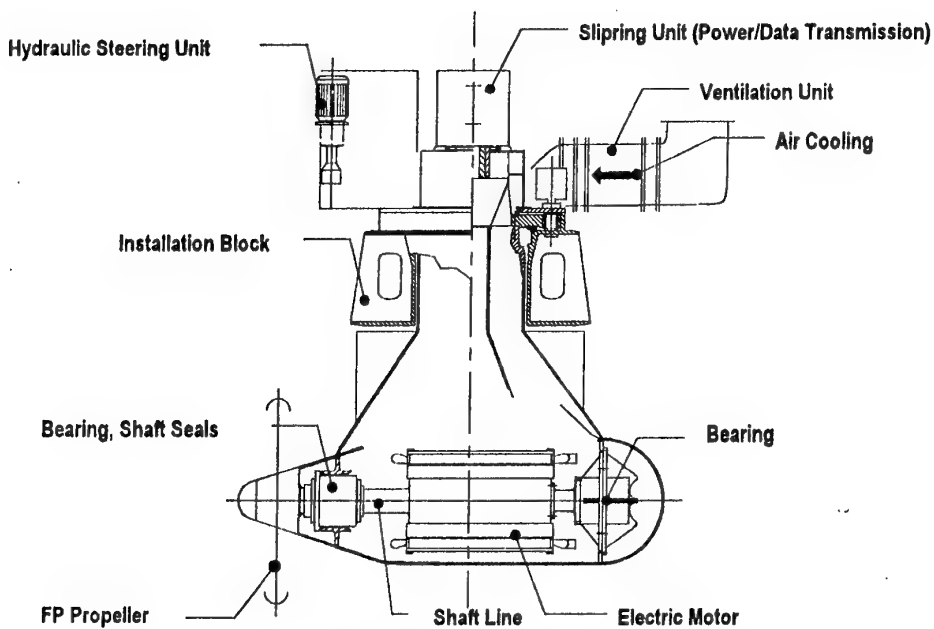
Fig. 1: Main components of an Azipod unit.

the confined area operations and during harbor maneuvers. The absence of the stern thrusters and the rudders makes a big difference in passenger comfort.

Conclusions

Recent experiences with the diesel-electric power plant concept combined with the Azipod propulsion system have proven the concept to be an attractive solution for various types of vessels. The improved total efficiency, in addition to other advantages such as enhanced maneuverability, redundancy, reduction of equipment, simplicity and proven reliability of the design, can be utilized in most ship projects of various types. The suitability of the concept for cruise ships is obvious, which the successful sea-trials of the M/S Elation prove.

The feasibility analysis for a new project should always be carried out together with the shipbuilder. The Azipod propulsion concept changes not only the way ships can be designed and operated but also how they are built.

Permanent Magnet Synchronous Motor For Ship Propulsion Drive

M. Rosu, V. Nahkuri, A. Arkkio, T. Jokinen, J. Mantere[*], J. Westerlund[*]

Helsinki University of Technology, Laboratory of Electromechanics, P.O. Box 3000, FIN-02015 HUT, FINLAND

[*] ABB Industry Oy, Synchronous Machines, P.O. Box 186, FIN-00381 Helsinki, FINLAND

Abstract

This paper describes a design of a permanent magnet synchronous motor with radial flux distribution. For these kinds of synchronous motors, the ship propulsion drive is a very interesting application, especially for podded drives, where the motor is incorporated in the propeller pod. Permanent magnet rotors do not have magnetization losses, which simplifies the rotor construction and cooling. This can be very useful in slow speed and podded drives. In this study, different permanent magnet motor configurations were analysed. Results are here presented mainly for different radial field permanent magnet motors. Numerical calculations of motor characteristics were performed with a two-dimensional finite element, time-stepping simulation program.

1 Introduction

In low-speed, high-power applications like electrical propulsion drives, development of motors towards higher specific outputs (power per volume unit) is going on. This is especially true in podded drives, where the motor is installed in the propeller pod, and where space savings can bring significant benefits. Permanent field synchronous motor concept gives good basis for further development of the whole drive configuration.

Interest in permanent magnets may not be obvious due to fairly high magnet prices and due to lower air gap flux densities, which can be achieved with magnets compared to those obtained with standard wound poles. However, recent developments both in magnet prices and in magnet characteristics give new interest to development of permanent magnet motors.

Development in production technology has brought new and more powerful permanent magnets available to users. Best characteristics are achieved with Neodymium-Iron-Boron (NdFeB) alloys. NdFeB gives higher energy product than earlier used Samarium Cobalt (SmCo) rare earth magnets. SmCo magnets permit higher operation temperature and high coercive field strength, but this material is expensive and also brittle, which makes handling and construction more difficult.

One disadvantage of NdFeB materials has been high temperature dependence of the coercive field strength. New compositions of NdFeB magnets are available with a fairly high coercive field strength at operation temperatures suitable for motor design without loosing too much in the energy product.

The clear benefits of a permanent magnet motor concept come from the absence of active windings in the rotor. Compared to synchronous motor with wound poles no excitation supply equipment is needed and losses in the rotor are minimal also compared to induction motor designs. The rotor construction without windings and with negligible or with only small losses gives a possibility to simplify the whole motor construction and to arrange more effective cooling for the motor. This leads to space and weight savings in the total construction, which can give clear advantages for the propeller drive e.g. in terms of the efficiency of the drive and thus in fuel consumption of the ship.

A variety of possible PM motor constructions have been presented in the literature. In this study, different types of permanent magnet motor configurations were analysed and judged according to their suitability for low speed propulsion motor applications with special focus on motor constructions in podded drives. In addition, the influence of several parameters like pole number, air gap length and magnet placing were considered in comparative calculations and in analysis of motor performance.

2 Method of Analysis

The prediction of the performance of the motor is based on the numerical solution of the magnetic vector potential in the core region of the machine. The magnetic field is assumed to be two-dimensional, and the two-dimensional field equation is discretized by the finite element method. The effects of end-region fields are taken into account approximately by constant end-winding impedances in the circuit equations of the windings. The circuit equations are solved together with the field equation.

The time-dependence of the field is modeled by the Crank-Nicholson method. The rotor is rotated by changing the finite element mesh in the air gap. The non-linear system of equations obtained at each time-step is solved by the Newton-Raphson method. Second-order, isoparametric, triangular elements have been used when computing the results of this paper. The details of the method of analysis are given in Ref. [1].

The permanent magnets are modeled using a linear magnetisation curve defined by the remanence flux density B_r and the coercive field strength H_c. During the time-stepping process, the state of the magnets is monitored by observing the flux density in the magnetisation direction of the magnets. If this flux density goes under a certain limit

a warning of the risk of demagnetisation is given. Eddy-currents in the magnets and the losses associated with them are calculated within the time-stepping analysis.

The main simplification in the model is the assumption of a two-dimensional magnetic field. Because of this, the permanent magnets are taken as bars continuous over the length of the machine. The eddy-currents flow along these bars and the eddy-current losses become larger than they would be in a real motor in which the poles are constructed of smaller pieces of permanent magnet insulated partially from each other.

3 Different PM - Topologies

The three main topologies of permanent magnet motors are: axial flux, transverse flux and radial flux operation principle.

Axial Flux Machines. The axial flux principle incorporates a disc type rotor and two disc type stators. The axially magnetized permanent magnets are located in the rotor disc. The flux produced by rotor poles flows through two annular air gaps into the stator core. A high pole number must be used to decrease the thickness of the flux carrying parts and to decrease the length of the winding overhangs. This allows a construction with many disc type stators and rotors within the axial length available and provides, as a consequence, a large air gap surface, which again means very high specific output (high torque/volume -ratio) [2].

Transverse Flux Machines. The transverse flux machine, also described as variable-reluctance permanent magnet machine, has a stator phase winding, usually having a simple circular form, exciting a homopolar mmf distribution in the air gap. This mmf is modulated by a pattern of stator teeth to produce a high order spatial harmonic of flux, which then interacts with a pattern of magnets on the rotor, with the same pole number, to produce torque. TF machines can efficiently have a very small pole pitch (high number of poles), which provides high specific output for the concept. The highest specific outputs can be achieved with multi-disc type constructions proposed e.g. in Refs. [3],[4].

Radial flux machines. Radial flux flow is the traditional and conventional operation principle for rotating electrical machines. Radial flux machines can be built efficiently for low or for high pole numbers [5].

When optimising the permanent magnet motor construction in relation to the size and weight, a high pole number is favourable, in all the three topologies. A higher pole number means a shorter pole pitch, and because flux carrying parts are directly related to the pole pitch, smaller thicknesses of stator and rotor yoke can be used. A smaller pole pitch means generally also a smaller permanent magnet thickness, which is important thinking of material costs. A smaller thickness of flux paths allows using a bigger air gap diameter with the same external diameter. With a bigger air gap diameter the motor can produce more torque.

Since the gearless propeller motor drives have low rotational speed, employment of a fairly high pole number is natural. But in respect to the mechanical characteristics a useful pole number may have certain limits. Constraints are coming mainly from the rigidity and characteristics of the magnetic core in relation to vibration and noise, stability against thermal stresses and various aspects of manufacturability.

When increasing the pole number, the feeding frequency will also increase. The increased frequency combined with a typically small air gap length can present considerable eddy current losses on the rotor surfaces due to harmonic distortion of the air gap flux caused either by slot harmonics or by converter harmonics. This must be considered in the PM motor dimensioning and design, especially in the case of surface mounted magnets.

Achieving high specific torque with axial field and transverse field topologies will require a high pole number and fairly complicated multi-disc constructions. Another disadvantage of the transverse flux machine is the low inherent power factor at full load [6].

Irrespective of the theoretically lower specific torque available from the conventional radial field motor concept, it is best suited for the constructional requirements and constraints of installation in a pod. Thus in this study, the radial field concept was selected to be the basis for more detailed studies and numerical analysis of motor performance.

4 Configurations Studied

The selected PM motor topology for further studies is the conventional radial field concept and the pole numbers selected were such that the output frequency of the converter will be below 50 Hz. With rotational speed equal to 150 rpm this means pole numbers less than 40.

Four radial field configurations, with different placing of permanent magnets, were first studied with respect to the electromagnetic torque as function of load angle. These four configurations are presented in Fig. 1, which shows their magnetic field distribution at load. All these rotor constructions have equal volumes of permanent magnets. Rotor types from a) to d) are:

a) surface mounted permanent magnets (SMPM)
b) pole shoe covered permanent magnets (PSPM), magnets mounted under laminated pole shoes
c) radially inserted permanent magnets in laminated core with flux barriers
d) tangentially inserted permanent magnets in laminated core, with maximum width of magnets

Configurations a) SMPM and b) PSPM clearly give the best torque per magnet volume ratios. In the inserted magnet types c) and d), the high portion of leakage flux limits the torque production. Because of the better torque per volume ratios, the constructions with surface mounted and pole shoe covered permanent magnets are chosen for a more detailed study presented in this work.

82

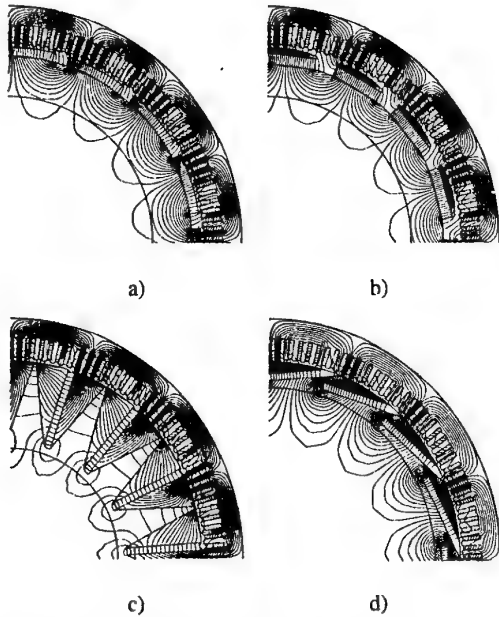a)   b)

c)   d)

Fig. 1. Magnetic field distribution at load for the four rotor configurations a), b), c) and d)

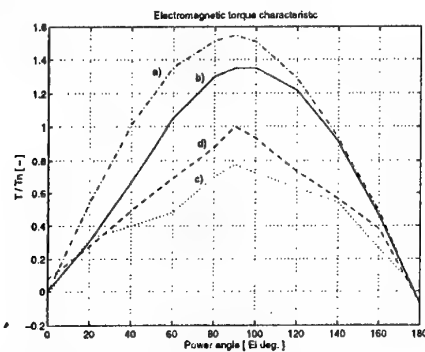The calculated electromagnetic torques as function of load angle are shown in Fig. 2.

Fig. 2. Air gap torque as function of load angle

5 Results

5.1 Comparison of Surface Mounted and Pole Shoe Covered Types

The following results have been calculated for a radial field type motor with two rotor versions:

a) surface mounted permanent magnets (SMPM) and

b) pole shoe covered permanent magnets (PSPM) according to Fig. 1. The stator is the same in both versions, also the air gap length as well as the volume of permanent magnet is kept constant.

With equal volumes of permanent magnets, the pole shoe version gives a lower power factor (Fig. 3a), and thus also a higher stator current, which will give higher stator winding resistive losses, Fig. 3 b.

Fig. 4 shows the harmonic distortion of the air gap flux density for both the rotor types at the rated load condition. The level of harmonics is of the same order in both the cases. The pole shoe type has a somewhat higher 3rd harmonic due to the smaller pole shoe width and bigger armature reaction. On the other hand, the 7th, 9th and 11th harmonics are clearly smaller with the pole shoe version. Slot harmonics (17th and 19th) have the same order of magnitude for both the types.

a)   b)
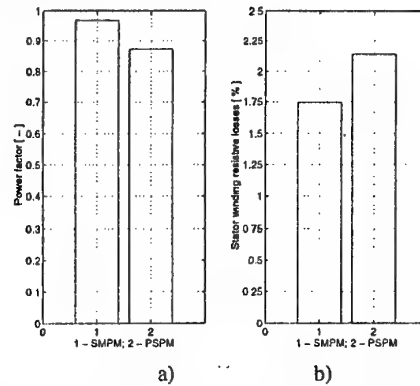
Fig. 3. Comparison of SMPM and PSPM types
a) Power factor b) Stator winding resistive losses
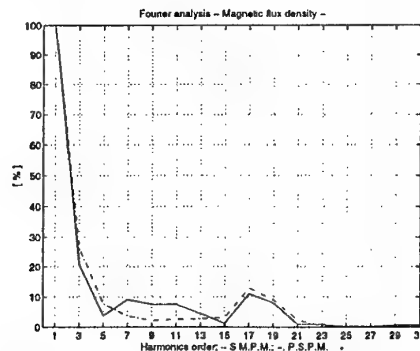
Fig. 4. Harmonic content of magnetic flux density
· · · · · SMSM ——— PSPM

The simulated harmonic content of the electromagnetic torques is shown in Figs. 5a and 5b. The pole shoe covered permanent magnet version has lower torque harmonics (6th, 12th and 18th) due to a better pole shape.
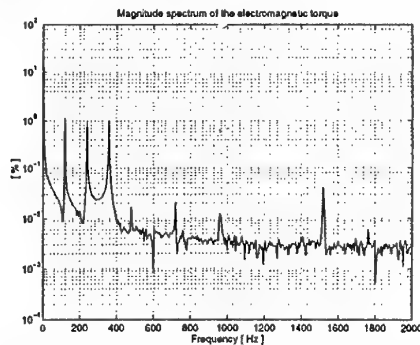
Fig. 5a. Harmonics in electromagnetic torque SMPM type

83
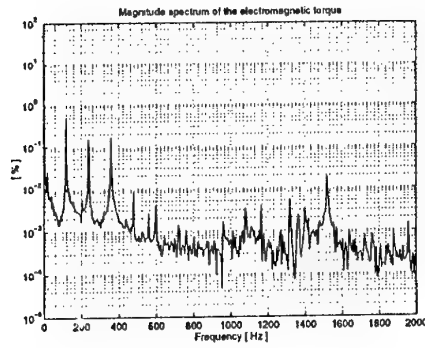
Fig. 5b. Harmonics in electromagnetic torque PSPM type

a)   b)
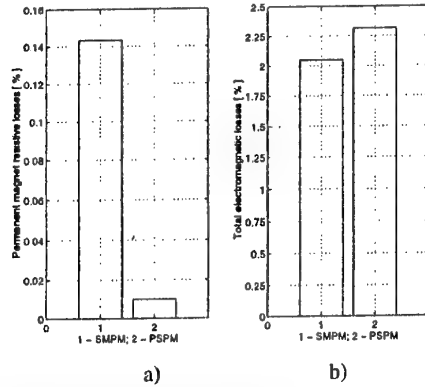
Fig. 6. Comparison of SMPM and PSPM types
    a) Permanent magnet resistive losses
    b) Total electromagnetic losses

The surface mounted permanent magnets version has considerably higher resistive losses in the magnets than the pole shoe version (with laminated pole shoes), as is shown in Fig. 6 a. However, concerning the total losses the surface mounted magnet type is still better due to the smaller stator winding losses (Fig. 3). The total electromagnetic losses are shown in Fig. 6 b.

In this study, the supply voltage of the motor was sinusoidal. In respect to surface losses in permanent magnets and to torque harmonics, similar calculations must be made also with actual current or voltage wave form of feeding converter.

5.2 Magnetic state of permanent magnets in nominal conditions

The demagnetisation of the magnets must be avoided in all loading situations. Fig. 7 shows the minimum flux density in the magnets at rated load for the both rotor versions.

The surface mounted magnet version is, as expected, much more sensitive to demagnetisation, although at the rated load still in safe operation state. In addition, maximum loading situation must be checked in respect to the magnetic state of permanent magnets.
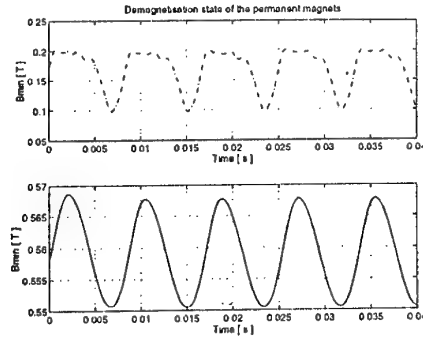
Fig. 7. Minimum magnetic flux density in permanent magnets at rated load
     · · · · · SMSM ——— PSPM

5.3 Magnetic state of permanent magnets in fault situations

The three-phase short-circuit is one of the most serious fault conditions from the operating state point of view. This situation, was analysed for the both configurations assuming that the rotation speed remains constant durring the fault situation.
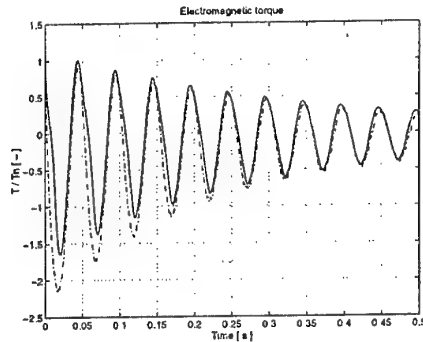
Fig. 8. Electromagnetic torque after the short-circuit
     · · · · · SMSM ——— PSPM

Fig. 8 shows the time variation of the ratio between the electromagnetic torque and rated torque due to the three-phase short-circuit. Fig. 9 shows the minimum magnetic flux density in permanent magnets at the three-phase short-circuit.

In time-stepping analysis of this transient phenomenon, the ratio between short-circuit current and rated current is equal to 1.55 for the surface mounted type and equal to 1.16 for the pole shoe covered type. This difference relates to the minimum magnetic flux density variation in Fig. 9.

According to Fig. 9 the analysed surface mounted type configuration will face quite high negative flux densities in fault situations. Whether it can withstand the situation without demagnetisation depends on temperature and on actual coercive force available from the magnets.

84
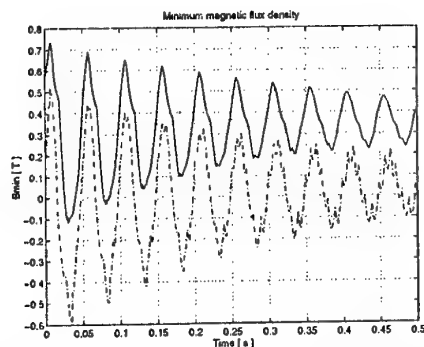
Fig. 9. Minimum magnetic flux density in permanent magnets at short-circuit condition
······ SMSM —— PSPM

6 Conclusions

Permanent magnet synchronous motors can bring significant space and weight savings in electric propulsion drives, especially in podded drives. There are many possible configurations of permanent magnet motor available. The traditional radial field concept offers a good basis for further development from the construction point of view.

The detailed study results were shown for a radial field PM motor equipped with two rotor versions: surface mounted permanent magnet rotor and pole shoe covered permanent magnet rotor. Both of these versions, with adequate dimensioning, seem to be suitable for the purpose. The surface mounted magnet type gives the required electromagnetic torque with smaller magnet volume than the pole shoe version, but is less favourable in respect to torque harmonics, permanent magnet resistive losses and sensitivity to demagnetisation. Magnetic state of permanent magnets must be checked in maximum operation conditions as well as in possible fault situations considering also the temperature of the magnets during these situations.

The analysis was made with a numerical 2D-FEM simulation tool with time-stepping method. This tool has shown to be effective in performance simulation of motors of radial field type. The work will be continued by including the actual current or voltage wave forms of the converter in the calculations.

References

[1] A. Arkkio, "Finite element analysis of cage induction motors fed by static frequency converters", **IEEE transactions on Magnetics, MAG-26, 2,** pp. 551-554, 1990.

[2] P. Letellier, "Electrical propulsion motors" **Proc. of Electric Propulsion – The Effective Solution? Conference,** London (U.K.), pp. 7.1-7.8, October 5th-6th, 1995.

[3] H. Weh, "Ten years of research in the field of high force density-transverse flux machines" **Proc. of SPEEDAM'96, Symposium,** Capri (Italy), pp. A3-1–A3-8, June 5th–7th , 1996.

[4] A. J. Mitcham, J. J. A. Cullen, "Motors and drives for surface ship propulsion: comparison of technologies" **Proc. of Electric Propulsion – The Effective Solution? Conference,** London (U.K.), pp. 4.1-4.10, October 5th-6th, 1995.

[5] M. Radaelli, L. Sozzi, P. Ehrhart, "Novel technologies with PM-machines for ship propulsion" **AES'97 (All Electric Ships),** pp. 17–22, 1997.

[6] M. R. Harris, G. H. Pajooman, S. M. Abu Sharkh, "The problem of power factor in VRPM (transverse-flux) machines" **EMD97, IEE Conference** Publication No. 444, pp. 386-390, 1-3 September 1997.

E-mail addresses for the authors:
Marius Rosu   Marius.Rosu@hut.fi
Ville Nahkuri   Ville.Nahkuri@tekla.fi
Antero Arkkio   Antero.Arkkio@hut.fi
Tapani Jokinen   Tapani.Jokinen@hut.fi
Juhani Mantere   Juhani.Mantere@fidri.mail.abb.com
Jan Westerlund   Jan.Westerlund@fidri.mail.abb.com

New Type of DC Commutatorless Motors for Ship Propulsion

B. Amin

Inrets-Cresta. 2, av.Gl. Malleret-Joinville, 94114 Arcueil France

Abstract:

In this paper, it is shown how some simple motor structures. associated with their appropriate converter circuitry. can work as conventional DC motors without requiring mechanical commutators. Instead, high power electronic commutators are used for this purpose. These commutators do not require any maintenance and do not suffer from the power range limitation of the mechanical commutators.

1-Introduction

A desirable electrical motor should have the characteristics of a DC motor without requiring a *mechanical commutator*. The latter is replaced by a set of power switches which are turned ON and OFF in sequence in order to direct the current within the active conductors. In addition. more cooling facilities and constructional simplicity would result if both the field and armature currents were supplied through the same *stationary* windings.

Clearly, such a motor would consist in two separate toothed structure, a model of which is shown below (**Fig.1**). Windings are lodged in the fixed part (stator) of the motor and are fed in sequence in the appropriate order. Consequently, the teeth of the moving part (rotor) tend to align themselves permanently with those of the stator. The resemblance between a conventional, separately excited DC motor and the presented motor is that, in both motors, the level of the torque is controlled by the level of the armature current while the speed is controlled by adjusting the magnitude of the applied voltage. The operational

principle of this type of motor has been well known since the end of the last century. However, power switches capable of commuting rapidly the current within the various phases were not available. Today, with the advent of modern solid-state power electronics, a reliable, converter-fed, single-side wound DC motor, using an *electronic commutator*, can be achieved. Indeed, many investigations have been undertaken in the recent years to study these types of motors, principally in the low and medium power range, under the name of switched reluctance motors (SRM) [1]. However, as shown below, these motors may exhibit, in the high power range, interesting performances, as well.

For the convenience of design [4], the number of teeth on the stator is taken as $4m$, were m is an integer; that of the rotor is $4m+2$. The total number of motor phases is $2m$ and the number of *simultaneously* active phases is m. The phase numbered k, $(k = 1,2...m)$ and that numbered $m+k$ are said to be *complementary*, that is, one is turned ON whenever the other is turned OFF. They are identified as Ph_k and $\overline{Ph_k}$. Note that if each phase is wound so as to determine a north and a south magnetic pole (which we assume to be the case). all the various $2m$ phases remain magnetically uncoupled.

2-Converter Structure

The converter is made of a three phase transformer with two coupled secondary windings: a feeding and a recovery windings, the latter having twice the number of turns than that of the former (**Fig.2**).

(Fig.1) Motor structure form=3
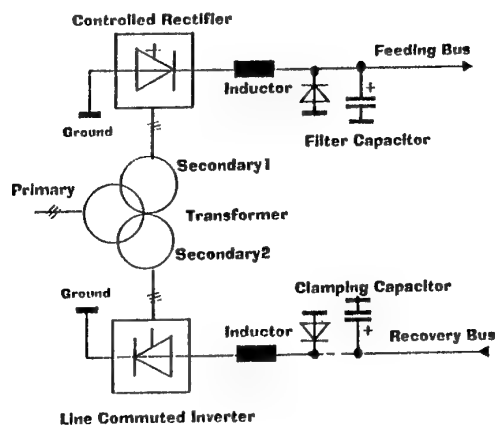
(Fig.2) The converter circuit layout
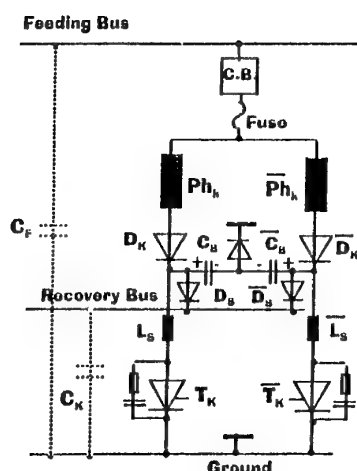
(Fig.3) A cell of an electronic commutator using Thyristors

(Fig.4) A cell of an electronic commutator using GTOs

A controlled rectifier bridge is used to provide the feeding voltage U_F available at the output of the filter capacitor C_F. An uncontrolled diode rectifier bridge can also be used. In this case, phase-voltages must be regulated by the pulse width modulation technique. This point is discussed in the next section.

A line commuted inverter is used to recover the energy of the phases being turned OFF. This energy is dumped by the capacitor C_K. The voltage U_K at the output of C_K is kept constant, equal to twice the voltage of the filter capacitor at full-load, by adjusting the firing angle of the inverter.

3-The Electronic Commutator

The circuit-layout of a cell of the electronic commutator is shown by (Fig.3) (the R-C protective components across the diodes are not represented).

Two complementary legs, corresponding to two complementary phases, are linked by "blowing capacitors" C_B. These are DC type capacitors and provide the means for commuting the thyristors T_k and $\overline{T}_k$. With Thyristors being used as power switches, the input voltage must be regulated by means of a controlled rectifier bridge, in conformity with the motor speed. The (Fig.4) shows an electronic commutator using GTOs. With this type of switches, one can regulate the input voltage by pulse width modulation; thus an uncontrolled diode rectifier bridge can be used in the converter section. Weak snubbers are necessary, however, for this operation. Instead, smaller capacitors, C_B, are required with GTOs. Pulse width modulation works as follows.

Assume that G_k is ON and $\overline{G}_k$ OFF. Now:

-Turn $\overline{G}_k$ ON.

-Measure the current flowing through the blowing capacitor C_B; when the maximum value is reached,
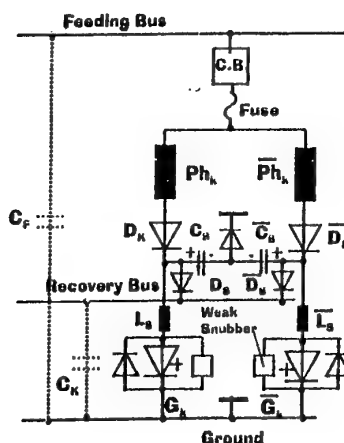
turn G_k OFF. At this moment, the current through G_k is normally nil and the switch commutes softly at zero-current. -Keep measuring the current through C_B; when this current has vanished (i.e. reaches a low threshold value), turn $\overline{G}_k$ OFF. Because of the large inductance of the phase, $\overline{Ph}_k$, a *small* amount of current keeps flowing within the di/dt limiting inductor, $\overline{L}_S$ (Fig.4). This current is dumped by the *weak* snubber provided across the switches.

-The current of the phase, Ph_k, keeps decreasing until G_k is turned ON again...

Notice that the chopping operation uses the *no-loaded* complementary switch, $\overline{G}_k$, for turning the *fully-loaded* switch, G_k, OFF.

The use of hard driven GTOs (IGCT) may bring further improvements by removing some of the components as the blowing capacitors.

4-Multi-Stage Electronic Commutator

The power rating of a cell can be increased by using a multi-stage circuit as shown in (Fig.5). In this figure, two thyristors are connected in series in each leg. In addition, the recovery capacitor is made of two units connected in series. The common point of the clamping capacitors is linked to the cathodes of the high side thyristors, as well as the anodes of the low-side thyristors, via the two voltage-sharing diodes, D_{SL} and $\overline{D}_{SL}$. Assume that switches T_{KH} and T_{KL} are ON and that $\overline{T}_{KH}$ and $\overline{T}_{KL}$ are OFF. In order to commute the current from the left switches to the right ones, first switch $\overline{T}_{KH}$ ON, and, immediately after, switch $\overline{T}_{KL}$ ON. Indeed, the low sided clamping capacitor, C_{KL}, acts as a buffer and limits the voltage across $\overline{T}_{KL}$ to U_F. Once $\overline{T}_{KL}$ is turned ON, the current flowing through T_{KH} and T_{KL} are "blown up"

87
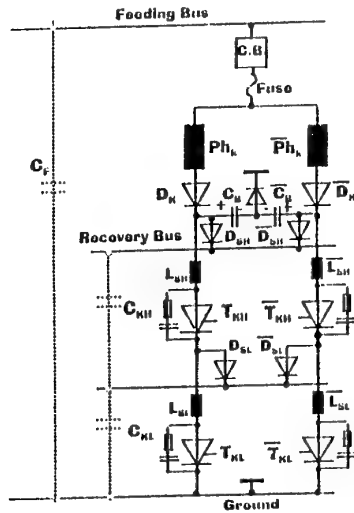
(Fig.5) A cell of a two-stage electronic commutator

and the two switches turn OFF. More than two levels can be achieved using this circuit, which
results in the achievement of high power electronic commutators.

5-Volt-Ampere Rating

The power factor of the motor is defined as:

$$PF = \frac{P_{mec} / \eta}{2m U_{rms} I_{rms}} \qquad (1)$$

where P_{mec} is the output power and η is the motor efficiency. U_{rms} and I_{rms} are the phase rms. applied voltage and current, respectively; m is the number of phases. The power switches must operate with a direct repetitive blocking capability factor, k_V, defined as:

$$k_v = \frac{V_{DRM}}{U_{rms}} \qquad (2)$$

where V_{DRM} represents the peak repetitive OFF-state blocking voltage of the chosen switches.
In addition, we shall label the safe-margin factor relative to the DC-link voltage as,

$$k_{v0} = \frac{V_{DRM}}{U_f} \qquad (3)$$

Similarly, the maximum rms. ON-state current of the switches must be within a safe margin factor, k_I, defined as:

$$k_I = \frac{I_{TRMS}}{I_{rms}} \qquad (4)$$

where I_{TRMS} represents the maximum rms. ON-state current of the switches. k_I depends on the

effectiveness of the cooling means provided, the working frequency and the nature of the switching operation (soft or hard!). The latter determines the amount of the commutation losses.
Combining eqs.(1), (2) and (3), the volt-ampere requirement per phase of the drive is written as:

$$V_{DRM} I_{TRMS} = \frac{k_V \cdot k_I}{PF} \frac{P_{mec} / \eta}{2m} \qquad (5)$$

The utilization factor of the switches is defined as:

$$k_{U} = \frac{k_V \cdot k_I}{PF} \qquad (6)$$

We shall compare the utilization factor of a SRM to that of a Y-connected, inverter-fed AC drive powered from the *same* DC-link voltage, U_F. Recall that, like an inverter-fed AC motor, each phase of a SRM may be controlled using *two* power switches, while the electronic commutator circuitry used in (Fig.3) uses one switch per phase. However, in the latter circuit the DC voltage available across each phase is only *half* of the full DC link voltage. At the blocking stage, each switch must withstand the *full* DC link voltage. Hence, the VA requirement of the drive is the same whether the one-switch per phase or the two-switch per phase commutator circuitry is used. The latter more resembles to the case of inverter-fed AC motors and, for the sake of clarity, will be used in the following discussion.
For a SRM operating under the full-wave mode, the DC-link voltage, U_F, and the applied rms. voltage per phase, U_{rms}, are numerically equal, since the input voltage is applied permanently, in positive or in negative, to the phases. However, for a Y-connected AC motor fed from a voltage-source inverter, the rms. voltage per phase and the DC-link voltage are related as $U_{rms} \cong 0.45 U_F$. Note that windings of industrial AC motors are mostly Y-connected with an isolated neutral point. Indeed, the circulating current in such a windings is nil, whatever being the degree of unbalance of the feeding lines.
On the basis of available data [5] concerning the performances of SRMs so far constructed and tested, the power factor of this type of machines operating under the full-wave mode ranges around: $PF \cong 0.25$ [5]. Comparatively, an AC motor may operate with a power factor ranging around: $PF \cong 0.9$. Consequently, the ratio of the utilization factors of an AC motor and a SRM of the same power and speed ranges is obtained as:

$$\frac{k_U(SRM)}{k_U(AC)} \cong 1.64 \frac{k_{v0}(SRM)}{k_{v0}(AC)} \frac{k_I(SRM)}{k_I(AC)} \qquad (7)$$

Next, because of the presence of the clamping capacitors across the power switches of the electronic commutator of an SRM (see Fig.), a lower value may reasonably be chosen for $k_{v0}(SRM)$ in comparison to

that usually used for $k_{vo}(AC)$. Let it be chosen: $k_{vo}(SRM) = 1.5$ and $k_{vo}(AC) = 2.0$. Thus it is obtained:

$$\frac{k_{v1}(SRM)}{k_{11}(AC)} \cong 1.25 \frac{k_{1}(SRM)}{k_{1}(AC)} \qquad (8)$$

If we assume comparable current safe margin for both drives, it is obtained:

$$k_{v1}(SRM) \cong 1.25 k_{v1}(AC) \qquad (9)$$

However, it must be pointed out that for the same speed range and under the full-wave mode, the switching frequency of a SRM usually is higher than that of an AC drive. Consequently, the k_1 factor in the SRM is usually higher than its counterpart in inverter-fed AC drive. As an example, a 4-pole AC motor rotating at 3000rpm would operate, under the full-wave mode, at 100Hz with a current safe margin factor of around $k_1 \cong 0.80$. A (R:14 ; S:12) SRM of the same power and speed would operate at 600H, with a current safe margin of around $k_1 \cong 0.50$. As a result, it is obtained: $k_{VA}(SRM) = 2. k_{VA}(AC)$.

The interest of the electronic commutator circuitry shown in (Fig.3) comes from the fact that switches can commute softly, under zero-current. This feature dramatically reduces the commutation losses and noticeably rises the value of the k_1 factors of SRMs. Moreover, switches gain the ability of commuting without a snubber (or using very weak snubbers), saving a huge amount of losses.

6-Design Example

It is not intended here to provide the values of the various motor parameters accurate to the last digit. However, on the basis of the data accumulated concerning the performances of SRMs so far constructed and tested, the various parameters of such a motor may be determined.

The designed example concerns a 20MW, 180rpm motors for ship propulsion. As compact as possible motor are appreciated in such applications. For this reason, a *multistack, axially* mounted toothed structure motor will be designed. Clearly, this structure is more complicated to construct than the classical radially toothed structure which requires the laminations to be simply stacked along the motor axis. However, the multistack, axially toothed structure motor requires the various elements of its magnetic circuit (teeth and yoke on the rotor and on the stator) to be separately stacked and axially fixed (welded, bolted...) on the rotor and stator drum. This configuration is shown in the (**Fig.6**). Furthermore, the armature winding of each motor is lodged, perpendicular to the motor axis (radially) in the stator slots (Fig.6).

Ten independent motor structure, of 2MW power each, are axially stacked in order to achieve a 20MW motor.
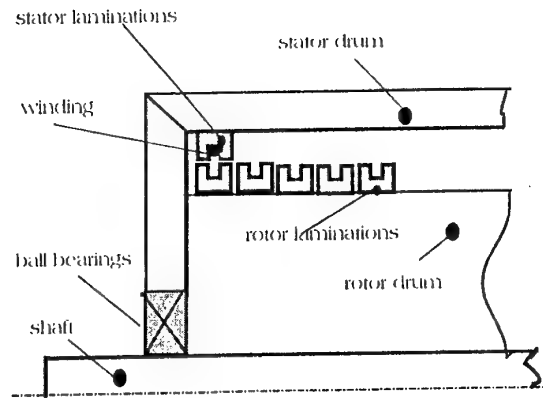
(Fig.6) 10-phase, axial mounted toothed structure

The stator of each motor is shifted from their neighbours by an angle corresponding to one tenth of the tooth pitch. This greatly improves the quality of the output torque of the multistack motor. Each motor is fed through its own electronic commutator the characteristics of which are the followings:

A cells of four-stage commutators using four 4.5kV, 3kA GTOs. These are standard components used today in the various fields of industry. Also, the characteristics of the converter are: feeding DC voltage: 6kV; recovering DC voltage: 12kV; voltage of each clamping capacitors: 3kV; capacitors

$C_{n} = \overline{C}_{n} = 12\mu F(16k1')$: di/dt limiting inductance

$L_{s} = 15\mu H$; snubber capacitors $2\mu F$. Note that, using an appropriate windings connection, it is also possible to use ten cells of double 2-stage commutators connected in parallel [6]. Each cell would operate under 3kV feeding voltage and 6kV recovering voltage; however, it would draw from the source twice as many amps than before.

The size of the laminations of which is made the magnetic circuit (stator teeth and yoke as well as the rotor teeth and yoke) of the motor are quoted in the (**Fig.7**). The other motor parameters are:

Number of stator teeth: 60; number of rotor teeth: 60; air gap: 4mm; rotor stack diameter: 3000mm; stack length: 250mm; stator and rotor tooth-width: 70mm; stator and rotor tooth-height: 130mm; stator outer diameter:3500mm; rotor inner diameter: 2500mm;
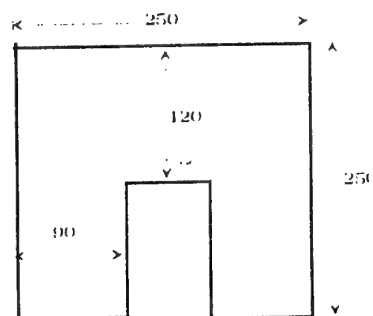
(Fig.7) Size of the laminations used.

89
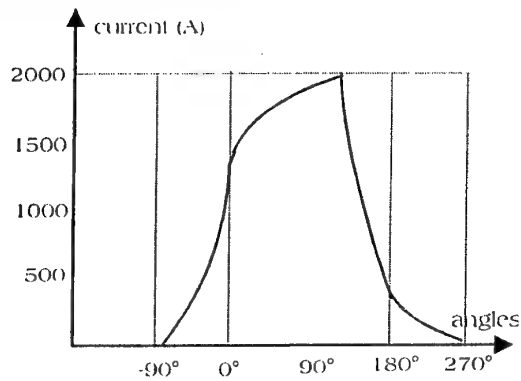
(Fig.8) Phase-current versus angular position in the full-wave functioning mode

number of turns of the armature winding: 24; flux linkage commuted in the rated regime:$\cong$17Wb; available slot area: $\cong$9100mm2; peak phase-current in the full-wave mode: $\cong$2000A (Fig.8); rated rms phase-current: $\cong$1300A; slot rms current: $\cong$32kA; slot feeling factor: $\cong$0.70; rated current density: $\cong$5.0A/mm2; switching frequency in the full-wave mode: 180Hz; copper mass: $\cong$0.55 tones; active iron mass: 3.4tones; rated copper loss (150°C): $\cong$45kW; rated iron lo (0.5mm, 2.6W/kg laminations) estimated to: $\cong$25k... motor efficiency around 0.97.

7- Some Comments Concerning the Designed Drive.

The average *static* torque of an SRM may be calculated from the eq.(11) written below [5]

$$T_s \cong k_t N_{act} (NI_{peak} - \frac{B_s \delta}{2\mu_0}) B_s LD \qquad (11)$$

where N_{act} is the number of teeth on the stator, NI_{peak} is the peak amps-turn per pole, δ is the air gap, B_s is the peak flux density under the teeth, L is the stack length, D is the stack diameter. k_T is an empirical coefficient the value of which is around: $k_t \cong 0.13$ [5].

Let it be assumed: $B_s \cong 2T$ and $I_{peak} = 2000A$ that is, NI_{peak}/pole=24kA. Using eq.(11) and the data concerning the motor parameters, it is obtained: $T_s \cong 170kNm$. The dynamic torque may approximately be estimated using the same eq.(11) provided that the rms. current, instead of the peak current, is used. Note that this statement is valid when optimum control of the ON and OFF firing angles is performed. Hence, for $I=1350A$, that is, $NI= 15.6kA$, and $B_s \cong 1.9T$, it is obtained: $T \cong 103kNm$.

-The weight of the active materials amounts to 40tones. The overall motor should weight less than 70 tones. This can be compared with that of some already existing 20MW, 180RPM, auto-sequentially commuted current source inverter-fed synchronous

motor which are reported to have an overall outer diameter of 5600mmm, an overall stack length of 3600mm and which weght 120 tones[2].

-Other projected Samarium Cobalt permanent magnet synchronous motor are reported to have comparable size and weight than the motor designed in the previous section. However, the permanent magnet motor would be far more expensive.

- The motor may easily be cooled since almost all the losses take place in the stator side. The best solution consists in providing the stator with an external tabular jacket inside which water flows.

- The motor develops a high quality torque since they run on ten shifted, simultaneously active phases. Indeed, let the rate of the torque ripple be defined as

$$\Delta t\% = 100\frac{T_{max} - T_{min}}{2T_{av}} \qquad (13)$$

where T_{max}, T_{min} and T_{av} are respectively the maximum, minimum and average torque over the period of time, Δt. In this case, the rate of the torque would be less than 5% [4].

-Acoustic noise, *if necessary*, can effectively be reduced by coating the motor with an insulator material. This technique works well with water-cooled motors using the flow of the water under the insulating coat.

-The electronic commutator can be realized in the modular form and does not require any maintenance. Moreover, it does not suffer from the power range limitation (around 5MW) of a mechanical commutator.

-The system exhibits a very high degree of availability, unequalled by conventional drives [3]. Indeed, there are ten *independent* cells within the same structure. Consequently, under any faulty conditions, the malfunctioning cell can be stopped while the other units continue to work as before.

8-Conclusion

In this paper it is shown how axially mounted toothed structure switched reluctance drives may operate in the high power, low speed ranges as effective commutator-less DC drives. The torque per unit volume (mass) ratio of such drives appears to be high which is appreciated in many specific applications. The likely superiority of the presented motor over inverter-fed AC motors of various structures, designed both with and without permanent magnets [2.7.8], requires deep attention for investigating the potentialities of these type of motors.

9-References

[1] **Lawrenson P.J.;** *"A brief status review of switched reluctance drives"* in: *EPE Journal. Vol.2. No.3. PP.133-144, Oct.1992*
[2] **Michaux R., Letellier P.;** « *Les machines discoïde à champ axial dans les systèmes de propulsion*

90

électrique» in: Rev. d'Elec. & Electron. (REE), No3, PP 37-41, March 1997.

[3] *Ahlqvist I.;* "Increasing availability through introduction of redundancy" in: Elect. Propulsion, The Effective Solution? Conf. Proceedings, Part1, Paper1, London 1995.

[4] *Amin B.;* "Structure of high performance switched reluctance machines and their power feeding circuitry", in: Eur. Trans. on Elec. Power, ETEP, Vol. 2 (1992), No.4, PP. 215-221.

[5] *Amin B.;* "Electromagnetic Performance Comparison in Electrical Machine» in: Eur. Trans. on Elec. Power, ETEP, Vol.2 (1992), No.2, PP. 83-90.

[6] *Amin B.;* "Some Original Structure of high Power Switched Reluctance Motors and Thier Power converters." In :acemp'95 Proc., Vol.2, pp.350-355, Kusadasi-Turkey

[7] *Kawabata T., Kawabata Y., Nishiyama K.;* «New Configurations of High Power Inverter Drives» in: PEMc'96 Proc., Vol.2, pp. 278-283, Budapest, 1996.

[8] Stemmler H., Guggenbach P.; «Configurations of High Power Voltage Source Inverter» in: european Power Electronics EPE, 1993, pp. 7-14

Magnetohydrodynamic Propulsion for Electric Ships

A. Leão Rodrigues

Department of Electrical Engineering
Faculty of Sciences and Technology
New University of Lisbon
2825 Monte de Caparica - PORTUGAL
e-mail: leao@uninova.pt

Abstract

This paper provides an overview of magnetohydrodynamic propulsion for marine vessels using superconducting coils. A theoretical analysis of magnetic field and efficiency of a linear thruster is described. The effect of magnetic field on thruster efficiency is also discussed.

Among other topics studied, analysis of magnetic field configuration in the various geometries of magnetohydrodynamic thrusters, by using the finite element method, is presented.

1 Introduction

Magnetohydrodynamic (MHD) propulsion for propelling sea water vessels has been studied since the early 1960's [1,2,3]. Recently there has been renewed interest in this subject both in USA [4] and Japan [5].

MHD sea water propulsion offers several advantages over conventional mechanical propellers. The absence of a mechanical propeller system leads to reduced vibration levels in the electric ship, and thus, to reduction in the mechanical noise generated. Gear reduction system for shafts is therefore no longer needed. Also, there is no physical restriction on the top speed of potential MHD sea water vessels, whereas the speed of conventional screw-driven ships is limited by the cavitation phenomenon.

Sea water conducts electric current by electrolytic ion exchange. Taking advantage of sea water's modest electric conductivity (~ 3.5 to 4.5 S/m, i.e. 10^{-5} less than Cu), the MHD propulsion of marine vessels has been subject of thecnical speculation and study for some years [6,7]. One of the key conclusions reached by different investigators is that large and powerful magnetic fields (8-20 Tesla) are required to achieve propulsion efficiencies comparable to those of conventional propellers. Recent interest in the MHD propulsion in some developed countries has been sparked by the possibility that developments in High Temperature Superconductors may lead to the design of such magnets.

Three basic forms of MHD propulsion have been studied. These are d.c. drive propulsion, a.c. induction propulsion and a variant of these which is an adaptation of the MHD induction pump. All these methods however, apply Lorentz force to provide kinetic energy to the fluid medium.

i) Direct current MHD is based on the interaction between a static magnetic flux density, created by a d.c. electromagnet on board and a d.c. current, perpendicular to the magnetic field, imposed by a voltage difference between two electrodes immersed directly in the conductive sea water.

ii) In the induction method, a magnet field is varied sinusoidally along the length of the vessel which generates a magnetic travelling wave. This magnetic travelling wave induces currents in the sea water and by interaction a thrust is produced in a similar way to a linear induction motor.

iii) The other scheme is to use an intermediate transducer to improve coupling between the electromagnetic travelling wave and the sea water. An externally generated magnetic travelling wave couples with a liquid metal transducer to set up a travelling pressure wave in the liquid. The consequent pressure fronts in the liquid metal produce ripples which are transmitted through a flexible membrane to a sea water duct. The travelling wave ripples in the membrane trap packets of sea water which are ejected from the duct to provide thrust. The system is known as a ripple motor.

The drawbacks of the latter two previous systems are the noise spectrum due to the necessity of a.c. operation and the serious constraint of developing a flexible membrane to separate the molten-metal driver from the sea water in the pump duct. Also, the generation of a.c. magnetic fields of magnitude 0.6 T with frequencies in the range of 50-60Hz may be difficult using superconducting magnets due to the a.c. losses. Therefore, the efficiencies of such induction drive propulsion systems operating in sea water are too low to be considered practical.

In order to improve propulsion efficiency, the MHD forces have to be large. This can be achieved basically by either increasing the fluid electrical conductivity or by increasing the magnetic field strength. The conductivity of the sea water can be enhanced by any seeding procedure. However, this has the drawback of leaving a detectable chemical signature behind the surface of the vessel. Increasing magnetic field strength (10-20T) is only possible using superconducting magnets and this opens the door for new designs for MHD thrusters.

2 Principle of operation of a linear d.c. MHD thruster

A schematic view of a linear d.c. MHD thruster is shown in figure 1. The following analysis is based on the channel geometry with rectangular cross section axb with a length ℓ, sufficiently long compared with depth b and width a. The fluid inside the duct (sea water) is considered non-magnetic, incompressible, non-viscid and electrically conducting with a conductivity σ.
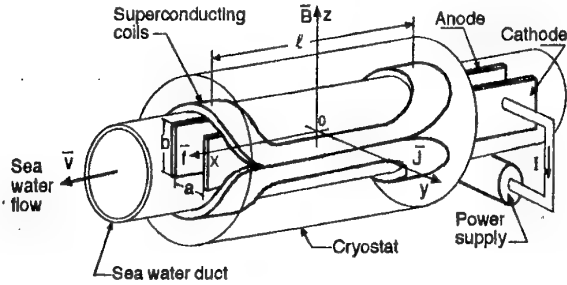
Fig. 1 - Linear MHD channel and excitation coils

Two superconducting saddle-shaped coils are immersed in a cryostat which set up a magnetic flux density $\overline{B}$ through the sea water. This can be expressed as

$$\overline{B} = B\overline{e}_z$$

where $\overline{e}_z$ is the unit vector in the z-direction. In figure 2a the flux plot of B at the middle duct is shown and figure 2b shows a 3D distribution of B in the plane $z = 0$, Here it can be observed that the steep slope at the end $\ell / 2$ of the duct is due to fringing of the magnetic field.

When a voltage U is applied across the parallel electrodes, a conducting electric current density J will flow through the sea water in the y-direction. The ideal material for electrodes and bus bars has not yet been found, but studies have been carried out for carbon, noble metals and compounds like TiRuO2 and TiIrO2. Using Ohm's law, the current density is given by

$$\overline{J} = \sigma(\overline{E}_g - \overline{E}_i) = \sigma\left(\frac{U}{a} - vB\right)\overline{e}_y \qquad (1)$$

where $\overline{E}_g$ is the gradient electric field of intensity U/a and $\overline{E}_i$ is the induced electric field due to the uniform jet speed $\overline{v}$ in the x-direction.

The interaction of this electric current with the magnetic field generates a Lorentz force per unit volume given by

$$\overline{f} = \overline{J} \times \overline{B} = \sigma B\left(\frac{U}{a}\right)\left(1 - \frac{v}{v}\right)\overline{e}_x.$$

Hence, the component of Lorentz force per unit volume along the x-direction is
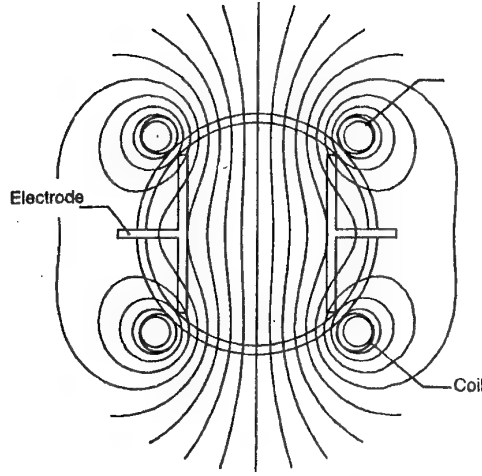
a) - Field plot at x=0
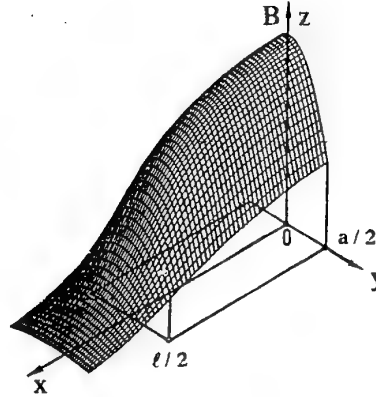
b) - Flux density distribution at z=0
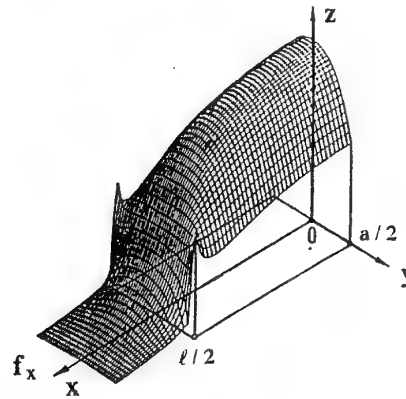
c) - Force per unit volume distribution

Fig. 2 - Flux and force distribution in a linear MHD channel

where

$$f_x = \sigma B\left(\frac{U}{a}\right)\Phi(\alpha) \qquad (2)$$

and

$$\Phi(\alpha) = 1 - \frac{v}{v} = 1 - \alpha \qquad (3)$$

$$v^* = \frac{U/a}{B}$$

is the duct critical speed and

$$\alpha = \frac{v}{v^*}$$

is the normalised speed. Figure 2c shows the force distribution per unit volume of sea water along half length ℓ/a of the duct, where the MHD thruster works as a hydraulic pump. By reaction, the jet speed v generated by the force impels the thruster in the opposite direction.

3 Thruster efficiency

Thruster efficiency η is defined as

$$\eta = \frac{P_{out}}{P_{in}} \qquad (4)$$

where P_{in} is the electric input power and P_{out} is the hydraulic output power.

Noting that the total resistance between electrodes is

$$R = \frac{1}{\sigma} \cdot \frac{a}{b\ell} \qquad (5)$$

and taking into account (1) and (3), the total electric current I across the surface $S = b\ell$ of the electrodes is given by

$$I = JS = \sigma \left(\frac{U}{a} - vB \right) b\ell = \frac{U}{R} \Phi(\alpha).$$

Then, the total input electric power supplied to the duct is

$$P_{in} = UI = \frac{U^2}{R} \Phi(\alpha) \qquad (6)$$

The total hydraulic output power becomes

$$P_{out} = \Delta p. ab. v \qquad (7)$$

where

$$\Delta p = \Delta p_{th} - \Delta p_{loss} \qquad (8)$$

is the net pressure difference between the two ends of the duct, Δp_{th} is the gross pressure difference and Δp_{loss} is the pressure drop due to hydraulic losses in the duct.

For an incompressible and non-viscid fluid, the pressure Δp_{th} inside the duct satisfies the differential equation

$$\frac{\partial p_{th}}{\partial x} = f_x. \qquad (9)$$

Substitution of (2) into (9) and integrating gives

$$\Delta p_{th} = \ell \sigma B \left(\frac{U}{a} \right) \Phi(\alpha) \qquad (10)$$

For a real conductive fluid as sea water, the pressure drop due to hydraulic losses of the duct is typically given by

$$\Delta p_{loss} = \frac{\lambda}{2\beta} \cdot \rho v^2 \qquad (11)$$

where λ is the dimensionless friction coefficient, ρ is the specific mass of the sea water ($\rho = 1025 kg/m^2$) and β is the duct shape factor given by

$$\beta = \frac{2b}{a+b} = 2 \frac{b/a}{1+b/a} \qquad (12)$$

In (12), $\beta = 1$ for $a = b$ (square duct).

Taking into account (10) and (11), the net pressure rise (8) through the working volume $ab\ell$ of the MHD duct thruster is

$$\Delta p = \ell \sigma B \left(\frac{U}{a} \right) \cdot \Psi(\alpha) \qquad (13)$$

where

$$\Psi(\alpha) = \Phi(\alpha) - \gamma \alpha^2$$

and

$$\gamma = \frac{\lambda}{2\beta} \cdot \left(\frac{U}{a} \right) \cdot \frac{\rho}{\sigma \ell B^3} \qquad (14)$$

is the dimensionless duct factor.

Substitution of (13) into (7) and taking into consideration (5), the actual hydraulic power becomes

$$\Delta P_{out} = \frac{U^2}{R} \alpha \Psi(\alpha). \qquad (15)$$

Finally, substitution of (15) and (6) into (4) gives for the thruster efficiency

$$\eta(\alpha) = \frac{\alpha \Psi(\alpha)}{\Phi(\alpha)} = \frac{\alpha(1 - \alpha - \gamma \alpha^2)}{1 - \alpha} \qquad (16)$$

Output hydraulic power (15) and thruster efficiency (16) are plotted versus normalised speed $\alpha = v/v^*$ in figure 3.

When the duct factor γ is not zero, the value of $\alpha = \alpha_P$ corresponding to the maximum hydraulic power ($dP_{out}/d\alpha = 0$) becomes

$$\alpha_P = \frac{\sqrt{1+3\gamma} - 1}{3\gamma} \qquad (17)$$

and is always less than 0.5. However, maximum thruster efficiency ($d\eta/d\alpha = 0$) is attainable for α_η greater than 0.5. The selection of $\alpha = v/v^*$ is therefore an essential parameter in designing a thruster for ship propulsion. In practice, it is reasonable to establish the design point α_{des} in the range $\alpha_\eta \geq \alpha_{des} \geq \alpha_P$ which corresponds to the hatched area shown in figure 3.

94
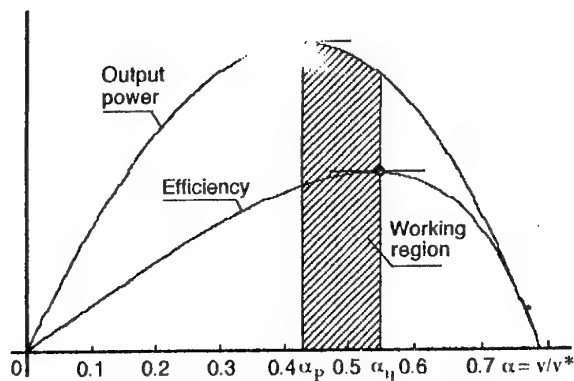
Fig. 3 - Thruster efficiency versus normalised speed

Fig. 4 - Efficiency versus magnetic flux density

As an example, for the values of $\lambda = 0.01$, $a = 0.8\,m$, $b = 1\,m$, $\ell = 5\,m$, $U/a = 600\,V/m$, $\sigma = 4\,S/m$, $\rho = 1025\,kg/m^3$, and if it is technically possible to obtain a magnetic field intensity of $B = 10\,T$, the duct factor resulting is $\gamma = 0.138$. Then, the design point based on the concept of (17) is $\alpha_{des} = 0.46$. The critical speed is $v^* = 216\,km/h$ or $v^* = 116\,knots$ and the jet speed becomes $v = 53\,knots$. The corresponding thruster efficiency is $\eta = 43\,\%$.

Besides the above mentioned ohmic losses and frictional losses there are some other losses that arise from three dimensional effects and may not be easily assessed by simple analysis. They include the electrical end losses that result from the fringing of magnetic flux lines at the ends of the electrodes. Some of these losses are significant. Less other significant losses include electrolytic effects, which lead to bubble formation.

Taking into account the nozzle area ratio $\delta = A_{in}/A_{out}$, where A is thruster cross section, a simple formula for the thruster electrical efficiency can be derived as

$$\eta = \frac{1}{1 + \delta \dfrac{\rho v}{\ell \sigma B^2}} \qquad (18)$$

This expression does not take into account the losses linked to the partial electrolysis of the sea water. For a thruster with a nozzle ratio $\delta = 1.25$, $\ell = 20\,m$ and taking $\rho = 1025\,kg/m^3$ and $\sigma = 4\,S/m$, the efficiency versus magnetic flux density, given by (18), is plotted in figure 4 for several ship speeds. The results show that the thruster efficiency decreases with the speed of the ship. There is a rapid increase in efficiency between $B = 5\,T$ and $B = 10\,T$, where the electrical efficiency reaches a value of 25 % for a ship speed of 10 knots.

These numerical examples emphasise the need for strong magnetic flux densities in order to have viable thruster performance. Further work on superconducting materials will be necessary to produce such fields and the work is now well in hand. Also efficiency can be increased using improved thruster geometry.
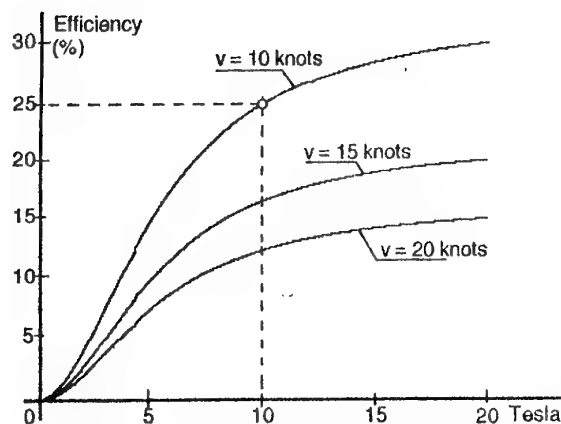
4   Thruster configuration

Many different types of MHD thrusters have been proposed which provide enhanced ship performance, operability, manoeuvrability, survivability and efficiency. As is the case for a.c. MHD, d.c. MHD may be internal (flow channelled) in a duct or external. Four distinct geometric configurations for MHD thrusters designs are considered. An essential characteristic for the excitation magnet would be its leakage field which as to be as low as possible. Therefore, magnetic flux density distribution set up by the superconducting coils are calculated using the MagNet CAD package.

4.1   Clustered Linear MHD Thruster

The Japanese MHD trials ship, the Yamato -1, uses twin clusters (port and starboard) of six linear MHD thrusters each as described previously.
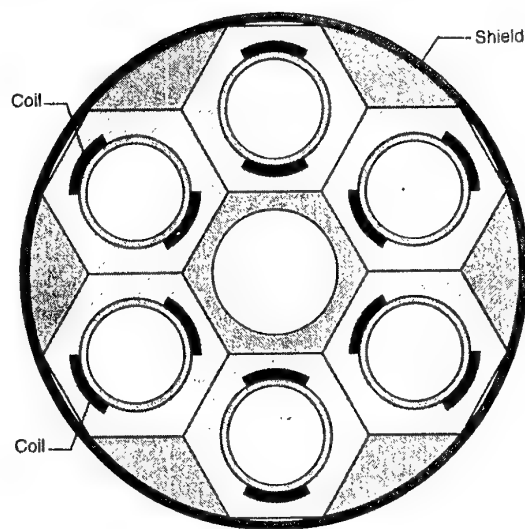
Fig. 5 - Cross section through one of the propulsion unit

95

Linear thrusters use a Cartesian geometry and require dipole magnets. These magnets require extensive structural support which limits the attainable field strength. A typical clustered dipole array is shown in figure 5. The hexagonal structure is ideal to bear strong electromagnetic forces.

Figure 6 shows the contour lines of magnetic field at the section of clustered linear MHD thruster. An outside magnetic shield minimises flux
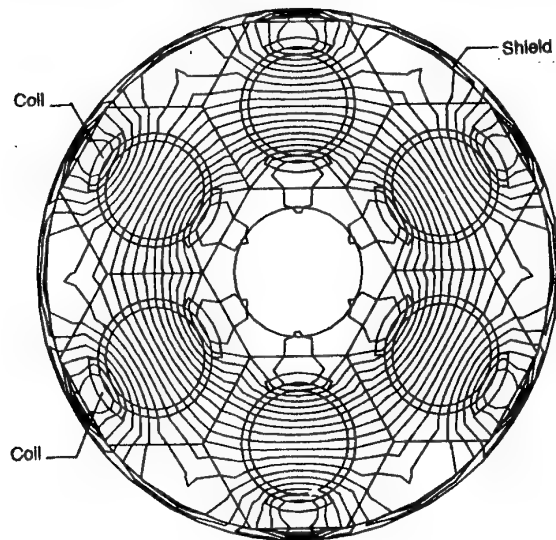
Fig 6 - Flux plot of the clustered linear MHD thruster

leakage avoiding the ship's magnetic signature and ill effects on neighbouring ships and structures due to the currents flowing in the water. The Lorentz force of each propulsion unit is 8 kN giving an efficiency of 18 %.

4.2 Toroidal Annulus MHD Thruster

The toroidal annulus type thruster can be thought as a clustered type with the superconducting coils mounted in a single unit. There are several superconducting coils in a racetrack shape placed around the thruster at regular intervals, as shown in figure 7. The magnetic field set up by the
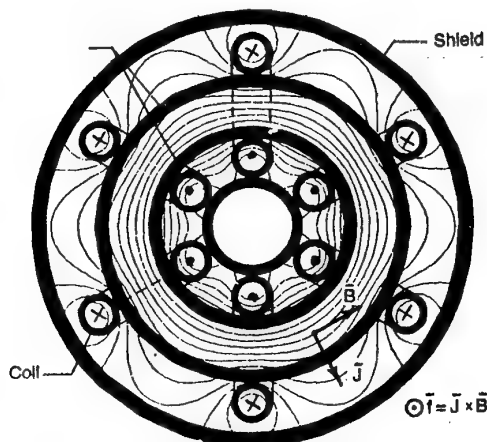
windings is in the azimuthal direction. This minimises the ship's magnetic signature.

Electrodes are placed such that an electrical current flows through the sea water are in the radial direction. The interaction of current and magnetic field results in a Lorentz force on the sea water along the length of the thruster.

4.3 Squirrel Cage MHD Thruster

The so-called squirrel cage MHD thruster consists of several superconducting coils situated externally around the hull of the vessel, as shown in figure 8.
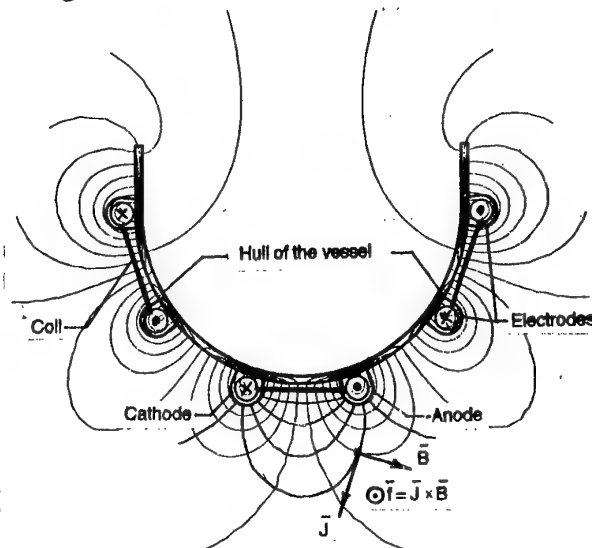
Fig. 8 - Flux plot of the squirrel cage MHD thruster

Electrodes are placed around the conductors which are housed with them. Anodes and cathodes are mounted alternately over the conductors to provide the necessary electric field which arches between the electrodes. The two fields interact orthogonally a short distance from the hull of the vessel to produce the Lorentz force. The disadvantage of this system is the strong magnetic signature of the ship.

4.4 Dual-solenoid MHD Thruster

A dual-solenoid type thruster consists of two concentric ducts through which sea water is channelled, as shown in figure 9. The magnetic

Fig. 7 - Flux plot of the toroidal annulus MHD thruster
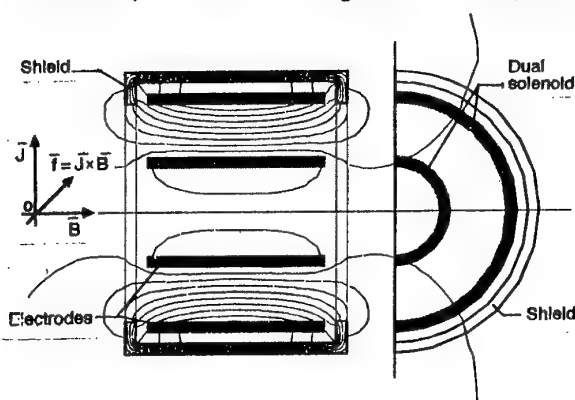
Fig. 9- Flux plot of the toroidal annulus MHD thruster

96

field set up by the windings is in the axial direction shielded externally to minimise the ship's magnetic signature.

The electrodes are located on opposite surfaces in the two concentric solenoids to generate a radial electric field. The orthogonal interaction of current and magnetic field produces a MHD flow in azimuthal direction, which is converted to an axial thrust by means of angled vanes.

A similar type of thruster with a single solenoid [8] is shown in figure 10. The solenoid winding is
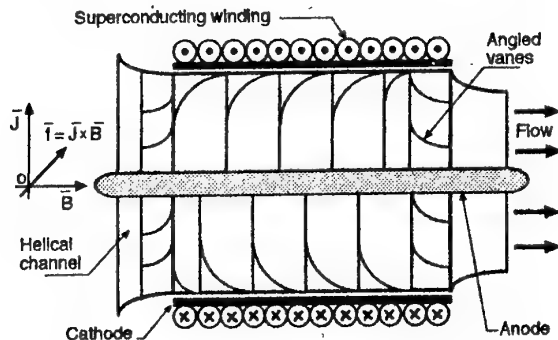
Fig. 10 - Helical MHD thruster

concentric to cylindrical electrodes producing an axial magnetic field and a radial electric field respectively. The channel, formed by the space between the electrodes, made by platinum-coated titanium, contains a helical insulator which guides the flow of water through the thruster. The helical flow deflected by vanes is converted into the desired axial flow.

5   Conclusions

The prospects of MHD propulsion of ships with a reasonable efficiency of conversion of electric power to useful power seems to be possible if large magnetic fields could be generated. One of the key technical issues will be the development of the MHD thruster superconducting magnets, support structures, and cryogenic cooling system for the coils.

The recent developments in present day superconducting magnet technology will significantly help in producing more efficient MHD thrusters. The huge magnetic energy stored in the field of the superconducting coils could serve as an emergency power supply in case of failure of the main system and to propel the ship for some further hours.

It must be noted that the clustered dipole, racetrack toroid and squirrel configurations the Lorentz force vector is parallel to the system axis, while the dual-solenoid it is in the azimuthal curvilinear vector direction. For the same conditions, the force vector varies for the four configurations, with the dual solenoid the lowest, the clustered and squirrel respectively next higher, and the toroid annulus configuration the highest.

As the system is a static device without a fixed shaft, gears or propellers, the noise generated from these sources are eliminated. Instead, the main source of noise would be due to the bubble formation arising from the electrolysis process between the electrodes and the sea water.

The MHD propulsion also offers reduced hydrodynamic drag, reduced maintenance and decreased detectability. This innovative MHD propulsion system offers an important contribution to the development of electric ships for the next century.

References

[1] - W. A. Rice, "U.S. Patent 2,997,013, August 22, 1961.

[2] - O. M. Philips, " The Prospects for Magnetohydro-dynamic Ship Propulsion" J. of Ship Research, March, 1962, pp 43-51.

[3] - S. Way, Propulsion of Submarines by Lorentz Forces in the Surrounding Sea," Amer. Soc. of Mechanical Engrs, Paper 64 WA/ENERG, Nov., 1964.

[4] - R. F. Rannelone,"Ship Integration and Construction Considerations", MHDs 91.

[5] - K. Imaichi," The Superconducting Magnetohydro-dynamic Propulsion System of *Yamato-1*", The Institute of Marine Sciences, 1992.

[6] - H. Weh, H. Mosebach, R. Palka, " Ship Propulsion with Electromagnetic Direct Drives, MHDs 91.

[7] - M. D. Doss. H. K. Geyer, " MHD Seawater Propulsion", Journal of ship Research, vol.37, n°1, March 1993, pp 49-57.

[8] - V. Bashkatov, "Reactive Forces in Magneto-Hydro-dynamics and Their Applications of MHD-Jet Propulsive Ocean Ships", MHDs 91.

*** * ***

NEW HIGH EFFICIENCY CURRENT FED DC-TO-AC INVERTERS

K. H. EDELMOSER & L. L. ERHARTT
Technical University Vienna
Power Electronics Section
Gusshausstr. 27-29, A-1040 Wien, Austria
Tel.: +43-1-58801-3886, Fax: +43-1-5042477, Email: edel@uxi.tuwien.ac.at

ABSTRACT:

A new high efficiency DC-to-AC inverter for stand alone and direct AC mains connection is described. The new inverter features very high efficiency and is well suited for solar and renewable energy as well as for aerospace applications. The structure uses only off-line switches to generate the AC output. Due to security reasons the input voltage (e.g. the voltage of the solar cells) is limited. Therefore, high currents on the primary side are necessary to obtain the required output power. The overall efficiency of the inverter depends to a high degree on the number of switching elements in the current path. The structure described here has only one active switch in the main current path.
Keywords: Inverter, High-Efficiency, Stand-alone PV systems

1. DERIVATION OF THE INVERTER STRUCTURE

Two well known state of the art single phase DC-to-AC inverter structures [1] are shown in Figs. 1.a and b. Figure 1.a is a voltage fed converter. To produce a sinusoidal voltage at U_C, the buck-switch S_1 is appropriately controlled. The conversion to an AC-signal is done by alternatively switching of S_2 and S_3 at twice the mains frequency. In Fig. 1.b a current fed inverter structure is depicted. Here the input current for the inverter stage (and therefore of the transformer) is controlled by S_1 to generate a sinusoidal current which is injected into the transformer. S_2 and S_3 are the inverter switches working at twice the mains frequency. Only off-line structures are examined, because on-line switches require additional, bulky overvoltage protection due to transients in the power grid (caused by lightning, switching events etc.). Studies have shown that the probability of failure increases if on-line switching is performed.

These conventional solutions require at least two semiconductor switches in the main current path to convert DC to AC. If the number of the active switches can be reduced, the efficiency and the realibility can be improved significantly. One approach is the structure in Fig. 1.c.
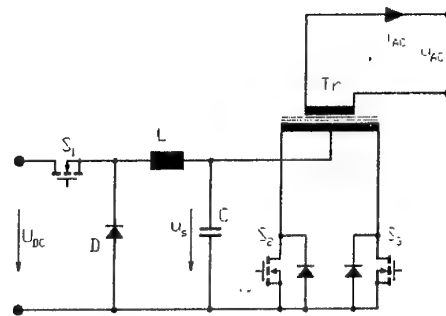
Fig.1.a. Principle of the conventional voltage-fed DC-to-AC converter
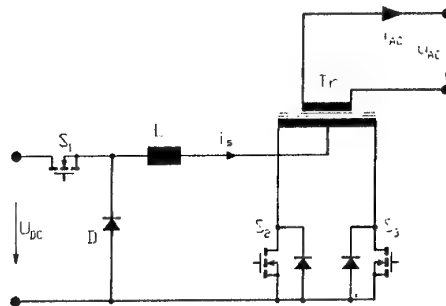
Fig.1.b. Principle of the conventional current-fed DC-to-AC converter
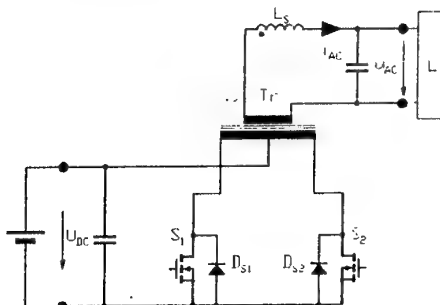
Fig.1.c. Principle of the advanced voltage-fed DC-to-AC converter

The method of efficiency improvement by overdimensioning of the semiconductor elements is overcome by topological improvement [2,3]. Moreover, the reduction of the number of the active elements leads to higher reliability and lower costs. Disadvantegeous is the fact, that the main transformer additionally is subject to high frequency operation.

2. THE NEW CONVERTER STRUCTURE

The structure shown in Fig. 2 shows the novel current-fed inverter topology. Again (as it is the case in Fig.1.c.), one operating stage is eliminated. The inductor L is split into two identical windings with high coupling on the same core L_A and L_B. Only two lowside switches are required (always only one active switch in the main current path). The splitted inductor L_A, L_B reduces the impact of the primary current, which alternates with switching frequency, on the mains transformer. An ordinary main transformer for 50 Hz operation is used, only the inductor is designed for the switching frequency. The necessary freewheeling diodes are realized by the antiparallel diods of the used FETs.
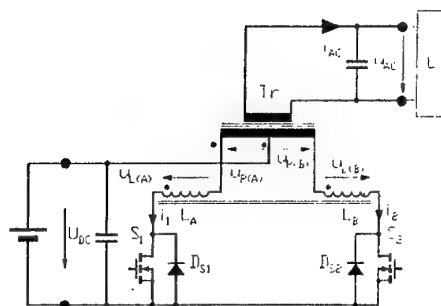
Fig.2. Principle of the advanced current-fed DC-to-AC converter

The continous mode operation of the inverter can be divided into four operational states (cf. Fig.3). During the positive half wave of the line voltage u_{AC} the switch S_1 is operating. Fig.3.a. shows the primary current path, when S_1 is on, Fig.3.b. shows the primary current path, when S_1 is off. The negative half wave is produced by switching S_2. The path of the primary current, when S_2 is on and off is depicted in Fig.3.c. and Fig.3.d., respectively.

a.)   b.)

c.)   d.)
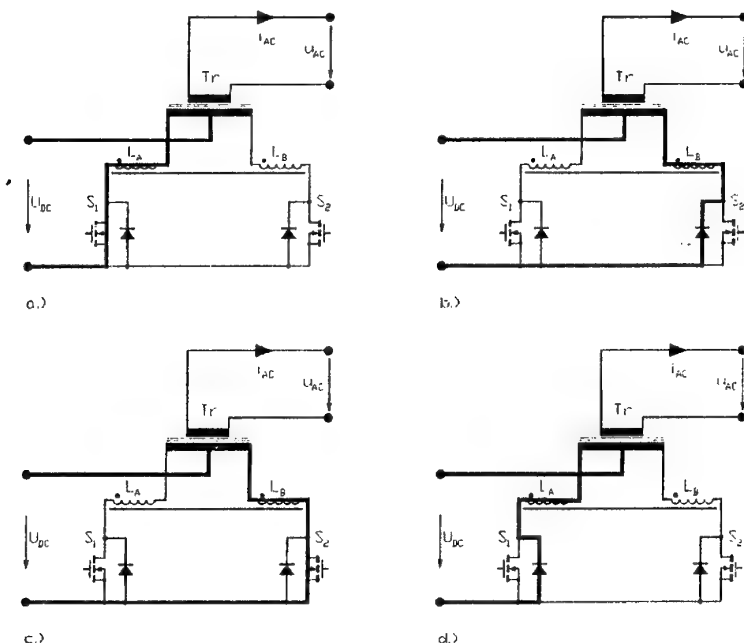
Fig.3. a-d operational modes of continous transformer current type inverter

a) S_1 is closed (S_2 is not in operation or off). The voltage

$$u_{P(A)} = \frac{1}{\ddot{u}} \cdot u_{AC},$$

is reflected on the primary winding of the main transformer. The voltage across the inductor L_A is

$$u_{L(A)} = U_{DC} - \frac{1}{\ddot{u}} \cdot u_{AC}.$$

99

The inductor L_A is energized and the rate of rise of the input current I_{IN} is given by

$$\frac{di_{in}}{dt} = \frac{u_{L(A)}}{L}.$$

The voltage across S_2 and D_2 during the magnetization interval (S_1 closed) is $2 * U_{DC}$.

b) S_1 is turned off (S_2 is not operating or turned on in order to shunt ist freewheeling diod D_2), the current commutates from L_A into L_B and decreases (current path through the antiparallel diode of S_2 and drives the right windings T_B of the transformer). S_1 has to block $2 * U_{DC}$. The demagnetization speed is

$$\frac{di_m}{dt} = \frac{-u_{L(B)}}{L}, \qquad \text{where}$$

$$u_{L(B)} = U_{DC} + \frac{1}{\ddot{u}} \cdot u_{AC}.$$

c) S_2 is closed (S_1 is not switching or off), the current of L_B increases and drives the right windings of the main transformer.

d) S_2 is open (S_1 is open or shunts ist freewheeling diod D_1), the current commutates from L_B to L_A and decreases (current path through the antiparallel diode of S_1 and drives the right windings of the main transformer).

Figure 4 depicts the input current within one switching cycle of S_1 in order to calculate the duty ratio α.
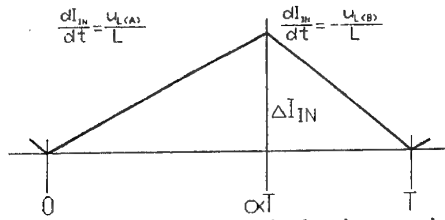
Fig. 4 Input current ripple in continuous operation mode

With

$$\frac{di_{(A)}}{dt} = \frac{u_{L(A)}}{L} = \frac{U_{DC} - \frac{1}{\ddot{u}} u_{AC}}{L}, \qquad (1)$$

$$\frac{di_{(B)}}{dt} = -\frac{u_{L(B)}}{L} = -\frac{U_{DC} + \frac{1}{\ddot{u}} u_{AC}}{L} \qquad (2)$$

and

$$U_{AC} = u_{AC} \cdot \sin(\omega t)$$

the duty ratio α (c.f. Fig. 4) is calculated to

$$\alpha = \frac{u_{L(B)}}{u_{L(A)} + u_{L(B)}} = 0.5 + \frac{1}{2 \cdot \ddot{u}} \cdot \frac{U_{AC}}{U_{DC}} \cdot \sin(\omega t).$$

$$(3)$$

As a result the variation of α due to the variing output voltage u_{AC} is described by

$$0.5 \le \alpha \le 0.5(1+k), \text{ with } k = \frac{1}{\ddot{u}} \cdot \frac{U_{AC}}{U_{DC}}. \qquad (4,5)$$

The variation of α depends on the factor k, where the winding ratio $\ddot{u}$ of the mains transformer is a free parameter. A large value of $\ddot{u}$ in relation to the ratio of U_{AC}/U_{DC} causes only a smal variation of α due to the line voltage u_{AC} and offers high control dynamics in every operating point. On the other hand it leads to higher primary transformer current. This can be a point of further optimization.

In the discontinous mode an additional state occures, where no current is flowing through the main transformer. The advantage of negligible turn on losses is compensated by the high peak current in relation to the mean value of the main transformer current.

The flux of the mains transformer changes its direction only at mains frequency, the commutation between L_A and L_B takes place at switching frequency. Because the inductor L (consisting of two identical windings L_A, L_B) can be designed for switching frequency its physical size is small. To minimize the required snubber circiuts for the semiconductor switches S_1 and S_2 the coupling of the two windings L_A and L_B of the inductor has to be as good as possible. If MOSFETs are used as power switches, a further improvement of efficiency can be achieved by shunting the free wheeling (body) diode by switching the FET. In the case of discontinous conduction mode the current has to be monitored to control the turn off point of time.

3. EFFICIENCY

To get a quick overview of the efficiency a simple first order model can be used. The load is ohmic and the transformer is idealized. To reduce the losses the diode will be shunted by the parallel transistor. Thus there is no difference whether the active or the passive switch is conducting. The used abbreviations are

u_{DC} input voltage,

R' reflected output load to the input,

R_L output load,

N_1 half primary winding,

N_2 secondary winding,

r_{DS} on resistance of the active switch,

r_{N1} winding resistance of the transformer,

$r_A = r_B = r_L$ resistance of one half of the coupled inductor,

100

$L_A = L_B = L$ inductance of one half of the coupled inductor.

The resistance of the leads can be included into the resistance of the windings. The reflected load to the primary can be calculated by

$$R' = \left(\frac{N_1}{N_2}\right)^2 \cdot R_L \quad . \tag{6}$$

Taking the positive half wave into account the current during the on time of the active switch S_1 (Fig.3.a) can be described by

$$\frac{di_{IN}}{dt} = \frac{u_{DC} - (R' + r_{DS} + r_A + r_{N1}) \cdot i_{IN}}{L} \tag{7}$$

and during the off-time of the active switch S1 (the current commutates into the parallel diode of S2 which will immediately shunted by S2) by

$$\frac{di_{IN}}{dt} = \frac{-u_{DC} - (R' + r_{DS} + r_B + r_{N1}) \cdot i_{IN}}{L} \quad . \tag{8}$$

As the current flows always through the same kind of resistors, the efficiency can be approximated by

$$\eta = \frac{R'}{R' + (r_{DS} + r_L + r_{N1})} \quad . \tag{9}$$

Low on resistances of the semiconductor switches and low copper losses of the magnetic parts are necessary to obtain high efficiency.

4. PROTOTYPE RESULTS

A 500W laboratory prototype is breadboarded. The input voltage is 12V, the winding ratio of the main transformer is (1 : 1) : 32. The control of the inverter is realized by a small microcontroller (PIC16C73A, operating at 20Mhz system clock), which does the whole control and calculation work.

Figure 5 shows the currents in the main power switches (c.f. Fig.2). The peak at the beginning of the conduction intervalls of i_1 is due to a parasitic resonance. The parasitic output capacity of S_2 is charged via the stray inductance of the loop defined by the commutating current (c.f. Fig.3.a. and b.).

The oscillogram Fig.6 shows the currents at the amplitude of the line voltage u_{AC}. The converter still works in the discontinuous mode. Thus, higher power ratings are still possible by choosing the continuous mode of operation.

Components, used in laboratory prototype (c..f. Fig. 5):

S_1, S_2	SUP75N03-04
D_A, D_B	MBR4045
D_P	13V-Transil, 1,5kW
D_{P1}, D_{P2}	28V-Transil, 1,5kW
C_{IN}	2 * 10000uF low ESR
C_O	1uF FKP-1
C_S	1000uF low ESR

R_1	0.68E / 5W / low inductance
R_2	180E / 1W
L_A, L_B	50uH, ETD49
Tr	Toroid, 7.2V/70A - 230V
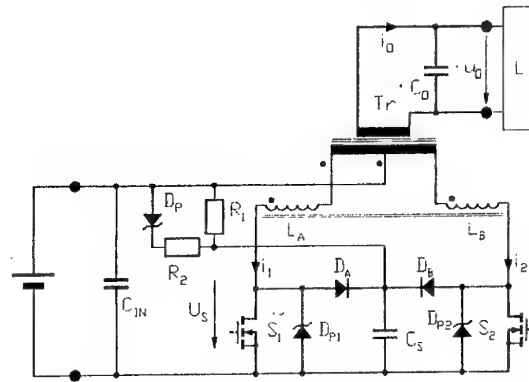
Fig.5. Laboratory prototype schematic
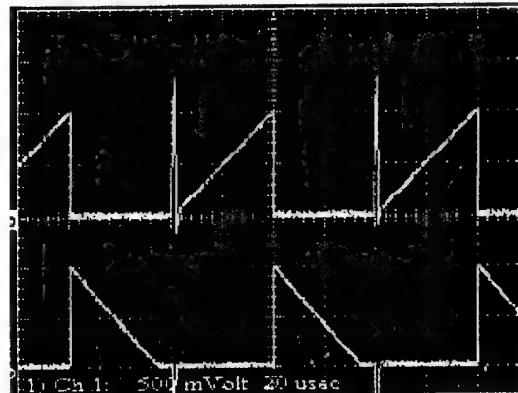
Fig. 6. Currents in the main power switches, 10mV/A = 50A/div. Upper trace: i_1, lower trace: $-i_2$
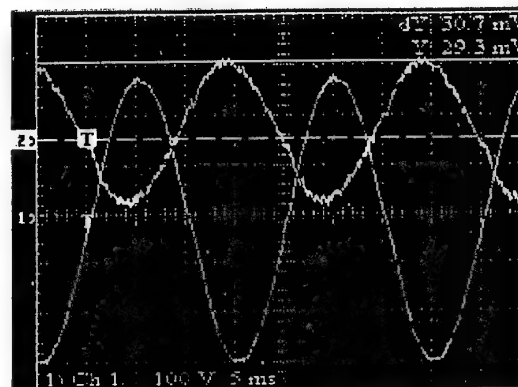
Fig. 7. Output voltage u_O (channel 1) and output current i_O (channel 2) (10mV/A=2A/div)

In Fig. 7 the output waveforms (current, voltage) of the load are given. The harmonics distortion of the output current is low (and therefore also the output voltage harmonics).

The efficiency is measured in the cases of two different switching frequencies, 20kHz (Table 1, Fig. 8) and 50kHz (Table 2, Fig. 9). Due to the switching losses the efficiency in the second case is lower than in the first case. As stated before, the ohmic resistance of the magnetic components should be as low as possible. Smal inductive components require a high switching frequency. Therefore the overall optimal switching frequency is located in the range from 20-50kHz and will be a task of further investigations.

Table 1: Inverter operating at 20kHz

Uin (V)	Iin (A)	Pin (W)	Uout (V)	Iout (A)	Pout (W)	Efficiency
12,6	0,22	2,8	233	0	0	0
12,5	5,52	69,0	230	0,26	59,8	0,86
12,2	9,18	112,0	224	0,46	103,0	0,92
12	14,02	168,2	221	0,73	161,3	0,95
11,6	27,9	323,6	216	1,4	302,4	0,93
11,1	49,56	550,1	208	2,41	501,3	0,91

Fig. 8. Inverter efficiency operating at 20kHz

Table 1: Inverter operating at 50kHz

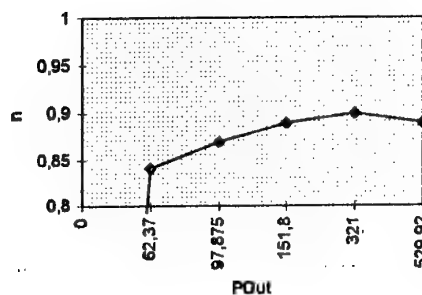| Uin (V)	Iin (A)	Pin (W)	Uout (V)	Iout (A)	Pout (W)	Efficiency
12,6	0,29	3,7	233	0	0	0
12,5	5,92	74,0	231	0,27	62,4	0,84
12,2	9,22	112,5	225	0,435	97,9	0,87
12	14,14	169,7	220	0,69	151,8	0,89
11,6	30,7	356,1	214	1,5	321	0,9
11,1	53,6	594,9	207	2,56	529,9	0,89

Fig. 9. Inverter efficiency operating at 50kHz

5. CONCLUSION

On the contrary to the conventional two stage solutions for DC-AC inverters which require at least two switches in the main current path, the inverter presented here consists of only one stage. This leads to a principal improvement of the efficiency, because only one switch is involved. The method of efficiency improvement by overdimensioning of the power semiconductor elements is overcome by topological improvement. Therefore, an additional potential of efficiency improvement is still available. The reduction of the count of active elements leads to higher reliability and lower costs. Due to the coupled inductor, which has to be dimensioned for the switching frequency, an ordinary 50 Hz main transformer with bifilar primary windings can be used.

ACKNOWLEDGEMENT

In Fig. 7 the output waveforms (current, voltage) of the load are given. The harmonics distortion of the output current is low (and therefore also the output voltage harmonics).

The efficiency is measured in the cases of two different switching frequencies, 20kHz (Table 1, Fig. 8) and 50kHz (Table 2, Fig. 9). Due to the switching losses the efficiency in the second case is lower than in the first case. As stated before, the ohmic resistance of the magnetic components should be as low as possible. Smal inductive components require a high switching frequency. Therefore the overall optimal switching frequency is located in the range from 20-50kHz and will be a task of further investigations.

Table 1: Inverter operating at 20kHz

Uin (V)	Iin (A)	Pin (W)	Uout (V)	Iout (A)	Pout (W)	Efficiency
12,6	0,22	2,8	233	0	0	0
12,5	5,52	69,0	230	0,26	59,8	0,86
12,2	9,18	112,0	224	0,46	103,0	0,92
12	14,02	168,2	221	0,73	161,3	0,95
11,6	27,9	323,6	216	1,4	302,4	0,93
11,1	49,56	550,1	208	2,41	501,3	0,91

Fig. 8. Inverter efficiency operating at 20kHz

Table 1: Inverter operating at 50kHz

Uin (V)	Iin (A)	Pin (W)	Uout (V)	Iout (A)	Pout (W)	Efficiency
12,6	0,29	3,7	233	0	0	0
12,5	5,92	74,0	231	0,27	62,4	0,84
12,2	9,22	112,5	225	0,435	97,9	0,87
12	14,14	169,7	220	0,69	151,8	0,89
11,6	30,7	356,1	214	1,5	321	0,9
11,1	53,6	594,9	207	2,56	529,9	0,89

Fig. 9. Inverter efficiency operating at 50kHz

5. CONCLUSION

On the contrary to the conventional two stage solutions for DC-AC inverters which require at least two switches in the main current path, the inverter presented here consists of only one stage. This leads to a principal improvement of the efficiency, because only one switch is involved. The method of efficiency improvement by overdimensioning of the power semiconductor elements is overcome by topological improvement. Therefore, an additional potential of efficiency improvement is still available. The reduction of the count of active elements leads to higher reliability and lower costs. Due to the coupled inductor, which has to be dimensioned for the switching frequency, an ordinary 50 Hz main transformer with bifilar primary windings can be used.

ACKNOWLEDGEMENT

References

[1] H. Schmidt: "Single Cell Module Integrated Converter (SCMIC)", 14th European Photovoltaic Solar Energy Conference, June 30 - July 4, Barcelona, pp. 355-360

[2] K. H. Edelmoser, F. A. Himmelstoß: "High Efficient DC-AC Inverter for Solar Application", 14th European Photovoltaic Solar Energy Conference, June 30 - July 4, Barcelona, pp. 314-318.

[3] K.Edelmoser, C.Anselmi: "Resonant Solar Converter for Direct Mains Connection Realized with a ZC-Switching SEPIC Variant Structure", Industrial Electronics Journal 1996, Vol. 80(2), pp341-354, 1996.

RESONANT MODE OPERATION OF INVERSE DUAL CONVERTER (IDC) FOR HIGH-POWER DC-DC APPLICATIONS

Birol ARİFOĞLU*   M. Oruç BİLGİÇ**
*Kocaeli University Department of Electrical Engineering
**Yıldız Technical University Department of Electronics Engineering

1. Introduction

The DC-DC converters for high power applications are some times needed in small size and low weight. Resonant IDC may be a good solution for these purposes. Since the switches in a resonant converter either turn on at zero voltage or turn off at zero current, therefore switching losses and switch dimensions are reduced. Thristors in that sense are good because they naturally turn-off at zero current.

This paper presents resonant mode operation of IDC. Resonant IDC is capable at voltage step-up or step-down control without a transformer. Since switches of resonant IDC can be turn-off at zero current it can be categorised in Zero Current Switching (ZCS) converters.

2. The IDC

To summarise the operation of the normal IDC [1] first will help to understand its resonant operation. The IDC is basically a modification of the Inductor Converter Bridge (ICB) [2].
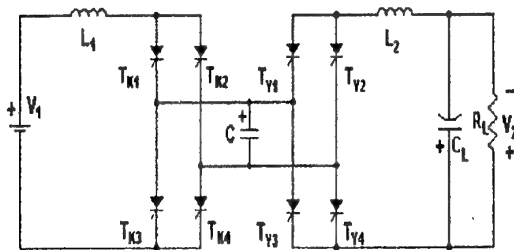
Figure 1 : IDC Circuit

The ICB is a two quadrant power supply developed for superconductive energy storage magnets in physics laboratories. The current source ICB DC-DC converter circuit has been modified to a voltage-regulated current-source DC-DC converter in the IDC, shown in figure 1.

The IDC can be divide two part, one is the source part ($T_{K1}, T_{K2}, T_{K3}, T_{K4}$) and the other is the load part ($T_{Y1}, T_{Y2}, T_{Y3}, T_{Y4}$). The source part works like a DC-AC converter and the load part like a AC-DC converter. The switching sequence on the source part is T_{K1}-T_{K4}, T_{K2}-T_{K3}, T_{K1}-T_{K4}, etc., and the same switching sequence and frequency is used on the load part, that is T_{Y1}-T_{Y4}, T_{Y2}-T_{Y3}, T_{Y1}-T_{Y4}, etc.. The phase difference (ϕ) between the source and load side switching may be used to control the output voltage [3]. The DC gain is the function of link capacitor, frequency and the phase difference.

$$\frac{V_2}{V_1} = f(C, \omega, \phi) \qquad (1)$$

Proper design and control guarantees continuos conduction in the input and output inductors and also proper commutation of the switching elements by the ac capacitor, C. The capacitor on the ac link serves two purposes: It temporarily stores the energy to be transferred from one side to the other and it also supplies the reverse voltage required for commutation. Output voltage control and input current continuity is accomplished by two control variables: the common converter frequency

104

and the difference of phase between the two converter.

3. Resonant IDC

The topologies of IDC and Resonant IDC are same but their control are different. The Current continuity is not necessary for resonant IDC. The Source side inductor and the AC capacitor works like a serial resonant circuit. Since the switching losses are small the frequency can be increased. Then the size of the components are reduced.

The switching sequence of IDC is same as it is in resonant IDC. The Currents of L_1 and L_2 are continuous at IDC but it is not continuous in the resonant IDC. Output voltage may be controlled by the time difference (t_1).

4. Principle of Operation of Resonant IDC

The source side switching sequence of resonant IDC are T_{K1}-T_{K4}, T_{K2}-T_{K3}, T_{K1}-T_{K4}, etc. and load side switching sequence are T_{Y1}-T_{Y4}, T_{Y2}-T_{Y3}, T_{Y1}-T_{Y4}, etc. but there is a t_1 time difference between source and load side switching. The currents of L_1 and L_2 and voltage of C are given in Figure 2.

The current of L_1 starts to rise when T_{K1}-T_{K4} turns on and falls to zero when the voltage of C reaches its maximum value. The load side switches T_{Y1}-T_{Y4} are turns on at t_1 and the energy stored in C starts to transfer to load side. The capacitor (C) voltage is constant while all switches are open. Similar operation repeats periodically.
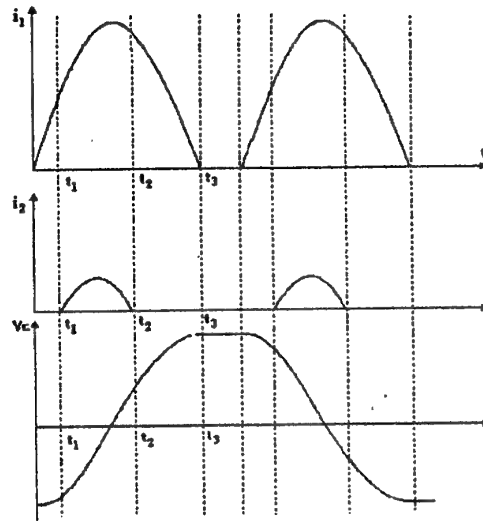
Figure 2. The currents of L_1, L_2 and voltage.

The switches turn off at zero currents due to the natural commutation. That makes the control of the switches easy.

5. Analytical Equations for Current and Voltage

There are four different topologies in resonant operation of IDC. These topologies are given in Figure 3.
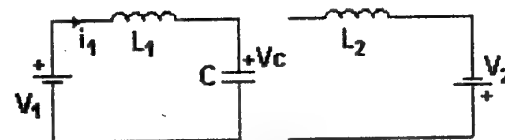
(a) Topology 1
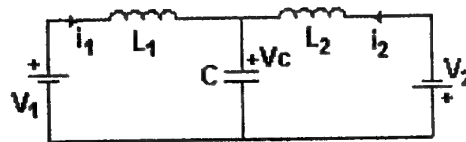
(b) Topology 2
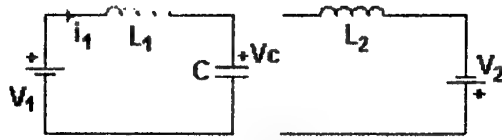
(c) Topology 3
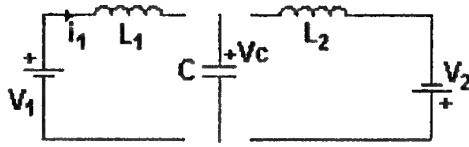
(d) **Topology 4**

Figure 3. Topologies of Resonant IDC

In these figures for the sake of simplicity load side is changed with a DC voltage source for the steady state. The mathematical analysis of each topologies are given below;

Initial conditions: $i(0^+)=0$, $V_C(0^+)=-V$

For topology 1; $\omega_0 = \dfrac{1}{\sqrt{L_1.C}}$ (2)

$V_C(t) = V_1 + \left[V_C(0^+) - V_1 \right].Cos(\omega_0 t)$ (3)

$i_1(t) = \left[V_1 - V_C(0^+) \right]\sqrt{\dfrac{C}{L_1}}.Sin(\omega_0 t)$ (4)

For topology 2; $a^2 = \dfrac{L_1 + L_2}{L_1 L_2 C}$ (5)

$V_C(t) = \dfrac{1}{aC} i_1(0^+) Sin(at) + V_C(0^+)$

$Cos(at) + \dfrac{L_2}{L_1 + L_2} V_1 (1-Cos(at)) -$

$\dfrac{L_1}{L_1 + L_2} V_2(1-Cos(at))$ (6)

$i_2(t) = i_1(0^+) \dfrac{L_1}{L_1 + L_2} [1-Cos(at) +$

$\dfrac{V_C(0^+)}{aL_2} Sin(at) + \dfrac{V_1}{L_1 + L_2}(t - \dfrac{1}{a} Sin(at)]+$

$\dfrac{V_2}{L_1 + L_2}(t + \dfrac{L_1}{L_2 a} Sin(at))$ (7)

$i_1(t) = i_1 (0^+) \left[\dfrac{L_1}{L_1 + L_2} + \dfrac{L_2}{L_1 + L_2} Cos(at) \right]$

$- \dfrac{Sin(at)}{aL_1} V_C(0^+) + V_1 \left[\dfrac{t}{(L_1 + L_2)} + \dfrac{L_2 Sin(at)}{aL_1(L_1 + L_2)} \right]$

$+ V_2 \left[\dfrac{t}{(L_1 + L_2)} - \dfrac{L_2 Sin(at)}{aL_1(L_1 + L_2)} \right]$ (8)

For topology 3; $\omega_0 = \dfrac{1}{\sqrt{L_1.C}}$

$V_C(t) = V_0 + \sqrt{\dfrac{L_1}{C}} i_1(0^+) Sin(\omega_0 t) +$

$(V_C(0^+) - V_1) Cos(\omega_0 t)$ (9)

$i_1(t) = i_1(0^+) Cos(\omega_0 t) + \left[V_1 - V_C(0^+) \right]$

$\sqrt{\dfrac{C}{L_1}} Sin(\omega_0 t)$ (10)

For topology 4 ; $i_1(t) = i_2(t) = 0$,
$V_C(t) = +V$

The variation of currents and voltages are obtained by the above equations and given in Figure 2.

6. PSpice Simulation of Resonant IDC

The following values are used for the simulation of the resonant IDC given in Figure 4.

    V1=20V.
    Ry=39Ω, Cy=2200μF
    L1=L1=1.1mH
    C=0.6μF

106

t1=15µs
f=5kHz
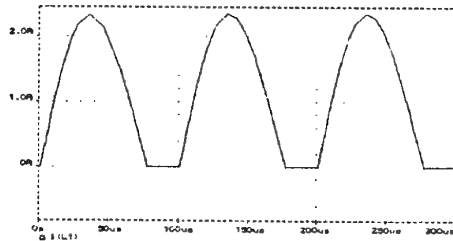
(a)
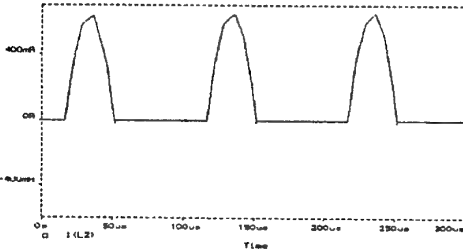
(b)
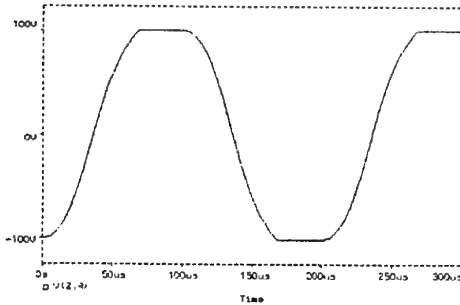
(c)

Figure 4. The link capacitor voltage and the inductors currents of resonant IDC circuit by PSpice, a) $i_{L1}(t)$; b) $i_{L2}(t)$; c) $V_C(t)$.

7. Experimental Results

A 300W proof of principle single phase resonant IDC was built in the Power Electronics Laboratory at Kocaeli University. Two 0.86mH inductors (L_1 and L_2) were wound on the iron powder cores. The link capacitor values were between 0.1 and 5µF for different experiments. The frequency range for the experiments were between 1 and 10kHz.

The oscilloscope outputs of voltage and currents for $L_1=L_2=0.86$mH, $C=5$µF, f=1.8kHz, $R_y=16\Omega$, $C_y=470$µF and $V_1=30$V are shown in figure 5. The PSpice simulation results for the same operating condition are shown in figure 6. The link capacitor voltage and the inductors currents of resonant IDC circuit at figure 5 and figure 6 are in accordance and there is no contradiction among them.
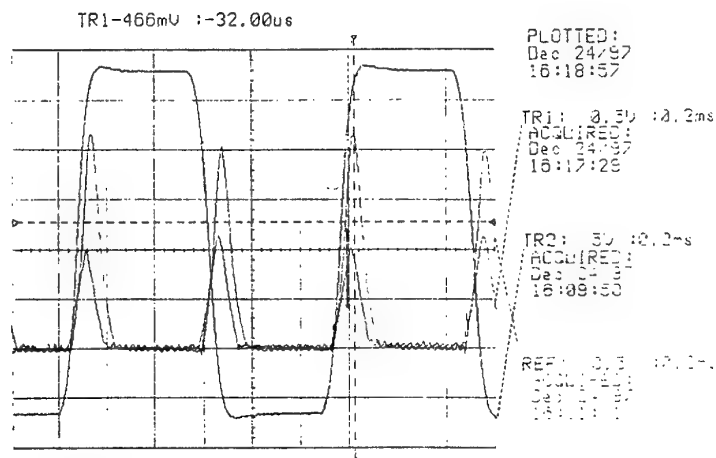
Figure 5. Experimental results for the link capacitor voltage and the inductors currents of the prototype resonant IDC.
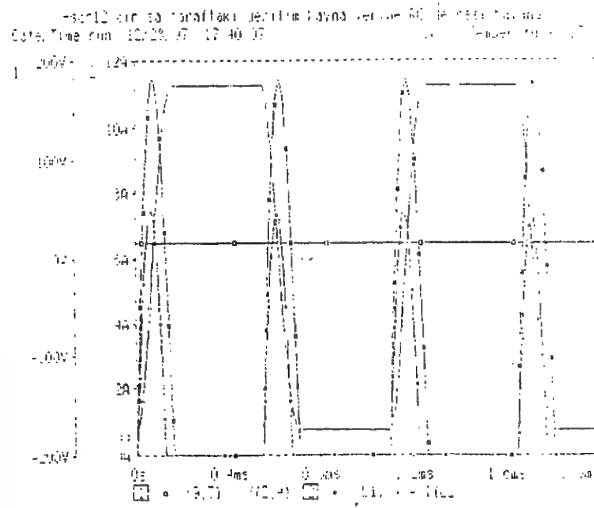
Figure 6. PSpice simulation results for the link capacitor voltage and the inductors currents of the resonant IDC.

8. Conclusion

In this work, firstly theoretical topologies are determined while IDC operates on resonant mode and expected curves of voltage and currents on capacitor and inductors are given. In order to define capacitor voltage and inductors current, some analytical equations are found by using nodal voltages in s-domain. Secondly all results are analysed for different value of inductors and capacitors by using Spice simulation program. Finally the circuit of resonant IDC is realised and the oscilloscope outputs of voltage and currents are obtained.

References

[1]   M. Ehsani, I. Husain, M.O. Bilgiç, "Inverse Dual Converter   (IDC)   for High-Power DC-DC Applications", IEEE Transactions on Power Electronics, Vol. 8,pp.216- 223 ,April 1993.

[2]   M.O. Bilgiç, M. Ehsani, "Analysis of ICB by Means of State-Space Averaging Technique", IEEE-PESC Conf. Rec., pp. 116-121, April 1988.

[3]   M.Ehsani, R.L.Kustom, R.W.Boom, "One-phase dual converter for two-quadrant power control of super conducting magnets", IEEE Trans. Magn., Vol. MAG-21, No:2, pp.1115-1118, March 1985.

Development of a 19 MW PWM Converter for U.S. Navy Surface Ships

Dr. Makhlouf Benatmane
Cegelec Projects, Ltd.
Boughton Road
Rugby, England CV21 1BU

LCDR Timothy McCoy, US Navy
Naval Sea Systems Command
2531 Jefferson Davis Hwy.
Arlington, VA 22242 USA

Abstract

The power electronics revolution of recent years has revived interest in electric propulsion for many types of ships, including military combatants. Today, integrated electric propulsion can be found aboard ferries, shuttle tankers, ice breakers and has virtually taken over the cruise ship market. In addition to the ownership cost advantages of electric propulsion, there are performance benefits for the military ship. These include increased survivability and reliability, reduced maintenance and manning requirements and arrangement flexibility. However, the military ship demands higher power density components, imposes more stringent signature requirements and subjects components to a harsher environment, including weapons effects such as underwater shock.

To meet these military requirements, an electric propulsion motor module is being developed as part of the U.S. Navy's Integrated Power System (IPS) advanced development program. This motor module consists of a 19 MW, 150 RPM, fifteen phase induction motor driven by a pulse width modulated (PWM) voltage source inverter. This paper concentrates on design considerations that led to the 15 phase PWM inverter drive selection and lessons learned in the detail design and manufacture of this technology at high power levels. When complete, the IPS motor module will be the highest power PWM motor drive in existence.

1. Introduction

Propulsion of a naval warship differs from virtually all other electric motor applications. In general, ship propulsion requires variable speed and reversing capability. The slow speed and small diameter constraints require very high torque motor designs ($\sim 10^6$ N-M). A seaway induces cyclic loading on the propeller and subsequently on the propulsion drive that should not be transmitted to the power distribution system. Therefore, the very tight speed regulation found in process plant drives is not suitable for ship propulsion. However, rapid reversal of the propeller direction is required for safely stopping the ship. Ships also require redundancy so no single failure will put the drive out of commission. Warships additionally impose stringent noise, vibration, electromagnetic compatibility, vibration and underwater shock requirements on all shipboard components.

2. Design Process

As part of the system design, a trade-off study was conducted to determine the optimum motor/converter configuration for the requirements of the Full Scale Advanced Development (FSAD) prototype. This proof of concept development phase emphasises minimum cost while meeting the military ship requirements. Reference [1] discusses some of the systems issues as well as other portions of the FSAD prototype system.

2.1 Electrical Design

The PWM driven induction motor was selected primarily to meet the severe size and acoustic noise constraints placed on the design. The robust and simple design of an induction motor was also considered lower risk in meeting the U.S. Navy's shock requirement. An induction motor was preferred over a synchronous motor primarily because of the added complexity, cost, weight and space of a synchronous machine. This induction motor's efficiency of 95.7 % at rated power is comparable to that of a synchronous machine. Slip is a minimal 1.23 % at rated conditions. Other advantages of the induction motor are more simple, rugged and reliable rotor design, no insulated rotor components and no added control complexity, losses or maintenance related to an exciter. The FSAD motor shown in Figure (1) is designed to meet all military requirements and detailed analyses have been performed which predict it will survive in that environment. Reference [2] discusses the FSAD motor in more detail.
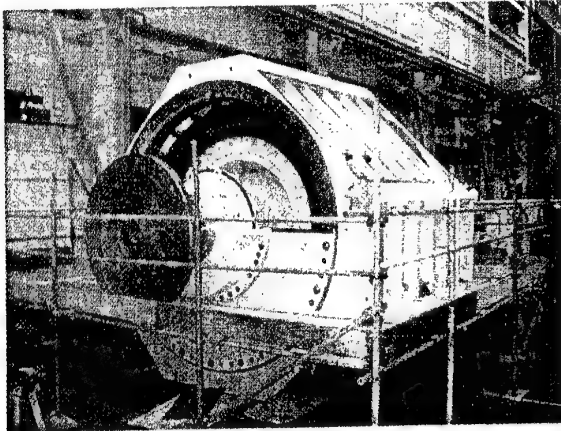
Figure 1: 19MW 150 RPM Motor

The fifteen-phase design was selected to achieve stator and rotor slot/phase/pole ratios of 1 to 1 to meet the very stringent acoustic requirements for a naval combatant ship. Although anywhere from five to twenty-one phases could have been fit within this stator design, fifteen phases was the optimal selection for best noise performance and minimal cost. Either more or less than fifteen phases would have resulted in increasing the complexity and cost of the stator with very little benefit in noise performance, reference [3].
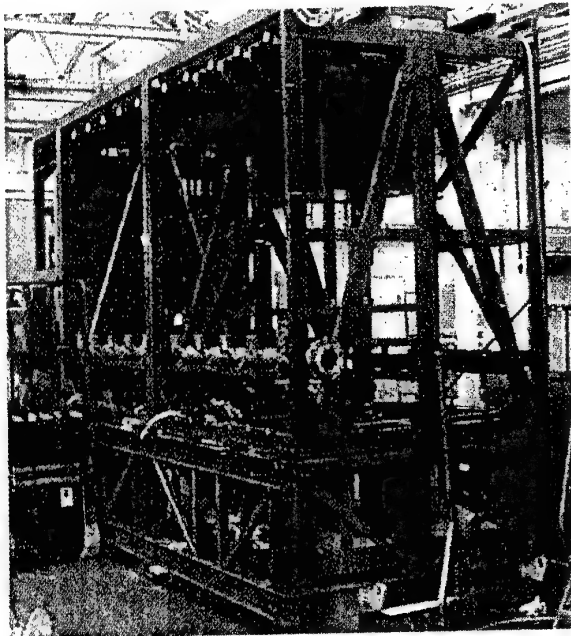
Figure 2: PWM Motor Converter

The FSAD motor converter's rated output is 21.8 MVA, 0-3700 V, 0-15 Hz, 15 phase, as shown in Figure (2). It is designed as three independent units that operate in synchronism. Each of the three units consists of one six pulse SCR-based recitfier bridge, one DC link and five series IGBT-based machine H-bridges, see Figure (3), all controlled by a separate microprocessor based controller. This design architecture allows the machine to be operated on 5, 10 or 15 phases under casualty conditions. The converter is depicted schematically in Figure (4).

The uncontrolled DC link voltage ranges from 6 kV at no load to 5.6 kV at full load. Presently there are no IGBTs capable of withstanding this voltage so for the FSAD prototype eight 1600 V IGBTs are placed in series in each H-bridge arm. This allows for n+1 redundancy in addition to the standard military practice of a 50% derating on each device. Because IGBTs normally fail open, an SCR is placed in parallel with each IGBT to be fired upon failure of the IGBT, as depicted in figure (3). The SCR is a sacrificial device, which immediately fails to a short circuit around the failed IGBT. This feature prevents the loss of a motor phase because of a single device failure and has been successfully tested several times during the initial H-bridge test programme.
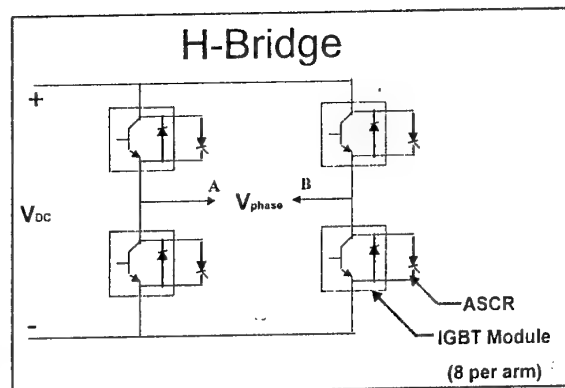
Figure 3: H-Bridge Schematic

Because of the high power levels and switching frequency, electromagnetic interference (EMI) is of particular concern in this converter design. The high voltage power system is electrically isolated from any sensitive user loads [3], so conducted emissions are not significant. However, radiated emissions both within the converter itself and those escaping from the converter must be strictly controlled.

Low level signals are transmitted fibre optically within the converter whenever possible, such as between the microcomputers and the IGBT gate driver circuit cards. A significant effort was expended in making the gate driver CCAs immune from interference. Standard packaging techniques are used to minimise the fields escaping from the converter enclosure. Additional EM field characterisation testing of both components and the

110
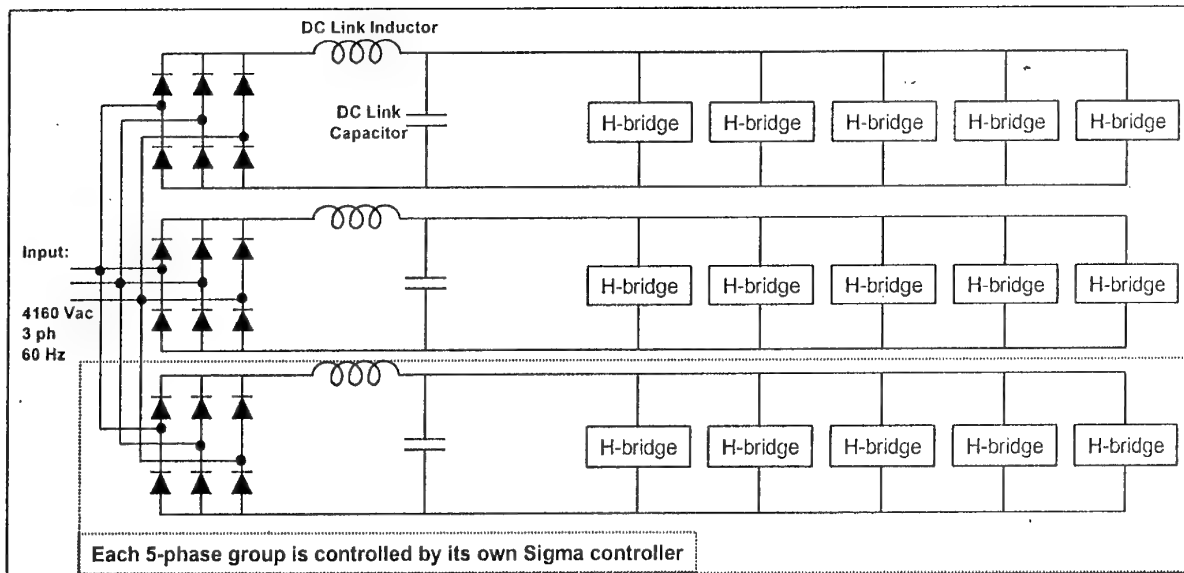
Figure 4: Converter Schematic

entire system will be conducted as part of the FSAD test programme.

2.2 Mechanical Design

The converter mechanical design is a space frame with non-structural steel cover panels attached to the frame. It is designed to meet military shock, vibration, EMI, temperature and humidity requirements. It is modular, with each supply and machine bridge separately removable for maintenance. All power cables enter from beneath and the auxiliaries (cooling pumps, heat exchangers, etc.) are positioned together at one end of the unit.

The converter is designed to meet U.S. Navy shock requirements when mounted on resilient shock mounts. Although [4] specifies testing methods, rather than shock acceleration levels, it is expected that acceleration levels on the order of ~35g would be seen by the converter. Shock design notably impacts the converter design, affecting everything from the frame to securing of cabling and bus bars. However, allowing equipment to be mounted on shock mounts, vice hard mounted to the ship's structure significantly reduces the shock levels seen by the equipment, thus minimising the impact on its design, cost and allowing it to be manufactured with commercial methods.

The drive is seawater cooled, using an air/water heat exchanger for the supply bridges, a Midel/water heat exchanger for the DC link inductors and direct seawater

cooled heat sinks for the PWM machine bridges. The machine bridge heat sinks are kept at ground potential by placing an insulating layer between each IGBT and the heat sink. Thermal tests on the bridges have proven this technique successful.

2.3 Machine Control

The DC link voltages are operated in an uncontrolled fashion. Although the recitifier bridges are SCR-based, they are essentially operated as diode bridges. The firing angle control is only used for controlling in-rush currents upon start-up and upon detection of a fault condition on the supply.

Because there is no need to precisely control rotor speed, a scalar control strategy is used. The design is simplified as no rotor position sensor is required and sophisticated sensorless vector control schemes that rely on estimation techniques are avoided. Figure (5) depicts a simplified control block diagram. Note that the 3x5 phase design allows using three controllers, so no single control system failure will render the entire drive inoperative. However, this control architecture adds more complexity since the three controllers must precisely synchronise the drive for proper operation. High speed fibre optic serial links between the three controllers pass signals for synchronising the 2kHz carrier signals, supply bridge thyrister firing, motor phase currents, speed reference, and phase rotation all at a 2msec update rate.

111

Figure 5: Control Block Diagram
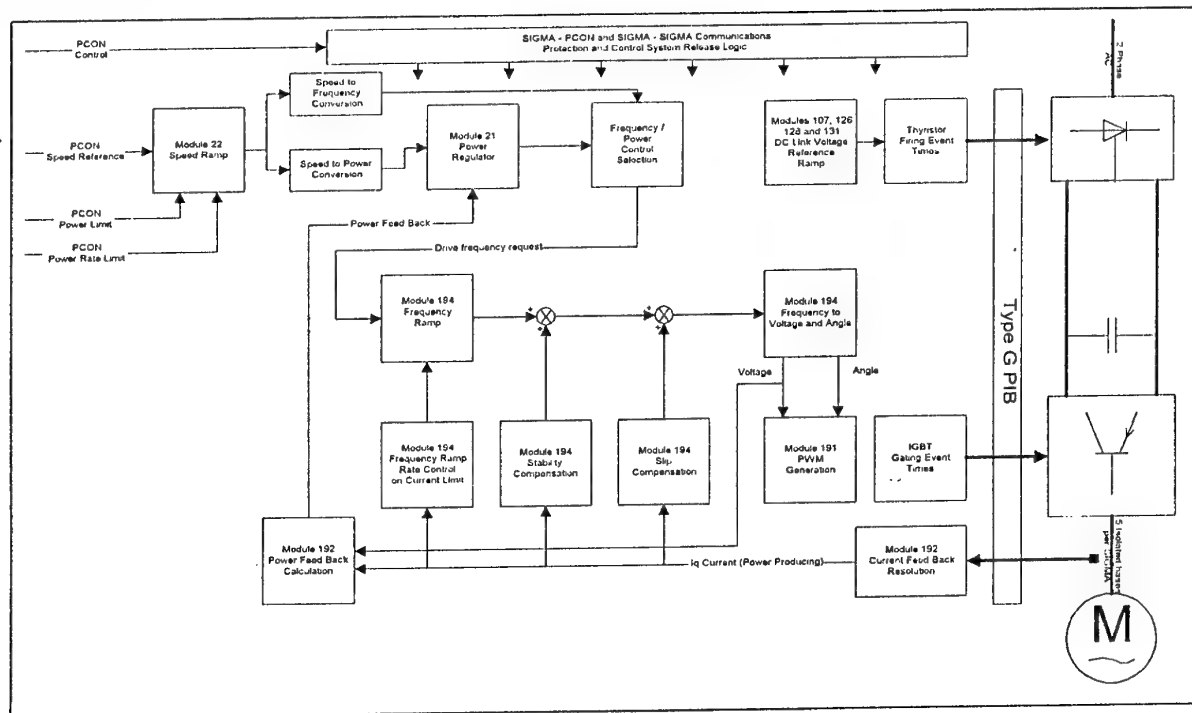
Presently, one of the three controllers is designated as a master with the others acting as slaves. The master provides the timing information used by the slaves to maintain proper synchronism. The master can either be manually selected by the operator or chosen automatically by the controllers themselves. As long as the master maintains communications with both slaves, full drive operation can be maintained. This allows for a failure of one of the three serial links with no adverse impact on the drive operation. All three controllers are also fitted with Ethernet communications to the ship's supervisory control system providing triple redundancy in this communications link as well.

Figure 6: PWM Switching Pattern

The machine bridges are switched using a differential unipolar PWM technique. Bipolar switching was contemplated, as it would eliminate common mode currents. However, analysis indicated this method would have caused unacceptably high circulating currents within the motor and was abandoned during the design phase. The common mode currents are kept within the motor/converter by utilising the cable conductor screens and additional cables tied from the motor frame to DC link midpoints to carry this current. The differential unipolar PWM switching pattern is depicted in Figure (6). Reference [5] discusses the overall grounding scheme in detail.

3. Advantages

A PWM converter was selected over a load commutated inverter (LCI) or cycloconverter for numerous reasons. Since a PWM converter does not require a synchronous motor to maintain a controlled load commutation, the advantages of an induction motor become available with the PWM drive. The PWM converter provides the ability to control the waveform for a more sinusoidal shape. This reduces harmonics resulting in lower motor noise than is possible with other converters.

Other advantages of PWM converters over LCI and cyclo-converters are a higher, more constant power factor for better efficiency, constant harmonic frequencies to ease any supply filtering required and smaller size and weight. The FSAD unit is only 2.0m x 4.0m x 2.5m high and weighs approximately 17,000 kg, significantly smaller than commercial units of any power topology. Table I compares the IPS design with standard commercial drive technology.

Converter (Type)	Rating (MW)	Volume (kW/m3)	Weight (kW/kg)
IPS (PWM)	19	905	1.12
UK Type 23 (rectifier)	1.5	191	0.28
USCG Healey (cyclo)	11.2	455	1.24
UK Oiler (synchro)	7.0	277	0.741

Table I: Comparison of Converter Technologies

The 3x5-phase architecture for both the power circuits and control system, offers triple redundancy and enhanced reliability over commercial dual wound three phase motors. This feature, combined with the n+1 IGBT redundancy allows for very high reliability required of a military system. The FSAD unit is predicted to have an availability of 0.9995 with a mean time to repair of two hours [3].

4. Conclusion

The U.S. Navy's Integrated Power System programme has developed a viable propulsion motor drive to meet the military requirements for Navy ships. While the design of this unit is somewhat developmental, the open system architecture will allow insertion of any technology that can meet the military requirements (matrix converters and permanent magnet motors are examples). This particular development was undertaken because studies have shown that PWM technology will be required to meet the needs of military ships.

This effort has more than tripled the power level to which PWM technology may be applied, opening up the entire commercial ship market to utilising this technology, if it can be shown cost effective. Sharing technology between the military and commercial markets will ultimately benefit both users achieve their somewhat disparate ends.

5. References

[1]   McCoy, T.J., Benatmane, M., "The All Electric Warship: An Overview of the U.S. Navy's Integrated Power System Development Program," International Conference on Electric Machines, 1998.

[2]   Benatmane, M., et. al., "Electric Power Generation and Propulsion Motor Development for U.S. Navy Surface Ships," All Electric Ship '98, London, U.K., 1998.

[3]   Integrated Power System, Propulsion Motor Module Design Document, CDRL-B041, Lockheed-Martin, Syracuse, NY 1996.

[4]   MIL-S-901D, "Shock Tests, High-Impact, Shipboard Machinery, Equipment and Systems, Requirements for."

[5]   Dalton, T., "Grounding Design Approach in the Integrated Power System for US Navy Surface Ships," ICEM '98, Istanbul, Turkey, 1998.

Power Unit for Research Submersible

Tapani JOKINEN
Helsinki University of Technology
P. O. Box 3000, FIN-02015 HUT, Finland
E-mail: Tapani.Jokinen@hut.fi

Jaakko LARJOLA
Lappeenranta University of Technology
P. O. Box 20, FIN-53851 LAPPEENRANTA, Finland
E-mail: Jaakko.Larjola@lut.fi

Igor MIKHALTSEV
P. P. Shirshov Institute of Oceanology
Russian Academy of Sciences
MOSCOW, Russia

Abstract

In the paper, the design solution of a 25 kW power unit for a research submersible is presented. The unit charges the batteries of the vehicle being able to operate at a depth of 6000 meters. The generator of the unit is a high-speed permanent magnet synchronous generator. The fuel of the power unit is hydrazine-water mixture. The system has been successfully tested.

1 Introduction

The scientific research submersibles have normally electric propulsion system. The energy storage is a rechargeable battery. In Russian 6000 meter *Mir 1* and *Mir 2* submersibles, the energy of the batteries is 100 kWh.

100 kWh energy is sufficient for normal planned missions; the crew becomes tired before the batteries are drained. Anyway, it was planned an alternative 200 kWh hydrazine hydrate power pack for abnormal long missions and allowing the use of energy consuming instruments.

2 Power unit

The main parts of the power unit are presented in Fig. 1. The fuel, hydrazine hydrate with 36 % of water ($N_2H_4H_2O$), is pumped from the fuel tank 1 to the reaction camber 2. The density of the fuel (1,035 kg/dm^3) is close to that of ocean water at 20 ^{0}C.

Thus, the weight of fuel container is nearly zero in submerged conditions. The fuel tank is a plastic sack. It is installed outside the pressure hull and therefore buoyancy is prevented as the chemical is consumed and replaced with seawater. Under normal conditions, the fuel is not inflammable, and it is ecologically safe enough.

In the reaction chamber 2, the fuel is catalytically dissociated, giving hot steam-gas products (mostly ammonia) under more than 700 bar pressure. Because of its physical characteristics, hydrazine hydrate is especially suitable for use in underwater devices.

The hot gases from the reaction chamber give their heat in the heat exchanger 3 to the secondary circuit 5. In the heat exchanger, most of the hot gases condense, so that the exhaust 4 to the sea is mainly liquid. Alternatively, the gases can be directed to an extra buoyancy soft tank. This important and unique feature provides buoyancy for lifting additional weight, for example, from the bottom.

The potential lift capability of the soft fuel / exhaust product tank was a factor that influenced the decision to proceed with the heat cycle selected instead of a Sterling thermodynamic cycle under consideration.

Our calculations and the known analysis of the content of ammonia in seawater show that draining the exhaust to the ocean brings no harm to the environment. Within a radius of 5 meters, the ammonia dissipates to natural concentration level.

114
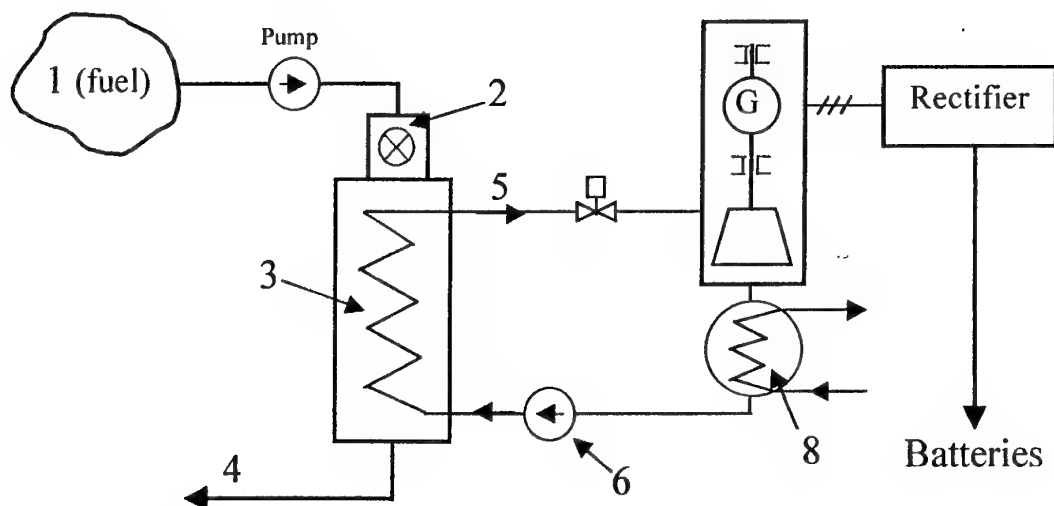
Fig. 1 Main parts of the power unit for a submersible 25 kW battery charger.

The secondary circuit is an organic Rankine cycle, where the working fluid is toluene ($C_6H_5CH_3$). The pump 6 feeds toluene to the heat exchanger 3, where it is vaporised and superheated. The vapour expands in the turbine of the turbogenerator 7 and condenses back to the liquid state in the condenser 8. The coolant used in the condenser is the ambient seawater.

3   Turbogenerator

Using a high rotational speed, the weight and size of the turbomachines and electric generators are small. The weight and size are approximately inversely proportional to the speed. Also to obtain a good efficiency, it is necessary that the turbine run very fast, in our case 40,000 to 48,000 rpm. The turbine, feed pump and electric generator are directly coupled; that is, no gearbox and no seals are used. The generator and turbine have common bearings, which are lubricated by the working fluid toluene. The pump 6 develops the required lubricant flow.

The whole secondary system is completely hermetic and should require maintenance only seldom. The high frequency current (750 Hz) produced by the generator is rectified and fed to the batteries. The output of the power unit is adjusted by the controlling the fuel flow.

3.1 Generator

The generator is a two-pole permanent magnet high-speed generator. High-speed permanent magnet machines can have several forms [1]. Fig. 2 shows the constructions of three different permanent magnet machines. In Fig. 2a the permanent magnets are on a ferromagnetic shaft and a retaining ring contains their centrifugal forces. The ring must be non-magnetic and it forms an additional magnetic air gap. Fig. 2b shows the inverse structure; the peripheral permanent magnets are on the inside of the external rotor. The rotor core may be the retaining ring and the magnetic air gap is equal to the mechanic air gap. In the third construction (Fig. 2c), the rotor consists of a cylindrical permanent magnet which is diametrically magnetised and reinforced by a retaining ring. The stator winding can be in the slots or in the air gap.

The construction 2a has been chosen for the generator of the submersible power unit. The rotor pole consists of 12 samarium cobalt magnets embedded in aluminium cylinder, Fig. 3. In axial direction there are two magnets and in circumferential direction six magnets. The pole angle is 135 ^{0}C. The division of the poles into smaller magnets is done to make the manufacturing easier and to avoid cogging torque that could prevent the starting of the generator. The retaining ring contains the centrifugal forces of the magnets. The retaining ring is made from titanium. The electric efficiency of the generator is high; including the losses in the rectifier and in the connecting cables, it is calculated to be 94%.
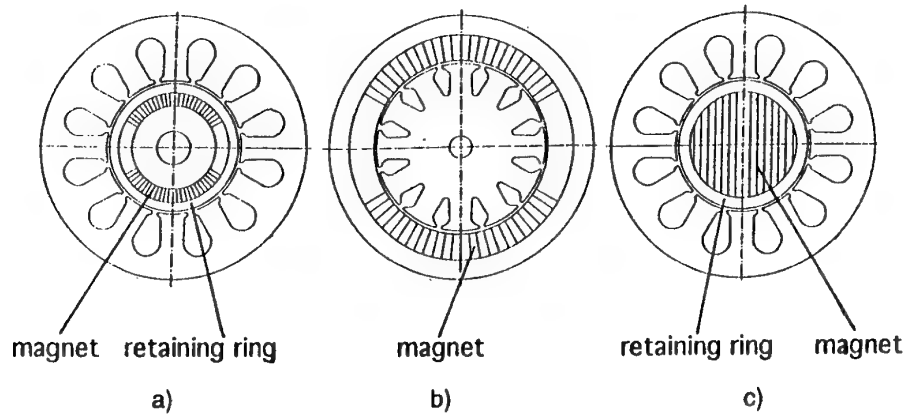
Fig. 2 Different kinds of permanent magnet machine constructions. a) Internal rotor - peripheral magnets, b) external rotor - peripheral magnets, c) internal rotor - cylindrical magnet.
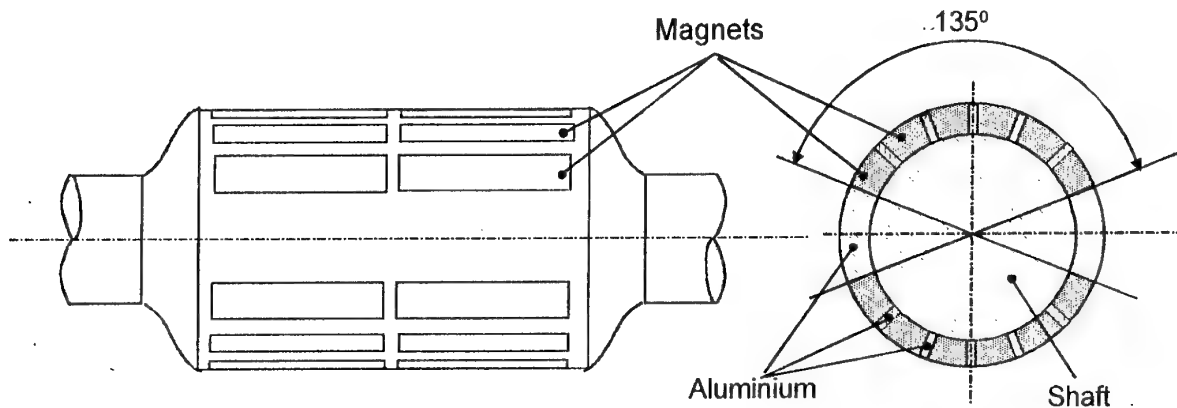
Fig. 3 The rotor of the submersible power unit's generator without the retaining ring.

3.2 Turbine

Pressure ratio over turbine is high, over hundred. Practical considerations limit the number of turbine stages to two. If a single stage turbine is used, both the inlet and the outlet velocity of rotor blades will be supersonic and the outlet velocity of stator nozzles will be highly supersonic. This causes certain design problems and results in reduced efficiency particularly at partial load [2]. Thus it is, after optimisation process, selected a two stage design, where the relative inlet velocity to each blade passage is subsonic, and outlet velocity always supersonic. Thus both stages work with a degree of reaction higher than zero, and the first stage rotor blades must be coated with a labyrinth seal ring in order to avoid leakage. In addition, the pressure differential over rotor blades causes an axial force, which is compensated with a compensation piston, provided also with a labyrinth seal. The principle of this construction appears in Fig. 4.

There are however problems also in this construction. In the first stator there are used for construction reasons only four nozzles, and the highly supersonic flow must travel c. 90° along a circular path, which causes losses. Later it is calculated, that a single stage radial design, optimised with CFD, should give the highest efficiency, but this new design is not yet tested [3]. However, despite the slightly lower efficiency than expected, the two-stage turbine design worked very well in the power pack.

116
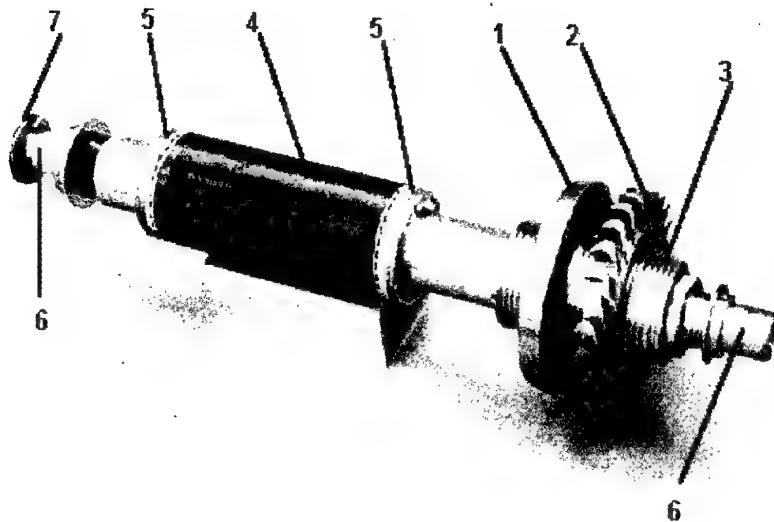
Fig. 4 The rotor of the high-speed turbogenerator. 1 turbine 1st stage rotor, 2 turbine 2nd stage rotor, 3 compensation piston, 4 generator rotor, 5 generator cooling fan, 6 radial bearing counter surface, 7 thrust bearing counter surface.

3.3 Bearings

Bearings of the rotor are situated to the free ends of the rotor. As the radial bearing type it is selected a tilting pad design, because the bearing must have good stability also at zero radial load [4]. In addition, the thrust bearing is a dynamic one, provided with taper-land bearing sectors. The thrust bearing disk diameter should be kept as small as possible in order to avoid losses. Thus, most of the axial load is compensated with the compensation piston of turbine. As the lubricant it is used the pressurised toluene. Both bearing housings are provided with labyrinth seals in order to minimise leakage. The remaining leakage of liquid toluene flows to condenser and is pumped back to the process. Thus, the whole turbogenerator is fully hermetic: there are no shaft outlets, and the leakage through labyrinth seals in turbine and in bearings happens only inside the turbogenerator housing. - Cooling of the generator is arranged with gaseous toluene, and it is circulated around with coated fans at the ends of generator rotor, see Fig. 4.

4 Tests

The whole power unit, Fig. 5, has been tested in a large (750 bar) hydraulic test chamber [5]. The cylindrical chamber with spherical end caps is 3.5 meters long (not including the end caps) and 2.5 meters in diameter. The test confirmed that the whole concept, the catalytic hydrazine dissociation unit, the organic Rankine cycle with toluene as working fluid, and the high-speed permanent magnet generator with toluene lubricated bearings worked as it was designed. The control system controlling the charging of the batteries worked also without any problems.

The consumption of hydrazine hydrate was 14,5 litre/kWh in a pressure of 500 bar (being equivalent to a depth of 5 km). The calculated value was a little bigger, 14,2 litre/kWh. In cold sea conditions, the actual consumption should be still lower, about 13 litre/kWh because of lower condensing temperature.

The whole system was mounted on a frame and the testing was repeated in the natural ocean environment in eastern mid-Atlantic to the depths of about 5000 m. The tests proved the normal, self-controlled operation as well as self-start and emergency-stop operations of the power unit. The test also proved the power unit's ability to blow out 500 litres of water immediately to provide additional buoyancy for rapid ascent.

117
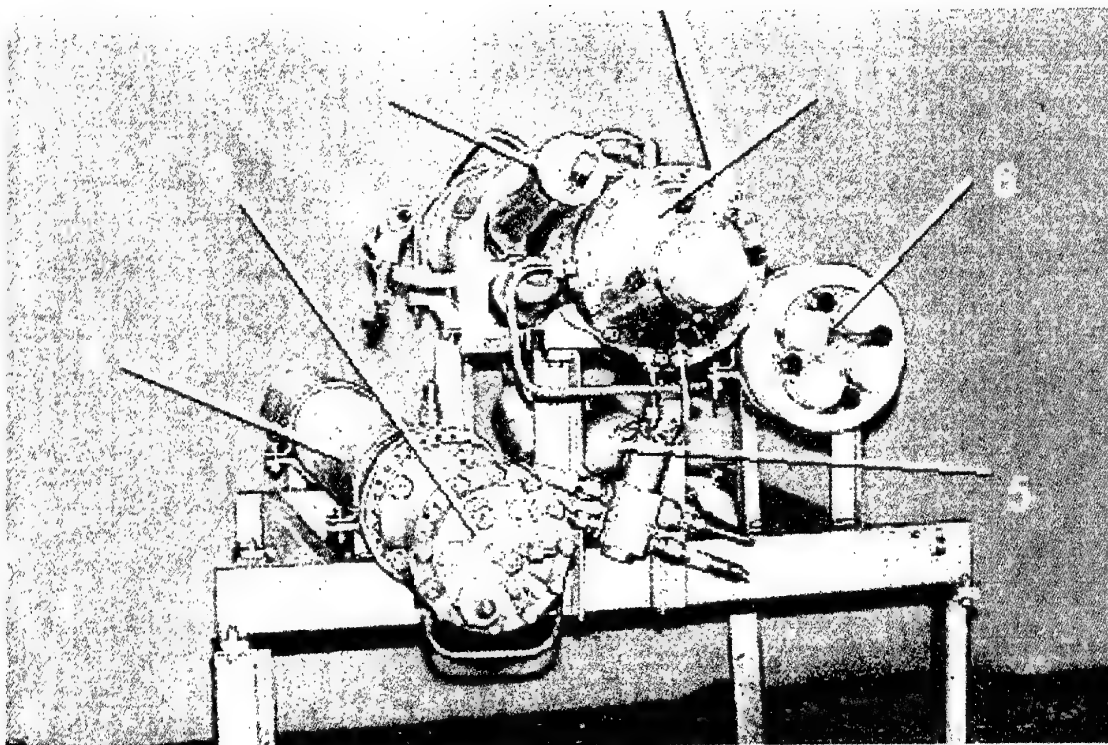
Fig. 5 The 25 kW power unit: 1 turbogenerator, 2 turbine valve, 3 reaction chamber, 4 heat exchanger, 5 condenser, 6 rectifier and control electronics.

5   Conclusions

The design of a 25 kW power unit for a research submersible is presented in the paper. The fuel used in the unit is hydrazine hydrate with 36 % water. The heat cycle is an organic Rankine cycle, where the working fluid is toluene. The generator is a high-speed permanent magnet synchronous generator that is directly coupled to the turbine and feed pump; no gearbox and no seals are used. The generator, turbine and feed pump have common bearings, which are lubricated by the working fluid toluene. The test done in a hydraulic test chamber and in the natural ocean environment proved the normal, self-controlled operation as well as self-start and emergency-stop operations of the power unit.

References

[1]   Jokinen, T.:" High-Speed Electrical Machines – a review". Electromotion, vol. 2 (1995) no 2, p. 111-116

[2]   Verneau, A.: "Supersonic Turbines for Organic Fluid Rankine Cycles from 3 to 1300 kW. Small high pressure ratio turbines". Von Karman Institute for Fluid Dynamics, Lecture series 1987-07

[3]   Larjola, J.: "The calculation of turbine in the static programme for ORC-process" (in Finnish). Lappeenranta University of Technology, Publ. No. EN B-100, 1996

[4]   Larjola, J., Backman, J.: "Oil free bearings in high speed technology". Stockholm Power Tech, June 18-22, 1995, Stockholm, Sweden, vol. Invited Speakers' Session, p. 63-68

[5]   Mikhaltsev, I.: "Boosting the Power Curve for Deep Ocean Systems". Sea Technology, (1993) April, p. 29-33

A Modular Medium Voltage PWM Inverter System for Electric Ship Propulsion

E. Cengelci*, B. Woo*, P. Enjeti*, C. Singh*

Power Quality Laboratory*
Department of Electrical Engineering
Texas A&M University
College Station, TX – 77843
Tel: 409-845-7466
Fax: 409-845-6259
Email: enjeti@tamu.edu

Abstract: In this paper a modular PWM voltage source inverter system suitable for adjustable speed drives (ASD) in electric ship propulsion is proposed. The modular inverter system is derived by combining three standard 3-phase inverter modules (power electronic building blocks-PEBB) and a 0.33 pu output transformer. The proposed system generates high quality multi-step 3 pu, low dv/dt PWM output voltages. The approach guaranties 100% utilization of each three-phase inverter module over the entire speed range. Further, employing random PWM modulation quiet operation of the ship propulsion system can be realized. Analysis, simulation, and experimental results are shown to validate the concepts.

1. INTRODUCTION

The recent trend is towards building an all electric ship with an adjustable speed drive powering the electric propulsion system. With the advances in power semiconductors and power electronic building blocks (PEBB) technologies, realization of Integrated Full Electric Propulsion (IFEP) of ships is now a reality. The IFEP concept has many benefits in operation as well as offers savings.

Power converters for medium voltage adjustable speed drive (ASD) systems are primarily current source inverter (CSI) based [5]. The CSI approach employs SCR/GTO devices and has the following disadvantages: higher cost per kW; suffers from stability problems; unsuitable for running multiple motors from a single inverter; can excite torsional resonance's in the motor; results in increase in motor heating and poor input current quality. On the other hand, the voltage source inverter (VSI) for medium voltage ASDs suffers from high output dv/dt; elevated common mode output voltage & dv/dt which necessitates additional motor insulation or a dedicated output isolation transformer in retrofit applications.

In this paper a new medium voltage PWM inverter topology is proposed [6]. The proposed inverter employs three standard 3-phase PWM inverter modules along with a 0.33 pu output transformer (Fig. 1). Each inverter module is balanced and is equally loaded and supplies 1/3 of the output power. The output voltage is 3 pu and is multi-step PWM of high quality. The advantages of the proposed system can be summarized as follows:

i. Only three standard 3-phase rectifier/inverter modules are necessary to generate medium voltage output.
ii. Each inverter is balanced in operation, equally loaded and supplies 1/3 output power.

(a)

(b)
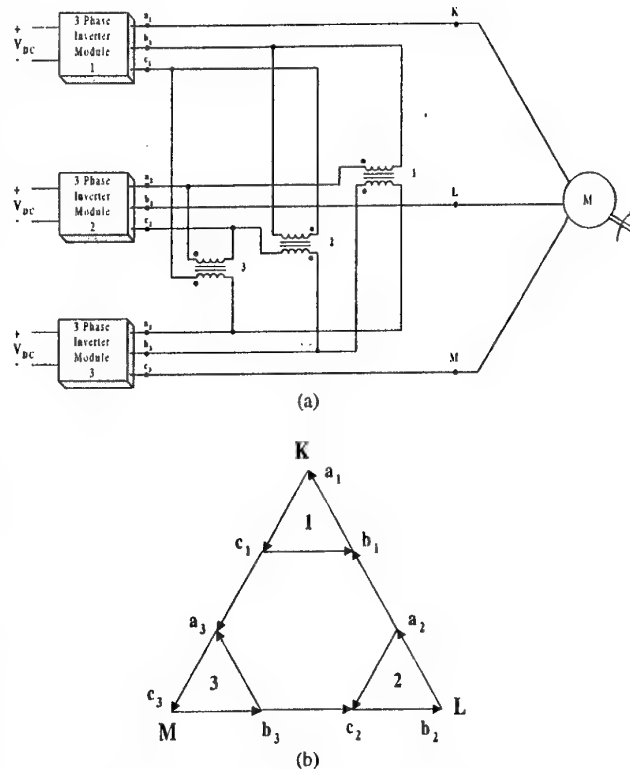
Fig. 1. (a) Proposed new medium voltage PWM inverter topology.
(V_{dc} = 1090V, IGBT's rated at 1700V for 2300V ac (rms) output)
(V_{dc}=1970V, IGBT's/IGCT's rated at 3300V for 4160V ac (rms) output)
(b) Vector diagram of the system with the fundamental voltages.

iii. Modular construction of the medium voltage inverter system facilitates the use of lower voltage IGBT devices, which are available in larger volume, easy maintenance and spare management.
iv. The output voltage is 3 pu, high quality multilevel PWM with low dv/dt.
v. The dc-link capacitive energy storage requirement is low due to balanced operation of each three-phase inverter module.
vi. The proposed system is suitable for powering constant/variable torque type loads over a wide speed range.
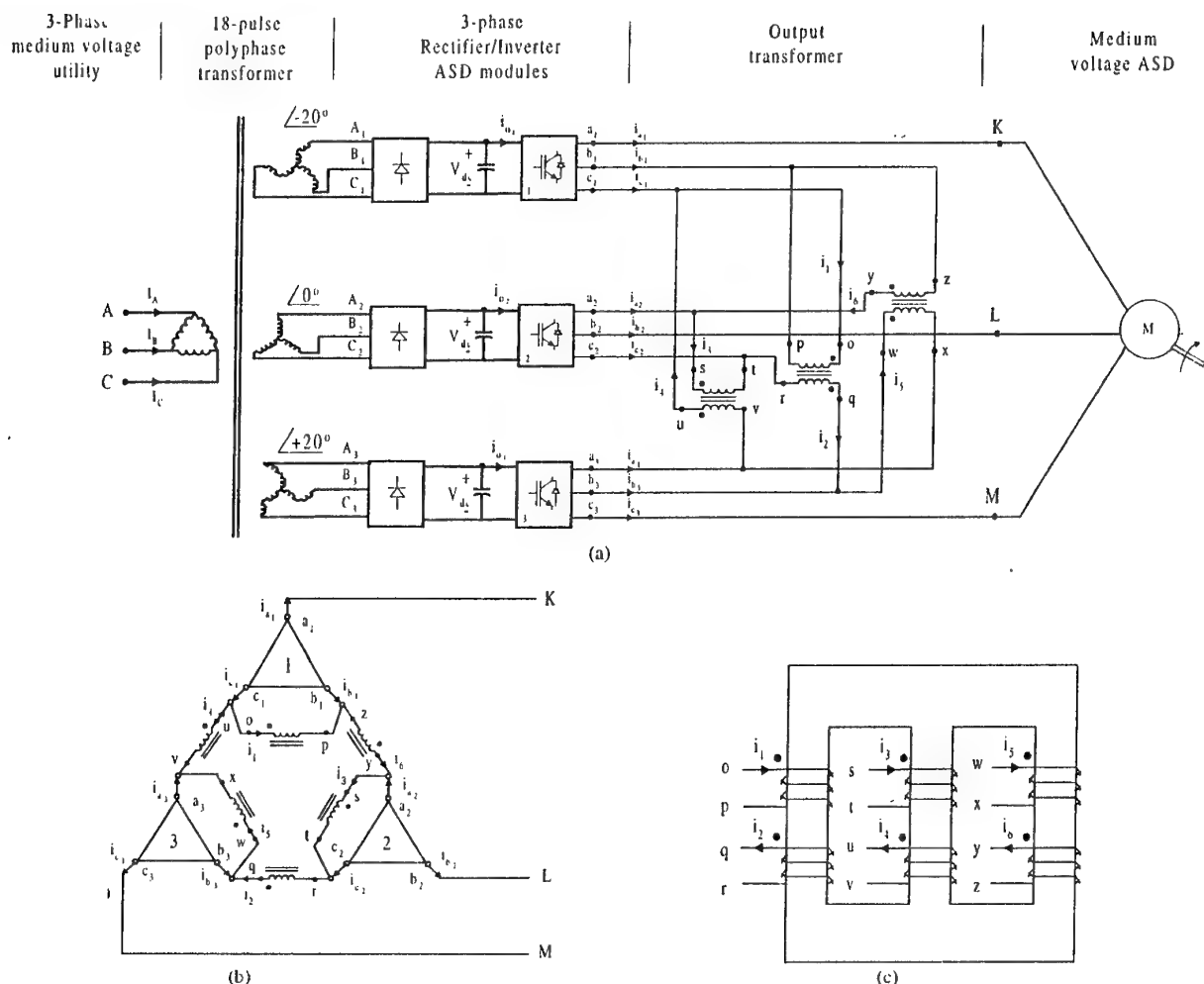
119

Fig. 2 (a) Complete medium voltage ASD with the proposed topology along with an 18-pulse input transformer for clean input power. (b) Connection of inverter modules and the output transformer. (c) Winding configuration of output transformer on a three-limb core.

vii.   The inverter system is flexible for generating different medium voltage levels for ASD applications.

viii.   The output transformer contributes to higher output voltage and eliminates any circulating current within the inverter modules.

2. OPERATION OF THE INVERTER SYSTEM

Fig.1a shows the interconnection of three standard 3-phase inverter modules along with an output transformer to generate higher output voltage. The vector diagram representing the complete inverter system is shown in Fig. 1b. Each three-phase inverter generating balanced three-phase output voltages is represented by a delta. For example, a_1, b_1 and c_1 (Fig. 1b) represent the inverter module-1 in Fig. 1a. Also three transformers of 1:1 turn ratio are connected to the inverter output (Fig. 1a). The purpose of the output transformer is to generate the vectors (Fig. 1a, 1b) c_1a_3, b_3c_2, a_2b_1 from inverter output voltage vectors a_2c_2, c_1b_1 and b_3a_3, respectively.

A more detailed connection diagram of the output transformer to accomplish this task is shown in Fig. 2. The output transformer therefore increases the output voltage and also ensures that the addition of voltage vectors (Fig. 1b) c_1b_1, b_1a_2, a_2c_2, c_2b_3, b_3a_3 and a_3c_1 is zero at any switching instant; this eliminates any circulating current within the loop.

The proposed inverter topology can power a 2300V adjustable speed drive system with a dc bus voltage $V_{dc} = 1090V$. Hence IGBT's rated at 1700V or higher can be employed. Further, a $V_{dc} = 1970V$ is sufficient to power a 4160V adjustable speed drive system. For 4160V output each inverter IGBT's/IGCT's could be rated at 3300V. Further details are available in section 3.

Fig. 2a shows an approach to interface the proposed inverter topology to electric utility via an 18-pulse transformer. The input transformer essentially has three secondary windings arranged in 0°, ±20° phase shift to achieve harmonic current cancellation in the

120

utility line currents. Since each three-phase inverter is loaded equally, the 5th, 7th, 11th and 13th, harmonic currents generated by each rectifier/inverter module are cancelled in the input line. This results in clean input power.

3. DESIGN EXAMPLE

In this section a detailed design example of a 2300V, 2000hp medium voltage inverter is discussed (Fig. 2).

Motor parameters:
Power $(P_o) = 2000HP$

Power factor $(pf) = 0.8$
Efficiency $(\eta) = 0.85$
Fundamental line-to-line voltage $(V_{KL}) = 2300V_{rms}$
Fundamental output frequency $f_o = 60Hz$

Apparent power (S) and line current $(I_{a_1,rms})$ of the motor can be calculated as follows:

$$S = \frac{P_o}{\eta \cdot pf} = 2200kVA \qquad (1)$$

$$I_{a_1,rms} = \frac{S}{\sqrt{3} \cdot V_{LL}} = 552A \qquad (2)$$

Since the rms inverter output currents are all equal and same as the load currents, each 3-phase inverter module should be rated for 552A.

The fundamental output voltages of inverter-1, -2 and -3 ($V_{a_1b_1}$, $V_{a_2b_2}$, $V_{a_3b_3}$) are given by [5] as follows:

$$V_{a_1b_1} = V_{a_2b_2} = V_{a_3b_3} = \frac{\sqrt{3}}{2\sqrt{2}} V_{dc} m_a \qquad (3)$$

From Fig. 1b,

$$V_{KL} = V_{a_1b_1} + V_{a_2b_2} + V_{a_3b_3} = \frac{3\sqrt{3}}{2\sqrt{2}} V_{dc} m_a \qquad (4)$$

By equating the output voltage V_{KL} in (4) to 2300V at 60Hz and assuming $m_a = 1.15$, we have

$$V_{dc} = \frac{2\sqrt{2} \cdot V_{KL}}{3\sqrt{3} \cdot m_a} = 1090V \qquad (5)$$

Further, the rms current of the IGBT and diode pairs,

$$I_{sw,rms} = \frac{I_{a_1,rms}}{\sqrt{2}} . \qquad (6)$$

From (2) and (6),

$$I_{sw,rms} = 390A \qquad (7)$$

Peak switch current is the same as peak motor current. Therefore,

$$I_{sw,peak} = 552 \cdot \sqrt{2} = 780A \qquad (8)$$

The IGBT's in inverters are rated at rms current of 390A and peak current of 780A. Further, IGBT's rated at 1700V or higher can be employed in each inverter module to operate at a $V_{dc} = 1090V$.

If we assume the same motor parameters in the previous design example, except the line-to-line voltage of the motor $(V_{KL}) = 4160V_{rms}$, the inverter ratings are as follows:

From (5) to (8), we have,

$$V_{dc} = 1970V , \quad I_{sw,rms} = 215A , \quad I_{sw,peak} = 431A$$

The IGBT's in inverters for 4160V motor design are rated at rms current of 215A and peak current of 431A. IGBT's rated at 3300V [7] can be employed in each inverter module to operate at a $V_{dc} = 1970V$

4. PWM CONTROL STATEGY

In this section the necessary PWM control strategy required to operate the proposed medium voltage topology (Fig. 1, Fig. 2) is discussed. It is obvious that for proper operation of the modular inverter system the three 3-phase inverter modules need to be synchronized. Further, the high frequency triangular carriers employed in each inverter are so chosen that a phase-shift of 120° exists between them. Then the overall output voltage v_{KL} (Fig. 4d) applied to the motor is not only multi-step in nature but also low in harmonic content.

Fig. 3 shows the intersection of high frequency triangular carrier signals and the low frequency modulating sinusoidal signal for one phase. Notice the 120° phase shift among the high frequency triangular carriers employed for the control of inverters 1, 2 and 3.

Fig. 4 (a), (b) and (c) show the line-to-line voltages of the inverters 1, 2 and 3, i.e. $v_{a_1b_1}$, $v_{a_2b_2}$ and $v_{a_3b_3}$, respectively. Fig. 4 (d) illustrates the overall output voltage v_{KL}, which is multi-step in nature.

Assuming that the triangular carrier frequency is much higher than the fundamental output frequency, the Fourier components of voltages $v_{a_1b_1}$, $v_{a_2b_2}$ and $v_{a_3b_3}$ can be expressed as follows [5]:

$$v_{a_1b_1} = V_{dc} m_a \sin(\omega t) + V_{dc} \sum_{h=2}^{\infty} A_h \sin(h\omega t)$$

$$v_{a_2b_2} = V_{dc} m_a \sin(\omega t) + V_{dc} \sum_{h=2}^{\infty} A_h \sin\left(h\left(\omega t - \frac{120°}{m_f}\right)\right) \qquad (9)$$

$$v_{a_3b_3} = V_{dc} m_a \sin(\omega t) + V_{dc} \sum_{h=2}^{\infty} A_h \sin\left(h\left(\omega t + \frac{120°}{m_f}\right)\right)$$

where h is the order of the harmonics in the inverter output
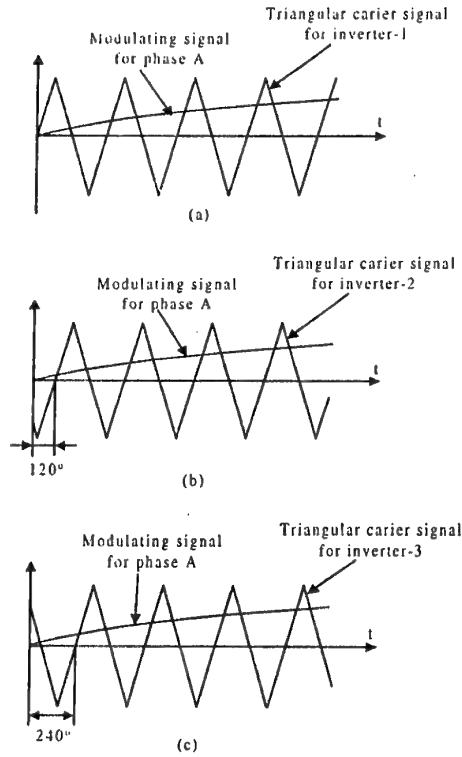
121

Fig. 3 PWM control strategy for the proposed topology (Notice the 120° phase-shift among the high frequency triangular carriers for inverters 1,2,3)
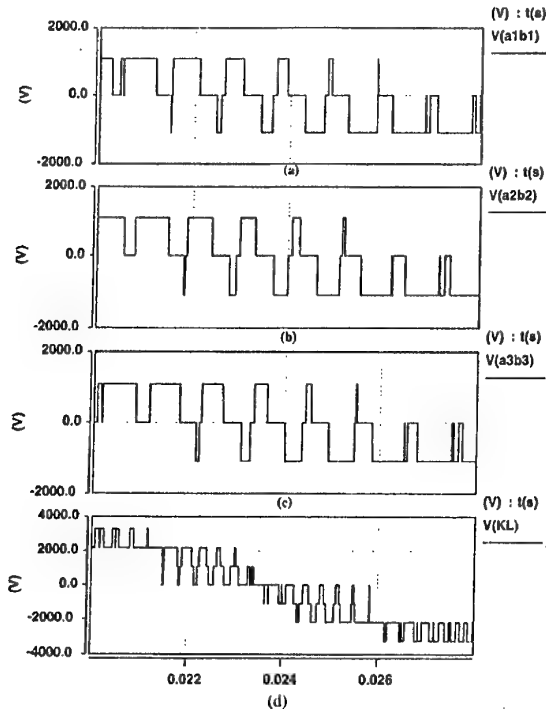

Fig.4 The voltages across "a" and "b" terminals of each 3-phase inverter and the voltage across the motor terminals K and L

voltage, A_h is the amplitude of hth harmonic and

$$m_f = \frac{f_s}{f_1} = \frac{\text{Frequency of triangular carrier signal}}{\text{Frequency of modulating signal}}$$

The phases of harmonics of $\pm h \cdot 120°/m_f$ in the expressions of $v_{a_2b_2}$ and $v_{a_3b_3}$ in (9) are primarily due to the inherent 120° phase-shifts among the high frequency triangular carrier signals (Fig. 3).

From Fig. 2 the overall inverter output voltage v_{KL} is,

$$v_{KL} = v_{a_1b_1} + v_{a_2b_2} + v_{a_3b_3}$$
$$= 3V_{dc}m_a \sin(\omega t) +$$
$$V_{dc}\sum_{h=2}^{\infty} A_h \left[1 + 2\cos\left(\frac{h \cdot 120°}{m_f}\right)\right]\sin(h\omega t) \qquad (10)$$

For sine-triangular PWM, h is given by [5] as,

$$h = m_f, m_f \pm 2, m_f \pm 4,$$
$$2m_f \pm 1, 2m_f \pm 3, 2m_f \pm 5,$$
$$3m_f, 3m_f \pm 2, 3m_f \pm 4, 3m_f \pm 6 \qquad (11)$$
etc.

Substituting (11) into (10) we can deduce that for a large value of m_f (i.e. high switching frequency) the harmonic components of h, around the side-bands of m_f, $2m_f$, $4m_f$, $5m_f$, are cancelled in v_{KL} in (10). The dominant harmonics in v_{KL} are around $3m_f$. Therefore, in the proposed PWM strategy the overall inverter line-to-line output voltage (v_{KL}) is multi-step with the dominant harmonics at three times the inverter switching frequency. Also the voltage v_{KL} experiences level change in steps of V_{dc}, which contributes to low dv/dt across the motor terminals.

5. SIMULATION RESULTS

In this section simulation results of the proposed system powering a 2300V motor detailed in the design example are discussed. The switching frequency is set at 1kHz for each inverter module in the simulation. Fig. 5 shows the line to-line output voltage of the inverter system across the motor terminal. It is clear from Fig. 5 that the voltage across the motor terminal is multilevel, therefore is of low dv/dt and its harmonic content is also low. Fig. 6 shows the motor currents, which are balanced and nearly sinusoidal. Lastly, Fig. 7 shows the three output currents of an inverter module, which are balanced.

6. EXPERIMENTAL RESULTS:

A scale down experimental prototype of the proposed inverter topology (Fig. 2) was tested in the laboratory for the following specifications:

Dc bus voltages: 110V
Motor power: 4kW

122
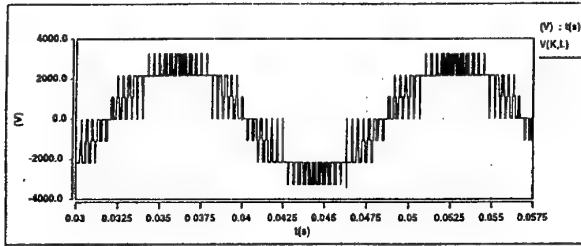
Fig. 5 Line-to-line multi-step PWM voltage across the motor terminals.
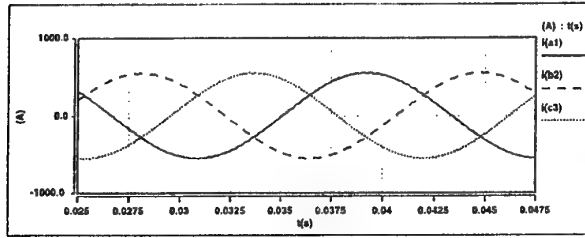
Fig. 6 The currents of the motor.
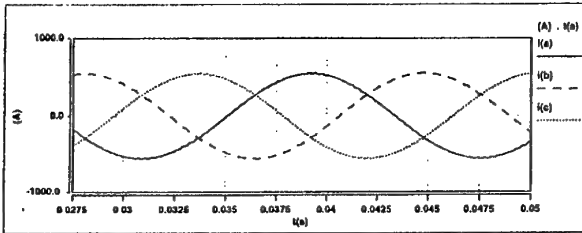
Fig. 7 Output currents of three-phase inverter modules.

Switching frequency: 1kHz
Fundamental output frequency: 50Hz
Fundamental voltage across the motor terminals: $260V_{rms}$

The control signals for the inverter system in Fig. 2 are obtained by using a DSP evaluation module of TMS320F240 of Texas Instruments. TMS320F240 is a fixed-point, 16 bit low cost DSP, incorporating a 20 MIPS processor designed specifically for motor drive applications. The block diagram of the PWM control system is shown in Fig. 8. The PWM control signals for inverter-1 and -2 are generated by the full compare and simple compare PWM channels of the DSP (Fig. 8). The control signals for inverter-3 are generated by software using GP Timer 3. The full compare unit is capable of generating gating signals with their dead-bands for inverter-1. However, the dead-band generation of gating signals for inverter-2 and-3 is obtained by hardware. The implementations of triangular carrier signals are done by the GP timers 1, 2 and 3. A sine table is used to implement the low frequency modulating sinusoidal signals. The gating signals generated in the control board are applied to the inverters via fiber optic isolation hardware. A protection signal from each inverter is fed back to the control hardware unit to ensure safe operation of the system.

Fig. 9 shows the experimental PWM line-to-line voltage of inverter-1. Fig. 10 shows the multilevel PWM voltage v_{KL} applied to the motor terminals. Fig. 11 shows the frequency spectrum of voltage v_{KL}. The dominant harmonics in v_{KL} are around 3kHz, i.e. three times the inverter switching frequency (Equation 10). Fig. 12 shows the motor currents i_{a_1}, i_{b_2}, i_{c_3} (Fig. 2). Fig. 13 shows the inverter-1 output currents i_{a_1}, i_{b_1}, i_{c_1}. These results demonstrate the feasibility of the proposed inverter topology. More extensive tests are underway and will be reported at the conference presentation.
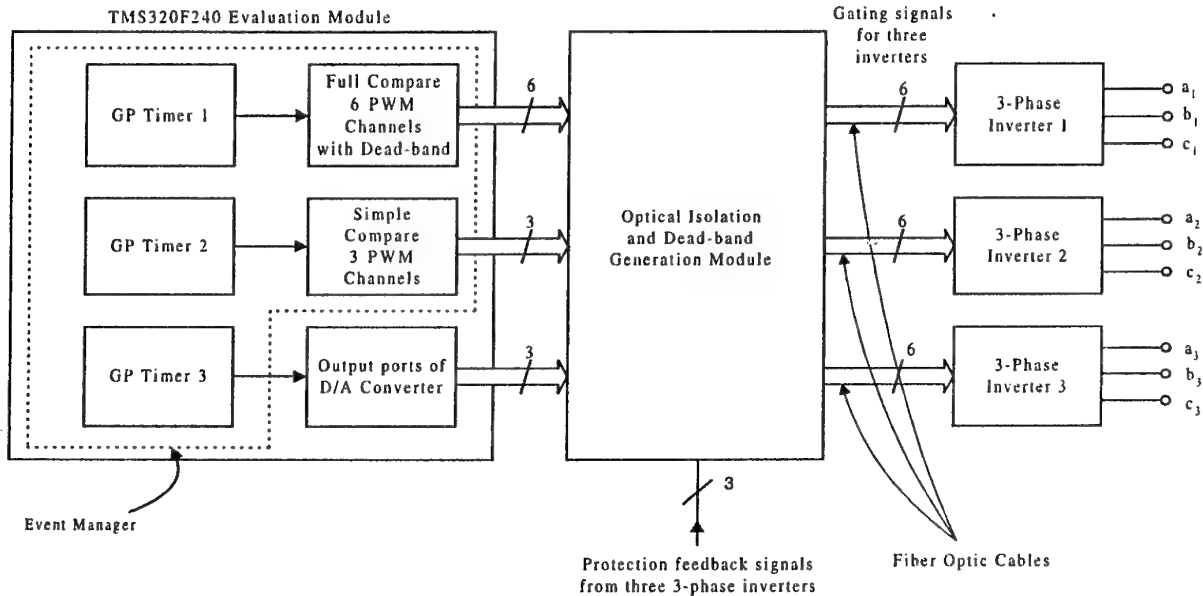
Fig. 8 DSP implementation of the PWM generation for the medium voltage inverter.
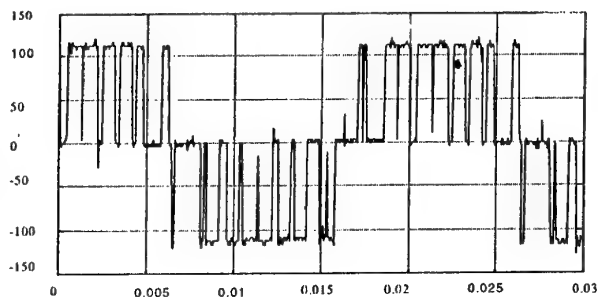
Fig. 9 Line-to-line output voltage of inverter-1 ($v_{a_1 b_1}$).
(Vertical scale: 50V/div, Horizontal scale:5ms/div)
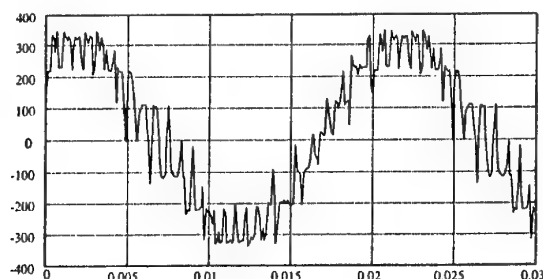
Fig. 10 The voltage across the motor terminals (v_{KL}).
(Vertical scale: 100V/div, Horizontal scale:5ms/div)
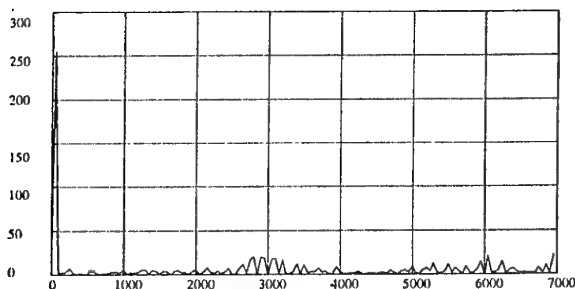
Fig. 11 Frequency spectrum of v_{KL}.
(Vertical scale: 50V/div, Horizontal scale:1kHz/div)
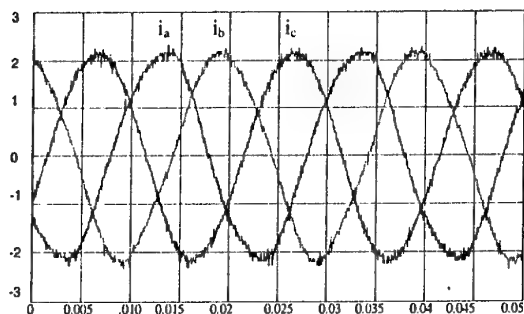
Fig. 12 Motor currents (i_{a_1} , i_{b_2} , i_{c_3}).
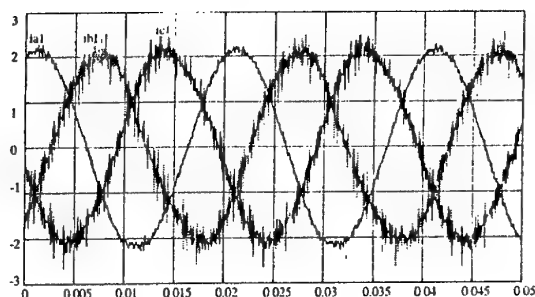(Vertical scale: 1A/div, Horizontal scale:5ms/div)

Fig. 13 Output currents of inverter-1 (i_{a_1} , i_{b_1} , i_{c_1}).
(Vertical scale: 1A/div, Horizontal scale:5ms/div)

7. CONCLUSIONS

In this paper a new medium voltage PWM inverter system for electric ship propulsion system has been proposed. The proposed approach is modular, flexible architecture suitable for different output voltage levels. Advantages of the proposed inverter topology include: high quality multilevel PWM output, low output dv/dt, and modular construction with the use of lower voltage IGBT devices. Analysis, simulation and experimental results demonstrate the feasibility of the proposed inverter system.

ACKNOWLEDGMENT

REFERENCES

1. D.A. Paice and C.W. Charles, "High voltage modular inverter and control system thereof",US Patent No: 4674024, June 16, 1987.
2. P. W. Hammond, "Medium voltage PWM drive and method", US Patent No: 5625545, April 29, 1997.
3. K. Opal, H. Abrams, P. W. Hammond, "Low and medium voltage PWM AC/DC power conversion method and apparatus", US Patent No: 5638263, June 10, 1997.
4. P. W. Hammond, "A New Approach to Enhance Power Quality for Medium Voltage Drives", *Petroleum and Chemical Industry Conference Record*, Sept. 1995, pp. 231-235.
5. N. Mohan, T. M. Undeland, W. P. Robbins, "Power Electronics: Converters, Applications, and Design," Chapter 8, 1995 Second Edition, John Wiley & Sons.
6. "Method and System of Medium Voltage Inverter Topologies For Adjustable Speed AC Motor Drive Systems", Texas A&M University, US Patent Application, 1998.
7. "Eupec IGBT Databook", Eupec Inc., 1998.

POSITION CONTROL OF AN INDUCTION MACHINE FED BY A NPC SEVEN LEVEL INVERTER

H.Gheraia* , E.M.Berkouk * , G.Manesse **

* Laboratoire d'Electronique de Puissance et de Commande
DER Genie Electrique et Informatique -ENP-
10, Avenue Hassen badi , El-Harrach , Alger, Algérie
Fax(213) 02.29.53.73 , E-mail : Berkouk @ ist . Cerist . DZ
** Laboratoire d'Electricité industrielle -CNAM-Paris
292,Rue saint 75141 Paris cedex 03-France

Abstract

In this paper we are interested to the position control of a high power induction machine fed by a seven level **NPC** inverter . We develop in first part a knowledge model of a seven level inverter **NPC** structure . Then, we present a triangulo-sinusoidal control strategy . In last part , we study the performances of the position control of an induction machine.

Key words : Induction machine, voltage inverter, multilevel, PWM strategy, field oriented control, Position control.

1 Introduction

. The alternating current machines used for the speed control in automation , submit at present time a spectacular development , in detriment of direct current motors , less performant in term of massique torque , and especially more onerous . This fact of state results from the fantastic development of power electronics components , and the data processing progress . In fact , nowadays , the rapidity of calcul and power of microprocessor allow the use , in control structure of these converters, of powerful automatic tools . Thus with self piloting , the control of synchronous motor becomes similar to a direct current motor one , and the absence of the mechanical collector assures its robustness . But the use of a permanent magnet at the rotor , as well as the cost that it leads, find its limits in harsh functioning condition : high temperatures or important overloads . So, we turn to the induction motor , which is cheap , strong and with a simple conception , associated to two or multilevel voltage inverter . These converters can be drived by different control strategies in order to get wanted performances . The two level inverters are limited in output voltage and power [5] . Thus to remedy to this limitation , new inverter structures are appeared . In this paper , we propose a seven level NPC inverter to fed great power induction machine. In this paper , we firstly remind the induction machine Park model then we present the seven level NPC inverter , develop a knowledge model of this inverter and a triangulo-sinusoidal strategy using six carriers . In the

second part , we study the performance of the control of the induction machine position using the field oriented control. The machine is fed by the seven level NPC inverter.

2 Modelling of the induction machine

2.1 Simplified hypothesis

We formulate the following hypothesis :
-The magnetic circuit saturation, foucault current, are neglected.
-The windings resistance do not varry with the temperature .
-We consider only the first space harmonic of the magnetomotrice power distribution of the stator and the rotor .
-Air gap is constant, the mutual inductances are sinusoidal functions of angles between the statoric and the rotoric axes frame.

2.2 Electrical equations of the induction machine

The figure(1) represents the six windings of the three phases induction machine .The general equations of voltages of the induction motor obtained, we write that the voltages applied to each phase is the whole of the ohmique drop and the inductive one caused by the total flux which cross this phase[1][2][3].
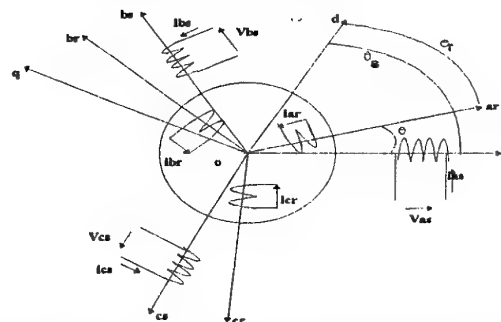

fig .1 schematic representation of an induction machine .

So, the induction machine model is defined by the following system :

$$\begin{cases} [V_s] = [R_s].[I_s] + \dfrac{d}{dt}[\Phi_s] \\ [V_r] = [R_r].[I_r] + \dfrac{d}{dt}[\Phi_r] \end{cases} \qquad (1)$$

The fluxes are linked to the current by an inductance matrix $[L(\theta)]$. This matrix can be decomposed to four blocks.

$$\begin{bmatrix} [\Phi_s] \\ [\Phi_r] \end{bmatrix} = \begin{bmatrix} [L_s] & [M_{sr}] \\ [M_{rs}] & [L_r] \end{bmatrix} \begin{bmatrix} [I_s] \\ [I_r] \end{bmatrix} \qquad (2)$$

with

$$[L_s] = \begin{bmatrix} L_s & M_s & M_s \\ M_s & L_s & M_s \\ M_s & M_s & L_s \end{bmatrix} \quad ; \quad [L_r] = \begin{bmatrix} L_r & M_r & M_r \\ M_r & L_r & M_r \\ M_r & M_r & L_r \end{bmatrix} \text{ and}$$

$$[M_{sr}] = [M_{rs}]^t = M. \begin{bmatrix} \cos\theta & \cos(\theta + \dfrac{2\pi}{3}) & \cos(\theta - \dfrac{2\pi}{3}) \\ \cos(\theta - \dfrac{2\pi}{3}) & \cos\theta & \cos(\theta + \dfrac{2\pi}{3}) \\ \cos(\theta + \dfrac{2\pi}{3}) & \cos(\theta - \dfrac{2\pi}{3}) & \cos\theta \end{bmatrix}$$

2.3 State form of the machine model

We introduce the **Park** transformation in the system (1), with the referential linked to the turning field . The induction machine model is defined by the following state system :

$$\begin{cases} \dot{X} = A.X + B.U \\ \dfrac{d\omega}{dt} = \dfrac{1}{J}.(p.Cem - p.Cr - f.\omega) \\ Y = X \end{cases} \qquad (3)$$

with : $X = (I_{ds} \quad I_{qs} \quad \Phi_{ds} \quad \Phi_{qs})$

$$A = \begin{bmatrix} \dfrac{-1}{\sigma}.(\dfrac{1}{Ts} + \dfrac{1}{Tr}) & \omega_{gl} & \dfrac{1}{\sigma.Ts.Tr} & \dfrac{\omega}{\sigma.Ls} \\ -\omega_{gl} & \dfrac{-1}{\sigma}.(\dfrac{1}{Ts} + \dfrac{1}{Tr}) & -\dfrac{\omega}{\sigma.Ls} & \dfrac{1}{\sigma.Tr.Ts} \\ -Rs & 0 & 0 & \omega_s \\ 0 & -Rs & -\omega_s & 0 \end{bmatrix}$$

$$B = \begin{bmatrix} \dfrac{1}{\sigma.Ls} & 0 \\ 0 & \dfrac{1}{\sigma.Ls} \\ 0 & 0 \\ 0 & 0 \end{bmatrix} \quad ; \quad U = \begin{bmatrix} V_{ds} \\ V_{qs} \end{bmatrix}$$

$Cem = p.(\Phi_{qr}.I_{dr} - \Phi_{dr}.I_{qr})$

$\omega_{gl} = \omega_s - \omega$

$\omega_s = d\theta_s / dt$

$\omega = d\theta / dt$

3 Seven level NPC inverter

The figure (2) present the seven level **NPC** voltage source inverter associated to the induction machine . The symmetry of the three phases seven level **NPC** inverter lets us to modelling it by leg . A Topological analysis of an arm show eight configurations possible . One of these configurations correspond to the case where all switches are turned off . The table (**I**) represents the control table of this inverter. f_{is} is the connection functions of the semi-conductor k_{is} (i: number of the arm ,and s: number of the semi-conductor). We define a following complementary control for an arm i of the inverter :

$$\begin{aligned} F_{i5} &= \overline{F_{i2}} \\ F_{i6} &= \overline{F_{i1}} \\ F_{i7} &= \overline{F_{i4}} \\ F_{i8} &= \overline{F_{i3}} \end{aligned} \qquad (4)$$

The output voltage relatively to the middle point **M** of an arm **i** of the inverter , using the connection functions of the switches is given as follow :

$$\begin{cases} V_{im} = F_{i1}.F_{i2}.\overline{F_{i3}}.\overline{F_{i4}}.Uc1 + F_{i1}.F_{i2}.F_{i3}.\overline{F_{i4}}.(Uc1 + Uc2) + \\ F_{i1}.F_{i2}.F_{i3}.F_{i4}.(Uc1 + Uc2 + Uc3) - \\ F_{i5}.F_{i6}.\overline{F_{i7}}.\overline{F_{i8}}.Uc1' - F_{i5}.F_{i6}.F_{i7}.\overline{F_{i8}}.(Uc1' + Uc2') - \\ F_{i5}.F_{i6}.F_{i7}.F_{i8}.(Uc1' + Uc2' + Uc3') \end{cases} \qquad (5)$$

By introducing the half arm connection functions , the system (5) becomes :

$$\begin{cases} V_{im} = (F_{i9}.Uc1 + F_{i10}.(Uc1 + Uc2) + f_{i1}^b.(Uc1 + Uc2 + Uc3)) - \\ ((F_{i11}.Uc1' + F_{i12}.(Uc1' + Uc2') + f_{i0}^b.(Uc1' + Uc2' + Uc3')) \end{cases} \qquad (6)$$

Where :

$F_{i9} = F_{i1}.F_{i2}.\overline{F_{i3}}.\overline{F_{i4}}$

$F_{i10} = F_{i1}.F_{i2}.F_{i3}.\overline{F_{i4}}$

$f_{i1}^b = F_{i1}.F_{i2}.F_{i3}.F_{i4}$

$F_{i11} = F_{i5}.F_{i6}.\overline{F_{i7}}.\overline{F_{i8}}$

$F_{i12} = F_{i5}.F_{i6}.F_{i7}.\overline{F_{i8}}$

$f_{i0}^b = F_{i5}.F_{i6}.F_{i7}.F_{i8}$

The system (6) can be written as follow :

$$\Rightarrow \begin{cases} V_{im} = (F_{i9}.Uc1 - F_{i11}.Uc1') + \\ (F_{i10}.(Uc1 + Uc2) - F_{i12}.(Uc1' + Uc2')) + \\ (f_{i1}^b.(Uc1 + Uc2 + Uc3) - f_{i0}^b.(Uc1' + Uc2' + Uc3')) \end{cases} \qquad (7)$$

The relation (7) shows that a seven level **NPC** inverter is equivalent to three three-level **NPC** inverters in series[4][6]. For the remain of the paper , we suppose :

$Uc1 = Uc2 = Uc3 = Uc1' = Uc2' = Uc3' = Uc$

The system (7) becomes as follow :

$$\begin{cases} V_{im} = \left\{ \left[F_{i9} + 2.F_{i10} + 3.f_{i1}^b \right] - \left[F_{i11} + 2.F_{i12} + 3.f_{i0}^b \right] \right\}.Uc \\ i = 1,2,3 \end{cases} \qquad (8)$$

126

We define the following functions :

$$\mathbf{f}_{i1}^{bT} = F_{i9} + 2.F_{i10} + 3.\mathbf{f}_{i1}^{b}$$

$$\mathbf{f}_{i0}^{bT} = F_{i11} + 2.F_{i12} + 3.\mathbf{f}_{i0}^{b}$$
(9)

The simple out put voltages of the inverter are given by the following matricial system :

$$\begin{vmatrix} V_{as} \\ V_{bs} \\ V_{cs} \end{vmatrix} = 1/3. \begin{vmatrix} 2 & -1 & -1 \\ -1 & 2 & -1 \\ -1 & -1 & 2 \end{vmatrix} . \begin{vmatrix} \mathbf{f}_{11}^{bT} - \mathbf{f}_{10}^{bT} \\ \mathbf{f}_{21}^{bT} - \mathbf{f}_{20}^{bT} \\ \mathbf{f}_{31}^{bT} - \mathbf{f}_{30}^{bT} \end{vmatrix} . Uc \quad (10)$$

This knowledge model is discontinued . To deduce The control model which must be continued ,we use the generating functions[6].

4 Six carriers triangulo-sinusoidal strategy of the seven level NPC inverter

4.1 Principle : This algorithm is deduced directly from the three phases three-level inverter [4][7]. We compare six , bipolar saw teeth carriers shifted by Th/6 (Th=1/m.f), m : represents the modulation index, with the reference voltages V_{ref_i} .These reference voltages are defined as follow :

$$\begin{cases} Vref_i = Veff.\sqrt{2}.\left(\sin(\omega.t - 2\,\Pi(i-1)/3\right) \\ i = 1,2,3 \end{cases}$$

$Veff.\sqrt{2} = r.Up\max$

with :

$Up\max$: The maximum value of the carrier.

r : rate modulation .

4.2 The strategy algorithm

$$Vref_i \geq Vp_s(s = 1,6) \Rightarrow \begin{cases} V_{is} = +Uc_s,(s = 1,2,3) \\ V_{is} = 0,(s = 4,5,6) \end{cases}$$

$$Vref_i \prec Vp_s(s = 1,6) \Rightarrow \begin{cases} V_{is} = 0,(s = 1,2,3) \\ V_{is} = -Uc'_{(s-3)},(s = 4,5,6) \end{cases}$$

$$V_{im} = \sum_{s=1}^{6} V_{is}$$

V_{im} : The voltage of the phase i relatively to the middle point **M** . Vp_s : The voltage of the carrier s .

The figures (4.*) show the performances of the three phases induction machine drive fed by this inverter and controlled by six carriers triangulo-sinusoidal strategy . The voltage harmonics are organised by family centred around multiple frequency of F'_p , with $F'_p = 6 \cdot m \cdot f$ (fig 4.3 et fig 4.5).This strategy is equivalent to single carrier triangulo-sinusoidal strategy with carrier frequency equal to $F'_p = 6 \cdot F_p$. This property shows that with six carriers , we can have a same spectrum of the output voltage with lower frequency than are carrier (in six ratio). We note the

presence of the edge and add harmonics , and particularly 2 and 4 (**fig 4.3**) . As consequence , the torque frequency of the machine is three time of the voltage one (**fig 4.6**).

5 The field oriented control

5.1 The principle of the field oriented control

The control by the field oriented is an expression appeared nowadays at literature treating the controlling technics of the electric motor. And the etymology leads us to an elementary notion, but more important of the electromagnetism .The force applied to a conductor crossed by a current and put in a magnetic field is equal to the vectorial product of the vector current by the field one. The amplitude of this force is maximal when the vector current and the field vector are perpendicular [8][9] This property is the basis of the field oriented control . We place with an optimal fashion the vector current and the result flux. The principle of this control was proposed firstly by **Blashke** at the beginning of the seventieth. Its led the induction machine behaviour and control being as a direct current one. It consist to place the reference (**d**-**q**) like the axe (**d**) coincides with the flux (current) vector **figure (3)** . In this paper we use the indirect field oriented control with the orientation of rotoric flux.
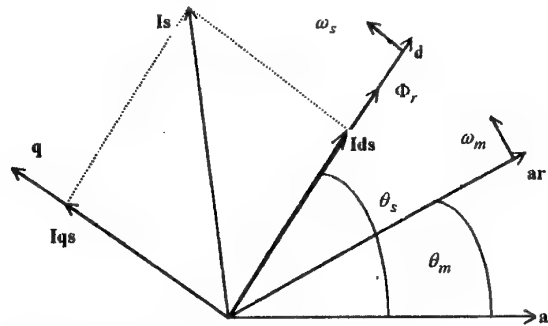

fig .3 The principle of the field oriented control.

5.2 Control of position by the indirect field oriented

The principle of this method of control consist, on do not use the amplitude of rotoric flux but only on its position. The figure(4) show a scheme of an indirect control applied to the induction machine[8].

5.3 The performances of the indirect field oriented control of the induction machine fed by a seven level NPC inverter

The figures (5.*) show the performances of the position control of the induction machine fed by a seven level inverter using the triangulo-sinusoidal strategy (with six carriers).

-The position follows quietly the references without passing **fig(5.1)**.

127

-The current (I_{qs}) and the torque are practically proportional **(fig 5.6)-(fig 5.3)**. -The flux (Φ_{qr}) is practically null **(fig 5.7)**
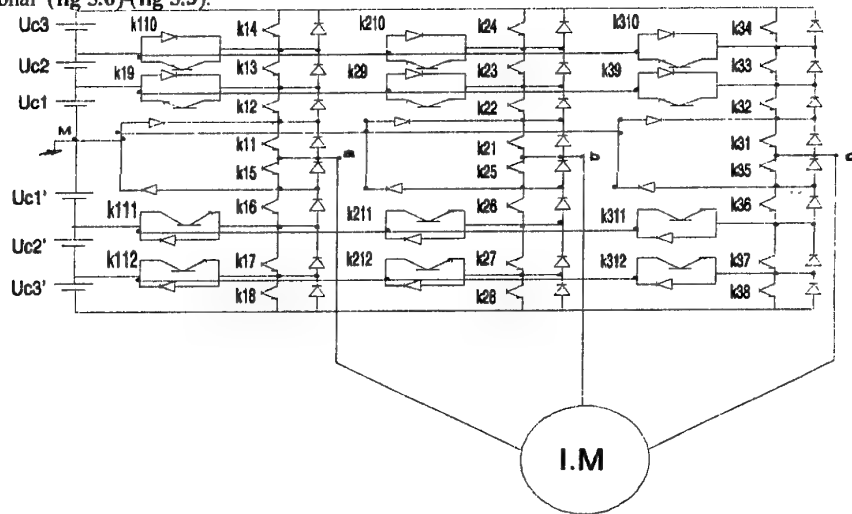

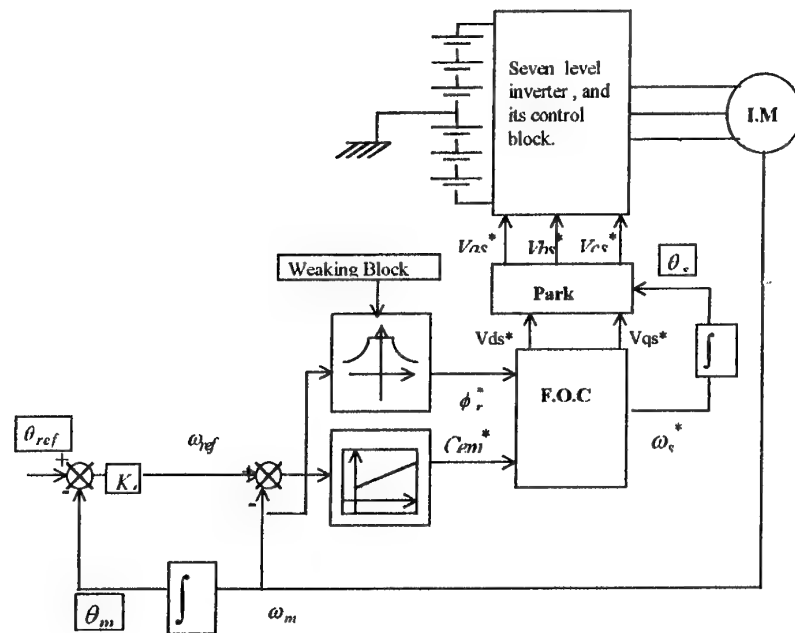fig .2 Three phase inverter of seven levels.

fig .4 Block scheme of the indirect field oriented control of the induction machine fed by an **NPC** seven level inverter .

Table. I Excitation table of arms (1) switches of the seven level inverter .

VAM	F11	F12	F13	F14	F110	F19	F15	F16	F17	F18	F111	F112
-3.uc	0	0	X	x	0	0	1	1	1	1	0	0
-2.uc	0	0	X	x	0	0	1	1	1	0	0	1
-uc	0	0	x	x	0	0	1	1	0	x	1	0
0	1	0	x	0	0	0	1	0	x	x	0	0
2.uc	1	1	1	0	1	0	0	0	0	x	0	0
3.uc	1	1	1	1	0	0	0	0	0	0	0	0
uc	1	1	0	0	0	1	0	0	x	x	0	0

128
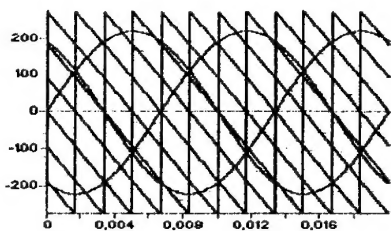
fig 4.1 The different signals of the triangulo-sinusoidal strategy (m=2,r=0.8).
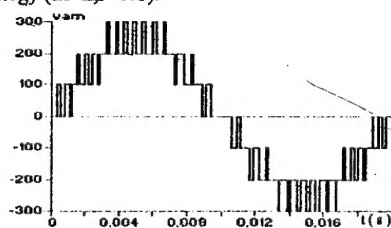
fig 4.2 The output voltage of the inverter vam (m=6,r=0.8)
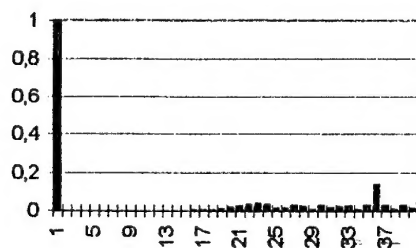
fig 4.3 Harmonics spectrum of the voltage vam
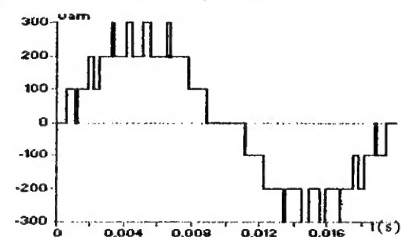
fig 4.4 The output voltage of the inverter vam (m=3,r=0.8).
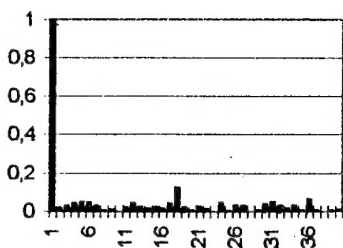
fig 4.5 Harmonics spectrum of the voltage vam.
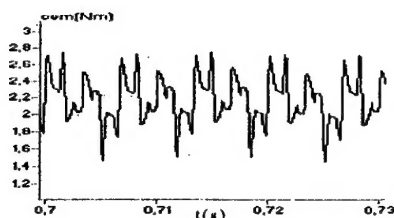
fig 4.6 electromagnetic torque in steady state (m=3,r=0.8).
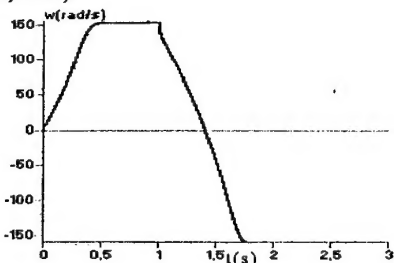
fig 4.7 Induction motor speed (m=3,r=0.8).
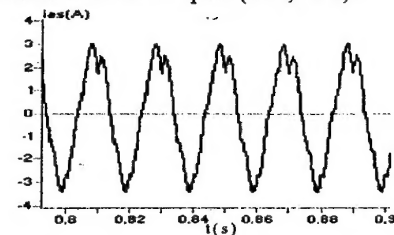
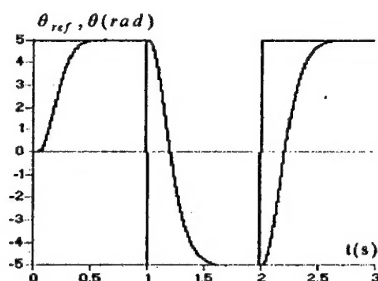fig 4.8 Phase « a » current of the induction motor in steady state (m=3,r=0.8).

fig 5.1 The real and reference position of the induction machine.
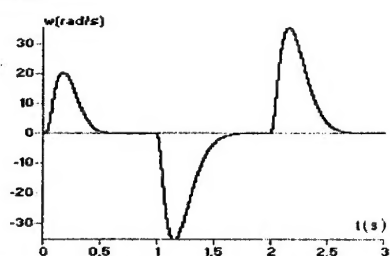
fig 5.2 The speed of induction motor.

129
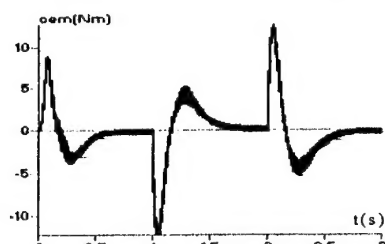
fig 5.3 The electromagnetic torque of the induction machine.
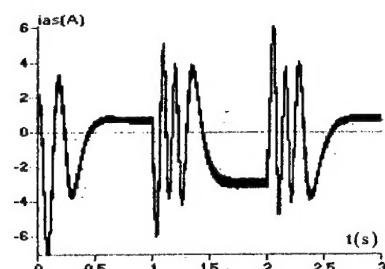
fig 5.4 The phase « a » current of the induction machine.
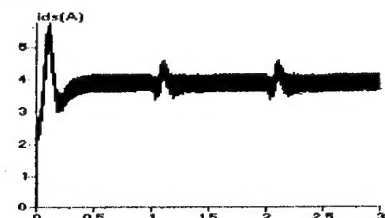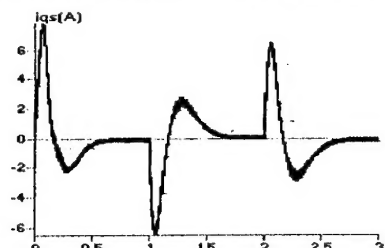

fig 5.5 The direct current Ids of the induction machine.

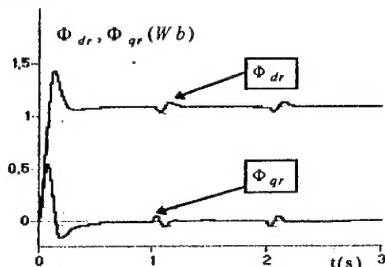fig 5.6 The quadratique Iqs current of the induction machine.

fig 5.7 The real direct and quadratic flux of the induction machine.

6 Conclusion

In this paper , we have developed the knowledge model of the three phases seven level **NPC** inverter , and we have showed that it is equivalent to three three -level **NPC** inverters (or six two level inverters). Then we have studied the six carriers triangulo-sinusoidal strategy , and showed that the harmonics frequencies are centred around multiple of 6.nf . We have used the indirect field oriented control to control the position of the induction machine fed by the **NPC** seven level inverter . The results obtained show that the position follows quietly its reference , and the component (Φ_{qr}) of the flux is practically Zero . The performances obtained for the whole system are full of promise to use it in the high voltage and great power fields as electrical traction .

References

[1] **P.C.Krause**, Analysis of electric machinery,edition MAC-GRAW HILL 1987.

[2] **J.Chatelain**, machine électrique ,tome 1,edition dunod 1983.

[3] **M.Boussak**, « contribution à la modélisation entrée sortie et l'identification paramétrique des machines à induction », **Thèse de Doctorat ,Paris VI,Paris1989.**

[4] **E.M.Berkouk**, « contribution à la conduite des machines asynchrones monophasée et triphasée alimentée par des convertisseurs directs et indirects, application aux gradateurs et onduleur multiniveaux », **Thèse de Doctorat,CNAM 1995.**

[5]**Y.B.Romdhane,E.M.Berkouk,G.Manesse**,Etude comparative entre un onduleur deux et trois niveaux pour la conduite d'une machine asynchrone triphasée», **EPE'94,SUISSE 1994 .**

[6]**E.M.Berkouk,Y.B.Romdhane,G.Manesse,** « Knowledge and control models for three-level voltage inverters »**IMACS'95,Allemagne 1995.**

[7] **E.M.Berkouk,Y.B.Romdhane,G.Manesse,** « PWM strategies to control three-level inverter.Application to the induction motors drive », **EPE'95,Espagne 1995.**

[8] **A.Faidalah,** « Contribution à l'identification et à la commande vectorielle des machines asynchrones » **Thèse de doctorat de l'INPL,France,Fev 1995.**

[9] **A.M. Trznadlowski**, « The field orientation principle in control of induction motors » **University of Nevada, Reno 1994.**

MIDDLE EAST TECHNICAL UNIVERSITY

The Middle East Technical University (METU) is one of Turkey's premie. state-financed institutions of higher education. Distinguished by its standards of teaching and research, by its use of English as the language of instruction and by its campus of unusual size and beauty, METU is a source of pride for all Turkey as well as an internationally respected institution. Its aims are to train students in scientific, technical, economic and social needs of a rapidly changing region. METU takes great pride in the achievements and looks forward to even greater accomplishments in the future.

The idea of a regional technical university originated in 1954 in recognition of the need for highly trained graduates in scientific, technical and professional fields to advance the development of Turkey and other countries in the region. In 1956, METU began instruction with four teachers and 40 students and continued to grow and develop in temporary quarters in the city until construction was initiated on the new campus 7 kilometres outside the city centre in 1962. Today, METU's modern campus, equipped with the most advanced scientific and technical facilities, serves over 20 000 students from all parts of the world with more than 2000 academic personnel.

METU is one of Turkey's most competitive universities. Of the students taking the National University Entrance Examination each year, over 40% of the 1000 applicants with the highest scores attend METU. Because demand to attend METU is so great, many of METU's departments have accepted the top 1% of the approximately one and a half million applicants taking this examination.

From its inception, METU has had an international perspective and has welcomed faculty and students from abroad. Because the language of instruction is English and because of its reputation for a high standard of education, students from many countries seek to enter METU's undergraduate and graduate programs. The number of foreign students at METU in any one year ranges from 800 to 1500 who come from over 50 different countries.

Electrical and Electronics Engineering Department

METU Electrical and Electronics Engineering Department started its education program with 25 students and 2 teaching members in 1958. Today, after 40 years of development, it is one of the biggest and the most developed departments of the university with around 1,000 undergraduate, 250 MSc and 80 Ph.D. students. With 36 professors most of which got at least one degree from respectable universities elsewhere and a staff around 100 including Research Assistants, it has reached a level of international recognition. Undergraduate program of the department has been declared substantially equivalent to similar US institutions by ABET until year 2002.

The aim of the department is to provide professional training in all major areas of electrical and electronics engineering, and at the same time to participate actively in applied and theoretical research. The students may specialise in the fields of circuits and systems, electronics, biomedical engineering, microwaves, communications, signal processing, control systems, computer engineering, electrical machines, power electronics, power systems and high voltage.

With its various research and teaching laboratories, the department has the most powerful infrastructure among similar institutions in Turkey. Computer facilities are extensive and the department runs its own computer network connected to INTERNET and the main ATM backbone of the university.

In the Electrical and Electronics Engineering Department, strong academic programs provide a background for the directed research that form a part of the MSc and Ph.D. programs. It is the policy of the department to encourage its members to take part in externally sponsored project works. These activities forming a beneficial link between the university and industry serve not only as a stimulus for a more intensive research environment in the Department but constitute a channel of information about the present and future needs of the industry to help in the improvement of the educational programs.

In 40 years, with thousands of successful graduates working in Turkey and abroad the department has become an internationally well known establishment in electrical and electronics engineering education. Considering its success in such a short time it is not difficult to foresee that it will continue to be a centre of excellence in 21st century as well.

40 years of excellence in EEeducation METU

AUTHOR AND CO-AUTHOR INDEX